Morphology of antennal hair field afferents, descending interneurons and mesothoracic motoneurons, and *in situ* calcium imaging of retrogradely labeled retractor coxae neurons in the stick insect

Inaugural-Dissertation

zur

Erlangung des Doktorgrades

der Mathematisch-Naturwissenschaftlichen Fakultät

der Universität zu Köln

vorgelegt von

Jens Goldammer

aus Köln

Köln

September 2013

Berichterstatter:
Prof. Dr. Ansgar Büschges
Prof. Dr. Peter Kloppenburg

Tag der mündlichen Prüfung:

16.10.2013

Zusammenfassung

Die Stabheuschrecke *Carausius morosus* ist ein etabliertes Tier für die Untersuchung von Laufbewegungen und Antennenbewegungen zur taktilen Erkundung der Umwelt. Neuroanatomische Studien sind hierzu aber nur limitiert vorhanden.

Im ersten Teil dieser Arbeit wurde die neuroanatomische Strukturierung des sensomotorischen Systems der Antenne von Stabheuschrecken untersucht. Dazu wurden Färbungen mittels Fluoreszenzfarbstoffen von Sinneshaaren antennaler Borstenfelder, welche als wichtige Gelenkwinkelsensoren fungieren, sowie Färbungen aller antennalen motorischen Nerven durchgeführt. Es konnte gezeigt werden, dass Afferenzen aller sieben Borstenfelder im Dorsallobus, einem deutocerebralen Neuropil im Gehirn, verzweigen und durch das Schlundkonnektiv zum Suboesophagealganglion (SOG) absteigen und dort terminieren. Des Weiteren wurden Doppelfärbungen von Borstenfeldern auf unterschiedlichen Segmenten der Antenne und von Borstenfelder mit unterschiedlichen Richtungseigenschaften angefertigt. Diese Färbungen zeigten ähnliche Projektionsmuster der unterschiedlichen Borstenfelder. Abweichungen wurden jedoch in einer unterschiedlichen Anordnung von synaptischen Boutons im Gehirn und SOG beobachtet. Innerhalb des Dorsallobus überlappen Projektionsmuster von Borstenfeld-Afferenzen mit Verzweigungen von antennalen Motoneuronen. Dies könnte bedeuten, dass direkte synaptische Kontakte möglich sind. Interessanterweise wurde in Präparaten mit Färbungen des Antennalnervens des Flagellums eine weitere Neuropilregion im Gehirn entdeckt. Diese Region ist abgegrenzt vom Dorsallobus und wurde bei Grillen als das ventrale Areal von Flagellum-Afferenzen (VFA) bezeichnet. Zusätzlich wurden Axone thorakaler Konnektive gefärbt, um absteigende Interneurone im Gehirn und SOG zu färben. Retrograde Färbungen von Halskonnektiven zeigten bis zu 410 Zellkörper (Gehirn: 205, SOG: 205), während bei Färbungen der Konnektive zwischen Pro- und Mesothorakalganglion 173 Zellkörper von absteigenden Interneuronen identifiziert wurden (Gehirn: 83, SOG: 90). Präparate mit Doppelfärbungen von Konnektiven und Borstenfeld-Afferenzen ergaben, dass Neuriten von absteigenden Interneuronen in der Nähe von Borstenfeld-Afferenzen zu finden sind. Dies lässt

vermuten, dass Signale von Borstenfeldern direkt über absteigende Interneurone zu thorakalen Netzwerken weitergeleitet werden.

Im zweiten Teil dieser Arbeit wurde die Morphologie von Motoneuronen, dorsalen ungepaarten medianen Neuronen (DUM) und sensorischen Neuronen untersucht. Dies erfolgte über durchgeschnittene laterale Nerven des Mesothorakalganglions mittels retrograder Applikation von Fluoreszenzfarbstoffen. Es konnte gezeigt werden, dass die Anzahl von Motoneuronen und DUM-Zellkörper erheblich höher liegt als bisher publiziert wurde. Die Zellkörper von exzitatorischen Motoneuronen bilden Gruppen in ganglionären Randbereichen und ihre Dendriten sind hauptsächlich in dorsalen und lateralen Bereichen des Ganglions zu finden. Insgesamt wurden neun DUM-Zellkörper gefärbt. Sechs dieser Neurone besitzen Axone im Nervus lateralis 5 (nl5), welcher die Retraktor coxae Muskeln innerviert. Die meisten gefärbten sensorischen Afferenzen terminieren in dem sogenannten ventralen Assoziationszentrum (VAC) des Ganglions. In der Nähe des Zellkörpers des "schnellen Extensor tibiae Motoneurons" (FETi) wurden 23 kleine Zellkörper entdeckt. Bei diesen Neuronen handelt es sich mit großer Wahrscheinlichkeit um sogenannte Sehnenrezeptoren. Die erzielten Ergebnisse wurden außerdem mit vorhandenen Publikationen von Stabheuschrecken und anderen orthopteroiden Insekten verglichen.

Im dritten Teil wird eine "Calcium (Ca^{2+}) -Imaging" Methode vorgestellt für das retrograde Beladen von durchtrennten Motoneuron-Axonen des nl5 mit einem Ca^{2+}-sensitiven fluoreszierenden Indikator. Intrazelluläre Ca^{2+}-Änderungen wurden induziert durch Applikation des muskarinischen Acetylcholinrezeptoragonisten Pilocarpine in die thorakale Öffnung des Tieres und durch taktile Stimulation des Tieres. Die gemessenen intrazellulären Ca^{2+}-Änderungen in Primär- und Sekundärneuriten von Retraktor coxae Motoneuronen sind sehr ähnlich und zeitlich gleichförmig. Berechnete Integrale von intrazellulären Ca^{2+}-Änderungen und Integrale der Retraktor coxae Motoneuronaktivität zeigten eine lineare Korrelation. Dies bedeutet, dass die gemessene Änderung des intrazellulären Ca^{2+} in Retraktor coxae Motoneuronen von der Aktivierung von spannungsabhängigen Ca^{2+}-Kanälen als Folge von Membrandepolarisierungen abhängig ist. Darüber hinaus war es möglich, Ca^{2+}-Transienten in lateralen DUM-Neuriten zu messen. Eine erste Analyse von Ca^{2+}-Änderungen in drei vermeindlichen DUM-Neuriten, ausgelöst durch Applikation von Pilocarpine, zeigte reguläre und gleichphasige intrazelluläre Ca^{2+}-Änderungen. Die Ca^{2+}-Erhöhungen in DUM-Neuriten zeigten weder mit der Aktivität von Protraktor coxae Motoneuronen noch mit der Aktivität von Retraktor coxae Motoneuronen einen festen Phasenbezug.

Abstract

The phasmid species *Carausius morosus* serves as an established animal for studying terrestrial locomotion and antennal movements for tactile exploration of the near-range environment, but neuroanatomical data is only limited available.

In the first part of this thesis, fluorescent dye stainings of antennal hair field sensilla, which are important antennal joint angle sensors, and stainings of all antennal motor nerves were performed to receive detailed insights into the neuroanatomical organization of the stick insects' antennal sensorimotor system. It was shown that afferents of all seven antennal hair fields (HF) send collaterals into the dorsal lobe, a deutocerebral neuropil region in the brain, and further descend through the circumoesophageal connective to the suboesophageal ganglion (SOG), where these afferents terminate. Moreover, double stainings of HFs located on different antennal segments and of HFs with different direction properties showed similar staining patterns, but differences were found in a spatially different formation of synaptic boutons within the entire depth of the dorsal lobe and within the SOG. In the dorsal lobe, HF afferents and projections of antennal motoneurons overlap, which could be an indication for direct synaptic contacts. Interestingly, stainings of the antennal nerve of the flagellum revealed another deutocerebral neuropil separated from the dorsal lobe, the ventral area of flagellum afferents described for crickets. Besides, thoracic connectives were stained to reveal somata of descending interneurons (DIN) located in the brain and SOG. Axonal backfills of cervical (neck) connectives revealed up to 410 cell bodies of DINs (brain: 205, SOG: 205), and backfills of connectives between the pro- and mesothoracic ganglia stained up to 173 DINs (brain: 83, SOG: 90). Furthermore, in double stainings of connectives and scapal HF sensilla it was observed that neurites of DINs seem to be in vicinity to afferents of HFs, which suggests that antennal HF signals are transmitted via a fast cephalothoracic pathway to thoracic motor centers.

In the second part, the morphology of leg motoneurons, dorsal unpaired median neurons (DUM), and sensory neurons in the stick insect mesothoracic ganglion were examined. For this, cut ends of lateral nerves were retrogradely labeled

with fluorescent dyes. Numbers of motoneurons and details of their structure by far exceed previously published data. Somata of excitatory motoneurons form clusters in the lateral ganglion cortex and their dendrites branch mainly in the dorsal neuropil. Nine DUM neurons were identified, six of which have axons in nervus lateralis 5, which innervates the retractor coxae muscles. Most sensory fibers terminate in the ventral association center (VAC). Twenty-three small cell bodies located close to the soma of the fast extensor tibiae motoneuron (FETi) likely belong to strand receptors. Stained structures are compared with previously published data from stick insects and other orthopteran insects.

In the third part, a calcium (Ca^{2+}) imaging method is introduced for retrograde loading cut ends of stick insect retractor coxae motoneuron axons with a Ca^{2+}-sensitive fluorescent indicator. Intracellular Ca^{2+} changes were induced either by the application of the muscarinic acetylcholine agonist pilocarpine into the thoracic cavity and by tactile stimulation of the animal's abdomen. The measured intracellular Ca^{2+} dynamics are very similar and temporarily uniform across primary and secondary motoneuron neurites. Calculated integrals of measured intracellular Ca^{2+} changes and integrals of retractor coxae spike activity revealed a linear correlation. This suggests that the observed changes in intracellular Ca^{2+} result from activation of voltage-gated Ca^{2+} channels by membrane depolarizations. Moreover, Ca^{2+} changes of lateral DUM neurites could be measured. A first analysis of pilocarpine-induced Ca^{2+} transients in presumed three different DUM neurites revealed regular and in-phase Ca^{2+} oscillations. These DUM neurite Ca^{2+} elevations have no fixed phase relation to either the protractor coxae nor the retractor coxae spike activity.

Contents

1. Introduction

Locomotion in a natural environment requires the perception of sensory information for orientation, localization or negotiation of obstacles, and recognition of food sources. For studying terrestrial locomotion and antennal movements for tactile exploration of the near-range environment, the phasmid species *Carausius morosus* serves as an established animal for the understanding of underlying behavioral and neuronal mechanisms (locomotion: e.g., reviewed in Bässler and Büschges, 1998; Büschges et al., 2008; Büschges and Gruhn, 2008; Cruse, 1990; tactile exploration: e.g., Dürr et al., 2001; Schütz and Dürr, 2011; Krause and Dürr, 2012; reviewed in Staudacher et al., 2005).
In the first part of this thesis, I investigated neuroanatomically the antennal sensorimotor system and descending interneurons in supra- and suboesophageal ganglia of stick insects. The second part deals about the morphology of mesothoracic motoneurons, modulatory dorsal unpaired median neurons, sensory neurons with a central cell body, and sensory afferents. In the third part, I will introduce a method for retrograde labeling a mesothoracic lateral nerve with a calcium-sensitive fluorescent dye for imaging free intracellular calcium in stick insect motoneuron neurites. The different contents in the present thesis are introduced in the following in three independent, separate sections.

1.1. Morphology of antennal hair field afferents and brain and suboesophageal descending interneurons

Tactile exploration is important for the detection of obstacles in the near-range environment. Many animals from invertebrates to vertebrates, use the tactile sense for active tactile searching and sampling of objects. For example, rodents and other mammals are equipped with whiskers for tactile sensing, whereas insects use a pair of antennae for sensing.

The insect antennae are regarded as true segmented limbs with muscles and sensory structures similar to thoracic walking legs (Staudacher et al., 2005). Evidence for similarities of antennae and legs are recognizable in homoeotic regenerates, where an amputation or a loss of a stick insect antenna leads to a regeneration as parts of a walking leg (e.g., Schmit-Jensen, 1914; Edwards et al., 1988).
The antenna of the stick insect *C. morosus* is composed of three functional segments: the scape, the pedicel, and a long thin flagellum. To explore the near-range environment it is necessary that the antennae are actively moved, in order to receive spatial information of the surroundings. Antennal movement patterns have been described in detail for crickets (Horseman et al., 1997), cockroaches (Okada and Toh, 2004), and stick insects (Dürr et al., 2001). During walking, the stick insect antennae are moved rhythmically and, furthermore, the antennal movements are coupled to stepping sequences of the front legs (Dürr et al., 2001). Each antenna is movable by means of two single-axis hinge joints with slanted axes, the proximal head-scape (HS joint) and the distal scape-pedicel joint (SP joint), whereas the flagellum can only be moved or bended passively (Mujagic et al., 2007; Dürr et al., 2001). The HS joint is controlled by a pair of levator muscles that move the antenna dorsolaterally, and a tripartite depressor muscle that moves the antenna ventromedially (Dürr et al., 2001). Whereas the SP joint is controlled by the antennal abductor muscle that moves the antenna ventrolaterally, and the antennal adductor muscle that moves the antenna dorsomedially (Dürr et al., 2001).

Kinematic leg analysis of blindfolded stick insects approaching a vertical rod revealed that antennal contact can elicit two types of reach-to-grasp front leg movements, so-called reaching and re-targeting movements (Schütz and Dürr, 2011). During reaching movement, the ipsilateral front leg has ground contact when the antenna touches the rod. The stance sequence of the front leg is first completed and then a movement similar to a leg swing phase occurs with an increased height of the foot trajectory. During re-targeting movement, the ipsilateral front leg performs a swing movement when the antenna touches the rod. Subsequently, the leg is moved towards the contact site of the antenna. Furthermore, Schütz and Dürr (2011) showed that the height of the last antennal contact location predicts the first leg contact site with the rod.

These reach-to-grasp movements after touching an object described by Schütz and Dürr (2011) require that antennal posture information is measured by antennal sense organs. The proprioceptive control of antennal movement patterns was described in detail for the cockroach (Okada and Toh, 2000, 2001) and recently for the stick insect (Krause et al., 2013). A particular group of sense organs, the antennal hair fields (HF; also known as Böhm's bristles, Böhm, 1911) situated close

to the joint membranes of the scape and pedicel encode directional information of the antennal position (cockroach: Okada and Toh, 2000, 2001; stick insect: Krause et al., 2013). Stick insect scapal and pedicellar segments carry seven HFs, these can be further divided into hair plates (HP) with up to 22 sensilla and hair rows (HR) with up to eight sensilla (Krause et al. 2013; Fig. 2.1). These tactile hairs have flexible and asymmetric sockets that allow a deflection of the sensillum in only one direction and a single hair is innervated by only one bipolar neuron (Staudacher et al., 2005). Ablation of HF sensilla affected drastically the working range of the antennal joints in cockroaches and stick insects, indicating their function as important joint angle sensors (Okada and Toh, 2000; Krause et al., 2013). For example, removal of the sensilla of the stick insect dorsal scapal HP caused an increase in the dorsal HS joint working range and, moreover, it was often observed that the animals pointed the antennae rearward or even folded it backward to nearly touch the abdomen (Krause et al., 2013).

Schütz and Dürr (2011) revealed furthermore that re-targeting movements of stick insect front legs begin within 40 ms after antennal contact. This implicates that antennal touch information is forwarded to thoracic ganglia via a fast cephalothoracic pathway. This can be accomplished by descending interneurons (DINs) that transmit signals from centers of the supraoesophageal ganglion (termed brain in the following) and suboesophageal ganglion (SOG) to motor networks of thoracic ganglia. DINs were reported in insects that respond to antennal tactile stimulation with very short latencies. In cockroaches, two identified brain and SOG DINs are considered to be involved in antennal guided escape responses (Burdohan and Comer, 1990, 1996). Schöneich et al. (2011) reported for the cricket, four brain and two SOG DINs that transmit antennal touch information from the flagellum with very fast conductance velocities ranging from 2.7 m/s to 5 m/s to the thorax. Moreover, Gebhardt and Honegger (2001) found five brain DINs in the cricket responding to forced antennal movement applied to the SP joint. Similar to the latter study, Ache and Dürr (2013) applied staircase ramp-and-hold stimuli to the SP joint of the stick insect antenna, while recording intracellularly from DIN axons in cervical (neck) connectives or in the anterior neuropil of the prothoracic ganglion. Ache and Dürr (2013) were able to characterize five functional groups of DINs sensitive to movement direction, velocity, and antennal joint angle: 1. Simple position-sensitive DINs which signal joint angle; 2. Dynamic position-sensitive DINs signaling joint angle with strong dependency on movement; 3. Unspecific movement-sensitive DINs which signal movement, and 4. and 5. On- and Off-type velocity-sensitive DINs, where the spike frequency is correlated with the SP joint angle velocity. The investigations by Gebhardt and Honegger (2001) and Ache and Dürr (2013) indicate that signals of antennal sense organs located at least

at the SP joints are transmitted directly via DINs to thoracic ganglia. Possible candidates for these sense organs are sensilla of antennal HFs. Furthermore, in contrast to the fast cephalothoracic pathway, a slower pathway exists for processing of antennal information that involves the central complex (CC) located in the protocerebrum of the brain as shown for cockroaches by multi-unit recordings in the CC during mechanical antennal stimulations (Ritzmann et al., 2008).

In general, insect antennae are equipped with a huge amount of sensory receptors for different modalities (reviewed in: Schneider, 1964; Staudacher et al., 2005). Along the antennal segments olfactory, thermal, gustatory (contact-chemosensory), and mechanosensory sensilla are located. The mechanosensory sensilla are essential for sampling surfaces, for object localization, or communication (Staudacher et al., 2005). Apart from HF sensilla, the filiform antennae of *C. morosus* carry various other sensory structures. At the distal edge of the pedicel a ring of campaniform sensilla (Hicks organ) and the Johnston's organ are situated. Along the flagellum, 40 to 50 campaniform sensilla, 600 to 700 gustatory sensilla, and 4000 to 4500 mechanosensory sensilla are distributed (Weide, 1960; Slifer, 1966; Monteforti et al., 2002; rev: Staudacher et al., 2005). Numbers of olfactory sensilla on the stick insect antenna are not known.
In other insect species, central projections of antennal sense organs and other mechanosensory sensilla have been well described and all afferent fibers converge in neuropils of the deutocerebrum (DC) of the brain (e.g., honeybee: Suzuki, 1975; Maronde, 1991; Ai et al., 2007; locust: Bräunig et al., 1983; cricket: Staudacher and Schildberger, 1999; cockroach: Nishino et al., 2005). Stainings of the antennal nerve of the honeybee revealed two prominent neuropils for antennal afferents, namely the antennal lobe (AL), where olfactory sensilla terminate, and the dorsal lobe (DL), where antennal afferents of mechanoreceptors terminate (Suzuki, 1975; Maronde, 1991). Motoneurons innervating antennal muscles have central projections within the DL of honeybees, too (Suzuki, 1975; Kloppenburg, 1995). The DL is therefore often referred to as the 'antennal mechanosensory and motor center' (AMMC; Rospars, 1988; Homberg et al., 1989). Furthermore, a third antennal neuropil in the DC of crickets was described by Staudacher and Schildberger (1999) and it was termed ventral area of flagellar afferents (VFA) because exclusively afferent fibers of the flagellum terminate there.

The movement kinematics of stick insect antennae are well investigated, but neuroanatomical data for antennal mechanosensory afferents are nonexistent. Thus, in the first part of the thesis, stainings of antennal HF sensilla and motor nerves were performed to receive information about the neuroanatomical organization of the stick insects' antennal sensorimotor system. In order to integrate and process

antennal sensory information in the brain, it could be possible that afferents from different HFs project, according to their location on the scape and pedicel, into different regions of the DC. Therefore, the central projection patterns of all antennal HFs are investigated concerning differences in arborizations, terminal neuropil regions, and vicinity to neurites of antennal motoneurons. Additionally, stainings of the antennal nerve and of dorsally situated solitary sensilla on the pedicel were performed to examine the relative locations of different terminal neuropil regions within the DC.

The clustering and numbers of DINs in the brain were reported in detail for the cricket (Staudacher, 1998) and the cockroach (Okada et al., 2003), but are lacking for stick insects. This is why axons in cervical (neck) connectives and axons in connectives between pro- and mesothoracic ganglia were stained to reveal numbers and distribution of DINs in the brain and SOG projecting to thoracic ganglia. According to the results by Schütz and Dürr (2011) and Ache and Dürr (2013) antennal sensory signals are transmitted rapidly to thoracic ganglia. Therefore, the vicinity of DIN neurites to scapal antennal HF afferents was examined to evaluate the neuroanatomical possibility of HF signals being transmitted via a fast-descending-pathway to thoracic motor centers.

1.2. Morphology of mesothoracic motoneurons, DUM cells, and sensory neurons with a central cell body[1]

It is well established that locomotor strategies like flying, swimming, or walking require coordinated rhythmic activity of antagonistic muscles (Orlovsky et al., 1999). Motor commands in vertebrates and invertebrates are centrally driven by local neuronal networks, so-called central pattern generators (CPG), which activate motoneurons (MN) that transmit signals in shape of action potentials to the performing skeletal muscles (e.g., reviewed in Pearson, 1993; Grillner, 2003). Typically, a mammalian limb muscle is innervated by several hundred MNs (e.g., Eccles and Sherrington, 1930), whereas arthropod limb muscles are innervated by just a few MNs. For example, the accessory flexor muscle of the Dungeness crab *Cancer magister* is innervated by one excitatory and one inhibitory MN only

[1]Parts of the introduction are already published: Goldammer J, Büschges A and Schmidt J. *Motoneurons, DUM Cells, and Sensory Neurons in an Insect Thoracic Ganglion: A Tracing Study in the Stick Insect Carausius morosus.* Journal of Comparative Neurology, 520(2), 230-257, 2012. The author contributions are as followed: JG, AB and JS designed research. JG performed experiments, analyzed data, prepared figures, tables and drafted the manuscript. JS edited the manuscript.

(Dorai Raj, 1964). Because of their small number, each arthropod MN is likely to have a distinct impact on the activity of the innervated muscle. Therefore, if one is interested in the neuronal control of insect locomotion, knowing the number of MNs innervating leg muscles and their position in the ganglion is crucial.

The phasmid species *C. morosus* and *Cuniculina impigra* are well established animals for studying the organization and coordination of neuronal networks controlling basic locomotor behaviors (e.g., Bässler and Büschges, 1998; Büschges et al., 2008; Büschges and Gruhn, 2008). During walking, the stepping sequence of a leg can be divided into two phases: (i) a stance phase, in which the leg has ground contact and generates force for the forward propulsion of the body, (ii) a swing phase, in which the leg is lifted and moved forward to reach the start position for the following step (Büschges et al., 2008). Each stick insect leg is movable by three main leg joints with its own sets of antagonistic muscles. The thoraco-coxal (ThC) joint is moved forward by the protractor coxae muscle and backward with the retractor coxae muscles. The levator and depressor trochanteris muscles lift or depress the coxo-trochanteral (CTr) joint, respectively. Whereas the femur-tibia (FTi) joint is extended with the extensor tibiae muscle and flexed with the flexor tibiae muscles.

In order to fulfill coordinated leg movements, it is necessary that each motoneuron (MN) pool innervating specific muscles is activated at the right phase of the step cycle. Experiments in the stick insect demonstrated that CPGs, located in the three thoracic ganglia of the ventral nerve cord, generate rhythmic and alternating activity in MNs. Topical application of the muscarinic acetylcholine (ACh) agonist pilocarpine onto a deafferented and isolated mesothoracic ganglion revealed alternating activity in antagonistic MN pools and, moreover, it was shown that the motor output of the different leg joints was not reliably cycle-to-cycle coupled (Büschges et al., 1995). These findings suggest that each main leg joint possesses its own individual CPG. Two further experiments revealed that inhibitory synaptic input onto MNs is probable to derive from CPGs: (i) application of pilocarpine onto a deafferented mesothoracic ganglion, or (ii) tactile stimulations applied to the abdomen of a stick insect, where all legs were removed, revealed that rhythmic activity of MNs underlies a tonic excitation interrupted by inhibitory phasic synaptic inputs (Büschges, 1998; Büschges et al., 2004). The tonic excitation of MNs during walking is assumed to originate from intersegmental and/or descending sources: First, it was shown that the amplitude of the tonic excitation of mesothoracic MNs was correlated with stepping sequences of the ipsilateral front leg (Ludwar et al., 2005). Second, removal of the brain decreased the amplitude of the tonic excitation of MNs (Westmark, 2007). Furthermore, MNs receive synaptic drive

of sense organs associated with the legs, either by rare monosynaptic connections directly onto MNs or via polysynaptic pathways involving intercalated component neurons of the CPGs (e.g., Burrows, 1996; Büschges, 2005; Büschges and Gruhn, 2008). Important sense organs for stick insects are for instance trochanteral and femoral campaniform sensilla (CS), which function as cuticular load and strain sensors, or the femoral chordotonal organ (fCO), which measures FTi joint flexion and extension (e.g., Büschges and Gruhn, 2008). Stimulation of these sense organs provide sensory feedback that can reset or entrain the MN rhythm (e.g., Hess and Büschges, 1999; Akay et al., 2001, 2004; reviewed in Büschges and Gruhn, 2008).

As yet, the complete CPG network architecture is not known (Orlovsky et al., 1999; Büschges, 1995; Burrows, 1996). For an elucidation of the networks controlling leg movements it is important to identify all involved neurons not only physiologically, but also morphologically. The knowledge of the aborization patterns of dendrites of neurons relative to prominent landmarks in thoracic ganglia, like fiber tracts, commisures, or neuropils, will help to draw conclusions about putative connections to other neurons that were already described or will be described in the future. The importance of neuroanatomical investigations can also be seen in the generation of 3D anatomical standard atlases for insect brains, where brain parts are digitally reconstructed. These atlases provide the basis to fit individually identified neurons into the reconstructed brain to gather information about the connectivity to other neurons or whole brain parts. Such brain atlases exist for example for *Drosophila* (Rein et al., 2002), the honeybee (Brandt et al., 2005), or the locust (Kurylas et al., 2008).

However, the locomotor networks for controlling leg movements are located in thoracic ganglia. For locusts, numerous studies about the morphology of thoracic neurons and sensory leg afferents are present (reviewed in Burrows, 1996). These studies range for example from mechanosensory neuropils (e.g., Pflüger et al., 1988), non-spiking interneurons (e.g., Siegler and Burrows, 1979; Watkins et al., 1985), local spiking interneurons (e.g., Burrows and Siegler, 1984), intersegmental neurons (e.g., Laurent, 1987) to muscle innervating MNs (e.g., Burrows and Hoyle, 1973; Watson and Burrows, 1982; Siegler and Pousman, 1990a, 1990b). Moreover, neuroanatomical and electrophysiological investigations revealed another neuron type with a particular morphology, the dorsal unpaired median neurons (DUM; e.g., Plotnikova, 1969; Crossman et al., 1971; Hoyle et al., 1974). These neurons are characterized by their position mainly dorsal at the ganglion midline, their efferent bilateral neurites projecting into lateral nerves, and the release of the biogenic amine octopamine in the periphery to modulate neuromuscular transmission (e.g., Stevenson and Spörhase-Eichmann, 1995; reviewed in Bräunig and Pflüger, 2001).

Moreover, sensory neurons were reported for orthopteran insects which have no cell bodies in the periphery, instead these sensory neurons have a special feature of a central cell body (Bräunig, 1982a, 1982b). The function of these sensory neurons in locusts is to innervate connective tissue strands in the thoraco-coxal joint (Bräunig and Hustert, 1980).
For other insect species less neuroanatomical data is present. For crickets, stainings of leg sensory afferents (Johnson and Murphey, 1985; Nishino, 2000), or of some coxal and tibial MNs are available (Laurent and Richard, 1986; Nishino, 2003). For cockroaches, the morphology of mechanosensory afferents was revealed by Collin (1985) and the distribution of MN cell bodies was investigated by Young (1969) and Iles (1976).

For stick insects, the ganglionic organization of fiber tracts and neuropil regions was revealed by the osmium/ethyl-gallate procedure (Kittmann et al., 1991). Central projections and terminal regions of body and leg sensory afferents were provided by Schmitz et al. (1991). The morphology of some thoracic non-spiking interneurons (NSI; Büschges, 1990; Büschges and Wolf, 1995; von Uckermann and Büschges, 2009) and intersegmental interneurons (Büschges, 1989) are known. Furthermore, the activity of DUM neurons during walking and the morphology of recorded neurons was investigated by Mentel et al. (2008). The authors categorize different types of DUM neurons according to their axons in different lateral nerves and, moreover, they showed that at least eight DUM neurons can be found in thoracic ganglia. At present, the total amount of mesothoracic efferent DUM neurons is still unknown.

As yet, a gross neuroanatomical description of stick insect leg muscle innervating MNs with respect to their arborizations in the neuropil of thoracic ganglia is only restricted available. For *C. morosus*, a map of retrogradely labeled meso- and metathoracic MNs was made by Storrer et al. (1986). The illustrations of whole-mount preparations in the study by Storrer et al. (1986) were captured by using camera lucida drawings that suffer from a lack of detail and allow only limited insights into the morphology of MNs, their cell body positions, their dendritic fields, and terminal areas of sensory afferents. Furthermore, DUM neurons were not labeled in previous studies about MNs (e.g., Graham and Wendler, 1981; Storrer et al., 1986; Hess and Büschges, 1997), indicating that the method used was improvable. This unsatisfactory situation and improvements in microscopy techniques, such as confocal laser scanning microscopy (CLSM), prompted in the second part of this thesis a re-investigation of the morphology and soma cluster sizes of mesothoracic MNs and the number of DUM cells in the stick insect by retrograde loading/backfilling cut ends of mesothoracic lateral nerves with fluorescent

dextran dyes. To receive detailed information about the distribution of neurites and terminal areas of sensory afferents within the entire depth of the mesothoracic ganglion, I performed anti-β-tubulin immunohistochemistry on thick vibratome sections to provide additionally transverse views with visualized landmarks as for example prominent longitudinal fiber tracts and neuropil regions. Moreover, the stainings are compared with previously published data from stick insects and other orthopteran insects.

1.3. *In situ* calcium imaging of retrogradely labeled retractor coxae neurons

Calcium (Ca^{2+}) plays a crucial role in various cellular processes, which range for instance from gene transcription, intracellular signaling, release of neurotransmitter, neuromuscular transmission, synaptic plasticity to even apoptosis (e.g., reviewed in Berridge, 1998, Berridge et al., 2000; Bootman et al., 2001; Augustine et al., 2003).

Ca^{2+} also serves as charge carrier to support the excitability and intrinsic firing properties of neurons. The importance of Ca^{2+} can be seen in the existence of numerous electrophysiological studies about the different types of low- and high-voltage-gated Ca^{2+} currents in invertebrate and vertebrate motoneurons (MN) (e.g., crab: Zhang and Harris-Warrick, 1995; insects: Hayashi and Levine, 1992; Mills and Pitman, 1997; Ryglewski et al., 2012; lamprey: El Manira and Bussieres, 1997; turtle: Hounsgaard and Kiehn, 1993; mouse: Carlin et al., 2000). Moreover, the firing properties of neurons can be regulated by Ca^{2+}-dependent currents. For the lamprey locomotor network, a Ca^{2+}-dependent potassium current was reported which is involved in spike frequency adaptation (SFA) and burst termination (El Manira et al., 1994).

About the role of Ca^{2+} in stick insects only limited data is available. A Ca^{2+} current in ventral longitudinal metathoracic muscle fibers was found by three electrode voltage clamp recordings (e.g., Ashcroft and Stanfield, 1982). Intracellular recordings of stick insect femoral chordotonal organ (fCO) afferents during electrical and mechanical stimulation of the fCO apodeme revealed that these afferents exhibit adaptation, which is mediated by a Ca^{2+}-dependent mechanism (DiCaprio et al., 2002). Westmark (2007) studied the tonic depolarization underlying flexor MNs during walking. She revealed that injecting BAPTA-1, a Ca^{2+} chelator, intracellularly into MNs decreased the amplitude of the tonic depolarization, which suggest that Ca^{2+} could support the generation of the tonic depolarization. Patch-clamp recordings of isolated stick insect leg MNs during application of acetylcholine

(ACh) showed a fast-desensitizing (I_{ACh1}) and a slow-desensitizing (I_{ACh2}) inward current (Oliveira et al., 2010). Morover, it was shown that nicotinic ACh receptors are the source of I_{ACh}, and patch-clamp recordings combined with Ca^{2+} imaging revealed that ~18% of the ACh induced current was carried by Ca^{2+} (Oliveira et al., 2010).

The development of Ca^{2+}-sensitive fluorescent indicators by Tsien and colleagues in the 80s of the last century (e.g., Tsien et al., 1985) provided reliable tools for measuring free intracellular Ca^{2+} by means of, e.g., CLSM or two-photon microscopy. The Ca^{2+} imaging technique has the advantage to study changes in free intracellular Ca^{2+} in many regions of a neuron's dendritic tree simultaneously, whereas intracellular or patch-clamp recordings are spatially limited to the recording site only. Moreover, the presence of voltage-gated Ca^{2+} channels in neurons and the influx of Ca^{2+} caused by membrane depolarizations due to action potentials allow to monitor activity patterns of single neurons or whole populations of neurons via Ca^{2+} imaging only (Göbel and Helmchen, 2007).
In the course of time, several different Ca^{2+}-sensitive fluorescent indicators and indicator loading techniques were developed for measurements of changes in intracellular Ca^{2+} in neurons (e.g., Takahashi et al., 1999; Göbel and Helmchen, 2007). Retrograde loading/backfilling the axonal pathways of neurons with Ca^{2+}-sensitive fluorescent dyes is one of the techniques to study Ca^{2+} transients. Such a loading of neurons with Ca^{2+} indicators (or variants of the technique) were used successfully in invertebrates (honeybee: Sachse and Galizia, 2002; *Drosophila* larvae: Macleod et al., 2003) and in vertebrates (e.g., zebrafish: Fetcho and O'Malley, 1995; lamprey: Viana di Prisco and Alford, 2004; chick embryo: O'Donovan et al., 1993; neonatal rat and mouse: Lev-Tov and O'Donovan, 1995; Bonnot et al., 2002).

As yet, Ca^{2+} imaging studies of insect MN neurites are spares. Duch and Levine (2002) investigated changes in free intracellular Ca^{2+} in neurites of the motoneuron 5 (MN5) of the moth *Manduca sexta* during different stages of postembryonic dendritic growth. In the cricket, Baden and Hedwig (2009) studied single-cell Ca^{2+} transients of adult tibial MNs by injecting the Ca^{2+} indicator intracellularly.

Retrograde loading of cut ends of nerves with fluorescent dextran dyes was used successfully in the second part of this thesis in order to study the morphology of mesothoracic MNs and DUM cells. Furthermore, the stainings revealed that MN neurites are mainly found in dorsal and lateral ganglion regions. This finding of MN neurites on the dorsal surface allows that stained neurites in tethered and exposed stick insects are accessible for Ca^{2+} imaging with a fluorescence microscope. In order to extend the current knowledge about Ca^{2+} in stick insect MNs and for studying synaptic input sites of MN neurites, a Ca^{2+} imaging method com-

bined with electrophysiological recordings could be a powerful tool for providing novel information towards the understanding of the neuronal control of locomotion. Therefore, in the third part of this thesis, a Ca^{2+} imaging method will be introduced for retrograde loading of stick insect retractor coxae MN neurites with a Ca^{2+}-sensitive fluorescent dextran dye that allows reliable and stable measurements of changes in free intracellular Ca^{2+} *in situ*.

2. Materials and Methods

2.1. Animals

Experiments were performed on adult female stick insects, *Carausius morosus* (de Sinéty, 1901), from a colony maintained at the University of Cologne. The colonies were kept at temperatures between 20 °C and 25 °C and at artificial light/dark rhythm. The animals were fed with blackberry leaves (*Rubus fructiosus*).

2.2. Staining of antennal mechanosensory afferents, antennal motor nerves, and descending interneurons

Staining of scapal and pedicellar hair fields

Animals were fixed dorsal side up with plasticine in a wax-coated petri dish. To gain access to the seven hair fields (HF) situated at the head-scape and the scape-pedicel joint (Fig. 2.1), the antennal segments needed to be deflected as much as possible, pointing away from the HF under study. The tips of the flagella were fixed with plasticine to prevent antennal movement. The HFs of interest were surrounded with Vaseline petroleum jelly (Weißes Vaselin, Medical Pharma GmbH, Bremerhaven, Germany) to build a well. Distilled water was filled into the well and HF sensilla were shaved at their base with a razor blade. Then, the water was replaced by a drop fluorescent dextran-coupled dye. In several cases, double staining procedures of scapal and pedicellar HFs were performed with tetramethylrhodamine dextran (TRDA, 5% in distilled water) for pedicellar HFs and fluorescein dextran (FDA, 10% in distilled water; both dyes 3000MW, Invitrogen, Eugene, OR) for scapal HFs. The wells were covered with Vaseline and animals

were kept for up to 72-96 hours at 4-7 °C. Double staining experiments of scapal and pedicellar HFs were performed in four combinations: 1. dorsal scapal HP (sHPd) and dorsolateral pedicellar HR (pHRdl), 2. ventral scapal HP (sHPv) and dorsomedial pedicellar HP (pHPdm), 3. dorsal scapal HP (sHPd) and ventrolateral pedicellar HR (pHRvl), 4. ventromedial scapal HR (sHRvm) and dorsomedial pedicellar HP (pHPdm).
After dye diffusion the head capsule was opened dorsally and supraoesophageal ganglion (termed brain in the following) and suboesophageal ganglion (SOG) were removed and cleaned from fat and connective tissue. Ganglia were then exposed to 20% Triton X-100 (Fluka, Buchs, Switzerland) in 4% paraformaldehyde (PFA) or 4% Roti-Histofix (Roth, Karlsruhe, Germany) for 20 minutes and subsequently fixed in 4% PFA or 4% Roti-Histofix for 2 hours at room temperature. Afterwards, ganglia were washed (3 x 10 minutes in 0.1 M phosphate-buffered saline, PBS, pH 7.2), dehydrated in an ascending ethanol series (30%, 50%, 70%, 90%, 2 x 100%, 10 min each step), transferred onto microscopic slides with cavity (Thermo Scientific, Braunschweig, Germany), cleared and mounted in methyl salicylate (Roth, Karlsruhe, Germany).

Staining of presumed mechanosensory hairs dorsally on the pedicel and the antennal nerve N1

In several specimens, sensilla of a scapal HP were stained in combination with labeling of presumed mechanosensory hairs situated dorsally on the pedicel (that are not arranged in HFs) or with stainings of the antennal nerve N1. Dorsal pedicellar sensory hairs were surrounded by Vaseline petroleum jelly, shaved in distilled water with a razor blade, and water was replaced with TRDA dye. In order to stain the antennal nerve, the flagellum cuticle was cut at least distally to the 2nd flagellum annulus and carefully removed to expose the antennal nerve that consists of two branches (Dürr et al., 2001). The nerve branches were cut with a pair of sharp scissors and placed in a Vaseline well filled with distilled water for up to 5 minutes. In few specimens, the brain was dissected out of the head capsule, and then nerve N1 was stained close to the brain in a Sylgard dish (Fig. 3.10 and Fig. A.5 in the appendix). After removal of the water the well was filled with TRDA dye. Specimens were kept and treated as described above.

Staining of antennal motor nerves

Staining of scapal HPs was done as described above. After 72 hours, the brain was removed and transferred into a Sylgard dish filled with stick insect saline (Weidler and Diecke, 1969). The antennal motor nerves N2/N3 or N4 (Dürr et al., 2001)

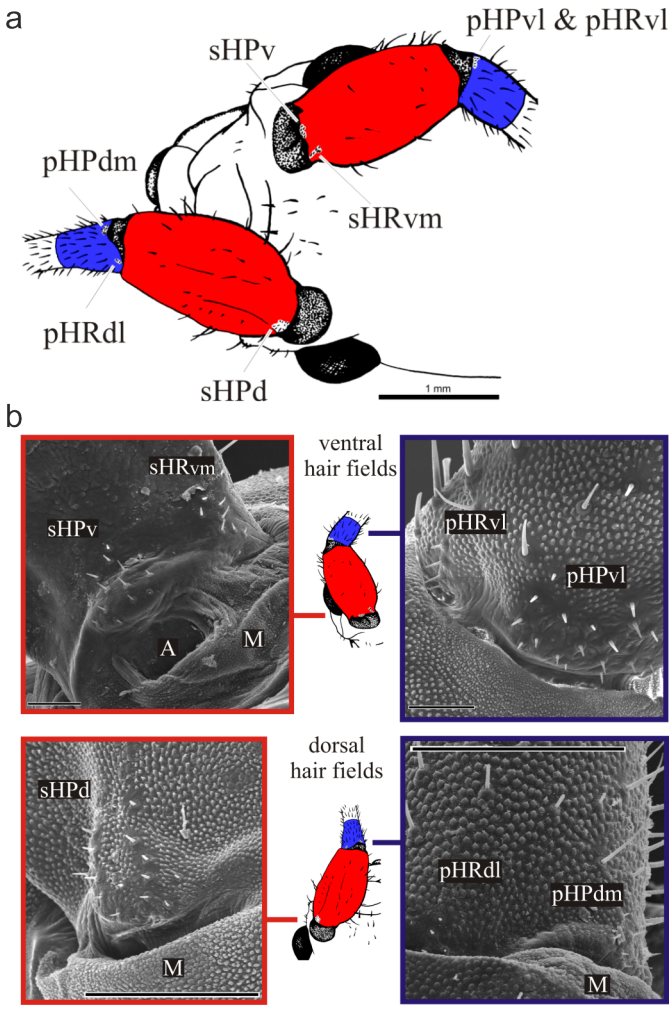

Figure 2.1. – **Location of the seven hair plates and rows (HP/HR) on *C. morosus* scapal (red) and pedicellar (blue) segments. a:** Top view of the head with the joints of left antenna deflected to their ventral extreme (maximum head-scape depression and scape-pedicel abduction) and the joints of the right antenna deflected to their dorsal extreme (maximum head-scape levation and scape-pedicel adduction). **b:** SEM images of the ventral (top) and dorsal (bottom) HPs/HRs. **d:** dorsal; **dl:** dorsolateral; **dm:** dorsomedial; **M:** soft articulating membrane; **v:** ventral; **vl:** ventrolateral; **vm:** ventromedial. Scale bars=100 µm. Adopted from Krause et al., 2013.

were placed in a Vaseline well filled with TRDA fluorescent dye. Nerves N2/N3 were stained together due to their close proximity of their nerve roots. Ganglia were kept for up to 24 hours at 4-7 °C. Afterwards, they were treated as described above.

Staining of descending interneurons

To label descending interneurons (DIN) of the brain and SOG, the animal was fixed ventral side up with plasticine. A small window was cut into the sternum between the SOG and prothoracic ganglion or between the pro- and mesothoracic

ganglia to expose the connectives of the ventral nerve cord. One connective was cut and surrounded by a well made of Vaseline petroleum jelly. At first, the well was filled with distilled water. After 5 minutes the water was replaced by TRDA. In some preparations, scapal HPs were stained in addition with FDA. Animals were kept for up to 96 hours at 4-7 °C before the brain and SOG were treated as described above. The prothoracic ganglion was also removed when axons of a connective between the pro- and mesothoracic ganglia were stained.

2.2.1. Anti-synapsin immunohistochemistry

Several brain whole-mounts were incubated with an antibody directed against the *Drosophila* synaptic protein synapsin (Klagges et al., 1996). To facilitate the antibody penetration, the ganglion sheath was treated for 30 s with small crystals of a proteolytic enzyme (Pronase E, Merck, Darmstadt, Germany). The enzyme was washed out by repeated rinsing with stick insect saline. Then, the detached sheath was manually removed with fine forceps and a pair of sharp scissors. Specimens were fixed and washed as described in sec. 2.2. Afterwards, ganglia were preincubated in 0.1 M PBS containing 5% normal goat serum (NGS, S1000, Linaris, Wertheim, Germany), 1% Triton-X 100 (Fluka, Buchs, Switzerland) and 0.1% sodium azide (AppliChem) for 1-2 hours to block unspecific antibody binding. The same solution was used for washes and the dilution of primary and secondary antibodies. The monoclonal mouse anti-synapsin antibody 'SYNORF1' (kindly provided by Prof. Erich Buchner, University of Würzburg) was applied at a dilution of 1:25 for 2 x 3 days at 4 °C. Subsequently, three washes of 2 hours each were carried out and ganglia were incubated with DyLight 633-conjugated goat anti-mouse IgG antibody (ThermoScientific) diluted 1:100 in blocking-solution for 2.5 days at 4 °C. Ganglia were washed 3 x 1 hour in PBS, dehydrated in an ascending ethanol series (30%, 50%, 70%, 90%, 2 x 100%, 10 minutes each step) and mounted in methyl salicylate.

2.2.2. Terminology of HFs, antennal nerves, innervated muscles, and brain orientation

The terminology of scapal and pedicellar HFs was adapted from Krause et al. (2013). The terminology of antennal nerves and their innervating muscle regions were adapted from Dürr et al. (2001).
Stick insects possess prognathous mouth parts, therefore, the brain is tilted backwards in the adult head capsule. Thus, all central projections stained in the brain

and general neuroanatomical descriptions of locations in the brain are related to the embryonic neuraxis, not to the body axis (Boyan et al., 1993). The top of the brain (according body axis) is neuronally ventral and the bottom part of the brain (according body axis) is neuronally dorsal. Cell body clusters of DINs within the brain were named, when possible, according to the nomenclature of Staudacher (1998).

2.3. Staining of mesothoracic motoneurons, DUM cells, and sensory neurons with a central cell body[1]

Animals were fixed dorsal side up on a foam platform by using dental cement (Protemp II, ESPE, Seefeld, Germany). To label neurons in the mesothoracic ganglion by backfilling through the cut ends of their axons the thorax was opened by a dorsal midline incision to expose the ganglion's lateral nerves (Fig. 2.2). The gut was moved aside and fat, connective tissue, some muscles, and tracheae were carefully removed. During the preparations the body cavity was perfused with chilled *C. morosus* saline (Weidler and Diecke, 1969). To expose side nerves that branch off the main leg nerve (nervus cruris, ncr) in the coxa it was necessary to remove dorsal and lateral parts of the coxa. *In situ*, cut ends of single nerves (except for sensory nerve nl1; Marquardt, 1940) were placed in a petroleum jelly well (Weißes Vaselin, Medical Pharma GmbH, Bremerhaven, Germany) containing TRDA or FDA (both 3000MW, 5% in distilled water; Invitrogen, Eugene, OR). To stain the whole DUM cell population in the mesothoracic ganglion all side nerves were cut and filled with dye. Nerve branches of ncr in the middle leg (flexor, F2 and RUI) were placed in wells inside or besides the femur after removal of the dorsal femoral cuticle. Wells were covered with petroleum jelly and animals were kept in a moist chamber at 4 °C for 24-48 hours for backfilling thoracic or coxal nerves and up to 72 hours for backfilling femoral nerves.

After dye diffusion ganglia were removed cleaned from fat and connective tissue, exposed to 20% Triton X-100 (Fluka, Buchs, Switzerland) in 4% paraformaldehyde

[1] The text for staining procedures of mesothoracic neurons and parts of the image acquisition in sections 2.3, subsections, and of section 2.4 are already published: Goldammer J, Büschges A and Schmidt J. *Motoneurons, DUM Cells, and Sensory Neurons in an Insect Thoracic Ganglion: A Tracing Study in the Stick Insect Carausius morosus.* Journal of Comparative Neurology, 520(2), 230-257, 2012. The author contributions are as followed: JG, AB and JS designed research. JG performed experiments, analyzed data, prepared figures, tables and drafted manuscript. JS edited the manuscript.

(PFA) or 4% Roti-Histofix for 20 minutes and subsequently fixed in 4% PFA or 4% Roti-Histofix for 2 hours. Afterwards, ganglia were washed (3 x 10 minutes in 0.1 M phosphate-buffered saline, PBS, pH 7.2), dehydrated in an ascending ethanol series (50%, 70%, 90%, 2x 100%, 10 minutes each step), transferred on microscopic slides, cleared and mounted in methyl salicylate (Roth, Karlsruhe, Germany).

2.3.1. Anti-β-tubulin immunohistochemistry on thick vibratome sections after retrograde nerve labeling

To visualize tracts, commissures, and neuropils in slices of ganglia a monoclonal anti-β-tubulin (T4026, Sigma) antibody was used to label tubulin as the main component of the cytoskeleton. Monoclonal anti-β-tubulin (mouse IgG1 isotype) is derived from the hybridoma TUB 2.1 produced by fusion of mouse myeloma cells and splenocytes from mouse immunized with purified rat brain tubulin (from Sigma-Aldrich product information; Gozes and Barnstable, 1982). Monoclonal anti-ß-tubulin specifically recognizes an epitope in the carboxy-terminal part of all five isoforms of β-tubulin (between amino acids 281-446; Sigma-Aldrich product information). The antibody has successfully been used in locusts to reveal longitudinal tracts, commissures, and neuropils (Kononenko and Pflüger, 2007). In the stick insect the staining pattern of tracts and commissures matches a previous study that utilized the osmium/ethyl-gallate procedure (Kittmann et al., 1991).
Ganglia with backfilled neurons were prepared, fixed and washed as described above and subsequently embedded in agarose (4% in PBS; 11380, Serva, Germany). Thick transverse sections (120 µm) were cut in PBS with a vibratome (Leica VT 1000S). Afterwards, slices were pre-incubated in PBS containing 3% Triton X-100 and 1% bovine serum albumin (BSA, Sigma-Aldrich) for up to 2 hours. Primary monoclonal anti-β-tubulin antibody was diluted 1:200 in PBS with 0.1% sodium azide (AppliChem GmbH). The tissue was incubated with the antibody for up to 72 hours at 7 °C. Slices were then washed in PBS with 0.1% sodium azide (1 x 20 minutes, 2 x 1 hour at room temperature; overnight at 7 °C) and subsequently incubated with Alexa Fluor 633-conjugated goat anti-mouse antibody (Invitrogen) diluted 1:400 in PBS containing 3% Triton X-100 and 1% BSA. Slices were kept for a duration of up to 72 hours at 7 °C. Thereafter, the sections were washed with PBS containing 0.1% sodium azide, dehydrated in an ascending ethanol series (as described above), transferred on microscopic slides, treated with xylene or methyl salicylate (Roth), and mounted in Permount (Fisher Scientific GmbH). Anti-β-tubulin immunohistochemistry was performed at least on two ganglia in which the same lateral nerves were backfilled.

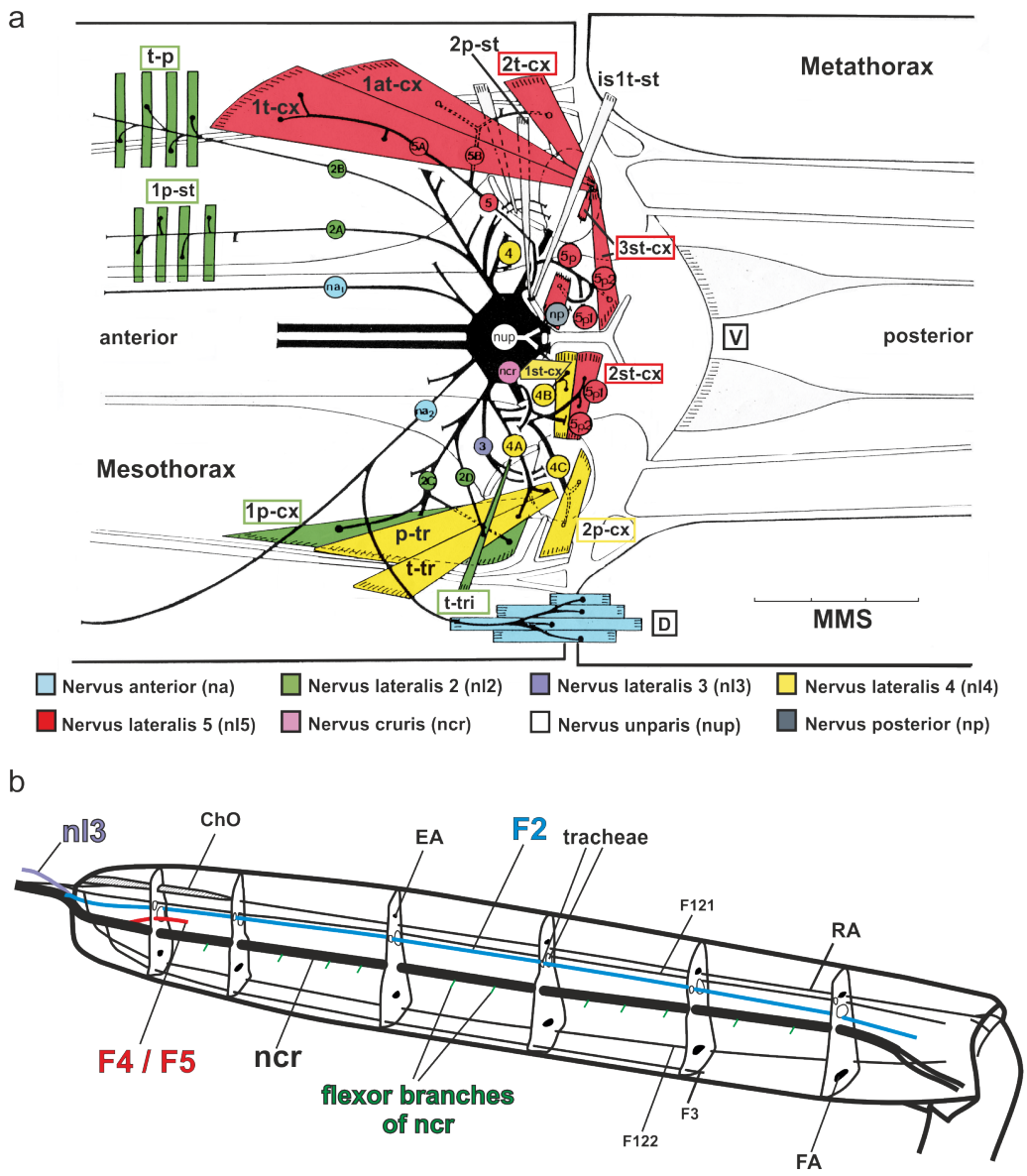

Figure 2.2. – **Schematic illustration of neuromuscular anatomy of the mesothorax (a) and nerves within the femur (b) of *C. morosus*. a: D** and **V**: dorsal and ventral longitudinal muscles; **2p-cx**, **1,2t-cx** and **1at-cx**: pleural and tergal retractor coxae muscles; **1p-cx**: protractor coxae; **is1t-st**: tergo-sternal muscle; **1,2p-st**: pleuro-sternal muscle (ventilation); **p-tr** and **t-tr**: pleural and tergal depressor trochanteris; **1st-cx**: sternal promotor of coxa; **2st-cx**: sternal adductor of coxa; **3st-cx**: sternal remotor of coxa; **t-p**: tergo-pleural muscle (ventilation), **t-tri**: tergotrochantinal muscle; MMS = millimeter. Modified after Graham (1985). **b: Femur of a right middle leg.** Transverse sections in the drawing show the three-dimensional nature of the reconstruction and give the relative position of apodemes of extensor and flexor tibiae muscles and of the two tracheae. **nl3**: nervus lateralis 3; **F4/5**: retractor unguis nerve (red); **F2**: femoral nerve branch 2 (blue) that innervates extensor tibiae; **ncr**: nervus cruris (main leg nerve); **ChO**: chordotonal organ; **EA**: transverse section of extensor tibiae muscle apodeme; **RA**: receptor apodeme of ChO; **FA**: transverse section of flexor tibiae muscle apodeme; **F121**, **F122**, **F3**: sensory nerves. Modified after Bässler (1977a).

2.3.2. Terminology of mesothoracic nerves, muscles, and ganglionic structures

The nomenclature of muscles and their innervating nerves were adapted from Marquardt (1940), Bässler (1977a), and Graham (1985) (see Fig. 2.2) and are listed in Tab. 3.3. The underlying designation of ganglionic structures such as tracts and neuropil regions (Fig. 2.3) based on the nomenclature by Kittmann et al. (1991). Central projections of stick insect proprioceptors (e.g., hair plates) and their target areas within the mesothoracic ganglion were named according to Schmitz et al. (1991). This neuroanatomical study is based on the analysis of 93 backfilled mesothoracic ganglia (note Tab. 3.3) and at least 18 ganglia in which backfilling was combined with anti-β-tubulin immunohistochemistry.

2.4. Image acquisition

Fluorescence images of whole-mounts or vibratome sections were captured with a confocal laser scanning microscope (LSM 510; Carl Zeiss, Germany) equipped with Plan-Neofluar 10x (0.65 NA) and Plan-Apochromat 20x (0.75 NA) objectives. FDA, TRDA and Alexa 633/DyLight 633 were imaged with 488, 543 and 633 nm excitation, respectively. Emission of TRDA was collected through a 560 long-pass (LP) filter or a 560-630 nm band-pass (BP) filter for double or triple labeled ganglia with Alexa 633/DyLight 633 and FDA. For emission of FDA and Alexa 633/DyLight 633 a 505-530 BP and a 650 LP filter was used, respectively. For documentation, optical sections of 1 to 5 µm overlap between all consecutive sections were made with the LSM 510 and its multi-track mode was used for double or triple labeled ganglia. In several brain and SOG images, the ganglion outline was captured by scanning the autofluorescence of the tissue. In double-labeled HF specimens, the TRDA staining patterns were occasionally copied into the projection of the FDA channel (after removal of stained structures) to obtain the ganglion outline basic on autofluorescence with 488 nm excitation.
For ganglia overviews or transverse sections, overlapping stacks were acquired and merged with CorelDraw software (vX6, Corel, Ottawa, Canada). Due to the low background of whole-mounts, shapes of mesothoracic ganglia were visualized by high gain overview pictures or by the range indicator function of the Zeiss LSM Image Browser (v4.2.0.121). Final figures were mounted in CorelDraw. If necessary, adjustments in contrast and brightness of images, and removal of artifacts and image noise on transverse sections were done in CorelDraw. Transverse sections

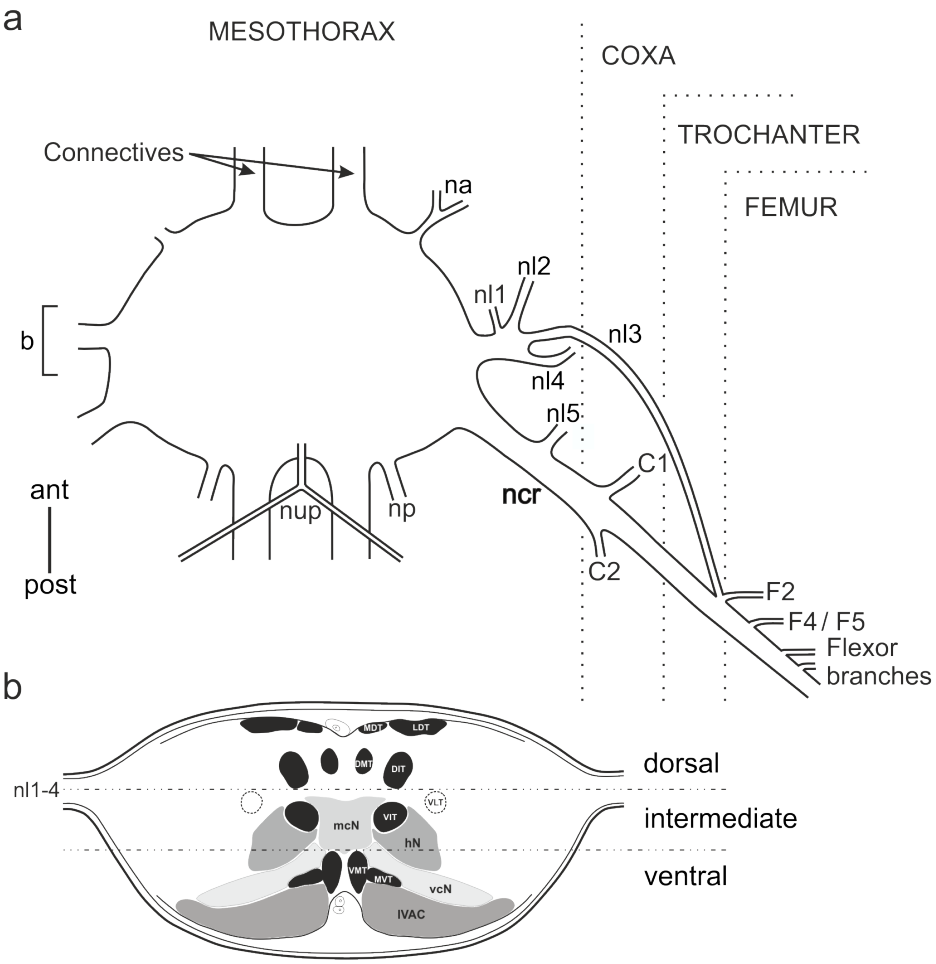

Figure 2.3. – **a: Schematic mesothoracic ganglion with lateral nerves and side branches of nervus cruris (ncr, main leg nerve)**. Bracket indicates plane of transverse section shown in b. **na**, nervus anterior; **nl1–5**, nervi laterali 1–5; **np**, nervus posterior; **nup**, nervus unparis; **C1–2**, coxa branch 1–2 of ncr; **F2**, **4**, and **5**, femoral branches 2, 4, and 5 of ncr. Nerve nomenclature adapted from Marquardt (1940), Bässler (1977a), and Graham (1985). **b: Schematic transverse section taken at mid-ganglion level as indicated in (a).** Horizontal lines indicate dorsal, intermediate, and ventral parts of the ganglion. Black fillings and dashed circles show longitudinal tracts, and gray shaded areas display prominent neuropils. **DIT**, dorsal intermediate tract; **DMT**, dorsal medial tract; **hN**, horseshoe neuropil; **LDT**, lateral dorsal tract; **lVAC**, lateral part of ventral association center; **mcN**, medial coarse neuropil; **MDT**, medial dorsal tract; **MVT**, medial ventral tract; **vcN**, ventral coarse neuropil; **VIT**, ventral intermediate tract; **VLT**, ventral lateral tract; **VMT**, ventral medial tract. Modified after Kittmann et al. (1991).

stained against β-tubulin were subsequently smoothed and overlaid with appropriate projections of retrogradely labeled nerves by using the ImageJ software, Version 1.42q (http://rsb.info.nih.gov/ij). Depth color-coded images of neurons were generated with the depth feature of the Zeiss LSM Image Browser. The depth-coded projections enabled recognizing the focal plane on where the cell bodies or neurites are localized within a z-stack. This is done by assigning a false color code of labeled structures as a function of the z-depth. This was important for determining

whether cell bodies are in the dorsal part (blue color) or in the ventral part (red color) of the ganglia. Thus, for example, the dorsal somata of efferent DUM neurons can be distinguished from the ventral somata of common inhibitors (CI) in the mesothoracic ganglion, despite the fact that they both lie close to the midline. Because microscopic slides without spacers were used minor distortion along the z-axis of mesothoracic ganglia is possible.

2.5. *In situ* calcium imaging of retrogradely labeled mesothoracic retractor coxae neurons

2.5.1. Preparation

A semi-intact preparation of the stick insect was used with the left front leg intact, while all other legs were amputated between the coxa and trochanter. The stick insect was fixed dorsal side up on a foam platform with dental cement (Protemp II, ESPE, Seefeld, Germany). In the following, a preparation is described that attempted to ensure respiration and vitality of the animal during the long dye labeling procedure.

Contralateral to the intact leg, a lateral incision along the body wall was made that exceeded from the anterior mesothorax to the middle metathorax. At the anterior and posterior ends of the incision two additional transversal cuts were made. The dorsal cuticle could then be lifted up (retractor coxae muscles needed to be intersected at the incision side) and fixed with steel pins at the side of the left front leg. This preparation allowed the dorsal vessel and the left spiracle to be intact. The unharmed gut was placed contralaterally to the left front leg in an encircled area around the thoracic cavity of the animal that was filled with stick insect saline to keep the gut moist and prevent it from drying out.

The thoracic cavity was filled with stick insect saline (Weidler and Diecke, 1969) and connective tissue was removed to expose the mesothoracic ganglion. The large longitudinal tracheae were left intact to allow respiration of the animal, whereas smaller tracheae traveling through the coxa needed to be removed very carefully to expose the mesothoracic lateral nerves. Ipsilaterally to the left front leg the tergo-sternal (is1t-st) and the pleuro-sternal (2p-st) muscles were cut ventrally at their insertion to have access to the p branch of nervus lateralis 5 (nl5) for cutting it (Fig. 2.2). The tendon of the three large tergal retractor coxae muscles were cut as well to have access to their innervating nerve. Nerve nl5 was then cut with a pair of very sharp scissors before bifurcating into the p branch and

the branch that innervates the pleural and tergal retractor muscles. Underneath the main leg nerve, nervus cruris (ncr), Vaseline petroleum jelly (Weißes Vaselin, Medical Pharma GmbH, Bremerhaven, Germany) was injected with a syringe that had a small flexible pointed tube at its cannula. Then, a tight Vaseline well was built around the cut end of nerve nl5. Distilled water was filled into the well that persisted for up to 5 minutes to allow crushed axons to open up. Then, water was replaced by a drop of 5 mM solution of the high affinity calcium (Ca^{2+}) indicator Oregon Green 488 BAPTA-1 dextran (OGB-1, 10.000MW, Invitrogen, Eugene, OR) dissolved in distilled water. The well was covered with Vaseline and the animal was kept mostly for 3 hours and up to 4 hours in the dark at room temperature for dye uptake. The stick insect saline was replaced several times during the diffusion of OGB-1. After dye diffusion, the Vaseline well and connective tissue dorsal to the ganglion were removed. The large longitudinal tracheae were cut anteriorly and were placed outside of the posterior end of the thoracic cavity.

2.5.2. Experimental setup

For imaging intracellular Ca^{2+} and for extracellular nerve recordings, the animal was placed on a steel platform (Fig. 2.4). In front of the animal's head a developed, movable ganglion holder (Electronics Workshop, Institute for Zoology, University of Cologne) was mounted via a micromanipulator to the platform. The ganglion was placed on the holder platform and a double-sided fork was manually set on the lateral edges of the ganglion. This fork was very important in order to decrease movement of the ganglion for imaging neurites properly. Ipsilaterally to the intact front leg one or two mircromanipulators were mounted and equipped with suction electrodes made out of borosilicate glass (tips were shaped manually to fit the recorded nerves). Extracellular recordings were made from the backfilled nerve nl5, the antagonistic protractor coxae nerve (nl2), or of the coxa branch 1 (C1) that innervates the levator trochanteris muscle. All other lateral nerves that were not extracellulary recorded from were crushed. The platform was installed on the stage of the imaging microscope and grounded to reduce electrical noise.

Pharmacological and tactile stimulation

Motor activity in retractor coxae neurons was induced pharmacologically with pilocarpine or through tactile stimulation of the animal.

Pilocarpine is a muscarinic acetylcholine agonist. From experiments in the crayfish, locust, and the stick insect it is known that pilocarpine activates central

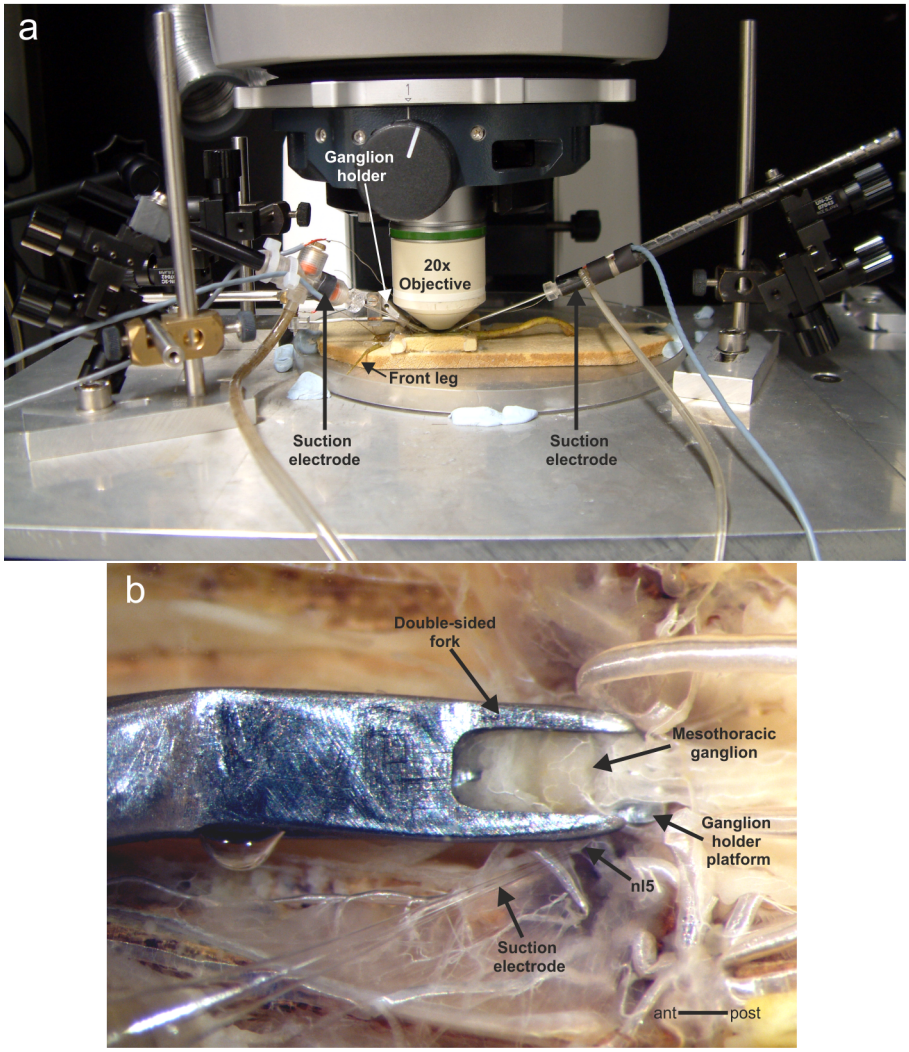

Figure 2.4. – Experimental setup for *in situ* Ca^{2+} imaging of retrogradely labeled retractor coxae neurons. a: Image of the experimental setup. **b:** Dorsal view of a mesothoracic ganglion *in situ* that was restrained against movement by a double-sided fork. The suction electrode records from an OGB-1 backfilled nl5 nerve stump.

pattern generating networks which elicit alternating rhythmic activity in antagonistic motoneuron pools (crayfish: Chrachri and Clarac, 1987; locust: Ryckebusch and Laurent, 1993; stick insect: Büschges et al., 1995). Stock solutions of pilocarpine (P6503, Sigma-Aldrich) were prepared in three different concentrations: 10^{-3} M, 3 x 10^{-3} M and 10^{-2} M. After starting the recordings, several drops of these solutions were applied into the mesothoracic cavity that was filled with stick insect saline, to reach a final pilocarpine concentration that was lower than the stock solution. In the experiments mainly the 3 x 10^{-3} M pilocarpine solution was used because it generated the most reliable motor pattern. It was attempted to receive a consistent alternating motor rhythm by crushing the anterior and posterior mesothoracic connectives.

For tactile stimulations, the animal's abdomen was gently touched with a paint-

brush to elicit stepping sequences of the front leg. The paintbrush was removed as soon as stepping of the front leg was observed. In general, long lasting stepping sequences were seldom and mostly the animal's abdomen was stimulated continuously to evoke motor activity.

2.5.3. Data recording and analysis

Optical measurements

Monochromatic light at 496 nm (Polychrome V, Till Photonics, Gräfeling, Germany) was applied through the epifluorescence port of the Zeiss Axio Examiner D1 microscope (Carl Zeiss, Jena, Germany). Changes in fluorescence emission of OGB-1 was detected at 524 nm by a cooled charged-coupled device camera (AxioCam MRm, Carl Zeiss, Jena, Germany). A 20x W-Plan Apochromat water immersion objective (1.0 DIC, working distance: 1.8 mm, Carl Zeiss, Jena, Germany) was used for imaging regions of interest (ROI). Depending on staining quality, the pixel resolution was set at 344 x 260 (binning factor 4 x 4) or 460 x 344 (binning factor 3 x 3) and sensitivity of the AxioCam was frequently digitally enhanced. Video data acquisition was sampled at frequencies between 16 Hz and 35 Hz using AxioVision software (V4.8.2, Carl Zeiss, Jena, Germany). To superimpose imaging data with electrophysiological recordings, a marker was placed into the running Ca^{2+} imaging sequence after starting the extracellular recordings with SPIKE2 software (v7.01, Cambridge Electronic Design, Cambridge, UK).
Optical recordings were pre-processed by using AxioVision software (v4.8.2, Carl Zeiss, Jena, Germany). Ca^{2+} imaging data have been background corrected by subtracting a ROI placed on the margin of the recorded images, where no indicator staining was visible. Thus, background values of each channel are subtracted over time from gray values of the measurement ROIs. The ratio-image was calculated by activating the confidence-mapping function (Tsien and Harootunian, 1990) of the AxioVision software to reduce noise. All values given are changes in fluorescence divided by backround intensity (F/F0). For figure preparation, changes in free intracellular Ca^{2+} ($[Ca^{2+}]_i$) were displayed in IGOR Pro 6 software (Wavemetrics Inc., Lake Oswego, USA) and if necessary $[Ca^{2+}]_i$ transients were smoothed and linearly fitted. Final figures were prepared in Corel Draw software (vX6, Corel, Ottawa, Canada).

Electrophysiological recordings

Extracellularly recorded signals were 100-fold amplified by a pre-amplifier (Electronics Workshop, Institute for Zoology, University of Cologne). Subsequently,

nerve recordings were amplified 10-fold and band-pass filtered (250Hz - 5kHz) with a 4-Channel / Signal - Conditioner (model MA102, Electronics Workshop, Institute for Zoology, University of Cologne). The output of the electrophysiological signals were digitized using an A/D converter (MICRO 1401mk II, CED, Cambridge Electronic Design) and recorded with a sampling rate of 12.5 kHz with SPIKE2 software (v7.01, Cambridge Electronic Design, Cambridge, UK) on a personal computer.
Electrophysiological recordings were pre-processed in SPIKE2 software for further data analysis. Extracellular recordings were rectified and smoothed (first order low pass filter, time constant $\tau = 50$ ms) to estimate the gross neuronal activity. Custom written SPIKE2 scripts were used to analyze recorded data. To mark bursts, burst criteria were defined in the SPIKE2 script as follows: max initial interval: 0.08 s, interspike interval: 0.2-0.4 s, min number events in a burst: 4; delete burst shorter than: 0.3 s and amalgamate bursts if inter-burst interval shorter than: 0.4 s. Further advanced analysis was performed with MATLAB software (vR2011b; The MathWorks, Inc., Natick, USA).

Data analysis

$[Ca^{2+}]_i$ elevations of measured ROIs were analyzed compared to the gross neuronal spike activity of the extracellular recordings by using custom written scripts with MATLAB software (vR2011b; The MathWorks, Inc., Natick, USA). The burst intensities of the extracellular recordings were measured as the integral under the rectified and smoothed recordings from the start to the end of the bursts. The onset and offset time points of marked bursts were used to calculate the integral under the $[Ca^{2+}]_i$ elevations. In order to calculate the $[Ca^{2+}]_i$ integrals, the measured Ca^{2+} transients were median filtered with a long time constant (τ=28 to 64 s) to remove the trend of the $[Ca^{2+}]_i$ traces due to dye bleaching. Therefore, $[Ca^{2+}]_i$ transients are slightly smaller as in the original traces. The integrals of burst activities and of $[Ca^{2+}]_i$ elevations were further divided by the burst duration in order to receive the mean integrals independent of burst duration. All values are given in arbitrary units [a.u.]. A regression analysis was used to analyze linear correlations between the integrals of mean burst activities and $[Ca^{2+}]_i$ integrals. Correlation coefficients were regarded significant at $P<0.001$.
Appropriate episodes of $[Ca^{2+}]_i$ elevations were chosen to calculate rise and decay time constants τ by using a custom script with MATLAB software. Depending on the shape of $[Ca^{2+}]_i$ transients, rise times were linearly or double exponentially fitted, from burst onset to the Ca^{2+} transient peak maximum. Decay time constants were exponentially fitted from the burst offset to the onset of the following burst.

Cross-covariance analysis of the different $[Ca^{2+}]_i$ transients in lateral DUM neurites and MN neurites were performed with MATLAB software. Time lags were defined from -15 to 15 s.

To analyze coupling of $[Ca^{2+}]_i$ transients in lateral DUM neurites to pro- and retractor coxae spike activity, the $[Ca^{2+}]_i$ transients were overlaid with reference to the pro- and retractor coxae burst cycle with a custom MATLAB script. The cycle was defined from the burst onset, corresponding to phase 0, to the onset of the following burst (phase 1). Each burst cycle was divided into 100 bins of equal width. Additionally, $[Ca^{2+}]_i$ transients of lateral DUM neurites were plotted at the time of pro- and retractor coxae bursts onsets to the end of the bursts. All $[Ca^{2+}]_i$ transients were aligned to start at the same time point of 0.

3. Results

3.1. Morphology of antennal hair field afferents and descending interneurons in stick insect brain and suboesophageal ganglion

Previous behavioral and electrophysiological experiments in the stick insect revealed that antennal hair field (HF) signals are crucial for antennal positioning and, moreover, signals of antennal sense organs are transmitted to thoracic ganglia (Schütz and Dürr, 2011; Krause et al., 2013; Ache and Dürr, 2013). In order to understand how the stick insects' antennal sensorimotor system is neuroanatomically organized, stainings of antennal mechanosensory afferents and motor nerves were performed. Furthermore, connectives were stained to reveal the number of descending interneurons (DIN) in the brain and suboesophageal ganglion (SOG). At last, the possibility of vicinity of scapal HF afferents to DIN neurites is examined.

3.1.1. Antennal HF afferents ramify in a distinct deutocerebral brain region and descend to the SOG

In this part, sensilla of all seven hair fields (HF; Fig. 2.1) were stained to reveal their projection patterns within the brain and SOG. The general morphology of antennal HF afferents is shown in Fig. 3.1 by using an example of the ventral scapal hair plate (sHPv).

Afferent fibers of sHPv enter the brain in a compact bundle, ramifying simultaneously and extensively in a distinct deutocerebral (DC) brain region where they form a dense multilayered dendritic meshwork. Several afferent fibers continue to travel anteromedially, terminating near the medial border of the anterior deuto- and posterior protocerebrum (PC). The tract seems to be homolog to tract 6I (T6I) in the honeybee, cricket, and cockroach (Staudacher et al., 2005). Noticeable are many varicosities or bouton-like structures that appear like beads on a chain along

their collaterals. These structures indicate possible neurotransmitter release sites. The deutocerebral brain region is a part of a diffuse neuropil that is often referred to as the 'antennal mechanosensory and motor center' (AMMC; Rospars, 1988; Homberg et al., 1989), or the dorsal lobe (DL; Suzuki, 1975; Kloppenburg, 1995) (more about brain neuropils in sec. 3.1.4). The sHPv stainings combined with anti-synapsin immunohistochemistry revealed that the lateral edge of the DL is curved, whereas the medial borders are not discernible (Fig. 3.1d-e). The sHPv fibers continue to travel from the DL posteriorly in tract 6II (T6II) with few boutons arising in a region slightly outside the DL. From there, the afferents descend through the ipsilateral circumoesophageal connective to the SOG. After reaching the SOG, the afferents travel posteriorly and slightly laterally on the ipsilateral side of the ganglion descending into deeper layers and terminating in intermediary neuropil regions (Fig. 3.1h). On their descending path, many bouton-like structures occur. Noticeable are few afferent fibers that terminate in lateral ganglion regions and develop several varicosities. The remaining fibers terminate in an inverted 'V'-shaped manner (Fig. 3.1f-g).

Central projections of all scapal and pedicellar HFs were evaluated for 29 brain and 25 SOG whole-mounts: sHPd: N=6 brain and SOG; sHPv: N=4 brain, N=3 SOG; sHRvm: N=4 brain, N=3 SOG; pHPdm: N=7 brain, N=5 SOG; pHPvl: N=3 brain and SOG; pHRvl: N=3 brain and SOG; pHRdl: N=2 brain and SOG. The staining patterns of the other six HFs were always very similar for all brain and SOG specimens (Fig. 3.2). All central projections showed HF afferent fibers projecting into the DL and sending collaterals in T6I to terminate near the medial border of the DC and PC. Within the SOG, all HF fibers travel posteriorly and slightly laterally to terminate beyond the central frontal plane (Fig. 3.2). No obvious differences were found. Differences might reflect the variability between preparations. Only in brain specimens of stained dorsomedial pedicellar HPs (pHPdm), it was observed that the anteromedially traveling neurites perform sometimes a slight turn in lateral direction to terminate shortly after (Fig. 3.2; Fig. A.2 in the appendix). In addition, it appears that the length and number of anteromedial collaterals in T6I differs, but variability was substantial observed for the same HF in different animals, too.

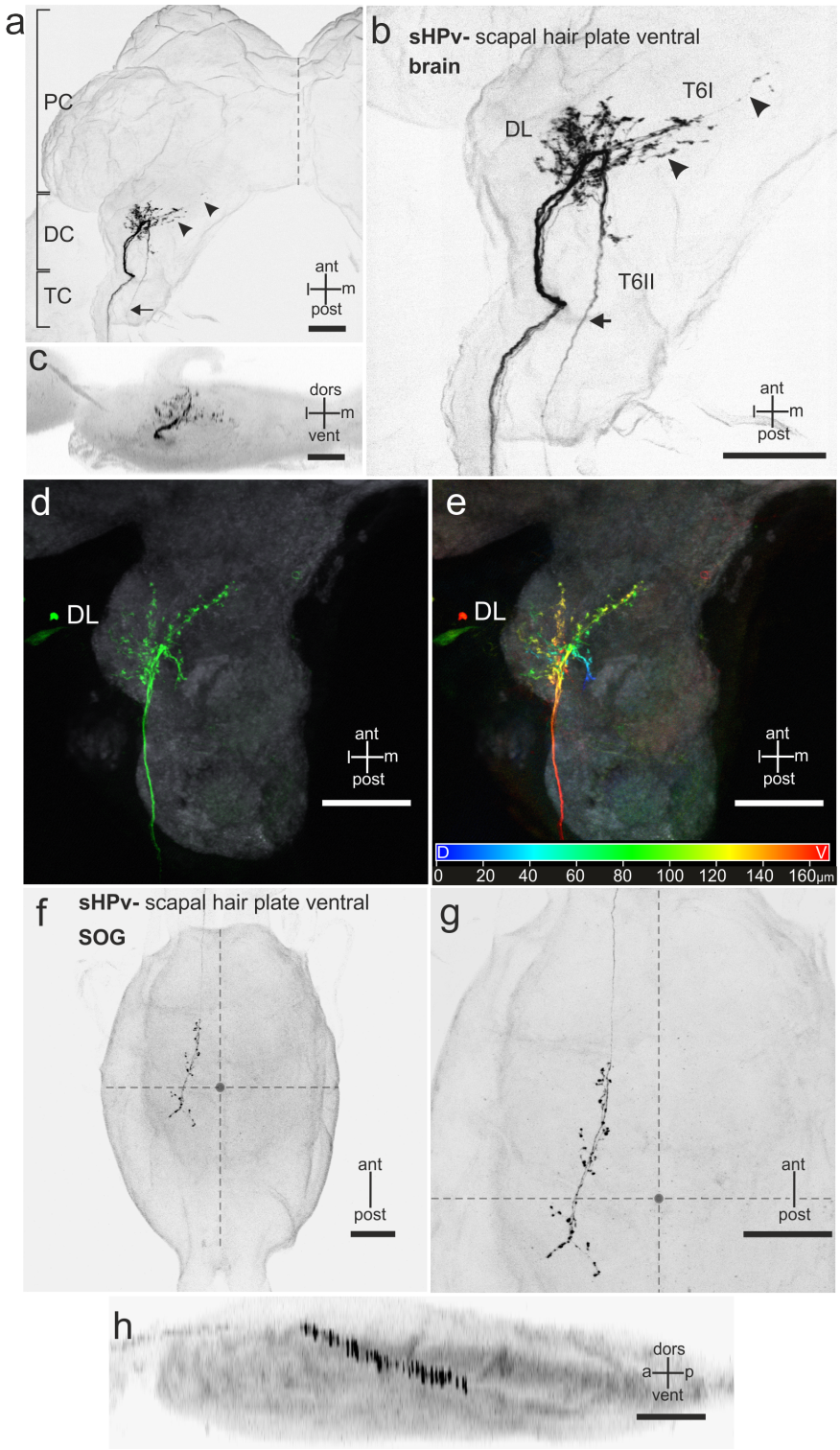

Figure 3.1. – **Central projections of stained sensilla of the ventral scapal hair plate (sHPv). a:** Overview with stained sHPv afferents in the brain. Brackets indicate approximately borders of the tritocerebrum (TC), deutocerebrum (DC), and protocerebrum (PC). Dashed line indicates brain midline. **b:** Magnification of (a). SHPv afferents enter the brain in a compact bundle to ramify in a distinct region of the DC, the dorsal lobe (DL; note also (d) and (e)). Several afferent fibers travel anteromedially in tract 6I (T6I) to terminate near the medial border of the DC (arrowheads). SHPv fibers travel posteriorly in T6II to descend to the SOG (arrow). **c:** Frontal view of (a). **d:** Another specimen with labeled sHPv afferents in combination with anti-synapsin immunostaining (gray) to reveal the DL neuropil in the DC. **e:** Depth color-coded image of (d) shows extensive multilayered arborizations within the entire DL. The depth is encoded from dorsal to ventral as blue to red. **f and g:** SOG whole-mount shows stained sHPv afferents that travel posterolaterally to terminate beyond the central frontal plane (dashed horizontal line). **h:** Lateral view of (f). SHPv afferents enter the SOG dorsally and descend to terminate in intermediate neuropil regions. Scale bars=100 µm.

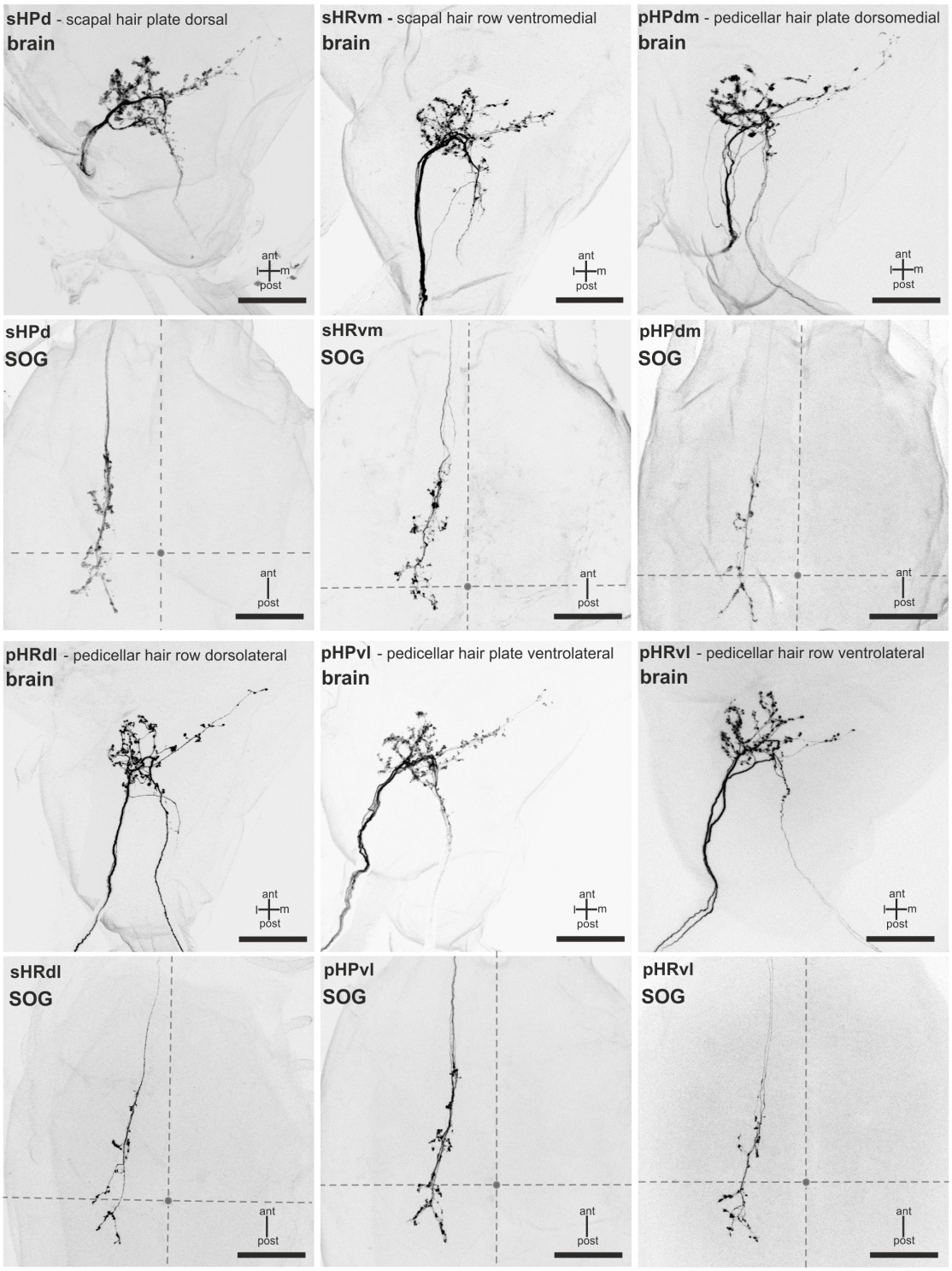

Figure 3.2. – **Whole-mounts of stained sensilla of the remaining six scapal and pedicellar HFs.** The stainings show that all HF fibers project to the DL of the brain and descend to the SOG with a similar projection pattern. Anteromedially traveling fibers of pHPdm sensilla (top row, right image) perform sometimes a slight turn in lateral direction before terminating. Scale bars=100 µm.

3.1.2. Double stainings of scapal and pedicellar HFs reveal differences in bouton formation

Afferents of sensory structures frequently form a somatotopic map in the central nervous system in which the spatial location of the receptor is preserved. For example, sensory neurons of the Johnston's organ in the honeybee (Ai et al., 2007), or antennal mechanosensory sensilla of bimodal (tactile and contact-chemosensory) bristles of cockroaches, which project successively into more medioventral regions in the DC and SOG (Nishino et al., 2005). To answer the question if sensory neurons of antennal HFs have different central projections according to their position at different scapal and pedicellar segments (segment specificity), or if their projections differ according to their dorsal and ventral location on the scape and pedicel (direction specificity), double labeling experiments were performed.

A staining investigated for segment specificity is shown in Fig. 3.3 by means of two HFs located dorsally on the scape and pedicel, respectively. The afferents of sHPd and pHRdl sensilla arborize intermingled within the entire DL. Their boutons are formed in spatially different locations through the entire depth of the DL and in T6I. The boutons appear frequently in close vicinity, but complete overlapping boutons were never observed. Only small areas of varicosities of different HFs can overlap slightly. In the SOG, the HF afferents travel through the same tract. Their boutons appear at slightly different locations with barely overlapping varicosities (Fig. 3.3). Example stainings examined for direction specificity are shown in Fig. 3.4 and in the appendix in Fig. A.1 by staining of HF sensilla located dorsally or ventrally at the scape and pedicel, respectively. The situation of the central projections of dorsal and ventral HF is similar as described above. Both HF afferents have boutons at different locations within the DL and in T6I. Similar results were also observed within the SOG. In the appendix, additional examples and depth-color coded specimens are shown in Fig. A.2 and Fig. A.3. The depth color-coded images illustrate the finding that boutons of different HFs can be found in similar layers and areas of the DL.

A somatotopic map requires a spatial and segregated distribution of HF afferents, where the position of the HF sensilla in the periphery is preserved. This implies, for instance, that ventrally located HF afferents possess more arborizations in a ventral part of the DL than dorsally situated HFs. On the other hand, the central projections of different HFs could be shifted, with respect to their location on the antennal segments, to medioventral regions similar as reported by Nishino et al. (2005) for antennal mechanosensory afferents of bimodal bristles. Here, the double stainings revealed no segment differences like a medioventral shift, and no differences according to a ventral or a dorsal location of the HF (direction speci-

ficity). Instead, the boutons of double labeled HF afferents are formed at different locations with no overlap to each other in the DL, T6I, and the SOG.

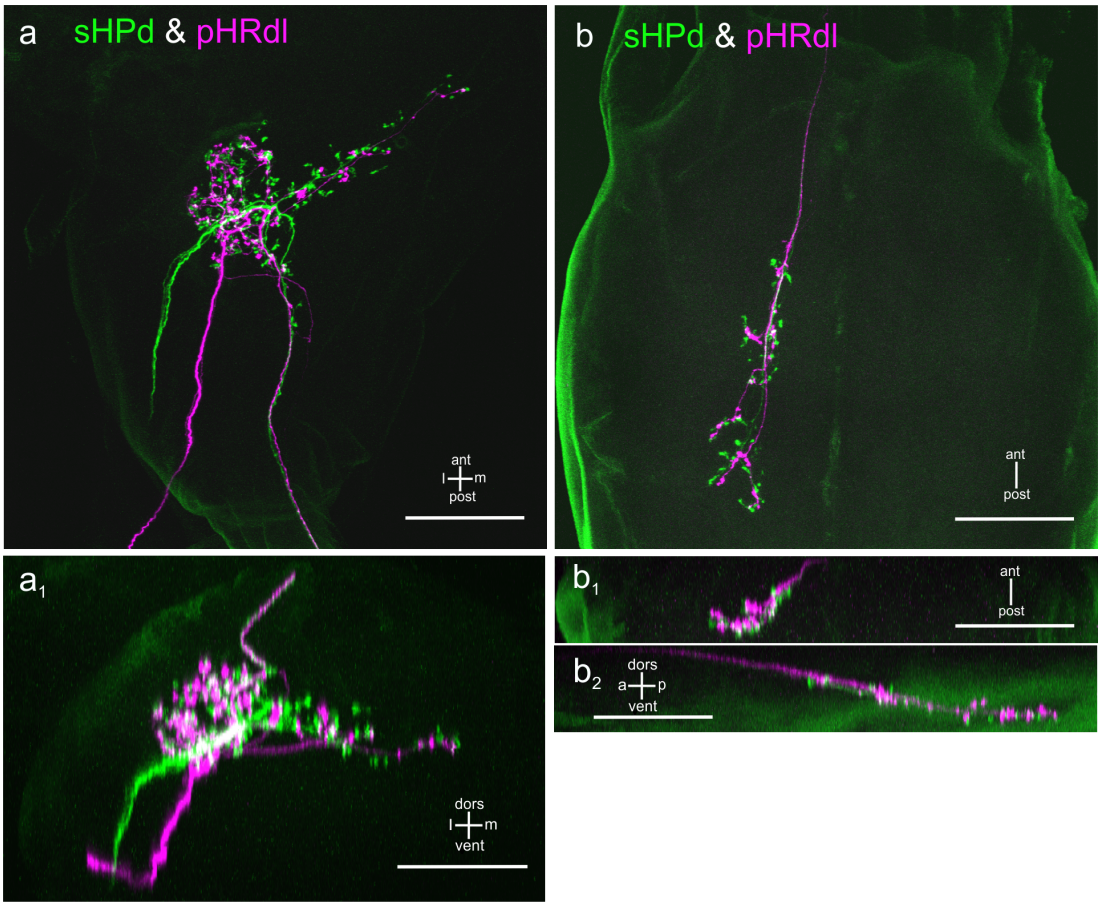

Figure 3.3. – Example of central projections of two dorsally situated HFs on the scape and pedicel investigated for segment specificity: sHPd (green) and pHRdl (magenta). a: Brain whole-mount. Stained afferents of sHPd and pHRdl enter the brain through different tracts until they ramify at the same region within the DL. Notice the different formation of synaptic boutons with almost non-overlapping regions (overlap indicated by white areas). Both HF fibers travel within the same tract to descend to the SOG. **a_1:** Frontal view of (a) shows no apparent regional differences in the arborization pattern. **b:** In the SOG afferents of both HFs travel through the same tract and boutons occur at slightly different locations with barely overlapping structures. **b_1:** Frontal view of (b) and **b_2:** lateral view of (b) shows also no obvious shifts in the projection pattern. Scale bars=100 µm.

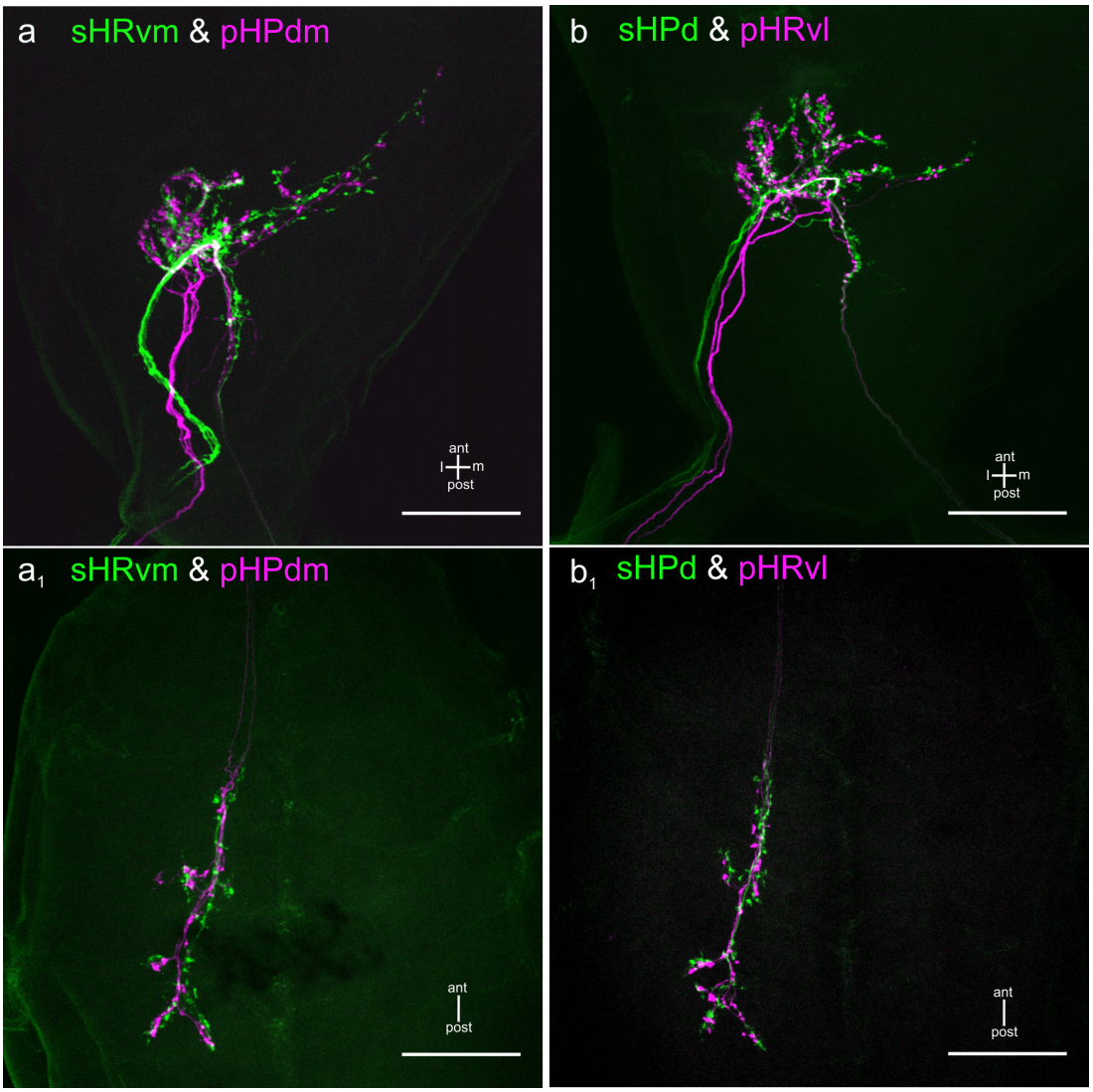

Figure 3.4. – Examples of central projections of dorsally and ventrally located HFs on the scape and pedicel examined for direction specificity. **a:** Brain whole-mount with stained sHRvm (green) and pHPdm (magenta) sensilla. Boutons of both HFs occur in close vicinity. Only small proportions of boutons slightly overlap with each other (overlap indicated by white areas). **a_1:** In the SOG, boutons of sHRvm and pHPdm afferents are found at slightly different regions. **b:** Brain whole-mount with labeled sHPd (green) and pHRvl (magenta) sensilla. Boutons are formed at different locations and in close vicinity. **b_1:** The staining pattern of sHPd and pHRdl afferents in the SOG is also very similar, but the boutons appear also at different regions. Scale bars=100 µm.

3.1.3. HF afferents and antennal motoneurons have overlapping dendritic fields in the dorsal lobe

This section adresses the question whether central projections of antennal motoneurons (MN) and HF afferents have overlapping dendritic fields in the DL of stick insects? Overlapping fields could indicate a reflex arc to improve the coordination of the antenna by supporting antennal movements or to change the direction of movements. Therefore, backfills of antennal motor nerves and stainings of scapal HFs with different fluorescent dyes were performed to investigate the sensorimotor system of the stick insect antennae. The stick insects' antennal MNs and the soma positions were previously described by Dürr et al. (2001).
Fig. 3.5 shows a specimen of a backfilled nerve N2 (innervates adductor muscle, MAd) and nerve N3 (innervates levator muscles, Lv) in combination with stained sHPv afferents. According to Dürr et al. (2001), eight neurons can be stained by backfilling nerves N2 and N3 (four Lv, three MAd, and the common inhibitory neuron, CI). The present stainings revealed also up to eight cell bodies in different regions. In contrast to Dürr et al. (2001), only one cell body was labeled anteroventrally (Lv1 or 2) and an additional weakly stained cell body was found dorsolaterally (Fig. 3.5, question mark). All neurites of levator and adductor MNs have extensive arborizations within the entire volume of the DL. Several MN arborizations were observed that extend in medial or posteromedial deutocerebral regions to terminate shortly after. Besides, a primary neurite was observed that reached a small cell body situated near the protocerebral bridge. This neuron is probably a strand receptor (see sec. 3.1.5). In the merged images it can be observed that projections of MN neurites and sHPv afferents have an extensive spatial overlap within the DL (Fig. 3.5).

Backfills of nerve N4 (innervates tripartite depressor muscles and nerve branch NAb innervates abductor muscle) were performed in combination with stainings of sHPd (N=1) or sHPv (N=2) sensilla. Dürr et al. (2001) reported four to six depressor (Dp) neurons (incl. CI) and two to five abductor (Ab) cell bodies (incl. CI). The whole-mounts here revealed similar numbers of seven and up to ten cell bodies (Fig. 3.6 and Fig. A.4 in the appendix). An additional weakly stained cell body was found near the posteroventrolateral cluster (question mark, Fig. 3.6). In another specimen, two weakly stained neurons were labeled near a Dp neuron (Fig. A.4 in the appendix). It is possible that one of these additionally stained cell bodies belong to the Ab4 neuron described by Dürr et al. (2001).
The dendritic fields of Dp and Ab MN neurites are similar as described for Lv and Ad MNs. Several MN neurites were observed that travel also in medial direction to terminate shortly after. The merged images of MN projections with stained

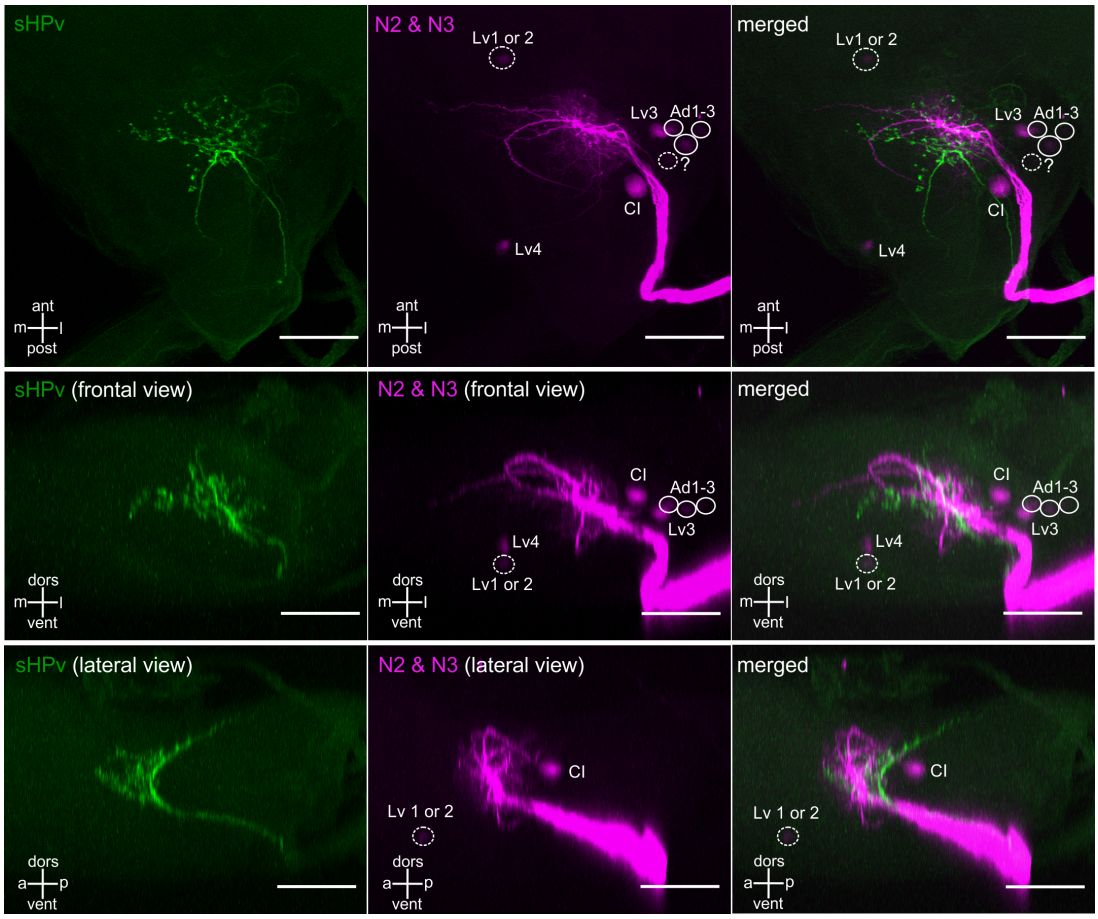

Figure 3.5. – Staining of sHPv sensilla (green) and antennal nerves N2 and N3 (magenta; innervate Lv and Ad muscles). Top row: Top views of a brain whole-mount with central projections of sHPv fibers and Lv and Ad MN neurites shows overlapping dendritic fields of sensory afferents and antennal MNs within the DL (merged image). **Middle row:** Frontal views. **Bottom row:** Lateral views. Lv1-4: levator MN cell bodies; Ad: adductor MN cell bodies (circles) and CI: common inhibitory neuron (Dürr et al., 2001). Scale bars=100 µm.

sHPd and sHPv sensilla show that the dendritic fields of Dp and Ab MN neurites spatially overlap with boutons of sHPd and sHPv afferents in the DL (see also Fig. A.4).

These overlapping fields of MN neurites with boutons of scapal HFs suggest that direct synaptic contacts between sensory neurons and MNs are possible within the DL. The overlapping fields of afferents from sHPv sensilla, which are deflected during depression of the scape with neurites of Lv MNs, may imply a feedback mechanism, to inhibit Dp MN firing and to excite Lv MNs for lifting the HS joint. In contrast, the sHPv afferents have also overlapping dendritic fields with Dp MNs. That could suggest a feedback mechanism, where the Dp MNs are enhanced in firing during deflection of sHPv sensilla to support the movement.

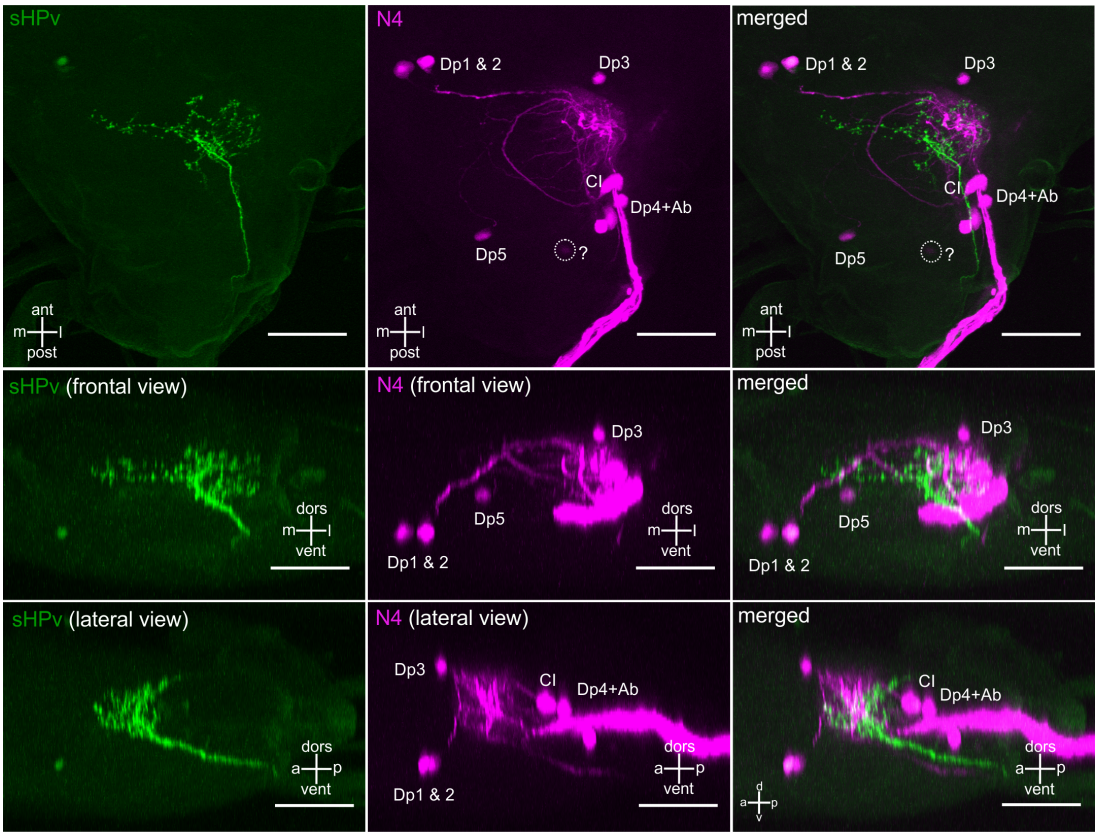

Figure 3.6. – Staining of sHPv sensilla (green) and antennal nerve N4 (magenta; innervates Dp and Ab muscles). Top row: Top views of brain whole-mount with central projections of sHPv fibers and Dp and Ab MN neurites. The merged image shows overlapping regions of sHPv boutons and MN neurites in the DL. One Dp cell body is apparent in the images of stained sHPv sensilla. **Middle row:** Frontal views. **Bottom row:** Lateral views. Dp1-5: depressor MN cell bodies; Ab: abductor MN cell bodies and CI: common inhibitory neuron (Dürr et al., 2001). The question mark indicates a weakly stained cell body. Scale bars=100 µm.

3.1.4. Antennal afferent fibers project into two different deutocerebral neuropils

To reveal terminal neuropil regions in comparison to central projections of antennal HFs, stainings of presumed mechanosensory hairs on the dorsal pedicel (not arranged in HFs) and stainings of the antennal nerve distally to the pedicel were performed.

Fig. 3.7 shows central projections of dorsally located presumed mechanosensory pedicellar sensilla and of sHPd sensilla. According to two pedicellar afferents entering the DC, it is assumed that at least two solitary pedicellar sensilla were stained successfully in each preparation. These afferents of dorsal pedicellar hairs enter the brain slightly more medially than HF afferents of sHPd. Moreover, the pedicellar hair afferents perform a turn in medial direction to ramify densely in a

brain neuropil located ventroposteriorly to the DL, with few arborizations extending in anterior direction. Interestingly, a pedicellar sensory fiber travels through the DL and it appears that a bouton is formed within the neuropil (asterisk, Fig. 3.7a).
In general, projections of sHPd afferents and of the pedicellar sensilla are separated from each other. However, sHPd afferents that leave the DL posteriorly in the direction of the circumoesophageal connective have boutons that slightly overlap with projections of dorsal pedicellar sensilla (arrow, Fig. 3.7 a and c). Afferents of both types descend through the circumoesophageal connective to the SOG. Within the SOG the fibers of dorsal pedicellar hairs travel more medially than HF afferents and descend into intermediary neuropil regions. During their path, these fibers ramify into finer branches and fan out with few branches terminating in the contralateral SOG portion, with respect to the staining side (arrows, Fig. 3.7 a_1 and b_1). Such a projection pattern was never seen in stainings of HF afferents. Both projections are almost separated from each other, only the first developed boutons might be in vicinity.

The brain neuropil with arborizations of the dorsal pedicellar hairs is similar to the ventral area of flagellar afferents (VFA) described for the cricket by Staudacher and Schildberger (1999). Therefore, stainings of the antennal nerve N1 distal to the second flagellum annulus were performed to visualize the terminal neuropil region of flagellar afferents.
Whole-mounts show a tract of massive stained flagellar afferents entering the brain in a broad band, ramifying posteromedially to the DL, in a region similar to the VFA neuropil in crickets (Fig. 3.8 and Fig. 3.9). The flagellar fibers diverge in bundles before reaching the VFA or take different paths within the VFA neuropil. Some of these afferents terminate medially, laterally or few fiber bundles ascend to intermediary and dorsal VFA parts. The branching pattern within the VFA is highly complex and due to the different pathways of flagellar fibers, it seems that spatial compartments and parallel terminal regions exist (Fig. 3.9a and c). Furthermore, the depth color-coded image revealed a cone-like appearance of the densely stained ventral part and more diffuse stained afferents on top of the core neuropil. In the cricket, Staudacher and Schildberger (1999) described a striped appearance of the VFA with an orderly structured projection pattern of flagellar fibers that might indicate a somatotopic arrangement. Such an orderly structured projection pattern of flagellar afferents is difficult to observe in the stick insect due to the large amount of labeled fibers that are not easy to trace within the heavily stained VFA.
Compared to labeled sHPd afferents within the DL, both neuropils are almost completely separated from each other. Only two regions showed vicinity of flagel-

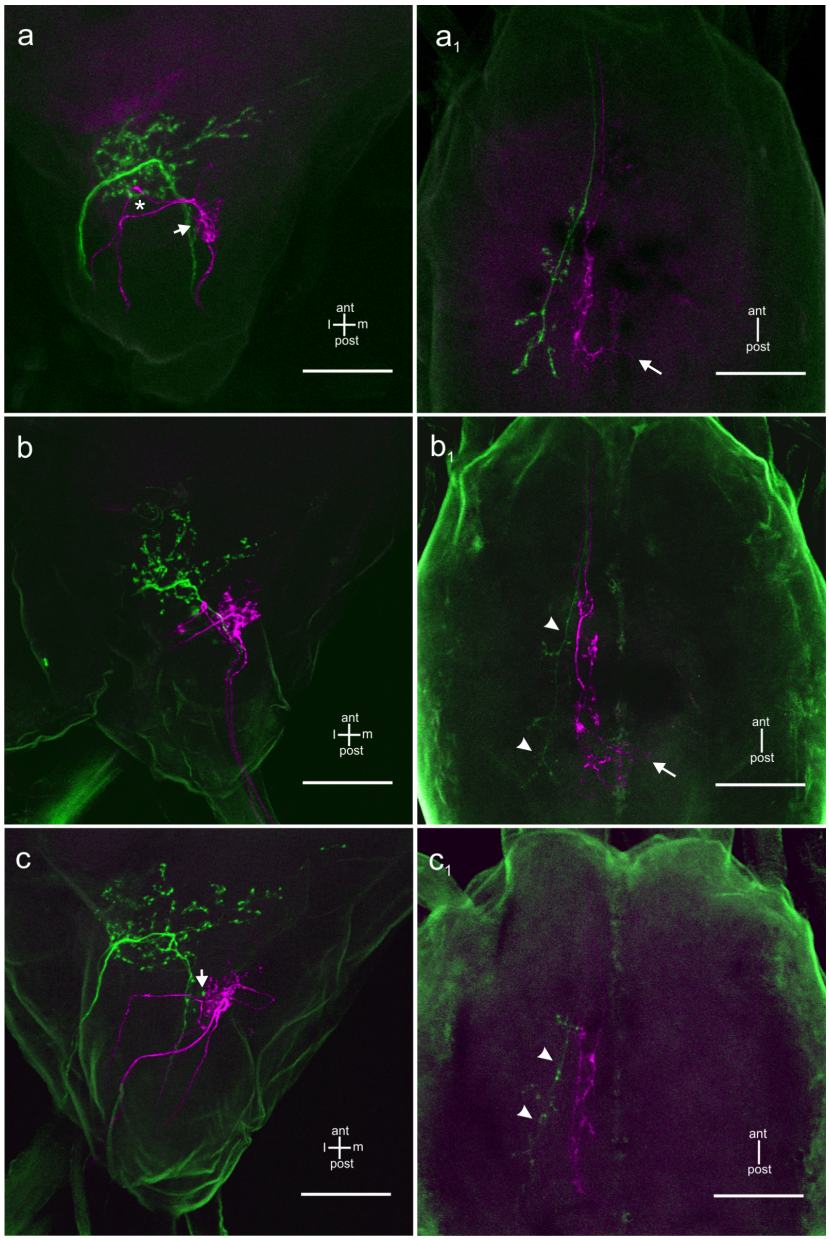

Figure 3.7. – Central projections of presumed mechanosensory hairs located dorsally on the pedicel (magenta) and of sHPd sensilla (green) in the brain and SOG. a-c: Brain whole-mounts revealed that dorsal pedicellar hairs project into a neuropil region ventrolaterally to the DL. The asterisk in (a) marks a fiber with a potential bouton that travels through the DL. The arrowheads indicate areas of close vicinity to sHPd boutons. **a_1-c_1:** Projections of dorsal pedicellar hairs in the SOG travel and terminate in neuropil regions more medial than sHPd afferents (arrowheads). The arrows mark sensory pedicellar fibers that terminate on contralateral ganglion sides. Scale bars=100 µm.

lar afferents with sHPd fibers: (i) along the anteromedially traveling sHPd fibers, and (ii) where the sHPd afferents leave the DL to travel towards the circumoesophageal connective (Fig. 3.9e). Particularly noticeable is the extraordinary weak labeling of olfactory flagellar sensilla within the antennal lobe (AL) (Fig. 3.9 b_1). The reason for this is probably the very small axon diameter of olfactory sensilla

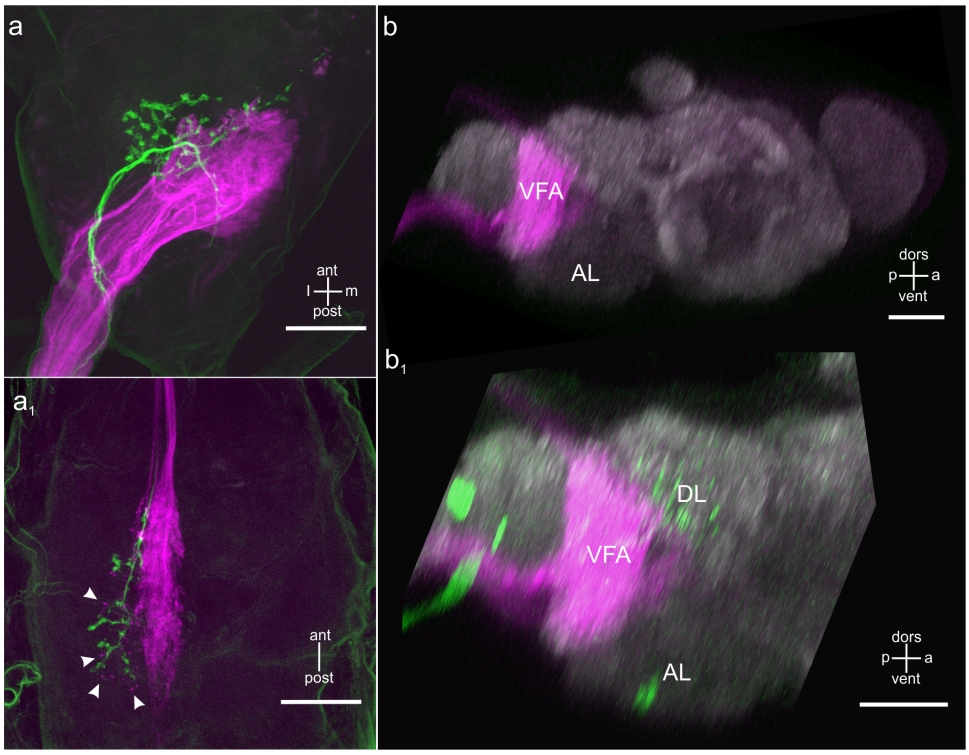

Figure 3.8. – **Stainings of antennal nerve N1 distal to the pedicel (magenta) and of sHPd sensilla (green). a:** Brain whole-mount show flagellar afferent fibers projecting into a large deutocerebral neuropil region that is similar to the cricket VFA neuropil (Staudacher and Schildberger, 1999). **a_1:** SOG whole-mount. Flagellar afferents travel and terminate in a broad band medially to sHPd fibers. The arrowheads mark bouton-like structures of flagellar afferents in vicinity to sHPd varicosities. **b and b_1:** Lateral views of another specimen with stained flagellar afferents and weakly stained sHPd sensilla in the DL (b_1) in combination with anti-synapsin immunohistochemistry (gray). The large VFA neuropil is located more dorsally than the antennal lobe (AL) and posteriorly to the DL (b_1). Scale bars=100 µm.

that were failed to stain with fluorescent dye.

A broad band of fine flagellar afferents were also stained within the SOG, where they travel mainly posteromedially to terminate in intermediary neuropil regions (Fig. 3.8). Fibers that reach the contralateral ganglion portion were not observed, but very weakly labeled flagellar afferents were found leaving the SOG to descend to the prothoracic ganglion (not shown). Moreover, the stainings revealed flagellar afferents that form bouton-like structures and terminate in the same neuropil region and in proximity to the sHPd afferents (Fig. 3.8a_1).

Taken together, afferents of solitary hairs located on the pedicel and afferents of the flagellum project in neuropils separated from the DL. Therefore, the DL is a neuropil which is innervated by afferents of scapal and pedicellar HF sensilla.

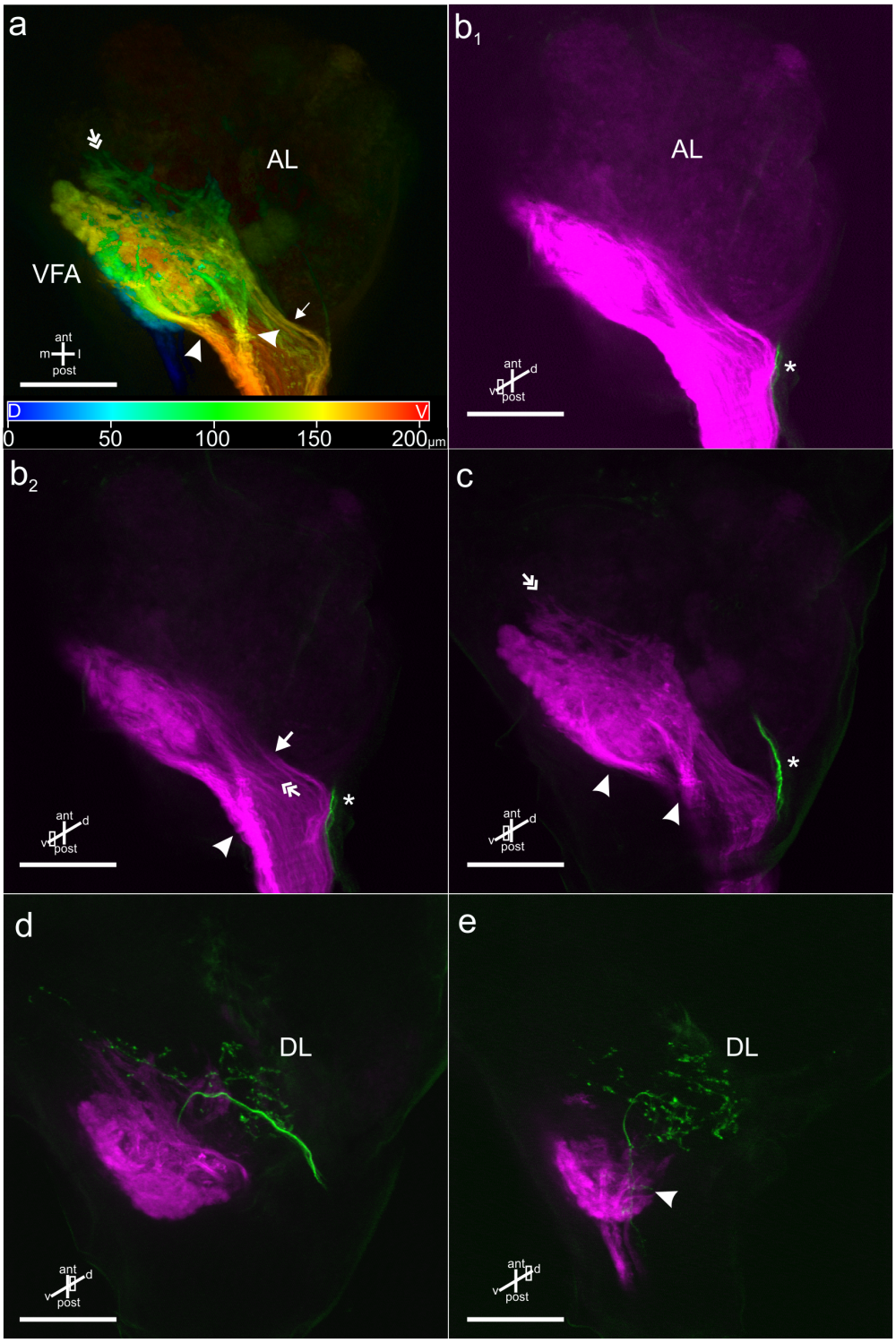

Figure 3.9. – Depth color-coded projection of flagellar afferents and optical sections of flagellar (magenta) and sHPd afferents (green). a: Brain with depth color-coded flagellar fibers. Depth is encoded from dorsal to ventral as blue to red. Image shows a diffuse staining in the AL and the dense cone-like VFA neuropil. Flagellar afferent fibers enter the brain broadly with fiber bundles arising that terminate in different VFA regions. Arrows mark broad bundles entering the VFA ventro- and ventromedially. Arrowheads indicate a bifurcating bundle with few fibers ascending into intermediate VFA regions. Double arrow marks parallel bands of terminal regions. **b_1-b_2:** Optical section of the ventral VFA with high contrast (b_1) revealed the diffuse AL staining and normal contrast (b_2). Arrow marks laterally traveling afferents, double arrow indicates medially running fibers, arrowhead marks a bifurcating bundle, and asterisks mark arriving sHPd fibers. **c:** Ventral and intermediary VFA neuropil. Arrowheads indicate bifurcating fibers, double arrow marks parallel terminal regions, and asterisk indicate entered sHPd fibers. **d:** Intermediary and dorsal VFA neuropil. SHPd fibers ramify in the DL laterally to the VFA. Only few boutons of anteromedially traveling sHPd fibers were found near flagellar fibers. **e:** Dorsal part of VFA. SHPd fibers traveling posteriorly, slightly overlapping with fibers of the dorsal VFA (arrowhead). Scale bars=100 µm.

3.1.5. Strand receptors and central projections of other antennal sense organs

As mentioned in sec. 3.1.2, backfills of antennal nerves N2/N3 revealed a small cell body near the protocerebral bridge (Fig. 3.10a and b). Its primary neurite travels anterolaterally followed by a medial turn around the anterior edge of the deutocerebrum. From there it travels anteriorly to reach its cell body (arrowheads, Fig. 3.10b). In the brain of the locust, Bräunig (1985) described four to five neurons in a similar location as shown here. These neurons innervate a connective tissue strand that spans between the scape to the head (tentorium). Therefore these neurons were termed strand receptors (Bräunig, 1985). So far, stainings in the stick insect revealed only one strand receptor neuron per brain hemisphere (Fig. 3.10b). Arborizations of the primary strand receptor neurite were not observed due to stained other afferents or MN neurites, but its primary neurite could be followed to a region near the DL.

At the distal edge of the stick insect pedicel two prominent sense organs can be found, the Johnston's organ and a ring of campaniform sensilla (Hicks organ). In order to investigate their possible central projection pattern, stainings of antennal nerves close to the brain were performed. These stainings revealed afferents traveling in a curved pathway through the DC and further into the posterior protocerebrum (arrowheads, Fig. 3.10c) than those of HFs, which tend to terminate earlier before reaching the protocerebrum. Furthermore, it seems that these afferents send also collaterals into the DL like HF sensilla. Similar stained afferents, but without an obvious curved pathway, are shown in Fig. 3.10d. The projection pattern appears to be similar to stained Johnston's organ afferents of honeybees that terminate in the posterior protocerebral lobe (Ai et al., 2007).

In the locust, Bräunig et al. (1983) stained antennal campaniform sensilla and their projection pattern resembles those of locust HFs. Bräunig et al. (1983) described the terminal projection pattern as a dense and plexus-like appearance. The Fig. 3.10c shows a broad band of anterolaterally stained afferents as shown for HFs, but their terminal region appears also dense and plexus-like (arrow). It might be that some of these afferents originate from campaniform sensilla, but that needs to be investigated further.

In the appendix, an image is shown of an afferent fiber that leaves the AL to terminate in an unknown neuropil region between the mushroom body and the central body (Fig. A.5 in the appendix). Similarly, recent work in the locust showed antennal afferent projections into the protocerebrum and these sensory neurons respond to downward temperature steps (P. Bräunig, personal communication).

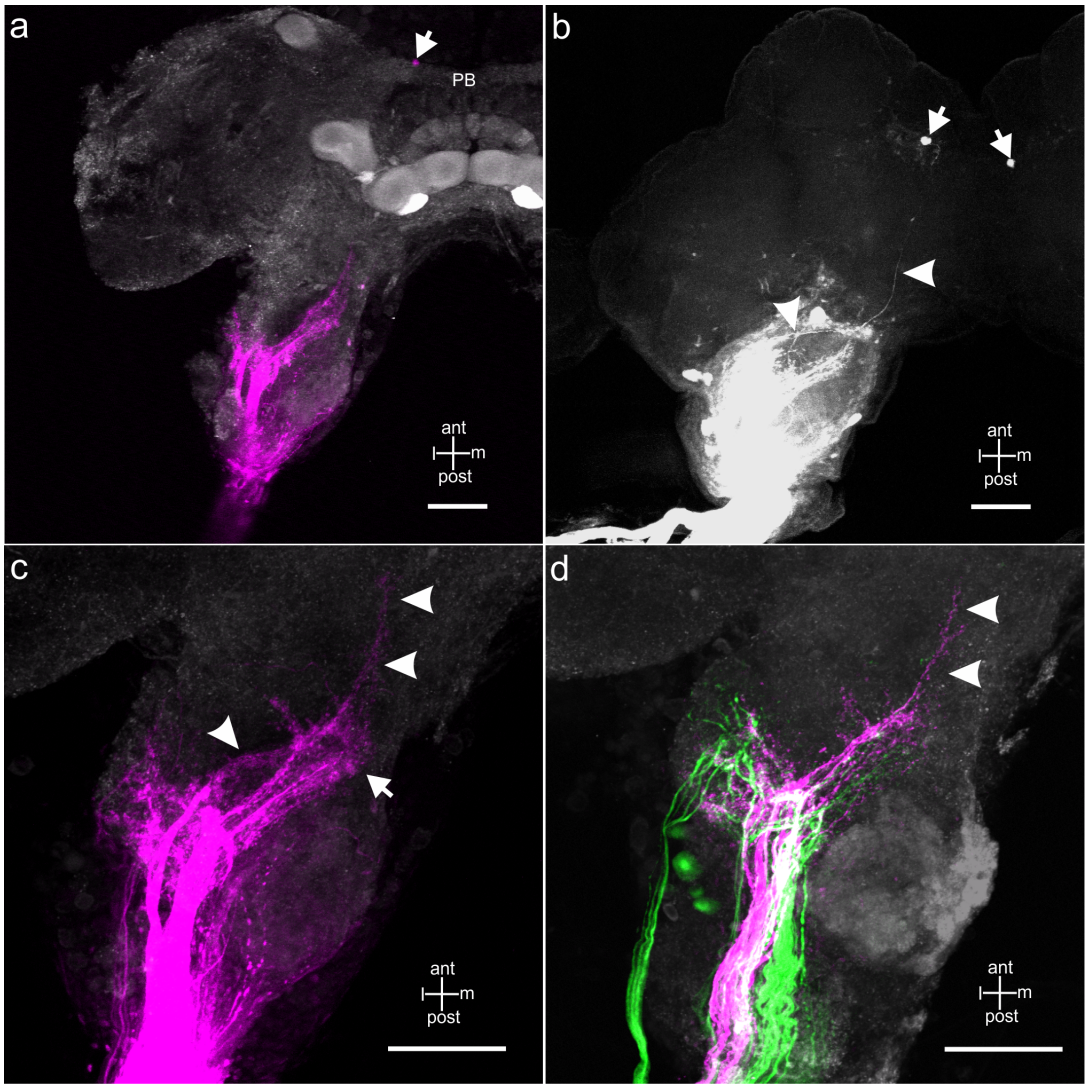

Figure 3.10. – Staining of the antennal motor nerves and nerve N1 close to the brain. **a:** Brain whole-mount with stained antennal nerves (magenta) and anti-synapsin immunolabeling (gray) revealed a small cell body near the protocerebral bridge (PB) that corresponds to a strand receptor neuron described for locusts. **b:** Brain whole-mount with stained antennal nerves shows the pathway of the primary neurite (arrowheads) of the strand receptor cell body (arrow). Here, the contralateral strand receptor cell body (arrow) was stained through contralateral antennal nerves. **c:** Arrowheads mark a curved pathway of possible afferents of the Johnston's organ. Arrow indicates a plexus-like terminal region of possible campaniform sensilla projections as shown for the locust. Afferents terminating in the VFA neuropil were not stained. **d:** Double-labeling of antennal nerve N1 and motor nerves revealed also possible Johnston's organ afferents (arrowheads), but without an obvious curved pathway as shown in (c). Scale bar=100 µm.

3.1.6. Brain and SOG descending interneurons

Neurons with a cell body in the brain and a descending axon have been named descending interneurons (DINs; e.g., Staudacher, 1998; Okada et al., 2003). The term is used also for neurons with cell bodies in the SOG with a descending axon (Kien et al., 1990), despite the existence of ascending interneurons (AIN) and intersegmental interneurons with similar properties. The following section describes the location and numbers of DINs in the brain and SOG, stained either through cervical (neck) connectives or through connectives between pro- and mesothoracic ganglia. In the experiments here, only one connective was stained per specimen. Soma clusters are named ipsilateral (i) or contralateral (c) with respect to the dyed connective. The nomenclature was adapted from Staudacher (1998).

DINs projecting to the prothoracic ganglion

Backfilling the cervical (neck) connective stained 164 to 205 (N=5; median: 176) somata in the brain. Fig. 3.11 and Fig. A.6 in the appendix show two depth color-coded brain specimens with labeled DINs, whereas in Fig. 3.12 thick optical brain sections are shown. DIN numbers and their clusters are summarized in Tab. 3.1. In the brain, these neurons are located in 19 soma clusters, nine ipsilaterally (i1-9), the pars intercerebralis cluster (pi), and seven contralateral clusters (c1-7). They are distributed in dorsal, intermediate, and ventral regions of the trito- (TC), deuto- (DC), and protocerebrum (PC). Noticeable are many stained cell bodies near the ipsi- and contralateral mushroom body calyces. The soma clusters i8, i5n, and c7 are not necessarily clusters because they often contain only one cell body. Nevertheless, due to their appearance at similar regions in different specimens and in comparable clusters in crickets and cockroaches, they were defined as clusters. In general, the cluster borders are often not easily discernible, due to a smooth transition in depth (see depth color-coded image). Therefore, the cell body counts for i2-i4, i7a-i7b, and c2-c4 have to be considered with care (Tab. 3.1). The cell body diameters range between 10 µm to at least 50 µm. One of the largest soma was found contralaterally in cluster c1. Probably it possesses the largest primary neurite, measuring ~10 µm in diameter. The distribution and branching of DINs can clearly be observed in the anti-synapsin immunostained images (Fig. 3.12). Note that, due to the huge amount of heavily stained neurites, it is not possible to distinguish between DIN dendrites and fibers of AINs. Nevertheless, a considerable amount of branching can be observed ipsilaterally in the lateral and posterior PC throughout ventral, intermediate, and dorsal parts (Fig. 3.12b-e). Apparent are two thick bundles of neurites, probably from AINs, traveling ipsilaterally to arborize and terminate in the PC. Few weakly labeled neurites run in the direc-

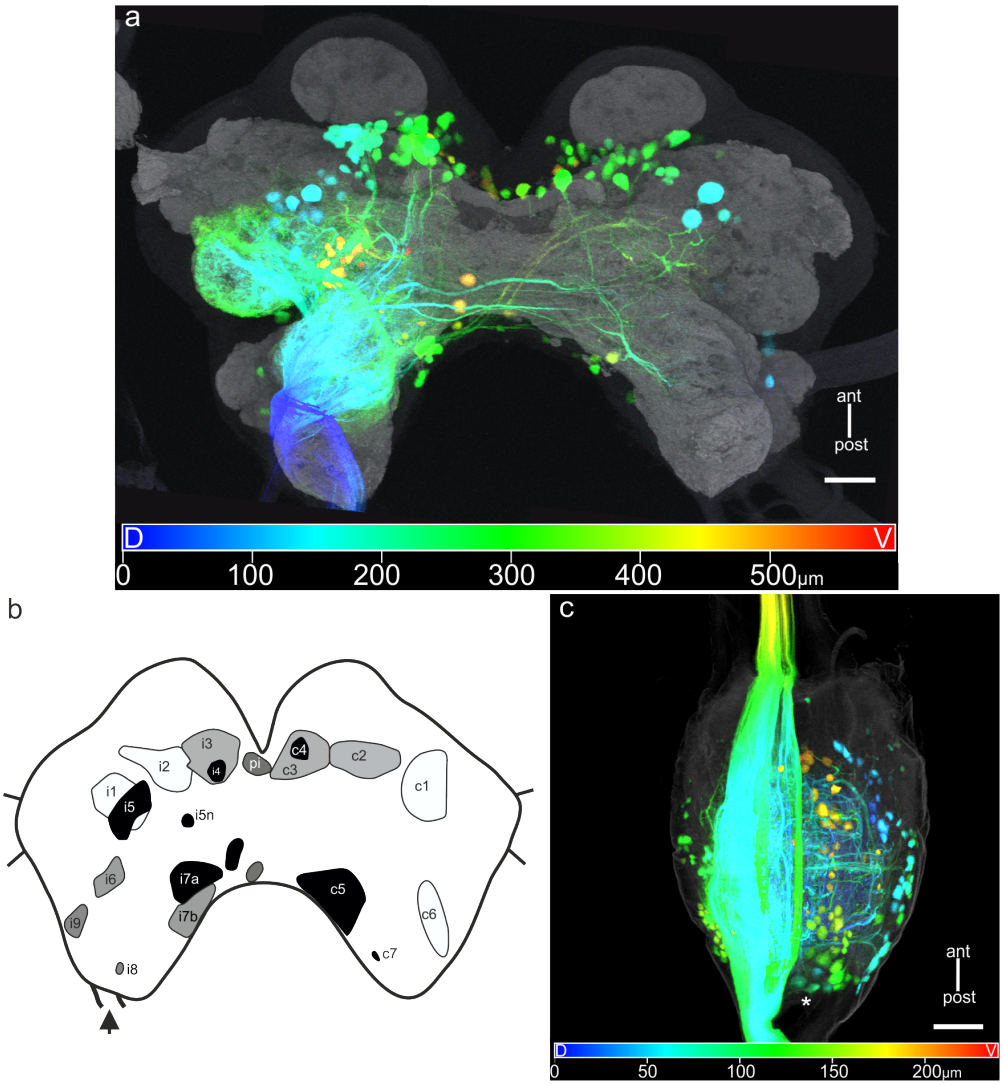

Figure 3.11. – DINs in the brain and SOG after staining a cervical (neck) connective. a: Depth color-coded brain combined with anti-synapsin immunostaining (gray). Brain outline was captured by scanning the autofluorescence of the tissue (dark gray). Depth is encoded from dorsal to ventral as blue to red. **b:** Schematic drawing shows the distribution of soma clusters in the brain, ipsi- (i) and contralaterally (c) to the site of the dyed connective (arrow). pi=pars intercerebralis cluster. dorsal=white with black outline; intermediate=gray; ventral=black. Unnamed clusters in the middle PC region were found rarely. **c:** SOG DINs stained through a cervical connective. Outline (gray) was captured by scanning autofluorescence. Depth coding as in (a). About 200 cell bodies were dyed in different regions and clusters, the majority ventrally. Arborizations of neurites are found densely in the core neuropil. At the posterior crotch of the SOG (asterisk) several DUM cells were stained. Scale bars=100 µm.

tion of the ipsilateral optic lobe (not shown). Numerous dendritic branches were also observed in the ipsi- and contralateral DLs and the VFA neuropils in the DC (Fig. 3.12b-c). Extensive arborizations were stained in a region between the central body (CB) and the ipsilateral AL (Fig. 3.12d), known as the lateral accessory lobe in moths and locusts (LAL; Homberg et al., 1988; Homberg, 1994). Ipsi- and

contralaterally to the dyed connective, dendritic branches were found in the intermediate and medial PC (Fig. 3.12c-e). No dendritic arborizations were observed in the AL, the central body (CB), and the mushroom bodies.

In the SOG, at least 161 and up to 205 (N=5; median: 183) cell bodies were stained through a cervical (neck) connective (Fig. 3.11c). The cell bodies are found in various clusters ipsi- and contralaterally to the stained connective in the whole depth of the SOG. Contralateral neurons were observed mainly dorsally, whereas the majority of neurons were found ventrally (partially masked by fibers running through; Fig. 3.11c). At the posterior crotch of the SOG several DUM neurons were stained. Their exact numbers could not be determined, but Hess (2008) estimated about six DUM neurons in the SOG of stick insects. Just after entering the SOG, fibers of descending and ascending neurons running through different longitudinal tracts. Several neurites are crossing through different commisures to the contralateral side. Extensive arborizations were found in the core neuropil of the SOG.

Table 3.1. – Soma clusters with numbers of brain DINs and their location, after staining a cervical (neck) connective for five specimens (N=5). d=dorsal; int=intermediate; v=ventral; DC=deutocerebrum; PC=protocerebrum; TC=tritocerebrum.

	i1 dPC	**i2**[1] dPC	**i3**[1] intPC	**i4**[1] vPC	**i5** vPC	**i5n** vPC	**i6** v/intDC/PC	**i7a**[1] vDC	**i7b**[1] intDC	**i8** int/dTC	**i9** intDC
1	8	21	20	5	25	2	3	7	6	1	3
2	9	25	22	7	22	2	3	9	7	1	0
3	11	22	38	6	28	0	4	10	10	1	2
4	15	19	29	3	19	1	2	8	9	1	2
5	11	21	23	4	24	1	3	8	3	1	4

	pi[1] vPC	**c1** dPC	**c2** d/intPC	**c3**[1] intPC	**c4**[1] vPC	**c5** vDC	**c6** dDC/TC	**c7** vDC	**single cells** various	**total #**
1	4	11	15	12	9	7	6	1	2	**168**
2	5	7	22	9	1	7	6	2	2	**168**
3	6	13	17	18	6	6	6	1	0	**205**
4	6	5	11	24	8	7	4	2	2	**177**
5	5	6	13	23	2	4	3	0	5	**164**

[1]Cluster borders are difficult to obtain. Few cell bodies counted for one cluster could also be counted for the neighboring cluster.

Compared to previous studies, the findings of 164 to 205 pairs of brain DINs in the stick insect is in agreement to the reported 135 to 181 brain DINs in the cricket (Staudacher, 1998) and to the cockroach with at least 235 brain DINs (Okada et al., 2003). The somata clustering of DINs is also comparable to the cricket and the cockroach with few differences (see discussion). However, counting the maximum numbers of brain and SOG somata, 410 pairs of DINs in the stick insect

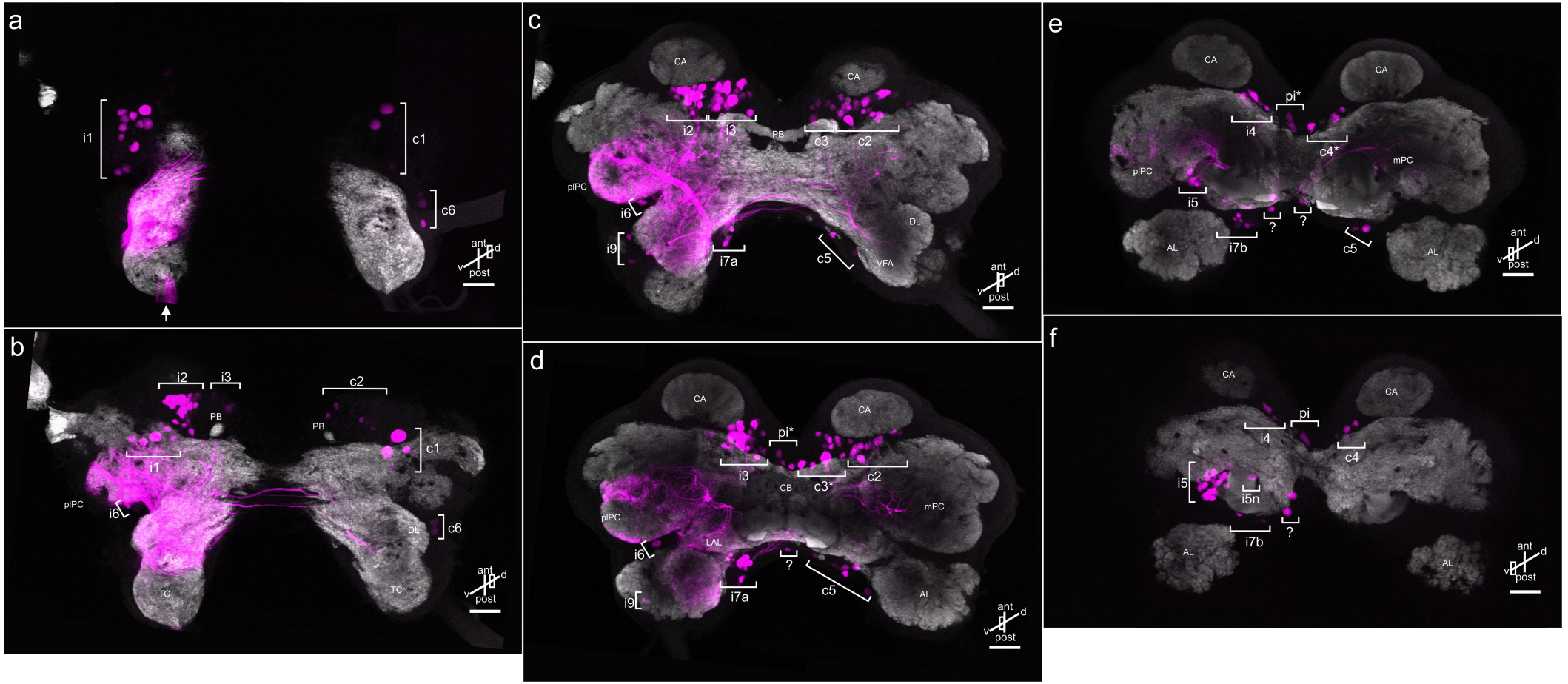

Figure 3.12. – **Thick optical brain sections with DINs (magenta) stained through a cervical (neck) connective combined with anti-synapsin immunostaining (gray). a-f:** Optical sections (same whole-mount shown in Fig. 3.11a) from dorsal (a) to ventral brain parts (f). Arrow in (a) marks the site of the dyed cervical connective. Indicated are soma clusters and prominent brain regions: AL=antennal lobe; CA=calyces; CB=central body; DL=dorsal lobe; PB=protocerebral bridge; VFA=ventral area of flagellar afferents. Arborizations occur in the ipsilateral and posterolateral protocerebrum (plPC), the lateral accessory lobe (LAL), the ipsi- and contralateral DLs and VFA, and in the medial contralateral PC (mPC) (b-e). Asterisks mark clusters with undefined borders and question mark indicates solitary neurons. The dark brain outline, e.g., the cell body rind, was captured by scanning the autofluorescence of the tissue. Scale bars=100 µm.

transmit signals from the brain and SOG to thoracic motor centers.

DINs projecting to the mesothoracic ganglion

Backfilling a connective between pro- and mesothoracic ganglia revealed 51 to 83 DINs (N=4; median: 68) in the brain (Fig. 3.13 and Tab. 3.2). They are distributed ipsilaterally in soma clusters i1-i7b, in the pars intercerebralis (pi) cluster, and contralateral clusters in c1-c6. No cell bodies were observed in clusters i8, i9, and c7 (Tab. 3.2). Arborizations of DINs were found, similar as described above, in the ipsilateral plPC, the ipsilateral LAL, the DL and VFA neuropil on both brain hemispheres, and within the contralateral mPC.

In the SOG, at least 69 and up to 90 somata (median: 82; N=4) were observed, with similar distributions and fewer arborizations in the neuropil than described above (Fig. 3.13c). For matters of completeness, intersegmental neurons of the prothoracic ganglion were counted, too. The stainings showed 90 and up to 115 neurons (N=4, median: 105), mainly ventrally and contralaterally to the dyed connective (Fig. 3.13d). Several neurons possess arborizations in the ipsilateral ventral association center (VAC), a prominent sensory neuropil.

Table 3.2. – Soma clusters with numbers of brain DINs and their location, after staining a connective between pro- and mesothoracic ganglia for four specimens (N=4). d=dorsal; int=intermediate; v=ventral; DC=deutocerebrum; PC=protocerebrum; TC=tritocerebrum.

	i1 dPC	**i2**[1] dPC	**i3**[1] intPC	**i4**[1] vPC	**i5** vPC	**i5n** vPC	**i6** v/intDC/PC	**i7a**[1] vDC	**i7b**[1] intDC	**i8** int/dTC	**i9** intDC
1	4	12	13	1	9	1	1	5	2	0	0
2	6	12	12	1	8	1	0	5	1	0	0
3	7	8	12	1	6	0	0	4	0	0	0
4	3	8	5	1	8	0	0	0	0	0	0

	pi vPC	**c1** dPC	**c2**[1] d/intPC	**c3**[1] intPC	**c4**[1] vPC	**c5** vDC	**c6** dDC/TC	**c7** vDC	**total #**
1	4	5	12	6	4	4	0	0	**83**
2	2	2	7	5	1	4	0	0	**67**
3	1	2	16	8	0	4	2	0	**71**
4	4	3	9	4	2	4	0	0	**51**

[1]Cluster borders are difficult to obtain. Few cell bodies counted for one cluster could also be counted for the neighboring cluster.

In comparison to cervical connective backfills, the number of stained brain and SOG DINs is less than half, with up to 173 neurons. This may indicate that a large number of DINs terminate in the prothoracic ganglion. On the other hand, the long dye traveling distance might be the reason for the limited numbers of

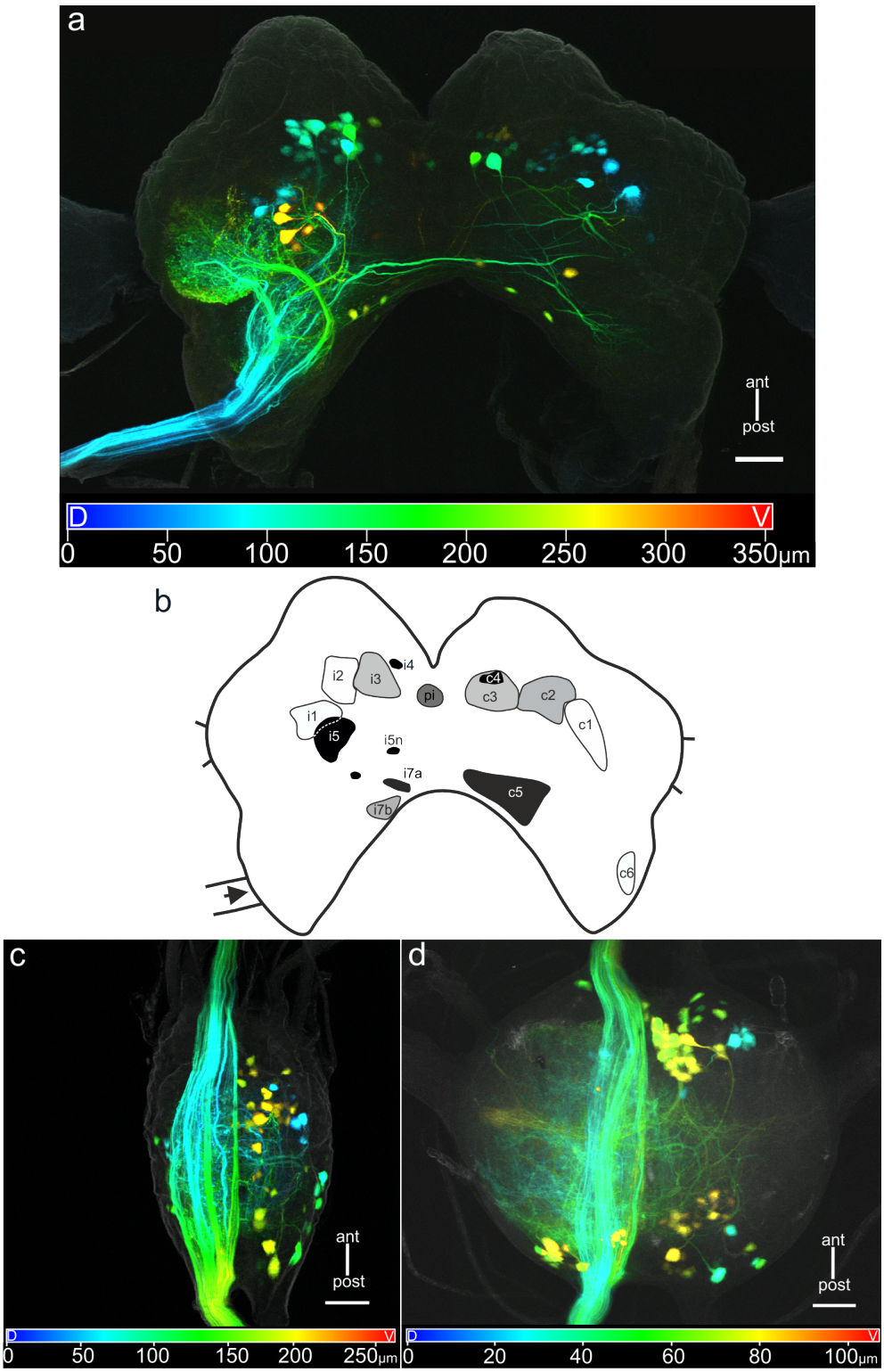

Figure 3.13. – DINs in the brain and SOG after staining a connective between the pro- and mesothoracic ganglion. a: Depth color-coded brain with slightly distorted z-axis. Brain outline was captured by scanning the autofluorescence of the tissue (gray). Depth is encoded from dorsal to ventral as blue to red. **b:** Schematic drawing shows the distribution of soma clusters in the brain, ipsi- (i) and contralaterally (c) to the site of the dyed connective (arrow). pi=pars intercerebralis cluster. dorsal=white with black outline; intermediate=gray; ventral=black. **c:** SOG DINs stained through a pro- and mesothoracic connective. Outline (gray) was captured by scanning autofluorescence. Depth coding as in (a). Approximately 80 cell bodies were dyed in different regions and clusters, the majority ventrally. Arborizations of neurites are found densely in the core neuropil. **d:** Intersegmental interneurons in the prothoracic ganglion after staining a posterior connective. Outline and depth coding as in (a) and (c). Approximately 100 cell bodies with axons to the mesothoracic ganglion were stained in ipsi- and contralateral ganglion regions. Scale bars=100 µm.

stained DINs, projecting to the mesothoracic ganglion. However, dyed connectives between meso- and metathoracic ganglia of cockroaches showed also a limited number of brain DINs, with 40 to 45 cell bodies (Burdohan and Comer, 1996).

3.1.7. Central projections of HF fibers appear to be in close vicinity to neurites of DINs

Stainings of cervical connectives and connectives between the pro- and mesothoracic ganglia revealed DIN neurites close-by or invading the ipsi- and contralateral DLs and VFA neuropils in the brain (Fig. 3.12c). This observation prompted the investigation whether central projections of antennal HFs have spatially overlapping regions with neurites of DINs.

Fig. 3.14 shows stained DIN neurites contralateral to a dyed connective between the pro- and mesothoracic ganglia and projections of scapal HPs sensilla. The images revealed that possible overlapping regions of DIN neurites with HP afferents exist. Vicinity of HF afferents and DIN neurites was found along the anteromedially traveling HP afferents in T6I (Fig. 3.14a_2-a_3, b_2-b_3), in the anteromedial DL (Fig. 3.14b_2), and in T6II, just after the afferents turned posteriorly to travel to the circumoesophageal connective (lower arrowheads; Fig. 3.14a_1 and b_1). In the ipsilateral DL, with respect to a stained connective between the pro- and mesothoracic ganglia, so far only one DIN neurite was found in the vicinity of sHPv afferents (Fig. 3.15a_1-a_2). Possible contacts were observed in addition along the anteromedially traveling afferents in T6I (Fig. 3.15 a_3). Another whole-mount with contralateral DIN neurites stained by backfilling a cervical connective is shown in Fig. 3.15. Numerous fine branches of DIN neurites invade the contralateral DL (Fig. 3.15b_1-b_3). Thus, it might be that not only HP afferents in T6I and T6II, slightly outside the DL, are in the vicinity of DIN neurites but also fine branches of DINs or even AINs within the DL.

As shown in section 3.1.1, stained antennal HF afferents descend from the brain to the SOG. In the appendix, images of two specimens are shown with stained DINs and HFs within the SOG (Fig. A.7 in the appendix). Within the descending pathway of the antennal scapal HF fibers and especially before and during terminating in the inverted 'V'-shaped manner, it appears that boutons of HF afferents are in the vicinity of neurites of SOG DINs or intercalated interneurons.

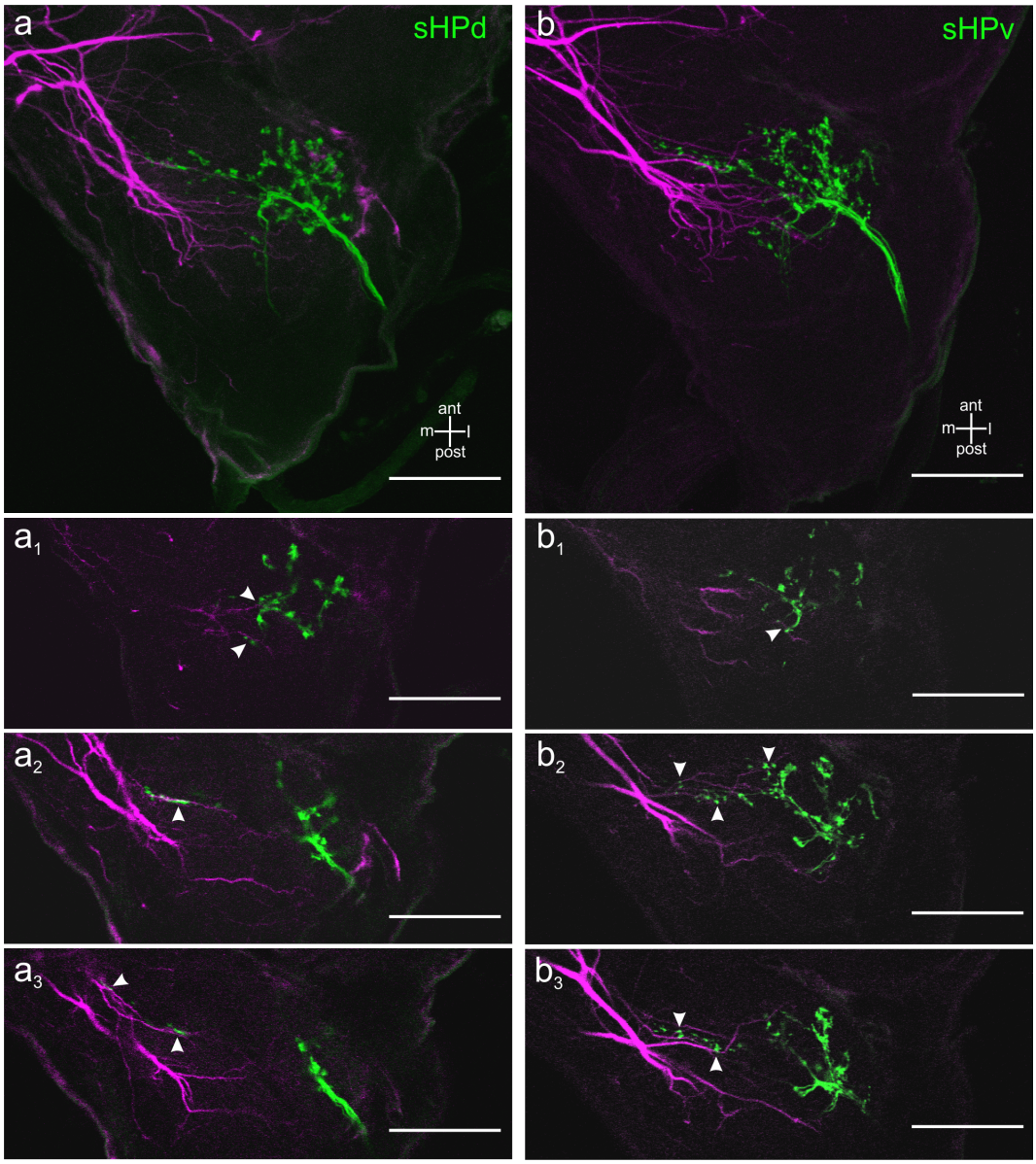

Figure 3.14. – Possible overlapping sites of DIN neurites and scapal HP afferents, contralaterally to the dyed pro-mesothoracic connective. a: Horizontal projection of sHPd afferents (green) and DIN neurites (magenta). **a_1-a_3:** Single images of (a) from dorsal to more ventral parts of the DL. a_1: DIN neurites invade slightly the DL and arrowheads indicate regions with overlap. Lower arrowhead marks vicinity of boutons in T6II (just after the afferent fibers begin to travel posteriorly) with DIN neurites. a_2-a_3: DIN neurites invading the VFA (medial) and vicinity of sHP afferents anteromedially in T6I with DIN neurites (arrowheads). **b:** Horizontal projection of sHPv afferents (green) and DIN neurites (magenta). **b_1-b_3:** Single images of (a) from dorsal to more ventral parts of the DL. b_1: DIN neurites in vicinity to sHPv afferents, just after turning posteriorly (arrowhead). b_2-b_3: Vicinity of DINs with sHPv afferents anteriorly in the DL and along T6I (arrowheads). Scale bars=100 µm.

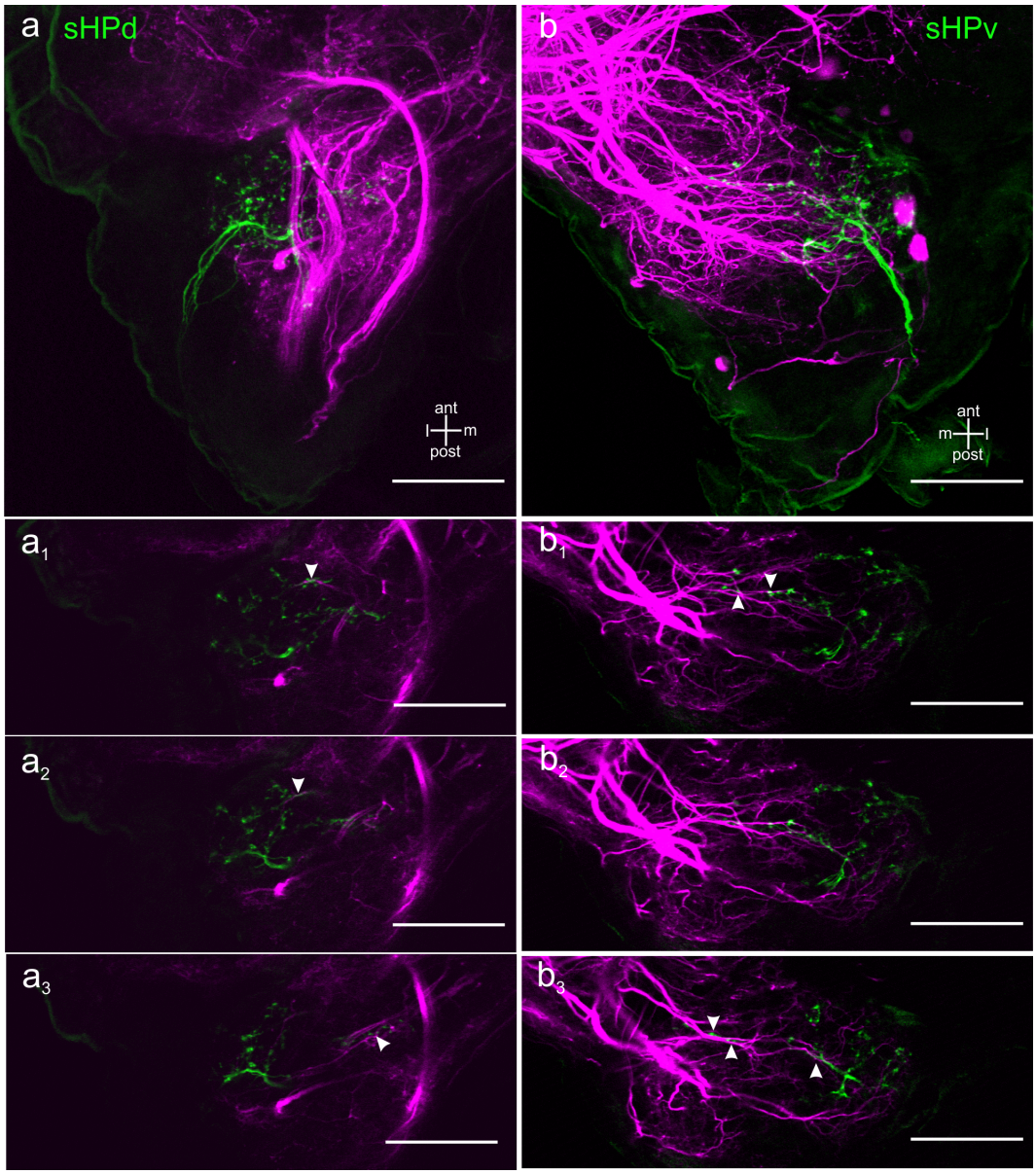

Figure 3.15. – Possible overlapping sites of DIN neurites and scapal HP afferents, ipsi- and contralaterally to a dyed connective. a: Horizontal projection of sHPv afferents (green) and DIN neurites (magenta) stained through a pro-mesothoracic connective. **a_1-a_3:** Single images of (a) from dorsal to more ventral parts of the DL. a_1-a_2: A DIN neurites invade slightly the DL and arrowheads indicate possible overlap. a_3: Possible overlap of sHPv afferents anteromedially in T6I with DIN neurites (arrowheads). **b:** Horizontal projection of sHPv afferents (green) and DIN neurites (magenta) stained through a cervical connective. **b_1-b_3:** Single images of (a) from dorsal to more ventral parts of the DL. b_1-b_2: DIN neurites in vicinity to sHPv afferents along T6I (arrowheads). b_3: Vicinity of DINs with sHPv afferents anteriorly in the DL and along T6I (arrowheads). Scale bars=100 µm.

3.1.8. Summary

The present chapter provides insights into the neuroanatomical organization of the mechanosensory and motor system of the stick insect antenna. All seven antennal HFs, located on the scape and pedicel, send collaterals into the DL, in T6I, and travel through T6II to descend through the circumoesophageal connective to the SOG, where these fibers terminate. Synaptic boutons were observed in the brain within the DL, along the fibers in T6I, and just after turning to travel through T6II. In the SOG, various sites with boutons occur during their descending pathway into deeper neuropil regions. The central projection patterns of all HFs appear very similar, but differences were found in spatially different formation of boutons within the entire depth of the DL and within the SOG. The HF afferents overlap in the DL with dendrites of antennal MN neurites, that could be an indication for direct synaptic contacts. Boutons of HF fibers in the DL, in T6I, and in the beginning of T6II are found in close vicinity of branches of DINs, suggesting that signals of HFs are probably transmitted to thoracic ganglia via a fast mediating pathway.

Afferent fibers of mechanosensory sensilla from the flagellum and also from presumed mechanosensory hairs of the pedicel converge in the ventral area of flagellum afferents (VFA), a neuropil region in the DC that is separated from the DL. These fibers descend also to the SOG, where they mainly terminate in neuropil regions more medially than HF fibers.

Furthermore, backfills of cervical (neck) connectives revealed up to 410 descending interneurons (DINs) in the brain and SOG (brain: 205, SOG: 205) that transmit signals at least to prothoracic motor centers. Backfills of connectives between the pro- and mesothoracic ganglia stained up to 173 descending interneurons (brain DINs: 83, SOG DINs: 90) projecting from the brain and SOG to mesothoracic motor centers. These stainings provide the neuroanatomical basis for studying the information flow from the brain to thoracic motor centers of the stick insect.

3.2. Morphology of mesothoracic motoneurons, DUM cells, and sensory neurons with a central cell body[1]

For the understanding of the neuronal control of locomotion it is important to know all involved leg muscle innervating motoneurons (MN), modulatory dorsal unpaired median neurons (DUM), and sensory organs associated with limbs. Therefore, retrograde stainings of all mesothoracic lateral nerves (except sensory nl1) of the stick insect were performed to receive information about the central projections of neurons with axons in specific muscle innervating nerves. Moreover, transverse sections of ganglia combined with anti-β-tubulin immunohistochemistry were prepared to provide information about stained structures in relation to prominent longitudinal fiber tracts and neuropil regions.

3.2.1. Nervus anterior (na)

Nervus anterior (na) initially ramifies into two side branches. Branch one joins with nervus unparis (termed also nervus transversus) and with nervus posterior of the prothoracic ganglion to innervate intersegmental muscles, dorsal longitudinal muscles, and the muscles of the heart (Fig. 2.2; Marquardt, 1940).
Backfills of both na branches revealed up to nine cell bodies (diam. 10–60 µm). Contralateral to the dyed nerve eight cell bodies are distributed dorsally in the anterolateral region of the ganglion (Fig. 3.16a,b), including two cell bodies localized slightly more medial. Their cell body processes (henceforth termed primary neurites; Wilson, 1979) travel in two separated tracts ultimately to enter nerve na. Dendritic branching occurs mainly in dorsomedian neuropil regions with branches that travel and terminate in ganglion areas ipsilateral to nerve na. At the ganglion center in the ventral cortex another neuron (diam. 32–45 µm) was stained (Fig. 3.16a,c). Its primary neurite leaves the cell body and several dendritic branches originate that project to posteromedial ganglion regions. The primary neurite ascends to the dorsal neuropil to run to the root of nerve na within the same tract as the neurites of the two slightly medial and contralaterally stained

[1]The results for mesothoracic motoneurons, DUM cells and sensory neurons with a central cell body in this section are already published: Goldammer J, Büschges A and Schmidt J. *Motoneurons, DUM Cells, and Sensory Neurons in an Insect Thoracic Ganglion: A Tracing Study in the Stick Insect Carausius morosus.* Journal of Comparative Neurology, 520(2), 230-257, 2012. The author contributions are as followed: JG, AB and JS designed research. JG performed experiments, analyzed data, prepared figures, tables and drafted the manuscript. JS edited the manuscript. The entire section, with minor modifications, is taken from the paper.

neurons. In one whole-mount an additional 60 µm cell body was labeled at the dorsal center (Fig. 3.16c). Due to the large soma, its dorsal position, and a weakly stained primary neurite that appeared to bifurcate forming two neurites, I conclude that the neuron is a DUM cell. The assumption is confirmed by data from Mentel et al. (2008), who described in the stick insect a DUM neuron with lateral projecting axons through nerves na and nl2 that was termed DUMna nl2.
Not only axons of efferent neurons but also several sensory afferents that are organized in two bundles travel through nerve na. These afferent fibers enter the ganglion together in a prominent bundle that descends to an intermediate ganglion region to diverge in two major bundles. Afferents of one bundle travel posteriorly to give rise to few dendritic branches that project semicircular in an intermediate neuropil region, probably the horseshoe neuropil (Kittmann et al., 1991; Fig. 3.16a, dashed line). Most of the afferent fibers follow a slightly curved path to posterior regions where they give rise to fine branches before they enter the ipsilateral connective to the metathoracic ganglion. Several fibers of the second and prominent bundle pass in a posteromedian direction through intermediary neuropil regions to terminate posteriorly, whereas the remaining afferents continue to descend to ventral regions of the neuropil, probably in the anterior part of the ventral association center (aVAC; Fig. 3.16a, arrow).

3.2.2. Nervus lateralis 2 (nl2)

Nervus lateralis 2 (nl2) ramifies into four branches: branch A innervates pleurosternal muscles, branch B the tergopleural ventilatory muscles, branch C supplies the protractor coxae (Bässler, 1983; Graham, 1985), and branch D innervates the tergotrochantinal muscle (Fig. 2.2; Marquardt, 1940).
Stainings of all nl2 branches together revealed a maximum of 22 neurons that are located in two different ganglion regions ipsilateral to nl2 and along the ganglion midline (Fig. 3.17a). One cluster with up to 17 cell bodies is located in the anterolateral region of the ganglion between the root of na and the anterior ipsilateral connective. About six cell bodies have relatively small diameters of 13–18 µm. The others are larger with diameters up to 50 µm. The depth color-coded image (Fig. 3.17b) and transverse sections (Fig. 3.17c) display the positions of these cell bodies in dorsal, intermediate, or ventral ganglion regions. The primary neurites of anterolateral neurons travel in two separate bundles through the ganglion until they run together to leave the ganglion via nl2. In the dorsal neuropil higher-order branches arise that spread in anterior and mainly posterior directions with a slightly descending course to deeper neuropil areas (Fig. 3.17d,e). One of the two main bundles is formed of neurites of ventrally located neurons (Fig. 3.17a,

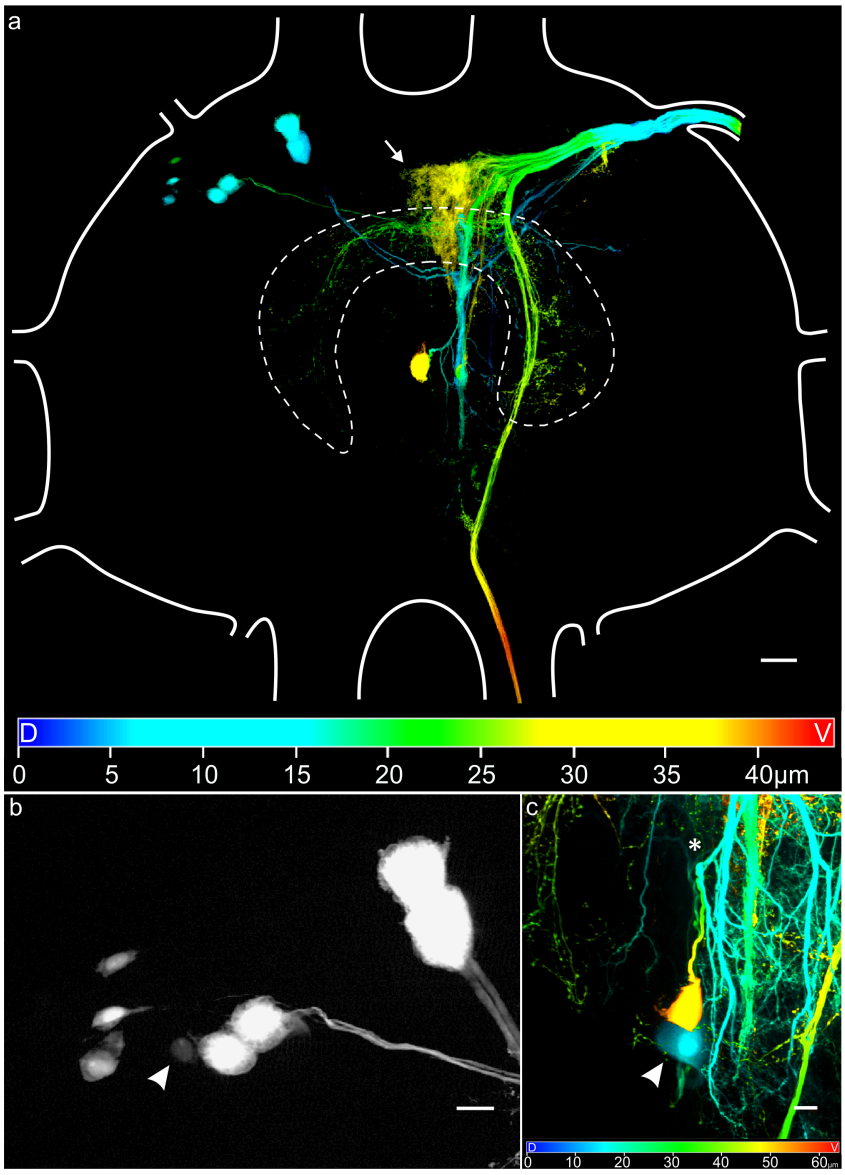

Figure 3.16. – **Backfill of nervus anterior (na). a:** Depth color-coded whole-mount. One cell body cluster is located anterodorsolaterally and contralaterally to the dyed nerve and one cell body was labeled ventrally at the ganglion center. Dashed line indicates sensory afferents projecting semicircular through the horseshoe neuropil (hN). Arrow marks sensory fibers terminating in ventral neuropil regions, probably the ventral association center (VAC). Depth encoded from dorsal to ventral as blue to red. **b:** High magnification shows seven contralateral cell bodies and a pale labeled neuron (arrowhead). **c:** Depth color-coded image of mid ganglion neurons in another whole-mount shows the ventromedian neuron (yellow) and a dorsal unpaired median (DUM) cell body, the DUMna nl2 neuron (arrowhead; Mentel et al., 2008). Asterisk marks DUM neurite T-junction. Scale bars=50 µm in a; 20 µm in b,c.

arrow) that ascend in posterior and slightly medial direction to the dorsal neuropil to bend laterally to join the neurite bundle of dorsally positioned cell bodies. During the lateral turn the primary neurites give rise to numerous secondary and tertiary branches that travel across the ganglion midline, where they split in different directions and then terminate in anterodorsomedial and posterodorsomedial

neuropil regions. Other neurites travel to the midline to turn posteriorly in order to terminate near the DUM cell bodies. The remaining neurites run slightly posteromedially followed by a medial bend, where additional branches originate. The second neuron cluster with up to six cell bodies is located in the posteromedian region of the ganglion (Fig. 3.17a,e,f). In two whole-mounts a maximum of four cell bodies, with diameters between 40–58 µm, were stained dorsally at the midline. Due to their position, diameters, and their bifurcating primary neurites these neurons were identified as DUM cells. Secondary lateral DUM neurites travel in the direction of nerves na, to the roots of nerves nl2–5, and to ncr. Four of these lateral DUM cell neurites were observed to enter these roots. It is possible that a fifth DUM neuron was stained in one preparation (Fig. 3.17a, dashed circle) but due to only four clearly visible DUM neurites I parenthesize that neuron in Tab. 3.3. Another cell body, with a diameter of 60–70 µm, is ventrally located (Fig. 3.17f). This neuron was designated by Bässler and Storrer (1980) and Graham and Wendler (1981) as the common inhibitory 1 (CI1) neuron. Its primary neurite ascends in an 'S'-shaped manner through the ventral and intermediate neuropil (Fig. 3.17e) to the lateral nerve roots and to the root of ncr. Higher-order branches emerge in the lateral ganglion region to enter the posterodorsal and the posterolateral neuropil (Fig. 3.17e).

A distinctive bundle of sensory afferents enters the ganglion that runs ventrally between the cortex and the ganglionic core to the ventral association center (VAC), where they ramify extensively in a fan-shaped pattern (Fig. 3.17a,c,d, arrowheads). The projection pattern of these afferents is similar to the one of a tactile hair on stick insect sternum that enter the ganglion through nerve nl1 (Schmitz et al., 1991).

In addition, backfills of branch C of nerve nl2 were performed that innervates the protractor coxae muscle (Bässler, 1983; Graham, 1985). Stainings revealed six to nine cell bodies (diam. 15–59 µm) anterolaterally, the CI1 neuron, and one to four DUM cells at the ganglion midline (Fig. B.1a-c in the appendix). Most of the anterolaterally cell bodies were labeled in ventral and intermediary ganglion regions except for one to two dorsally located cell bodies. One of these dorsal neurons showed in the majority of backfills the largest cell body diameter (51–59 µm) of the group. Sensory afferents were observed that travel and terminate ventrally in the VAC as described above. Additionally, sensory afferents were observed in a single whole-mount that enter the ganglion as a compact bundle that bifurcates just after entry (Fig. B.1c). Fibers of one bundle run in a posterolateral direction to terminate in intermediary regions near the root of nerve ncr. The remaining fibers continue to travel medially to ramify and terminate in intermediate parts of neuropil at the ganglion midline.

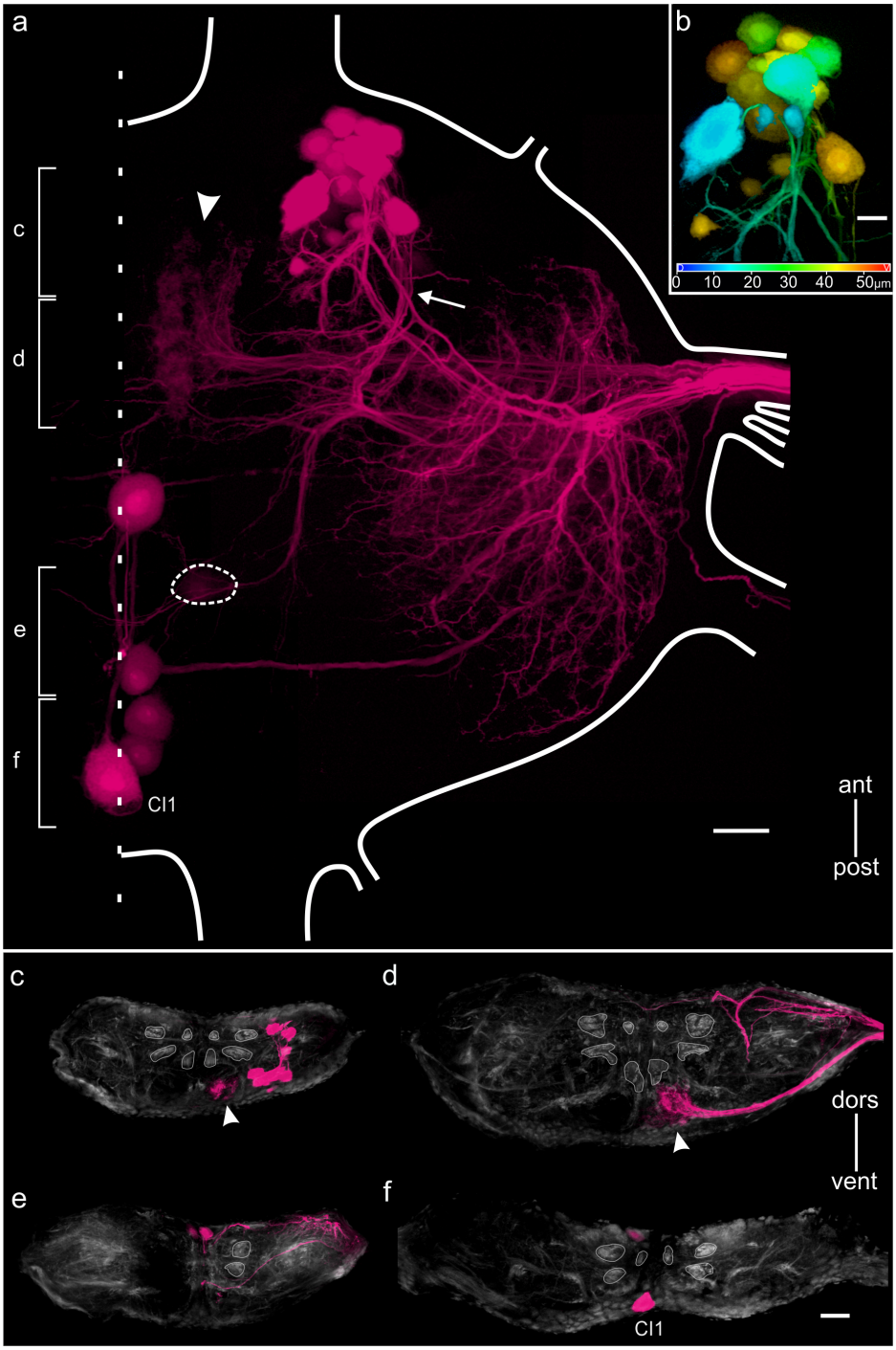

Figure 3.17. – **Backfill of nervus lateralis 2 (nl2). a:** Whole-mount with anterolateral cell cluster with 17 cell bodies and a cluster at the ganglion midline (dashed line). Midline cluster contains cell bodies of the common inhibitor 1 (CI1) cell body and at least four DUM neurons. Dashed circle indicates position of presumed fifth DUM cell body. Arrow indicates neurite bundle of ventral anterolateral cell bodies and arrowhead marks sensory afferents that ramify close to midline (note also arrowheads in (c,d)). Brackets indicate levels of transverse sections shown in (c–f). **b:** Depth color-coded image of anterolateral cell cluster from (a). Depth encoded from dorsal to ventral as blue to red. **c–f:** Transverse sections taken at levels indicated in (a). Sections show positions of stained cell bodies and MN arborizations in dorsal and lateral neuropils. Arrowheads (c,d) mark several sensory afferents terminating in VAC. Scale bars=50 µm in a,c–f; 20 µm in b.

3.2.3. Nervus lateralis 3 (nl3)

Nervus lateralis 3 (nl3) innervates the extensor tibiae, the accessory levator and depressor trochanteris (Storrer et al., 1986). Within the trochanter nl3 joins the root of the femoral nerve F2 just after it originates from nerve ncr (Fig. 2.3a; Bässler, 1977a).

Backfills of nerve nl3 revealed up to 33 cell bodies distributed in three cell body clusters, two on the ipsilateral side and one medial (Fig. 3.18a). One cell cluster with at least 24 neurons is located anterolaterally between the origin of na and the anterior ipsilateral connective (Fig. 3.18a,b,e). The large and ventral cell body (diam. 43–54 µm) in this group belongs to the fast extensor tibiae (FETi) MN that was electrophysiologically identified by Bässler and Storrer (1980). FETi is surrounded by a large number of small neurons (diam. 10–18 µm). Their function in stick insects is still unknown, but they are probably strand receptors, the only sensory neurons in insects known with central cell bodies, as described for the locust (Bräunig and Hustert, 1980; Bräunig, 1982b). The primary neurites of these receptors travel in a curve and apart from the FETi primary neurite to the nl3 nerve root (Fig. 3.18a, dashed yellow lines) with few arborizations terminating in medioventral ganglion regions. The second cell body cluster is located anterior of the origin of the lateral nerves and it contains seven neurons (Fig. 3.18a,c,f). The largest cell body in this group (diam. 43-50 µm) is the slow extensor tibiae (SETi; Bässler and Storrer, 1980). The diameters of the smaller neurons range between 13–25 µm. The characteristics of FETi's and SETi's neurites will be described below when neurons stained by backfilling nerve F2 are described (Fig. 3.23). The last cell body cluster is located posterior at the ganglion midline and it contains the ventral located CI1 and one DUM neuron (Fig. 3.18a,d,g,h).

Numerous sensory afferents from dorsal and ventral coxal hair plates (HP) enter the ganglion through nerve nl3. Schmitz et al. (1991) described their appearance in a dorsal view as a broad 'A' with its base located medially (Fig. 3.18a, solid blue line). Within the ganglion these afferent fibers project to four discrete target areas termed rostro-dorso-lateral terminal area (rdl), rostro-ventro-intermediate terminal area (rvi), caudo-ventro-intermediate terminal area (cvi), and caudo-dorsal-lateral terminal area (cdl) (Schmitz et al., 1991). Afferents terminating in the cvi and cdl areas form two bundles termed intermediate longitudinal bundle (ilb) and lateral longitudinal bundle (llb) (Schmitz et al., 1991). In the target areas the afferent fibers develop various bouton-like structures generally at their endings. Additionally, several ventrally running afferents were identified that terminate in a ventromedial neuropil region, in close proximity to the VAC. Another single sensory neurite that travels medially through an intermediate region, before reach-

ing the midline, bifurcates in an anterior and a posterior branch. The posterior branch descends through the ipsilateral posterior connective to the metathoracic ganglion (Fig. 3.18a, double arrows), and the anterior branch travels underneath the ventral intermediate tract (VIT) through the upper horseshoe neuropil (hN) (Fig. 3.18a,f, double arrowheads) to descend through the contralateral connective to the metathoracic ganglion (not shown). In contrast to Schmitz et al. (1991), few fibers were observed in transverse sections that terminate in the lateral part of the ventral association center (lVAC) (Fig. 3.18f).

3.2.4. Nervus lateralis 4 (nl4)

Nervus lateralis 4 (nl4) consists of three branches: branch A innervates the pleural and tergal depressors of the trochanter (DpTr), branch B supplies the sternal DpTr, and branch C the pleural remotors of the coxa (Fig. 2.2; Graham, 1985).
Staining of all nl4 side branches together revealed a maximum of 13 cell bodies organized in two clusters ipsilateral to the dyed nerve and on the ganglion midline. One cluster with up to nine neurons (diam. 25–60 µm) is located anterolaterally (Fig. 3.19a,b). Transverse sections and depth color-coded images show that two of these cell bodies are positioned dorsally and the remaining neurons more ventrally (Fig. 3.19b,d,e). Their primary neurite pathways, dendritic arborizations, and terminal areas are quite similar to those from neurons with axons in nerve nl2. The second cluster is located posterior at the ganglion midline and it contains three DUM neurons and the CI1 cell body (Fig. 3.19a,c,f).
In two whole-mounts four sensory afferents were observed that travel through the ventral neuropil to terminate in ventromedial and ventroposterior regions of the neuropil, the VAC (Fig. 3.19a,f, arrowheads).

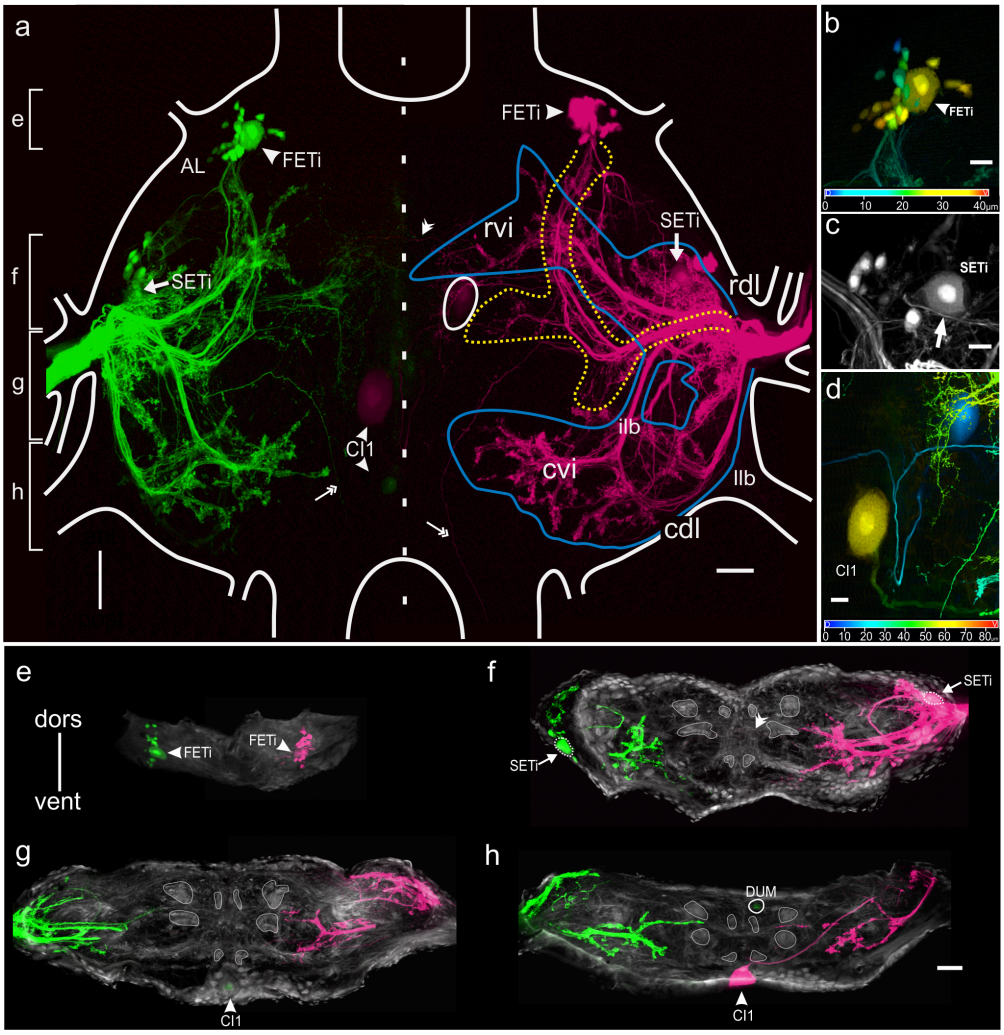

Figure 3.18. – **Backfill of nervus lateralis 3 (nl3). a:** Whole-mount of ganglion with bilaterally labeled nl3 nerves; fluorescein dextran (green), tetramethylrhodamine dextran (magenta). Brackets indicate levels of transverse sections shown in (e–h). In each hemiganglion an anterolateral cell cluster, consisting of the fast extensor tibiae MN (FETi; arrowheads) and up to 23 smaller cell bodies, was stained (see also (b)). Seven cell bodies including the slow extensor tibiae (SETi) were stained (arrows) close to the roots of lateral nerves. The CI1 cell bodies and a DUM cell (solid white circle) were labeled midline (dashed line). Dashed yellow lines accentuate the fiber bundle and arborizations of the small anterolateral cell body neurites. Double arrowhead marks a neurite that projects through the horseshoe neuropil (hN; note also (f)). Double arrows indicate neurites that descend to the metathoracic ganglion. Solid blue line marks sensory afferents of coxal HPs and prominent fiber bundles (for abbreviations, see text). **b:** Depth color-coded image of fluorescein dextran filled anterolateral neurons in (a) shows FETi's cell body ventrally surrounded by small neurons (note also (e)). Depth encoded from dorsal to ventral as blue to red. **c:** Projection view of the green colored lateral cell body group in (a) shows SETi's cell body with primary neurite (arrow) and six cell bodies. **d:** Depth color-coded projection of midline cell bodies reveals ventral CI1 (yellow) and a DUM cell (blue). **e–h:** Transverse sections of bilaterally labeled nl3 nerves. Sections taken at levels indicated in (a). Double arrowhead indicates a neurite that projects through hN to the contralateral side to descend through contralateral posterior connective to the metathoracic ganglion. Scale bars=50 µm in a,e–h; 20 µm in b–d.

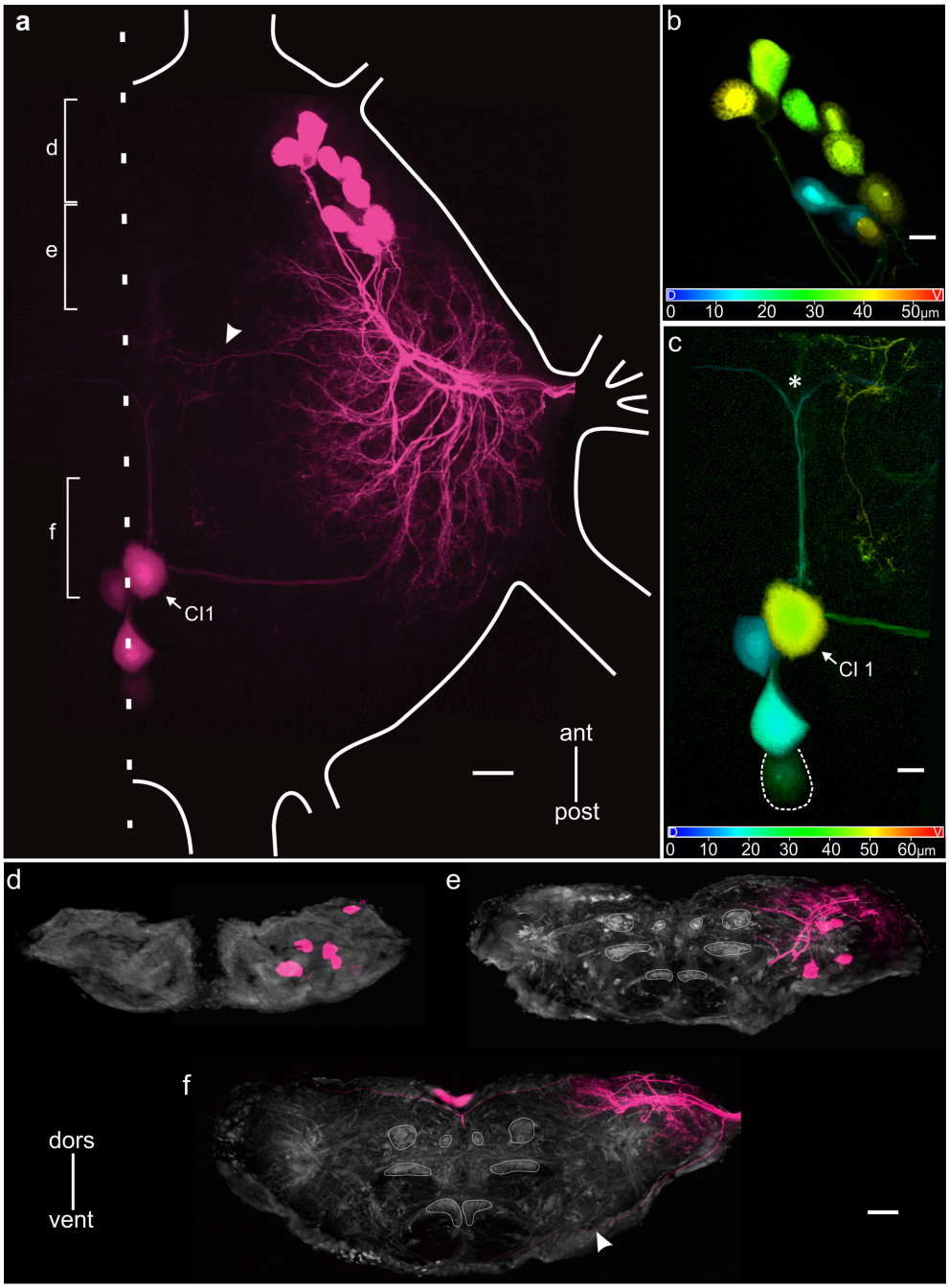

Figure 3.19. – **Backfill of nervus lateralis 4 (nl4). a:** Whole-mount with an anterolateral cluster with nine cell bodies and a second neuron group at the ganglion midline (dashed line) were labeled. Midline cluster contains CI1 cell body (arrow) and three DUM cells. Arrowhead marks sensory afferents that ramify close to midline (note also arrowhead in (f)). Brackets indicate levels of transverse sections shown in (d–f). **b:** Depth color-coded image of the anterolateral cell cluster in (a). Two cell bodies (blue) are dorsally situated (note also (e,f)). Depth encoded from dorsal to ventral as blue to red. **c:** Depth color-coded image of midline cell bodies in (a) shows the ventral position of CI1 (greenish yellow) and three DUM cells (blue). Dashed white circle marks a weakly stained DUM cell; asterisk indicates DUM neurite T-junction. **d–f:** Transverse sections were taken at the levels indicated in (a). Sections show the positions of cell bodies and cell body arborizations only in dorsal and lateral neuropils. f: Arrowhead marks sensory afferents terminating in the VAC. Scale bars=50 µm in a,e,f; 20 µm in b,c.

3.2.5. Nervus lateralis 5 (nl5)

Nervus lateralis 5 (nl5) is the first branch of ncr and it innervates the tergal remotors (Marquardt, 1940) which were renamed retractor coxae (Bässler, 1983; Graham, 1985). The entire nl5 consists of three branches: branches A and B innervate the tergal retractor coxae muscles (1t-cx, 1at-cx, and 2t-cx), and branch p supplies the sternal remotor (3st-cx) and the adductor coxae (2st-cx; Fig. 2.2; Graham, 1985).

Backfills of all nl5 side branches together revealed up to 31 cell bodies distributed in three posterior cell clusters, two of which are ipsilateral to the dyed nl5 and one at the ganglion midline, except for one to two cell bodies (diam. 10–40 µm) localized in the anterolateral ganglion region (Fig. 3.20a, asterisks). The first cell group with up to 18 cell bodies (diam. 13–50 µm) is located posterolateral, near the ncr root (Fig. 3.20a,b,f,g). Due to their cell body positions within the cortex the formation was termed the posterolateral cell cluster (PL). Medial to the PL group resides the posteroventromedial cluster (PVM) with up to seven neurons (diam. 20–30 µm; Fig. 3.20a). The depth coded image (Fig. 3.20b) and transverse sections (Fig. 3.20f,g) show that these cell bodies are slightly more ventrally positioned in comparison to the PL cell bodies. Almost all primary neurites of neurons of both groups form two dense and separate bundles that ascend dorsally where they unite and then travel together in a broad neurite band to the root of ncr. Within the dorsal neuropil extensive ramifications of higher-order branches occur that spread over the anterior, lateral, and posterior ganglion regions, descending into slightly deeper ganglion layers. The third cell cluster is located at the ganglion midline and it contains the CI1 cell body and at least five DUM neurons, but I am certain that a total of six DUM cells can be stained via all nl5 branches (see below and Fig. B.2 in the appendix). Noticeable are also several fine branches arising just after the CI1 primary neurite leaves the cell body (Fig. 3.20f, arrow). They travel dorsally in the direction of the DUM cell bodies and slightly lateral toward the dorsal intermediate tracts (DIT). Similar secondary CI1 neurites were also found at CI1 in meso- and metathoracic ganglia of locusts (Burrows, 1973; Watson et al., 1985).

The arrowheads in Fig. 3.20a,e,f indicate several sensory afferents that travel ventrally through the posterior ganglion region followed by a turn in slightly anterior direction to ramify and to terminate in the VAC. Such a projection pattern of sensory fibers was shown by Schmitz et al. (1991) for single tactile hairs on the stick insect trochanter.

Through separate backfills of nl5 branches A, B, and p, stained cell bodies could be related to the PL and/or PVM cluster. Stainings through branch nl5A revealed

12 cell bodies, with seven of them located within the PL cluster and five cell bodies at the ganglion midline, including CI1 and four DUM neurons (not shown). Whole-mounts of nl5 branch B revealed up to 16 cell bodies in the PL group and one neuron in the PVM cluster (not shown). Interestingly, 17 cell bodies were labeled by backfills of nl5 branches A and B together (Fig. B.2 in the appendix); in addition, the CI1 cell body and up to six DUM neurons could be detected (Fig. B.2). Backfills of branches A and B together and of branch B alone revealed the same neuron pool sizes. This observation might indicate that neurons innervating the tergal retractor coxae (1t-cx) have also axons through side branch B that supplies the remaining two tergal retractors (1at-cx and 2t-cx). Retrograde labeling of the nl5 branches A and B on the same ganglion side with different fluorescent dyes revealed that up to six cell bodies were labeled with both dyes and confirmed the observation (Fig. 3.20hi–hiii). Stainings of branch nl5p alone show that six cell bodies are located in the PVM cell group, two cell bodies in the PL cluster and the CI1, and up to two DUM cells were identified at the ganglion midline (Fig. B.3 in the appendix). The one to two anterolateral cell bodies occur only in whole-mounts in which all nl5 branches were backfilled together or in a preparation where a single p branch was filled. It is unclear if axons of these cell bodies run through the p branch or if their appearance was caused by dye contamination due to damaging other side nerves or nerve connections. Furthermore, in a single whole-mount in which the nl5 branches A and B were backfilled together almost all primary neurites of neurons of both groups form two dense and separate bundles that ascend dorsally where they unite and then travel together in a broad neurite band to the root of ncr. In the ventral ganglion region a sensory neurite can be observed that does not terminate in the VAC, but instead leaves the ganglion through the anterior ipsilateral connective to the prothoracic ganglion (Fig. B.2).

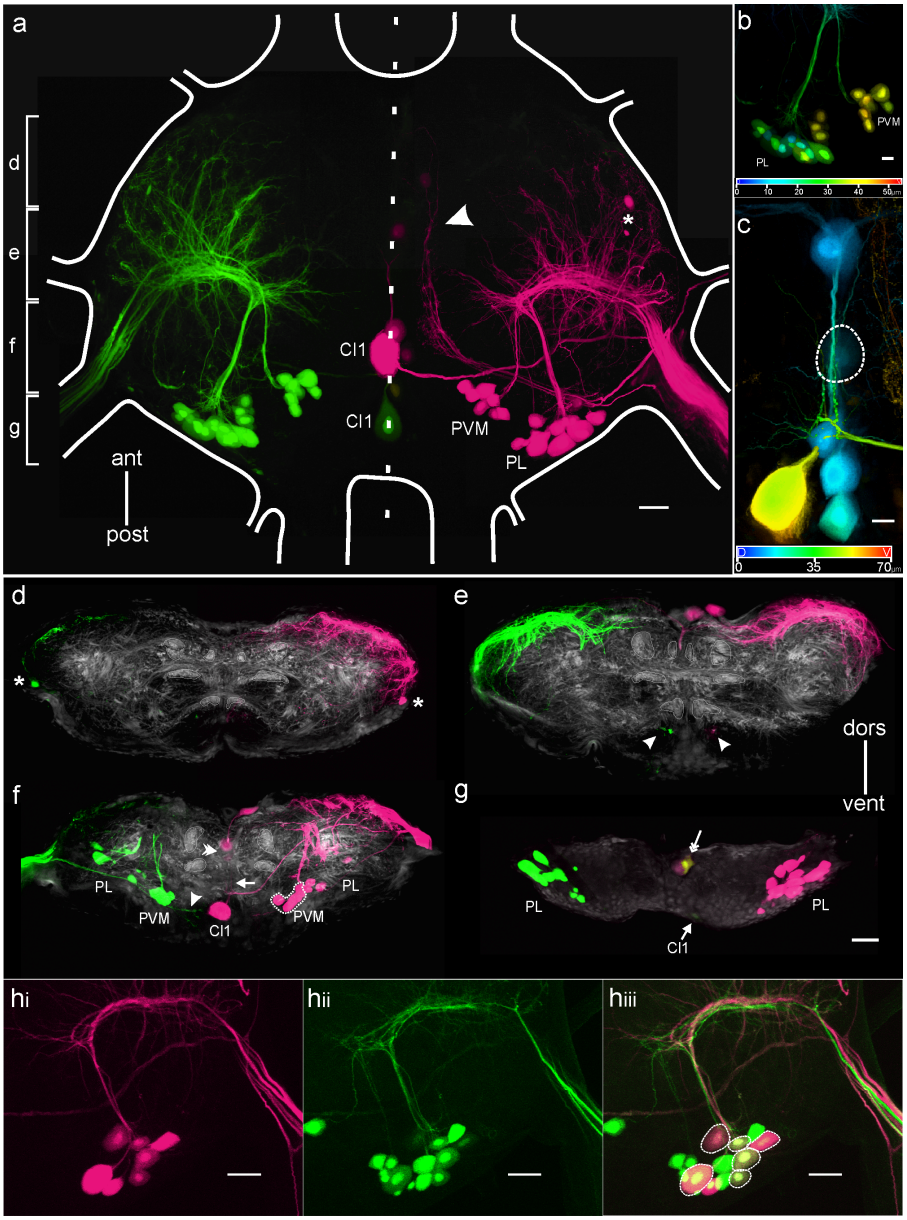

Figure 3.20. – **Backfill of nervus lateralis 5 (nl5). a:** Whole-mount of ganglion with bilaterally dyed nl5 nerves; fluorescein dextran (green), tetramethylrhodamine dextran (magenta). Brackets indicate levels of transverse sections shown in (d–g). In each hemiganglion two posterior cell body clusters were stained, the posterolateral (PL) and posteroventromedial (PVM) cluster. A third neuron group is located midline (dashed line) and consists of five DUM cells and the CI1 cell body. Two small and anterolaterally stained cell bodies were marked by an asterisk (note also asterisks in (e)). Arrowhead indicates several sensory afferents (note arrowheads in (e,f)). **b:** Depth color-coded image of the fluorescein dextran dyed neurons in (a) shows that the PL cell body cluster is more ventrally located than PVM. Depth encoded from dorsal to ventral as blue to red. **c:** Depth color-coded image of midline cell bodies reveals ventral CI1 cell body (yellow) and five DUM cells (blue). **d–g:** Transverse sections show positions of the different cell body clusters. The PVM cluster in (f) is indicated by a dashed line. MN arborizations occur only in dorsal and lateral neuropils. Asterisks in (d) mark the anterior labeled small cell bodies; arrowheads in (e,f) point to sensory afferents terminating in the VAC. f: DUM cells (double arrowhead) appear to be within the ganglionic core due to projecting all optical slices on a single plane. Arrow marks fine secondary branches arising from CI1s primary neurite. g: A DUM cell (double arrow) was double-labeled through bilateral staining of nl5. **hi–iii:** Ipsilateral staining of nl5 branches A and B with different fluorescent dyes shows six double-labeled cell bodies (dashed circles; hiii). This might indicate that neurons innervating the tergal retractor coxae (1t-cx) have also axons through nl5 branch B that supplies the remaining tergal retractor muscles (1at-cx and 2t-cx). Scale bars=50 µm in a,d–f,hi–iii; 20 µm in b,c.

3.2.6. Coxa branch 1 (C1) of nervus cruris (ncr)

Nerve C1 innervates the levator trochanteris muscle (Marquardt, 1940).
Backfills of nerve C1 revealed up to 15 cell bodies located in three distinct ipsilateral regions and at the ganglion midline (Fig. 3.21a). In the anterolateral region eight cell bodies (diam. 21–46 µm) are located. Anterior of the origin of the lateral nerves seven cell bodies are clustered laterally and in most whole-mounts two cell bodies appear slightly separated from the rest (Fig. 3.21a,b, asterisk). Anterior of the lateral cell group an additional single cell body was identified (Fig. 3.21a,b, arrowhead). The primary neurites of five cell bodies localized in the lateral cell cluster form a prominent bundle that ascends dorsally in medial direction followed by a hairpin turn to travel to the root of ncr. The primary neurite of the anterior single cell body and the two remaining primary neurites of the lateral stained neurons join the main bundle at the neurite hairpin turn (Fig. 3.21b, arrow) to travel within the same tract to the ncr nerve root. The second neuron group is located posterolaterally and it contains three cell bodies (Fig. 3.21a,c). Their positions are similar to that of the nl5 PL neurons and their primary neurites appear to run through the same tract. The smallest neuron in the PL cell group is probably a MN that supplies the levator stretch receptor muscle (LvSR; Schmitz and Schöwerling, 1992). The third cell cluster was located at the ganglion midline and it contains the CI1 neuron and up to three DUM cells (Fig. 3.21d).
Furthermore, several sensory afferents were stained through nerve C1 (Fig. 3.21a,g). The projection pattern and terminating areas of those fibers are comparable to sensory afferents from coxal HPs in whole-mounts of the nl3 (Fig. 3.18a, solid blue line).

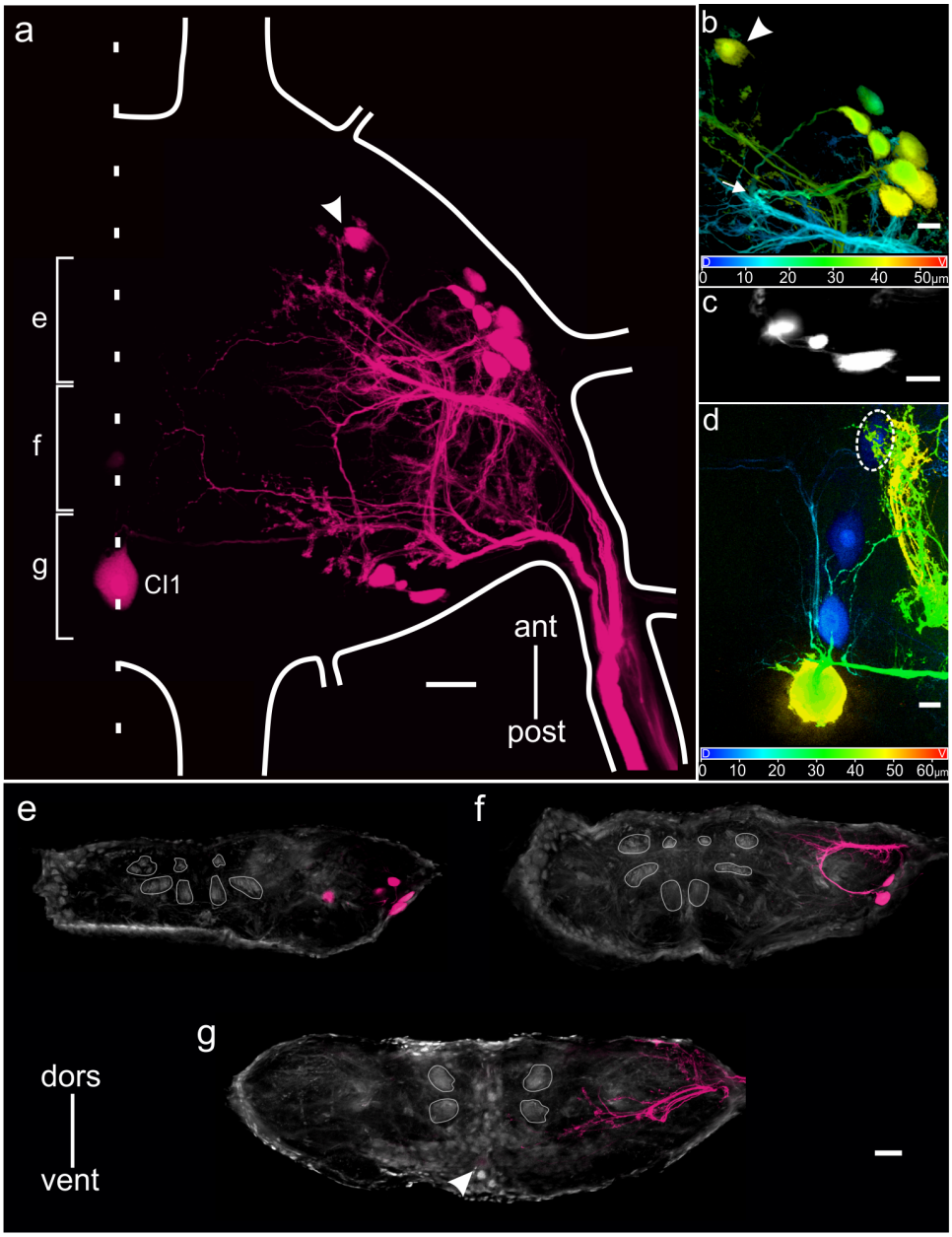

Figure 3.21. – **Backfill of coxa branch 1 (C1) of ncr.** **a:** Whole-mount with three different clusters of cell bodies and a more anterior positioned cell body (arrowhead). One cluster with seven cell bodies is located near the lateral nerve roots, one posterolateral (PL) cell group with three neurons, and four cell bodies at the midline (see also (d)). Brackets indicate levels of transverse sections shown in (e–g). **b:** Depth color-coded image of the nerve origin cell cluster in (a) shows intermediate and ventral distribution of cell bodies (note also (e,f)). Arrow marks turning point of primary neurites. Depth encoded from dorsal to ventral as blue to red. **c:** Single image of the PL cluster shows three cell bodies. The smallest cell body is possibly a MN that innervates the levator stretch receptor muscle. **d:** Depth color-coded image of the midline neurons in (a) shows the ventral position of CI1 (greenish yellow) and three DUM cells (blue). Dashed white circle marks a DUM cell that is masked by sensory afferents. **e–g:** Transverse sections show the positions of cell bodies, the occurrence of MN arborizations only in the dorsal and lateral neuropil. Sensory afferents terminate in dorsolateral, intermediate, and ventral parts of the ganglion. Scale bars=50 µm in a,e–g; 20 µm in b–d.

3.2.7. Coxa branch 2 (C2) of nervus cruris (ncr)

Nerve C2 supplies the posterior coxal depressor trochanteris (Marquardt, 1940). Retrogradely labeled C2 revealed at least seven cell bodies ipsilateral to the dyed nerve and at the midline. In the anteroventrolateral region a large cell body (diam. 52–66 µm) is located that belongs to the fast depressor trochanteris MN (FDTr; Fig. 3.22a; Schmitz, 1986). The primary neurite of the FDTr neuron ascends dorsally in a posterior direction until it bends towards the ncr origin. Close to FDTr's cell body several secondary neurites and higher-order branches ascend dorsally or remain within the ventrointermediate neuropil area (Fig. 3.22c). Extensive arborizations were stained in the dorsal neuropil (Fig. 3.22d). In a posteromedian position at least six cell bodies were labeled (Fig. 3.22a,b). At the ganglion midline the ventral CI1 and two DUM cells were stained. In one whole-mount a third cell body was labeled that is likely a DUM cell but typical secondary (lateral) DUM neurites could be clearly related to two DUM neurons only (Fig. 3.22b, arrowheads). In a posteromedial position three cell bodies were stained (Fig. 3.22a,e), one of which is situated dorsally (diam. 40–57 µm) and was identified as the slow depressor trochanteris MN (SDTr; Schmitz, 1986). The remaining cell bodies (diam. 40–62 µm; Fig. 3.22a,e, arrows) are ventrally located in a position typical for common inhibitory neurons 2 and 3 (CI2 and CI3) that innervate the flexor tibiae and muscles of the tarsus and claw (Fig. 3.24; Fig. 3.25). Their appearances in backfills of nerve C2 come as a surprise because the depressor's only inhibitory input is thought to be the CI1 neuron (Schmitz, 1986).
In addition to MNs, nerve C2 carries axons of sensory afferents with a similar but less prominent projection pattern as coxal HP afferents in backfills of the nerves nl3 (Fig. 3.18a, solid blue line) and C1 (Fig. 3.21a).

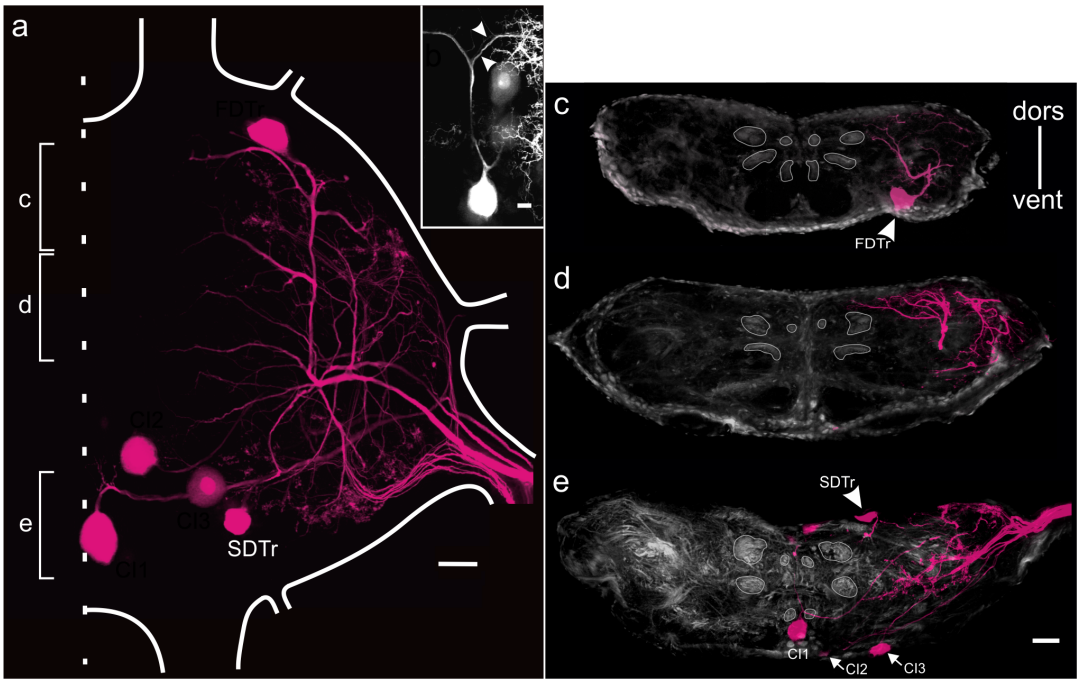

Figure 3.22. – **Backfill of coxa branch 2 (C2) of ncr. a:** Whole-mount shows anterolaterally the fast depressor trochanteris MN (FDTr) and four large cell bodies in the posteromedial ganglion region, including CI1 and the slow depressor trochanteris (SDTr; note also (e)). Brackets indicate levels of transverse sections shown in (c–e). **b:** Projection view of the posterodorsal ganglion region at the midline (dashed line) shows three DUM cells but only two lateral DUM neurites (arrowheads). **c–e:** Transverse sections show the ventral position of the FDTr (c), CI1 and of the two large posteromedially stained cell bodies (arrows in (e)), and the dorsal location of the SDTr cell body (e). Several sensory afferents terminating in the dorsolateral, intermediate, and ventral neuropil (e) similar to coxal HP afferents labeled through nerve nl3 (Fig. 3.18). Scale bars =50 µm in a,e–g; 20 µm in b–d.

3.2.8. Femoral branch 2 (F2) of nervus cruris (ncr)

As shown in Fig. 2.3a, nerve F2 originates from ncr just distal to the fusion of nl3 and ncr (Bässler, 1977a). This anatomical feature leads to the situation that axons of extensor tibiae MNs (FETi, SETi, and CI1) traveling within nl3 are also running through F2.

Whole-mounts of retrogradely labeled F2 nerves revealed up to six cell bodies located in three ipsilateral and posteromedial ganglion regions (Fig. 3.23a). The large anteroventrolaterally located soma (diam. 46–60 µm) belongs to the fast extensor tibiae MN (FETi; Bässler and Storrer, 1980; Fig. 3.23a,b), whereas the slightly smaller slow extensor tibiae MN (SETi; diam. 42–52 µm; Bässler and Storrer, 1980) is located ventrolateral and anterior of the lateral nerve roots (Fig. 3.23a,c). In the posteromedian ganglion portion CI1 and up to three DUM cell bodies were labeled (Fig. 3.23a, marked with dashed circles). Clearly observable are the

pathways of FETi's and SETi's primary neurites and their dendritic branches in the depth color-coded hemiganglion (Fig. 3.23a) and also in transverse sections (Fig. 3.23b–e). FETi's primary neurite ascends dorsally with a posterolateral course to the root of nerve nl3. Three large dendritic branches arise in the anterolateral-intermediate ganglion region just after FETi's primary neurite left the cell body. The first second-order branch descends slightly in a posterolateral course to branch out in finer dendrites which dive into the ventral neuropil (Fig. 3.23a,b). The second large branch proceeds posterolaterally where minor branches occur that terminate in dorsolateral-intermediate neuropil regions, close to SETi's cell body (Fig. 3.23a,b). The third branch emerged nearby the second branch and it ascends dorsally in a posterolateral direction to arborize in several finer dendrites that terminate in medial, posterior, or lateral parts of the dorsal neuropil (Fig. 3.23a,b). Further higher-order dendritic branches arise during FETi's curved primary neurite pathway to the nl3 nerve trunk and they course to anterior, medial, and posterior regions of the dorsal neuropil (Fig. 3.23a,c). SETi's primary neurite ascends medially to the dorsal neuropil where it performs a hairpin loop (Fig. 3.23a, asterisk) to travel slightly dorsally of FETi's primary neurite to the origin of nerve nl3 (Fig. 3.23c). Just after SETi's primary neurite leaves the cell body several minor dendritic branches occur that terminate mainly in anteroventrolateral and anterolateral-intermediate neuropil areas (Fig. 3.23a,c). Within the dorsal neuropil higher-order dendritic branches appear that spread in anterior and posterior direction (Fig. 3.23a). The dendritic fields of both SETi and FETi dendrites extend over the posterodorsal ganglion region (Fig. 3.23a).

The axons of MNs leave the ganglion via nerve nl3, whereas at least 20 axons of sensory cells that were found in nerve F2 enter the ganglion through ncr. In whole-mounts and transverse sections two prominent projections of sensory afferents can be observed. The projection pattern of same afferents is similar to but less prominent than that of coxal HP afferents in nerve nl3 (Fig. 3.18a, solid blue line), C1 (Fig. 3.21a), and C2 (Fig. 3.22a) backfills. The remaining sensory afferents enter the ganglion as a compact bundle that bifurcates just after entry. Fibers of one bundle run in an anteroventrolateral direction (Fig. 3.23a, double arrow) to terminate near nerve roots nl2–4, whereas the remaining fibers continue to travel ventromedially followed by a bend in slightly anterior direction to expand and terminate in the VAC (Fig. 3.23, arrowheads). The identity of these afferents is not clear.

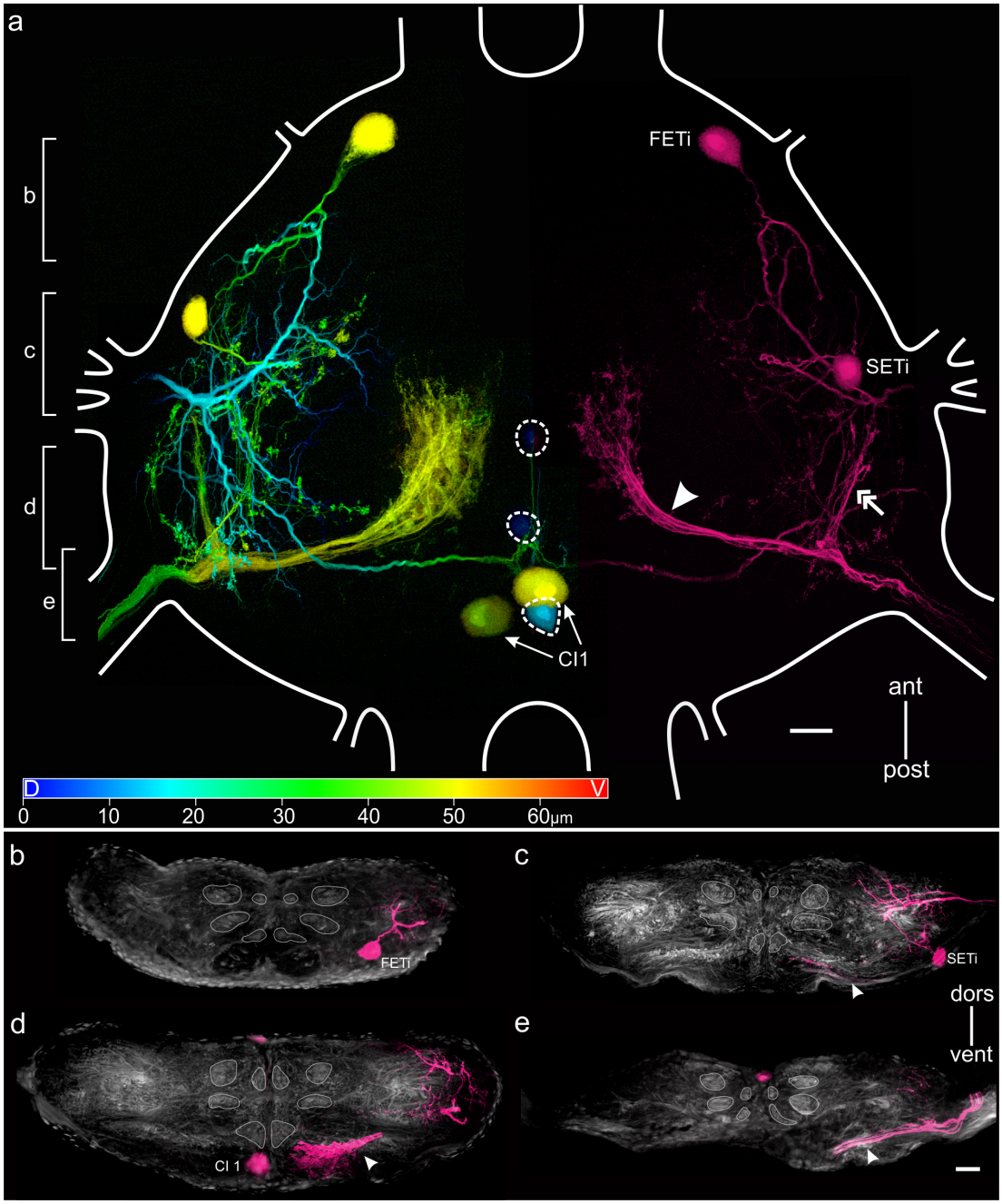

Figure 3.23. – **Backfill of femoral branch 2 (F2) of ncr. a:** Whole-mount of ganglion with bilaterally labeled F2 nerves; depth color-coded hemiganglion (left side). The fast extensor tibiae (FETi) cell body is situated anteroventrolaterally, the slow extensor tibiae (SETi) is ventrally located near the lateral nerves (note the loop in SETi's primary neurite, asterisk). In the posteromedian ganglion region two CI1 neurons and three DUM cells (dashed white circles) were labeled. A compact bundle of sensory afferents enter the ganglion through ncr. Few fibers run ventrally in an anterior direction (double arrow) to terminate laterally. The remaining fibers travel ventrally to the VAC (arrowhead and arrowheads in (c–e)). Brackets indicate levels of transverse sections shown in (b–e). Depth encoded from dorsal to ventral as blue to red. **b–e:** Transverse ganglion sections taken from two different whole-mounts at the level indicated in (a). FETi neurite arborizations occur in ventral and lateral neuropil regions (b), few higher-order branches arise before the axon leaves through nerve nl3 (c). SETi's primary neurite possesses arborizations similar to FETi neurites but they are not distinctive in anterolateral ganglion parts. Arrowheads indicate sensory afferents terminating and ramifying in the VAC. Scale bars=50 µm.

3.2.9. Flexor tibiae branches of nervus cruris (ncr)

In nine whole-mount preparations a minimum of 10 and a maximum of 29 cell bodies were stained. In the anterolateral region eight to 25 cell bodies (diam. 16–70 µm) are located mainly in ventral and intermediate ganglion regions except for one to two cell bodies that are localized more dorsally (Fig. 3.24b,d,e). Their primary neurites ascend in a compact bundle posteriorly with a slightly medial course. Below the mid-ganglion level they change course to project through the posterolateral ganglion portion into the ncr nerve root. At the point where the primary neurites bend toward ncr several dendritic branches arise that travel in medial direction to terminate nearby the ganglion midline (Fig. 3.24f,g). In posteromedial regions two to five neurons were stained (diam. 42–62 µm). Two large ventrally located cell bodies appeared in similar locations as two cell bodies labeled by backfilling nerve C2 (Fig. 3.22) and nerves F4 and F5 (Fig. 3.25a,c). These neurons are probably common inhibitory neurons 2 and 3 (CI2 and CI3). In four whole-mount preparations one to three DUM cells were weakly labeled (diam. 43–57 µm; Fig. 3.24c). Furthermore, various sensory afferents enter the ganglion through nerve ncr. In the ganglion two prominent fiber bundles can be distinguished that run parallel (Fig. 3.24a). Afferents of one bundle run in a tract with a slightly anteromedial orientation. The afferents of the second bundle proceed in posteromedial direction (Fig. 3.24a). Besides these bundles, after entering the ganglion, several fibers turn anterolaterally and terminate in the ventrolateral-intermediate neuropil, mainly the horseshoe neuropil and the lateral part of the VAC (Fig. 3.24f,g). In addition, transverse sections show afferent fibers that ascend after ganglion entry to terminate in dorsolateral-intermediate neuropil regions (Fig. 3.24e–g; asterisks). Other fibers within the posteromedial bundle continue to run ventromedially. Some of these fibers branch off in anterior direction to converge with anteromedial traveling afferents. The remaining afferents of both bundles proceed medially to project into the horseshoe neuropil before reaching the ganglion midline (Fig. 3.24f,g; arrowheads). Few whole-mount preparations showed a third bundle of afferents which run centered between the antero- and posteromedial fiber bundle to bifurcate before reaching the midline to project again into intermediate neuropil regions (not shown).

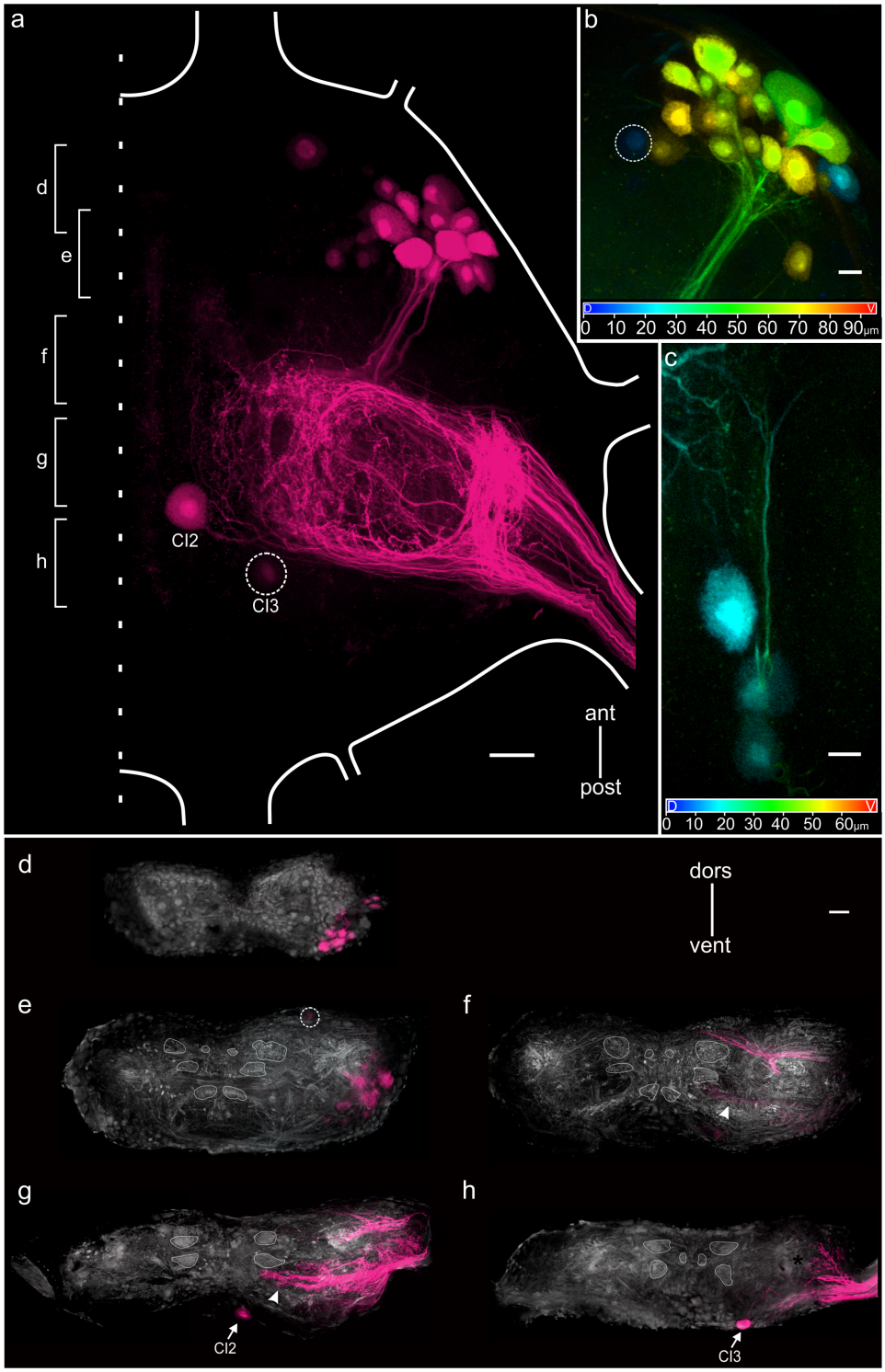

Figure 3.24. – **Backfill of flexor tibiae branches of ncr. a:** Whole-mount shows distinct anterolateral cell cluster and close to the midline (dashed line) cell bodies of the common inhibitory neurons CI2 and CI3 (dashed circle). Brackets indicate levels of transverse sections shown in (d–h). **b:** Depth color-coded image of the AL cell cluster of a different whole-mount shows 24 cell bodies distributed in ventral, intermediate, or dorsal ganglion regions (see also (d,e)). One dorsally situated and weak stained neuron was marked by a dashed circle. Depth encoded from dorsal to ventral as blue to red. **c:** Depth color-coded image of the dorsomedian ganglion region shows three DUM cell bodies and DUM T-junction (asterisk). **d–h:** Transverse sections taken from three different whole-mounts at levels indicated in (a). Cell bodies and primary neurite arborizations occur only in dorsal and slightly intermediate ganglion regions (f,g). One weakly and dorsally stained cell body in (e) was surrounded by a dashed circle. Arrows point at CI2 and CI3 cell bodies and arrowheads in (f,g) mark sensory afferents terminating in the horseshoe neuropil (hN). Note afferents that terminate in dorsolateral-intermediate parts of neuropil (asterisk; (g,h)). Scale bars=50 µm in a,d–h; 20 µm in b,c.

3.2.10. Femoral branches 4 and 5 (F4/5) of nervus cruris (ncr)

Nerves F4 and F5 supply the femoral retractor unguis I (RUI) muscle, the first of three muscles parts that share a common apodeme to flex the claw (Bässler, 1983; Radnikow and Bässler, 1991).

Backfills of nerves F4 and F5 were always performed together and revealed three to nine cell bodies distributed in two ganglion parts. A cell cluster of three to six cell bodies (diam. 23–60 µm) is located anterolaterally (Fig. 3.25a,b). Their primary neurites ascend posteromedially to the dorsal neuropil where dendritic branches occur that project to anterior, posterior, and medial regions of the neuropil. In the posteroventromedial region two large cell bodies (diam. 43–63 µm) were labeled in six (out of eight) preparations at the locations of the common inhibitory (CI2 and CI3; Fig. 3.25a,c) neurons that were also stained through the flexor branches of ncr. In three whole-mounts one to two DUM neurons (diam. 43–54 µm) were labeled at the ganglion midline (Fig. 3.25c).

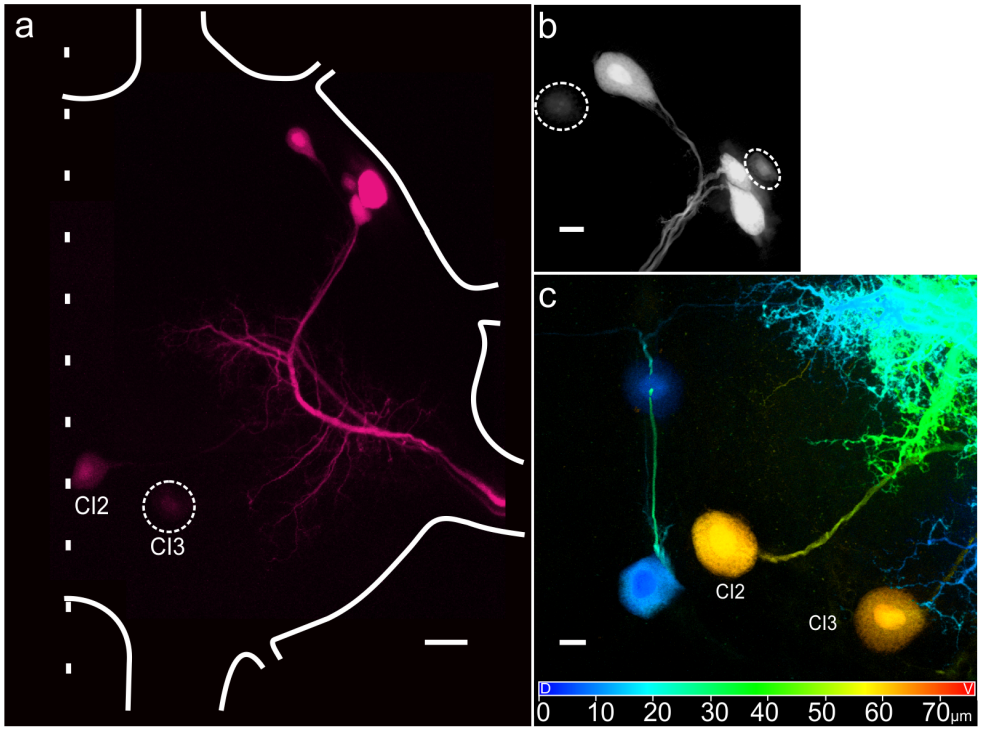

Figure 3.25. – Backfill of femoral branches 4 and 5 (F4 and F5) of ncr. a: Whole-mounts with cell bodies labeled anterolaterally and close to ganglion midline cell bodies of the common inhibitory neurons CI2 and CI3 (dashed circle). **b:** Projection view of the anterolateral cell cluster of a different preparation shows three heavily and two weakly labeled cell bodies (dashed circles). **c:** Depth color-coded image of posterior ganglion region shows CI2, CI3, and two DUM cells (blue) in ventral and dorsal positions, respectively. Depth encoded from dorsal to ventral as blue to red. Scale bars=50 µm in a, 20 µm in b and c.

3.2.11. Nervus unparis (nup)

Nervus unparis (nup) leaves through the dorsal ganglion surface (Fig. 2.3a) to split soon in two side branches (nervi transversi) that branch out further (Marquardt, 1940). One branch supplies intersegmental lateral muscles, whereas the other branch joins nervus posterior (np) of the mesothoracic ganglion and nerve na of the metathoracic ganglion (Marquardt, 1940).
Backfills of nerve nup revealed at least 14 to 15 cell bodies situated in three different posterior ganglion portions (Fig. 3.26d). In the posteroventromedial ganglion region up to five cell bodies (diam. 13–40 µm) were labeled but only four of them were found in most whole-mounts. These cell bodies are usually arranged in pairs on the left and right hemiganglion, respectively (Fig. 3.26f). The remaining cell bodies were stained in two posterodorsolateral cell clusters on both ganglion sides; each group contains up to five small neurons (diam. 18–36 µm; Fig. 3.26d and e). Noticeable are also two neurites that emerged close to the root of nup to travel through both anterior connectives to the prothoracic ganglion. In one preparation another neurite was labeled that runs through the entire hemiganglion to leave the ganglion via the anterior and posterior connectives with a side branch leaving through nerve np (Fig. 3.26d). Due to the symmetrical staining pattern it is most likely that such a neurite is also found in the other ganglion portion but this was never observed in any preparation.

3.2.12. Nervus posterior (np)

One side branch of nerve np supplies ventral longitudinal muscles and a second branch joins nup and the nerve na of the metathoracic ganglion (Marquardt, 1940). Backfills of nerve np revealed at least 18 mid-sized and small cell bodies (diam. 6–50 µm) localized ipsi- and contralateral in posterior ganglion regions (Fig. 3.27a). Almost all neurons are ventrally positioned except for a large dorsomedially stained neuron. In two preparations a neuron occurred that lies on the contralateral ganglion side anteroventrolaterally (not shown). Furthermore, two neurites were found in one whole-mount that ascend through both anterior connectives to the prothoracic ganglion similar as described above for a nup backfill (Fig. 3.27a, arrowheads). Again, another neurite was stained in a whole-mount that descends ipsilaterally through one posterior connective (not shown).

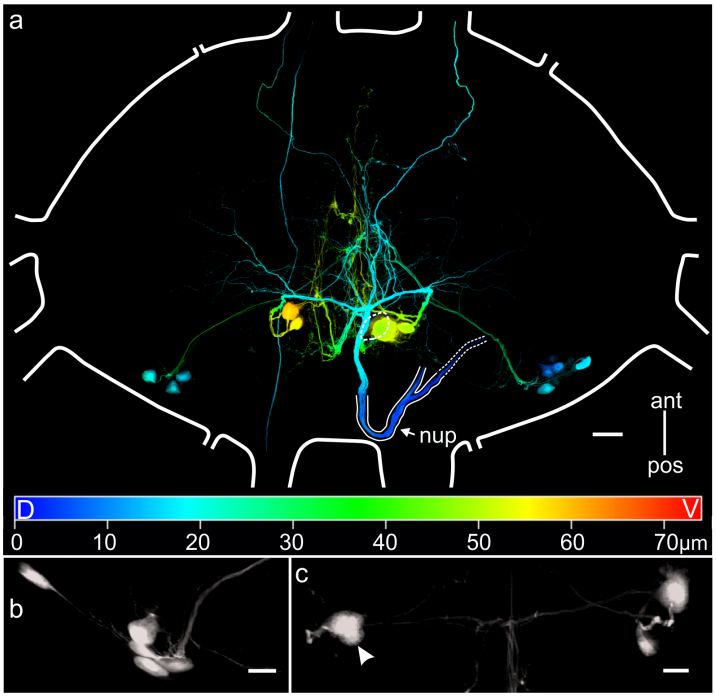

Figure 3.26. – **Backfill of nervus unparis (nup).** a: Depth color-coded whole-mount shows cell bodies in posteroventromedial regions and posterodorsolaterally on both ganglion sides. Depth encoded from dorsal to ventral as blue to red. **b:** Projection view of the lateral cell cluster of a different whole-mount shows clearly five small cell bodies. **c:** Projection view of posteroventromedial cell bodies as observed in most whole-mounts. Arrowhead marks a masked cell body. Scale bars=50 µm in a; 20 µm in b,c.

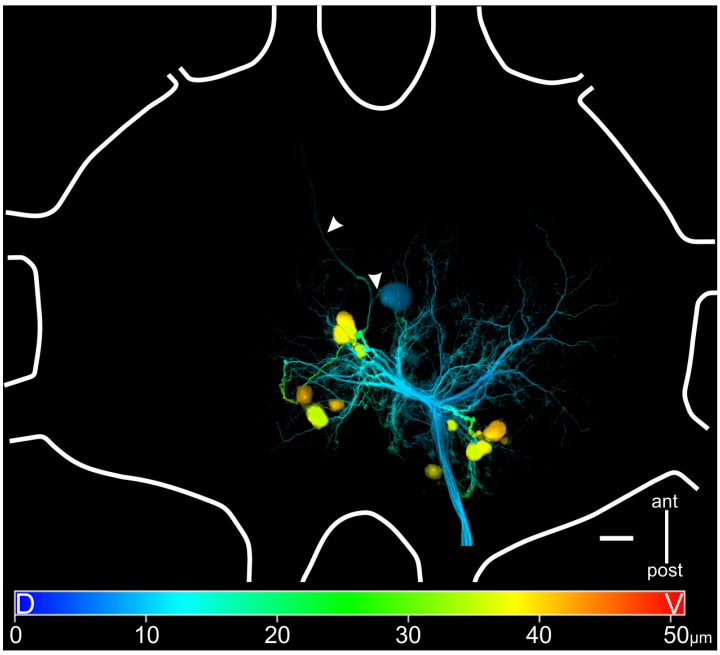

Figure 3.27. – **Backfill of nervus posterior (np).** Depth color-coded whole-mount shows cell bodies mainly ventrally in a medial region. Arrowheads indicate two weakly labeled neurites that ascend through both anterior connectives to the prothoracic ganglion (entire neurite pathway not visible). Depth encoded from dorsal to ventral as blue to red. Scale bar=50 µm.

3.2.13. Backfill of all thoracic nerves (DUM neuron population)

Backfilling nerve roots usually labels DUM cells. Mentel et al. (2008) assume that at least nine DUM cells are located in the mesothoracic ganglion of stick insects. To determine the number of DUM neurons within the mesothoracic ganglion all thoracic nerves were backfilled together (except for nerve np). In whole-mounts seven to nine DUM cells were identified with all cell bodies (diam. 40–60 µm) in the dorsoposteromedian ganglion region, near the posterior crotch where the posterior connectives originate (Fig. 3.28a,b).

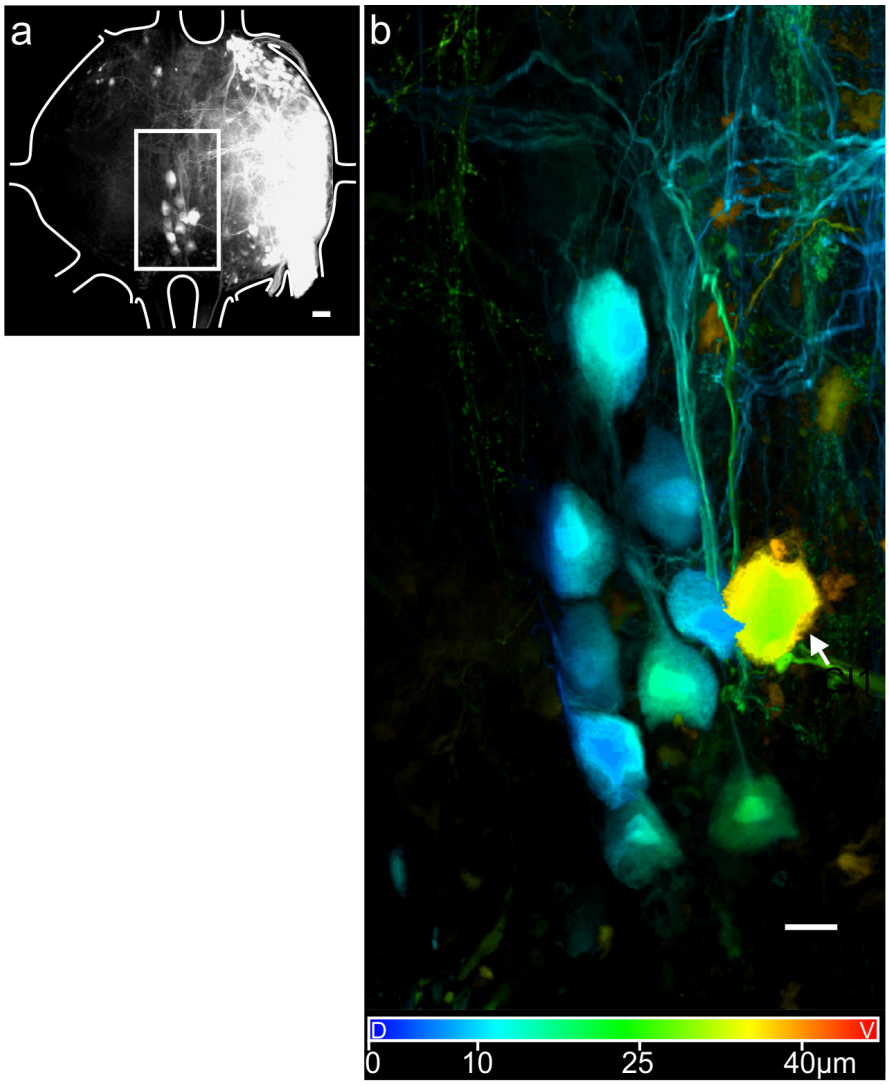

Figure 3.28. – DUM cells in the mesothoracic ganglion. a: Whole-mount with all thoracic nerves backfilled. **b:** Depth color-coded image of framed area in (a) shows cell bodies of nine DUM cells (blue and/or greenish blue) and CI1 (arrow). Scale bars=50 µm in a; 20 µm in b.

Table 3.3. – Summary of backfilled mesothoracic nerve roots, target muscles (see also Fig. 2.2), and numbers of stained neurons.

Nerve [1,2]	Branch	Muscle(s) and Abbreviations [1,2]	Number of stainings (N)	Motoneurons	DUM cells	Sensory neurons with a central cell body	Total number of stained neurons	Number of neurons published
Nervus anterior (na)	1 2	connection with np and nup of prothoracic ganglion, intersegmental muscles dorsal longitudinal, muscle of the heart	N=3	7-9	1		**9 (10)**	8 [5]
Nervus lateralis 2 (nl2)	A B C D all	pleuro-sternal (1p-st) tergo-pleural (t-p) ventilation muscles protractor coxae (1p-cx) tergo-trochantinal (t-tri)	N=6 N=6	6-9 + CI 1 12-17 + CI 1	1-4 4(5?)		**9-12** **22(23?)**	5-8 [4] 9 [5]
Nervus lateralis 3 (nl3)		accessory depressor trochanteris, accessory levator trochanteris, and extensor tibiae	N=6	8 + CI1	1	9-23	**33**	26–29 [5]
Nervus lateralis 4 (nl4)	A B C	pleural (p-tr) and tergal (t-tr) depressors of trochanter sternal (1st-cx) depressor trochanteris pleural (2p-cx) remoter coxae	N=7	8–9 + CI1	3		**13**	10 [5]
Nervus lateralis 5 (nl5)	A B p all	tergal retractor coxae (1t-cx) tergal retractors coxae (1at-cx and 2t-cx) sternal remotor (3st-cx), and sternal adductor (2st-cx)	N=4 N=3 N=2 N=6	7 + CI1 16-17 + CI1 8-9 + CI1 22-25 + CI1	4 4 2 5 (6)[1]		**12** **21-22** **11 (12)** **29 (31-32)**	3-8 [4] 18 [5]
Coxa branch 1 (C1)		levator trochanteris (3cx-tr), levator stretch receptor organ (LvSR) [8]	N=6	9-11 + CI1	3		**15**	9 [5]; 10 [6]
Coxa branch 2 (C2)		depressor trochanteris (2cx-tr)	N=7	4 + CI1	2 (3?)		**7 (8?)**	3 [5]; 3 [6]
Femoral branch 2 (F2)		extensor tibiae	N=5	2 + CI1	3		**6**	2 [3]; 3 [5]
Flexor branches of nervus cruris		flexor tibiae	N=9	8–25 + CI2 and CI3	0-3		**29**	12–18 [5]
Femoral branch 4 and 5 of nervus cruris		retractor unguis I (RUI)	N=8	3–7 (incl. CI2 and CI3)	1-2		**3-10**	3 [5]
Nervus unparis (nup)		intersegmental lateral muscles (isL1t-st; isL2-st)	N=5	9–14	-		**14 (15?)**	18 [5]
Nervus posterior (np)		ventral longitudinal muscles	N=5	11-18	-		**18**	18 [5]
All mesothoracic nerves			N=5		7-9			8 [7]

CI=common inhibitory neuron; DUM = dorsal unpaired median neuron. Numbers indicate maximum numbers of neurons stained in a single whole-mount.
Numbers in parenthesize indicate total number of neurons as estimated from different whole mounts. ? indicates uncertain estimate. [1]The sixth DUM neuron appeared in a single backfill of nl5 branches A and B (Fig. B.2).
[1] Marquardt, 1940; [2] Graham, 1985; [3] Bässler and Storrer, 1980; [4] Graham and Wendler, 1981; [5] Storrer et al., 1986; [6] Hess and Büschges, 1997; [7] Mentel et al., 2008; [8] Schmitz and Schöwerling, 1992.

3.3. *In situ* calcium imaging of retrogradely labeled mesothoracic retractor coxae neurons

Calcium ions (Ca^{2+}) play an important role in various neuronal processes, e.g., release of neurotransmitters or as 2nd messengers (e.g., Berridge, 1998; Augustine et al., 2003). In the stick insect, mesothoracic motoneurons (MN) receive tonic excitatory input during front leg stepping (Ludwar et al., 2005). The intracellular injection of the Ca^{2+} chelator BAPTA-1 into MNs decreased the amplitude of the tonic depolarization, indicating a possible role for Ca^{2+} in supporting the tonic depolarization (Westmark et al., 2009). Moreover, neuroanatomical data revealed that in the stick insect MN neurites are mainly found in dorsal ganglion regions, especially neurites of retractor coxae (RetCx) MNs that have axons in nervus lateralis 5 (nl5) (note sec. 3.2.5 or Fig. 3.20), and therefore are accessible for Ca^{2+} imaging studies. Besides, nerve nl5 has its origin close to the mesothoracic ganglion that is beneficial for short dye loading times and it carries a large number of 22-25 excitatory MNs (sec. 3.2.5 or Tab. 3.3).
The aim of this set of experiments was to determine whether Ca^{2+} imaging of retrogradely labeled neurons in the exposed but intact stick insect is feasible to investigate MN activity optically. This method could expand the current knowledge of the neuronal control of locomotion, particularly to gain more insights into the physiological properties and synaptic input sites of stick insect MN neurites. Here, first results of the developed methodological approach are presented which allows to investigate intracellular Ca^{2+} dynamics in a population of backfilled mesothoracic RetCx neurons *in situ*.

3.3.1. Pilocarpine-induced Ca^{2+} transients in RetCx neurons

Rhythmic activity in RetCx neurons was induced pharmacologically by the muscarinic acetylcholine (ACh) receptor agonist pilocarpine. From experiments in the crayfish, locust, and stick insect it is known that pilocarpine activates pre-motor networks, e.g., central pattern generating networks (CPGs), which elicit alternating rhythmic activity in antagonistic MN pools (Chrachri and Clarac, 1987; Ryckebusch and Laurent, 1993; Büschges et al., 1995). The induced motor output in stick insects share some similarities with the step-phase transitions during locomotion of intact animals (Büschges et al., 1995).

Pilocarpine-induced Ca^{2+} transients in RetCx neurons and ProCx spike activity

Fig. 3.29 shows one of the first successful experiments, demonstrating that the observed changes in the relative (F/F0) fluorescence results from changes in the concentration of free intracellular Ca^{2+} ($[Ca^{2+}]_i$) in RetCx MN neurites. The application of pilocarpine into the thoracic cavity elicited an increase in tonic spike activity in the antagonistic ProCx MNs, simultaneously accompanied by a transient elevation of $[Ca^{2+}]_i$ above resting level in all defined regions of interest (ROI) along RetCx neurites. Two minutes after the application bursts of larger excitatory ProCx MN units occur (Fig. 3.29). The $[Ca^{2+}]_i$ transients of RetCx neurites increased in anti-phase with the recorded ProCx motor output. After a transition phase, where ProCx MN units were silent and the RetCx $[Ca^{2+}]_i$ transients remained elevated, an alternating and regular pilocarpine rhythm was established. The magnified traces display clearly (Fig. 3.29c) that the change in $[Ca^{2+}]_i$ started with the offsets of ProCx bursts and decreased with the onset of a successive ProCx bursts. The measured $[Ca^{2+}]_i$ amplitudes reached up to 6% fluorescence change from baseline level. Across all defined ROIs, temporally uniform $[Ca^{2+}]_i$ transients were observed.

Pilocarpine-induced Ca^{2+} transients in RetCx neurons and RetCx spike activity

To compare the measured increase in $[Ca^{2+}]_i$ with the actual motor output of the RetCx MNs, the backfilled nl5 nerve stump was recorded in a set of experiments extracellularly. In the following section, three examples of pilocarpine-induced $[Ca^{2+}]_i$ transients in comparison to extracellular RetCx motor activity are presented.

$[Ca^{2+}]_i$ elevations and RetCx MN spike activities of the first example are shown in Fig. 3.30. After the application of pilocarpine, the tonic spike activity of small RetCx MNs increased and shortly after larger spikes of MN units occur. With increasing tonic spike activity, $[Ca^{2+}]_i$ increased simultaneously in all three defined ROIs along primary neurites (Fig. 3.30c). After 90s, a regular motor rhythm was established and $[Ca^{2+}]_i$ increased in-phase with the recorded motor output (Fig. 3.30d). After 300 s, the pilocarpine-induced motor rhythm changed to bursts with longer durations followed by a short burst of very large MN units. With the occurrence of these very large MN spikes, the $[Ca^{2+}]_i$ transients show a huge increase of up to 30% fluorescence change (these very large $[Ca^{2+}]_i$ transients will be further examined in sec. 3.3.2).

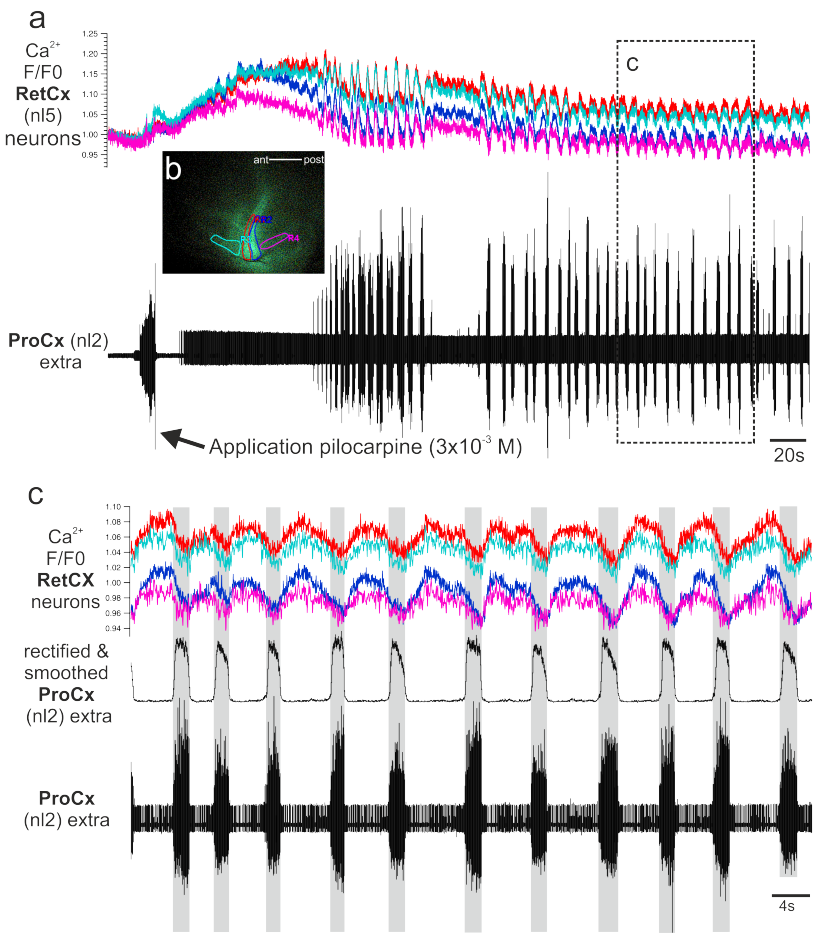

Figure 3.29. – Pilocarpine-induced $[Ca^{2+}]_i$ transients in RetCx neurons and spike activity in the antagonistic ProCx nerve. a: Experimental time-course. Application of pilocarpine (arrow) induced $[Ca^{2+}]_i$ elevations in RetCx neurons and tonic spike activity in the extracellular recording of nerve nl2 that carries the axons of ProCx MNs. After 2 min clearly defined bursts of activity in ProCx MNs occurred in anti-phase to relative changes in fluorescence (F/F0) of all measured ROIs along RetCx MN neurites. **b:** Image with marked ROIs. ROIs were defined along primary neurites (red, blue), along anterior (cyan), and posterior (magenta) ganglion regions. **c:** Magnification of boxed traces in (a) with established, regular motor rhythmicity. RetCx neurons show $[Ca^{2+}]_i$ changes with amplitudes of up to 6% in all ROIs in anti-phase to bursts of the antagonistic ProCx MNs (gray bars).

Furthermore, the shapes of measured $[Ca^{2+}]_i$ elevations remarkably reflected rectified and smoothed extracellularly recorded burst intensities of RetCx neurons (Fig. 3.30c and d). To examine these observations in more detail, the integrals under the rectified and smoothed burst intensities and the integrals of the $[Ca^{2+}]_i$ transients were calculated for each burst and divided by the burst duration. The corresponding value resembles the mean MN activity and mean $[Ca^{2+}]_i$ intensity for each burst in arbitrary units [a.u.]. The distribution of $[Ca^{2+}]_i$ and burst activities for the entire experimental time course and for episodes of the experiment are shown in Fig. 3.31a-d. The linear regression shows a significant correlation.

Moreover, the plot revealed an accumulation of small values around 0.008 arbitrary units [a.u.] along the x-axis. The reason is presumably that the calculated mean $[Ca^{2+}]_i$ intensity might not reflect the actual burst activity in the second half of the experiment (see also plot for 2nd half of experiment; Fig. 3.31c) due to assumed dye bleaching of the indicator. The correlation becomes clearer when only the mean values of the first part of the experiment (till timepoint 300 s) are plotted, where the motor activity was defined regular, the values show a linear relationship for all three ROIs (R=0.837-0.89; Fig. 3.31b). Such a distribution was expected according to the observed similar shapes of rectified and smoothed RetCx burst activities and $[Ca^{2+}]_i$ transients. The linear correlation of $[Ca^{2+}]_i$ and burst activity suggests that MN action potentials are the determinant of the measured $[Ca^{2+}]_i$ transients, by activating voltage-gated Ca^{2+} channels (VGCC).
Moreover, rise and decay times were calculated for few $[Ca^{2+}]_i$ elevations. For the first occurring $[Ca^{2+}]_i$ transients due to bursts of MNs (Fig. 3.31b_1), mean rise times were calculated as 0.13 s ± 0.015 s (mean ± SD) and mean decay times calculated as 0.86 s ± 0.241 s. Whereas, for four very large and three large $[Ca^{2+}]_i$ transients, in the second half of the experiment (Fig. 3.31d_1), faster rise times and longer decay times were calculated (mean rise: 0.074 s ± 0.012 s; mean decay: 1.039 s ± 0.154 s).

Fig. 3.32 and Fig. 3.34 show two additional examples of pilocarpine-induced $[Ca^{2+}]_i$ transients combined with recordings of RetCx nerve activity. Both examples revealed, as shown above (Fig. 3.30c), an increase in $[Ca^{2+}]_i$ in-phase to RetCx bursts. The extracellular recorded RetCx nerve activity was only partially regular in the beginning of the experiments, whereas the rhythm changes frequently and RetCx bursts follow each other very shortly (Fig. 3.34d). The $[Ca^{2+}]_i$ transients are mainly uniform across all defined ROIs. The only exception was found for $[Ca^{2+}]_i$ transients of ROI3 that showed slightly different $[Ca^{2+}]_i$ elevations, when spikes of smaller units occurred (asterisk; Fig. 3.34d).
The calculated integrals of RetCx bursts and $[Ca^{2+}]_i$ elevations are shown in Fig. 3.33a and Fig. 3.35. Both graphs revealed a linear relationship as shown for example 1 (Fig. 3.31b). Moreover, the graph for example 3 (Fig. 3.35) revealed a similar accumulation of small values. Here, the reason for small values is assumed to be the result of small $[Ca^{2+}]_i$ transients close to noise during burst of very small MN units. Due to short burst intervals in the experiment, rise and decay time constants could not be calculated for the third example, because the decay to baseline level was seldom accomplished.

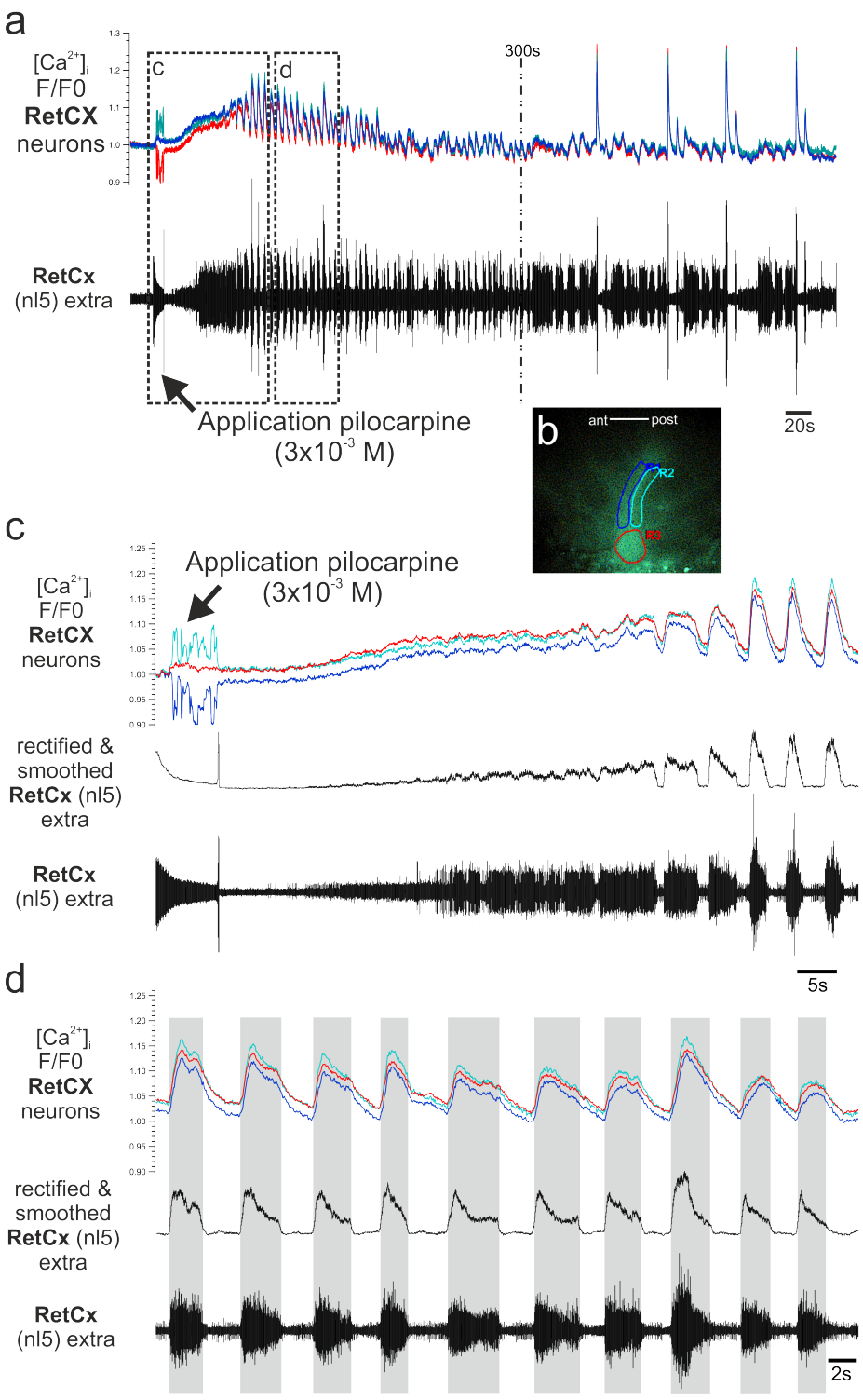

Figure 3.30. – **Example 1 of pilocarpine-induced $[Ca^{2+}]_i$ transients and spike activity in RetCx neurons.** **a:** Time-course of pilocarpine-induced $[Ca^{2+}]_i$ elevations in primary neurites of RetCx neurons and extracellularly recorded spike activity of RetCx MNs. First, tonic active MN units occurred (see (c)) followed by a phase of regular rhythmicity (see (d)). After 300 s the rhythm changed and large excitatory MN units occurred accompanied by very large $[Ca^{2+}]_i$ transients of up to 30% fluorescence change (see next section). **b:** Image with three defined ROIs along primary neurites. **c:** Magnification of boxed traces in (a) show pilocarpine-induced tonic activity of some small MN units with a simultaneous increase in intracellular Ca^{2+} (F/F0). After 83 s clearly separated bursts occurred in-phase to relative changes in $[Ca^{2+}]_i$ fluorescence of RetCx neurites. **d:** Magnification of second boxed area in (a) with established rhythmicity. Note the similar shape of $[Ca^{2+}]_i$ elevations compared to rectified and smoothed extracellular activity of RetCx MNs.

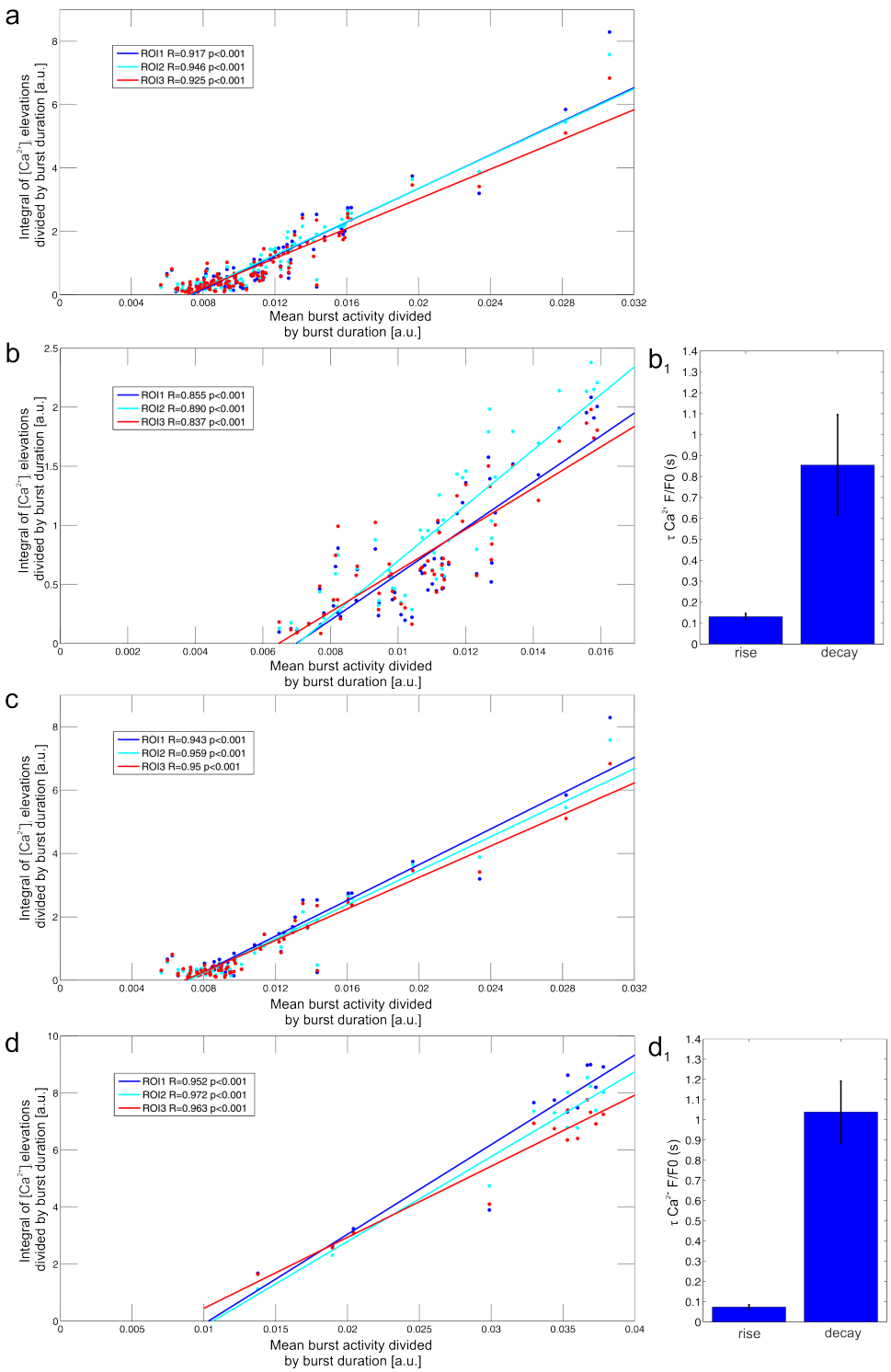

Figure 3.31. – **$[Ca^{2+}]_i$ integrals and mean RetCx burst activities, and time constants for example 1 (Fig. 3.30). a:** $[Ca^{2+}]_i$ integrals and mean RetCx burst activities for the entire experiment. Apparent is an accumulation of integrals around 0.008 arbitrary units [a.u.] along the x-axis, probably due to calculated mean $[Ca^{2+}]_i$ intensities that might not reflect the actual burst activity (see also (c)). **b:** $[Ca^{2+}]_i$ integrals and mean RetCx burst activities till 300 s show a linear correlation as expected. **b_1:** Mean rise and decay times for the first, seven occurring $[Ca^{2+}]_i$ elevations of ROI1. Mean rise times: 0.13 s ± 0.015 s (mean ± SD); mean decay times: 0.86 s ± 0.241 s. **c:** $[Ca^{2+}]_i$ integrals and mean RetCx burst activities from 300 s to the end of the experiment shows large integrals and a accumulation of values around 0.008 [a.u.]. **d:** $[Ca^{2+}]_i$ integrals and mean RetCx burst activities for nine very large $[Ca^{2+}]_i$ elevations of up to 30% fluorescence change and four smaller transients in the 2nd half of the experiment (see Fig. 3.30a). **d_1:** Mean rise and decay times for four very large $[Ca^{2+}]_i$ transients of ROI1 with up to 30% fluorescence increase. Mean rise: 0.074 s ± 0.012 s; mean decay time: 1.039 s ± 0.154 s.

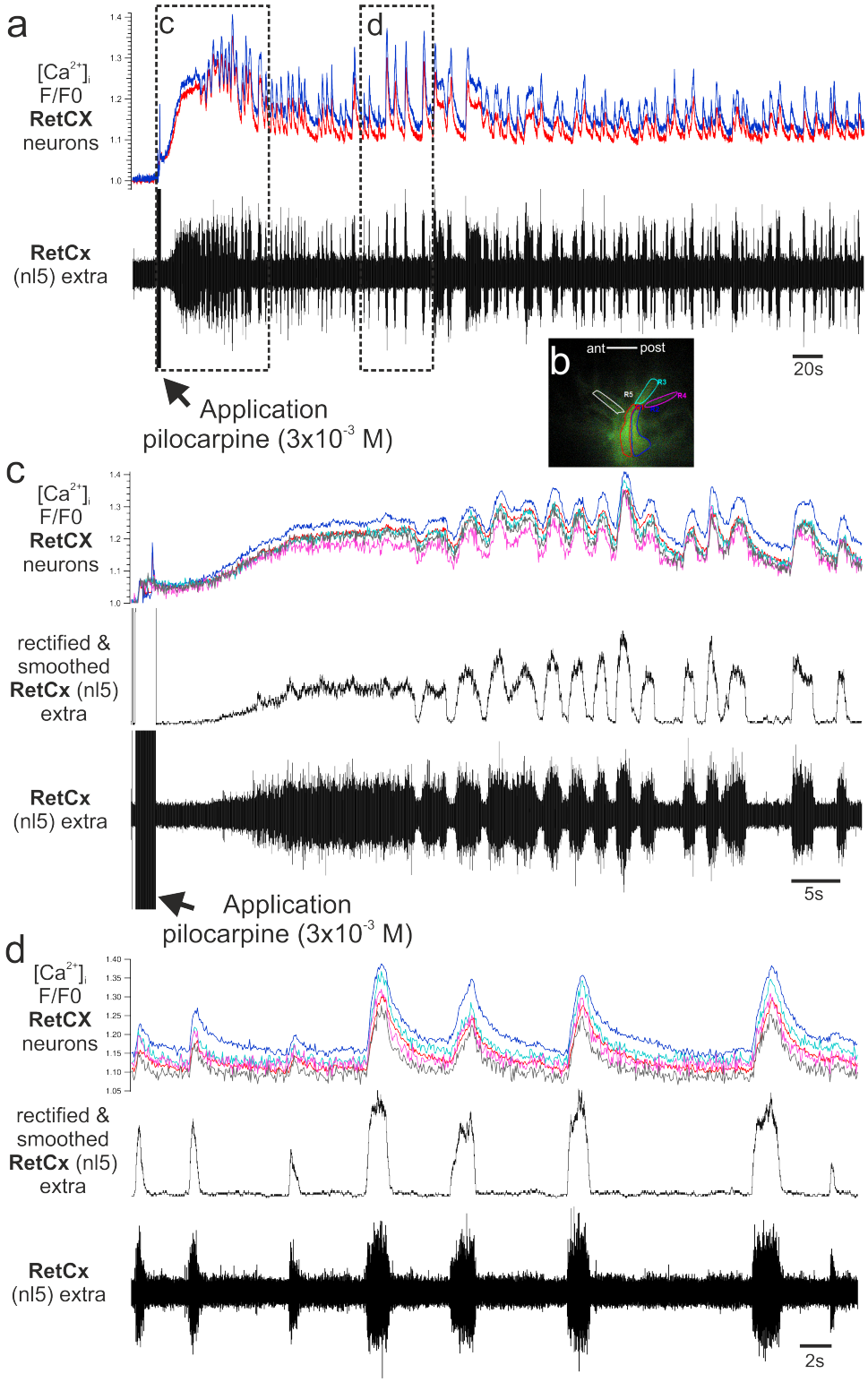

Figure 3.32. – Example 2 of pilocarpine-induced $[Ca^{2+}]_i$ transients and spike activity in RetCx neurons. **a:** Time-course of pilocarpine-induced $[Ca^{2+}]_i$ elevations in primary and secondary neurites of RetCx neurons and extracellularly recorded spike activity of RetCx MNs. First tonic activity occurs (see (c)), followed by rhythmic bursting of MN units in the entire time course (see (d)). **b:** Image with five defined ROIs, three along primary neurites (red, blue and cyan), one ROI along anterior (white=gray in magnified F/F0 traces), and one ROI along posterior (magenta) secondary neurites. **c:** Magnification of boxed traces in (a) show pilocarpine-induced tonic activity of some small units. Simultaneously, the relative changes in $[Ca^{2+}]_i$ increased uniformly in all ROIs. After ~50 s clearly separated bursts occur in-phase to $[Ca^{2+}]_i$ transients of RetCx neurites. **d:** Magnification of second boxed area in (a) with an episode of bursts of small and larger RetCx MN units and their corresponding $[Ca^{2+}]_i$ elevations. Calculated rise and decay times for the episode are shown in Fig. 3.33.

Rise and decay time constants were calculated for a short epsiode with seven $[Ca^{2+}]_i$ transients of example 2 (Fig. 3.33d). The rise times for five defined ROIs are similar (rise: ROI1: 0.152 s ± 0.04 s; ROI2: 0.201 s ± 0.064 s; ROI3: 0.193 s ± 0.07 s; ROI4: 0.184 s ± 0.071 s; ROI5: 0.159 s ± 0.058 s), whereas the decay times are longer for ROIs defined along primary neurites than of secondary neurites in anterior and posterior ganglion regions (decay: ROI1: 1.175 s ± 0.359 s; ROI2: 1.097 s ± 0.443 s; ROI3: 0.844 s ± 0.268 s; ROI4: 0.683 s ± 0.190 s; ROI5: 0.823 s ± 0.283 s).

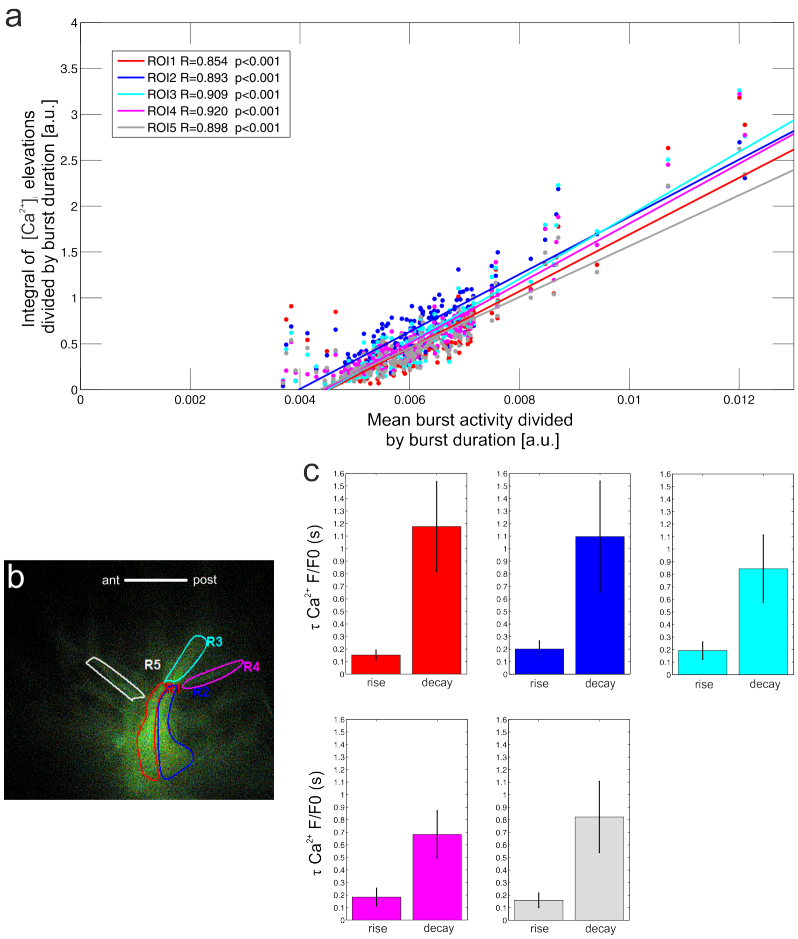

Figure 3.33. – **$[Ca^{2+}]_i$ integrals and mean RetCx burst activities, and time constants for $[Ca^{2+}]_i$ transients of example 2 (Fig. 3.32). a:** $[Ca^{2+}]_i$ integrals and mean RetCx burst activities for five ROIs of the entire experiment show a linear relationship of recorded burst activities and measured $[Ca^{2+}]_i$ elevations. **b:** Image with five defined ROIs. **c:** Calculated mean rise and decay time times for seven $[Ca^{2+}]_i$ elevations shown in Fig. 3.34d. Across ROIs, rise times are faster than decay times. ROI1 and 2, along primary neurites, have the largest decay times. Error bars denote standard deviation.

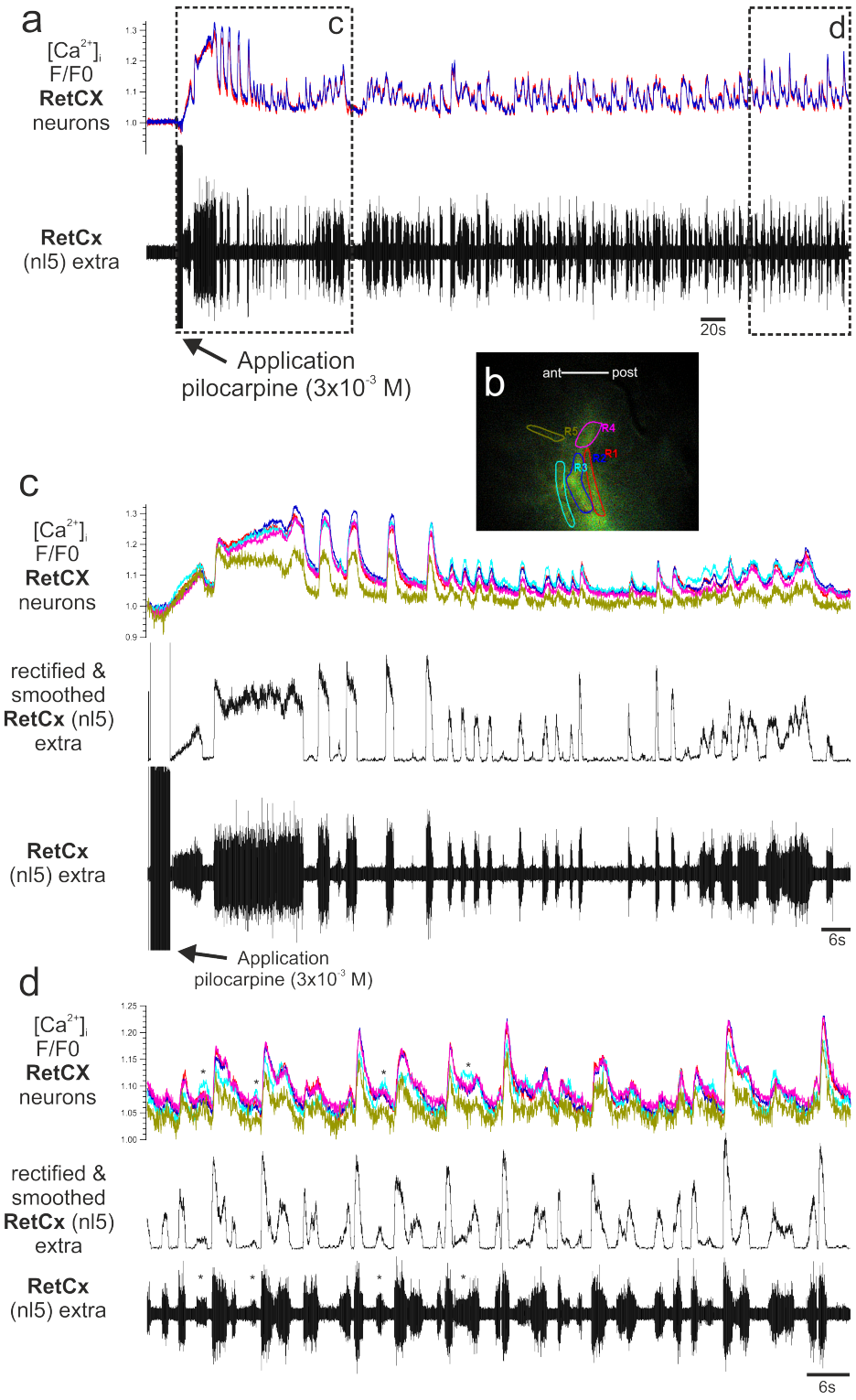

Figure 3.34. – **Example 3 of pilocarpine-induced $[Ca^{2+}]_i$ transients and spike activity in RetCx neurons.** **a:** Time-course of pilocarpine-induced $[Ca^{2+}]_i$ elevations of RetCx neurites and extracellularly recorded spike activity of RetCx MNs. Only ROI1 and 2 are displayed. **b:** Image with five defined ROIs along primary and secondary neurites. **c:** Magnification of boxed traces in (a) show that pilocarpine-induced activity in some small units followed by a broad burst with larger MN units. The relative changes in $[Ca^{2+}]_i$ increased from baseline level of up to 32%, whereas ROI5 (yellow; along secondary neurites) showed a more noisy signal and only an increase of up to 20% with no further elevation compared to ROIs1-4. All ROIs revealed uniform $[Ca^{2+}]_i$ elevations similar in shape to the rectified and smoothed extracellular activity. **d:** Magnification of second boxed area in (a) with rhythmicity, but not regular, because RetCx bursts follow each other very shortly. Shape of $[Ca^{2+}]_i$ elevations reflect the rectified and smoothed extracellular activity of RetCx MNs. ROI3 (cyan) revealed slightly different $[Ca^{2+}]_i$ elevations during bursts of small MN units (asterisks in upper and lower traces).

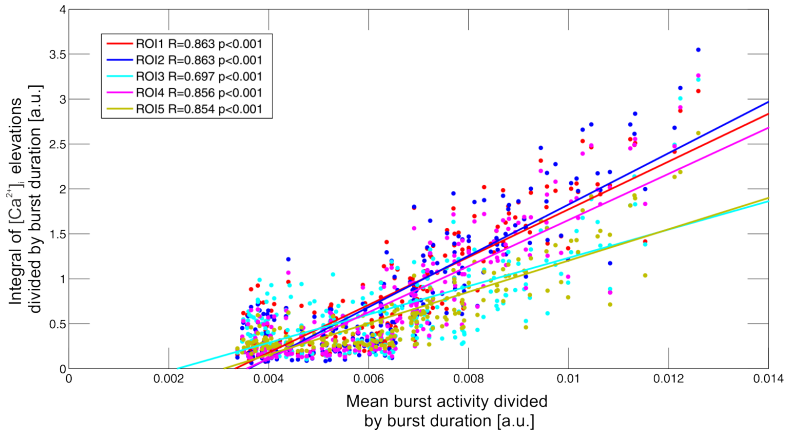

Figure 3.35. – $[Ca^{2+}]_i$ integrals and mean RetCx burst activities for entire experimental time course of example 3 (Fig. 3.34). $[Ca^{2+}]_i$ integrals and mean RetCx burst activities for five ROIs show a linear relationship of recorded burst activities and measured $[Ca^{2+}]_i$ elevations. Apparent are small integral values at 0.004 to 0.0065 [a.u.] along the x-axis. Reasons are presumably very small $[Ca^{2+}]_i$ elevations close to noise during bursts of small MN units (see Fig. 3.34).

3.3.2. Large Ca^{2+} transients in RetCx neurons during pilocarpine-induced activity

In the pilocarpine experiments, frequently, very large $[Ca^{2+}]_i$ transients with an increase of up to 30% fluorescence change occurred. As shown earlier for example 1 (Fig. 3.30), the RetCx motor rhythm changes to bursts with longer durations, followed immediately by a short burst of large RetCx units accompanied by a very large $[Ca^{2+}]_i$ transient. A magnification of such an event is shown in Fig. 3.36a.
Similar large RetCx $[Ca^{2+}]_i$ transients were observed in the interval of a burst of small ProCx units and a successive burst of larger ProCx units (Fig. 3.36b). The situation resembles a pilocarpine-induced motor pattern described by Büschges et al. (1995) and was termed spontaneous, recurrent pattern 3 (SRP3) of activity. The pattern involved a burst of excitatory extensor tibiae MNs. During this burst, first a RetCx burst occur and then activity switches to a ProCx burst (Büschges et al., 1995). Whether the observed pattern shown here is equal to SRP3 is unclear, because the activity of extensor tibiae MNs was not recorded during the experiment.
Furthermore, very large RetCx $[Ca^{2+}]_i$ transients were observed in-phase with large excitatory levator trochanteris (LvTr) units, immediately before the onset of a ProCx burst (Fig. 3.36c). The occurrence of these large Ca^{2+} transients in-phase to large units of LvTr units was observed in two different experiments. However, the motor pattern observed here has slight similarities to SRP2 described by Büschges et al. (1995) (see discussion).

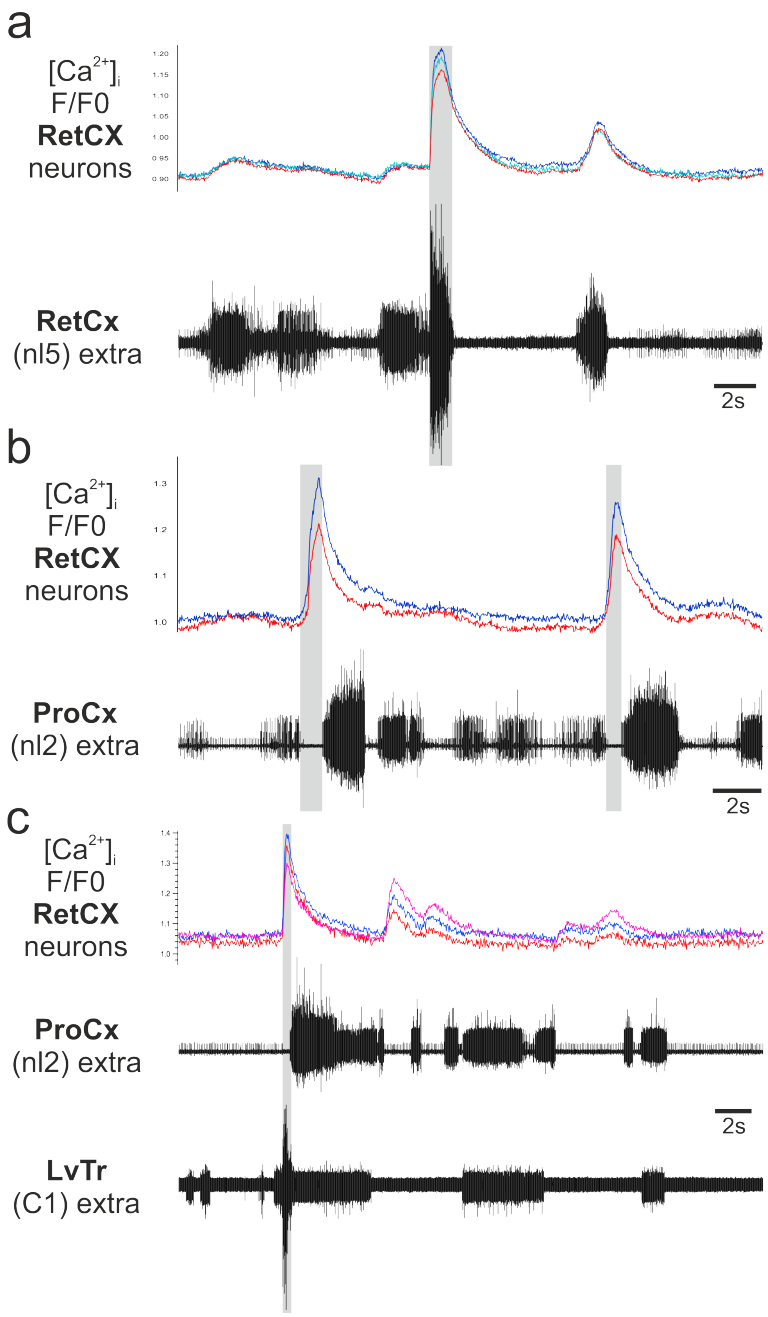

Figure 3.36. – **Large $[Ca^{2+}]_i$ transients in RetCx neurons during pilocarpine-induced activity. a:** Large $[Ca^{2+}]_i$ transients of up to 30% fluorescence change occur, when large RetCx MN units are active (gray bar) (magnification of a large $[Ca^{2+}]_i$ transient shown in Fig. 3.30a). **b:** Occurrence of large $[Ca^{2+}]_i$ elevations of up to 30% fluorescence change in the interval of two successive ProCx bursts (gray bars) at a pilocarpine concentration of 10^{-2} M. Here, an assumed spontaneous, recurrent pattern (SRP3; Büschges et al., 1995) of activity occurs. **c:** Occurrence of a large $[Ca^{2+}]_i$ transient in RetCx neurons during a burst of large levator trochanteris (LvTr) MN units (bottom trace; gray bar) and immediately before the onset of a ProCx bursts.

3.3.3. Pilocarpine-induced Ca^{2+} transients in RetCx MNs and lateral DUM neurites

The methodological approach presented here allows to measure an increase in intracellular Ca^{2+}, besides in MN neurites, also in lateral neurites of dorsal unpaired median neurons (DUM). The staining pattern revealed three lateral neurites of DUM neurons that could be identified in close proximity (Fig. 3.37b; ROI6-8). Whether these neurites have their origin in three different DUM cells is not clear, because DUM neurites divide into several branches before they project through different lateral nerves of the ganglion (e.g., Fig. B.2a and d in the appendix). Therefore, neurites of the same neuron or of two DUM neurons could be imaged just after splitting into side branches.

Fig. 3.37a shows the experimental time-course of pilocarpine-induced $[Ca^{2+}]_i$ elevations in RetCx MNs and lateral neurites of DUM neurons. Just after the application of pilocarpine into the thoracic cavity, the $[Ca^{2+}]_i$ fluorescence change increased simultaneously in ROIs1-5 of MN neurites and in DUM neurites (ROIs6-8; Fig. 3.37c). During $[Ca^{2+}]_i$ transients of very large RetCx units (e.g., last burst in Fig. 3.37c and first bursts Fig. 3.37d), a simultaneous increase in free $[Ca^{2+}]_i$ in DUM neurites was observed. The reason is assumed to be caused by fluorescence light that scatters into the defined DUM neurite ROIs, due to very large $[Ca^{2+}]_i$ transients in MN neurites.

Moreover, the $[Ca^{2+}]_i$ transients in DUM neurites oscillate rhythmically. Cross-covariance analysis of the DUM ROIs revealed a prominent peak at lag zero and additionally periodic peaks (Fig. 3.38b-c). This indicates that the DUM neurite $[Ca^{2+}]_i$ oscillations are regular and in-phase to each other, especially apparent for ROI6 vs. ROI7 and ROI7 vs. ROI8. Cross-covariance analysis of MN ROI1 vs. DUM ROI6 revealed no periodic peaks.

To further analyze whether the DUM neurite $[Ca^{2+}]_i$ oscillations have a phase relation to either the RetCx or ProCx motor activity, the DUM $[Ca^{2+}]_i$ changes were plotted over the RetCx and ProCx burst cycles (Fig. 3.39c-h). Additionally, DUM neurite $[Ca^{2+}]_i$ transients were overlaid with respect to the time of RetCx and ProCx burst onsets, respectively (Fig. 3.39c_1-h_1). Neither of these plots show any systematic phase relation to neither the RetCx nor the ProCx motor activity. Few DUM neurite $[Ca^{2+}]_i$ oscillations start with the onset of a burst, but this appears to be by chance, because DUM neurite $[Ca^{2+}]_i$ transients were found to decay at the bursts onsets (e.g., Fig. 3.39c_1 and d_1). The present finding is in agreement with results by Baudoux et al. (1998). They investigated locust DUM neuron activity induced by pilocarpine with intracellular recordings and found only a coupling of DUM neuron activity to bursts of levator trochanteris MNs.

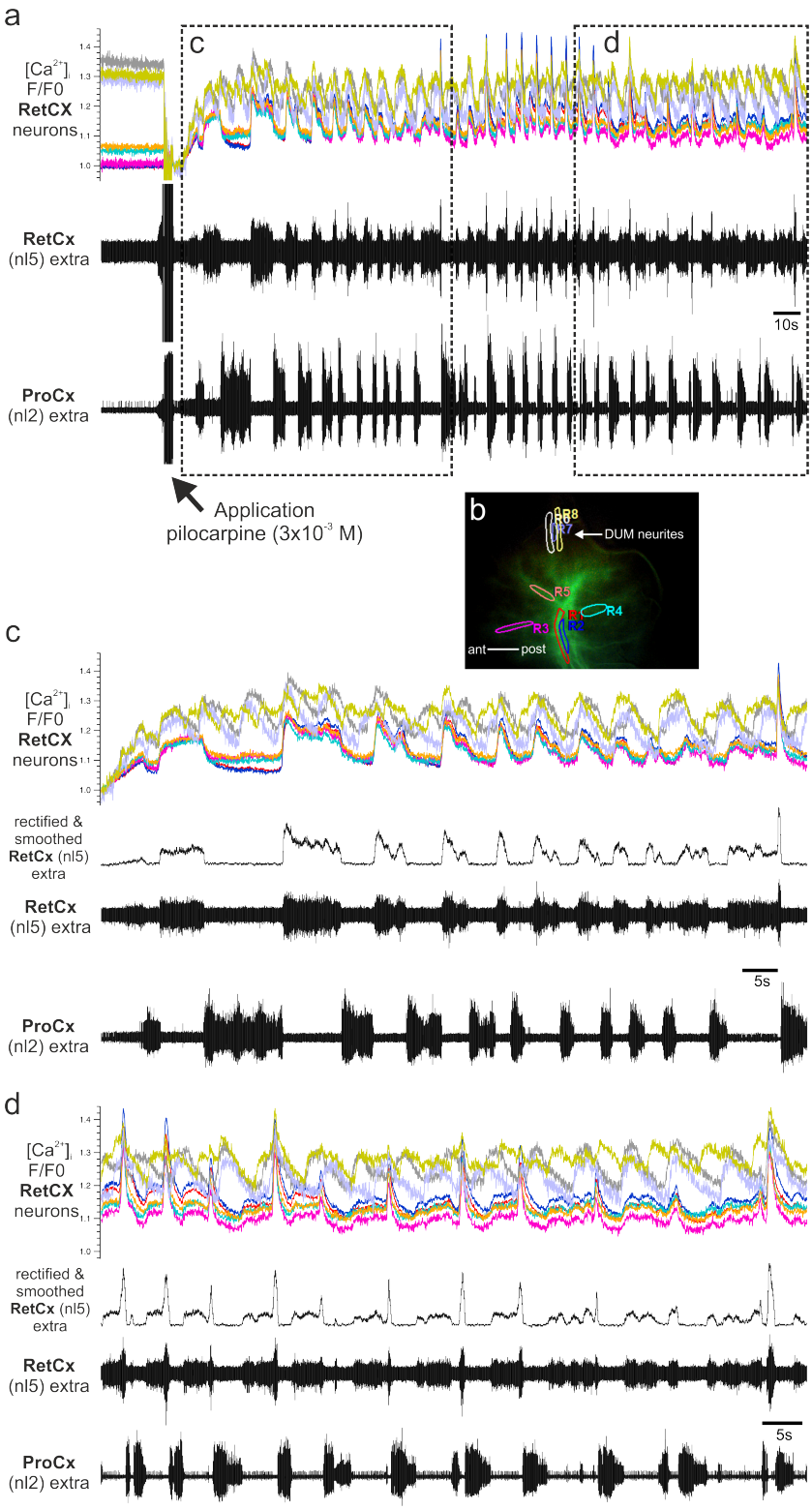

Figure 3.37. – Pilocarpine-induced $[Ca^{2+}]_i$ transients in RetCx MNs and lateral DUM neurites, and spike activity of RetCx and ProCx MNs. a: Time-course of pilocarpine-induced $[Ca^{2+}]_i$ elevations in primary neurites of RetCx MNs and lateral DUM neurites. **b:** Image with defined ROIs1-5 on RetCx MN neurites and ROIs6-8 on DUM neurites (arrow). **c:** Magnification of boxed traces in (a) show that shortly after the application of pilocarpine $[Ca^{2+}]_i$ transients occur across all ROIs. $[Ca^{2+}]_i$ elevations of ROIs1-5 are in-phase to the extracellularly recorded activity of RetCx MNs. $[Ca^{2+}]_i$ transients of DUM neurites (gray, lavender blue and yellow traces) oscillate rhythmically. The DUM $[Ca^{2+}]_i$ elevations increase further when large RetCx $[Ca^{2+}]_i$ transients occur (e.g., peak at the end of the Ca^{2+} trace). **d:** Magnification of second boxed area in (a). Again, $[Ca^{2+}]_i$ elevations of DUM neurites are rhythmically active and increase further during the occurrence of large RetCx $[Ca^{2+}]_i$ transients.

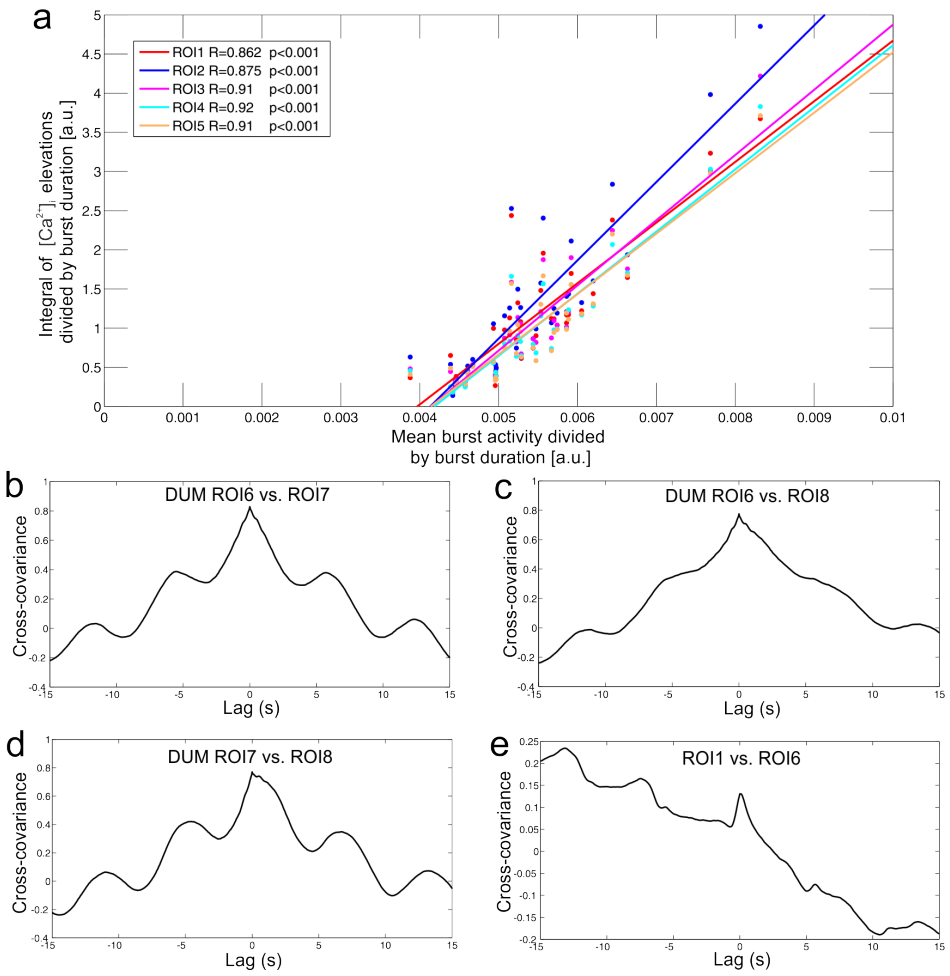

Figure 3.38. – **$[Ca^{2+}]_i$ integrals and mean RetCx burst activities and cross-covariance analysis of DUM neurites $[Ca^{2+}]_i$ oscillations. a:** $[Ca^{2+}]_i$ integrals and mean RetCx burst activities for ROIs1-5 (Fig. 3.37) show a linear relationship of recorded burst activities and measured $[Ca^{2+}]_i$ elevations. **b-d:** Cross-covariance analysis of $[Ca^{2+}]_i$ elevations in lateral DUM neurites. Periodic peaks indicate that DUM $[Ca^{2+}]_i$ oscillations are regular and in-phase to each other, particularly apparent for ROI6 vs. ROI7 (b) and ROI7 vs. ROI8 (d). **e:** Cross-covariance analysis of $[Ca^{2+}]_i$ in MN neurites ROI1 vs. DUM ROI6 shows no regular and in-phase $[Ca^{2+}]_i$ elevations.

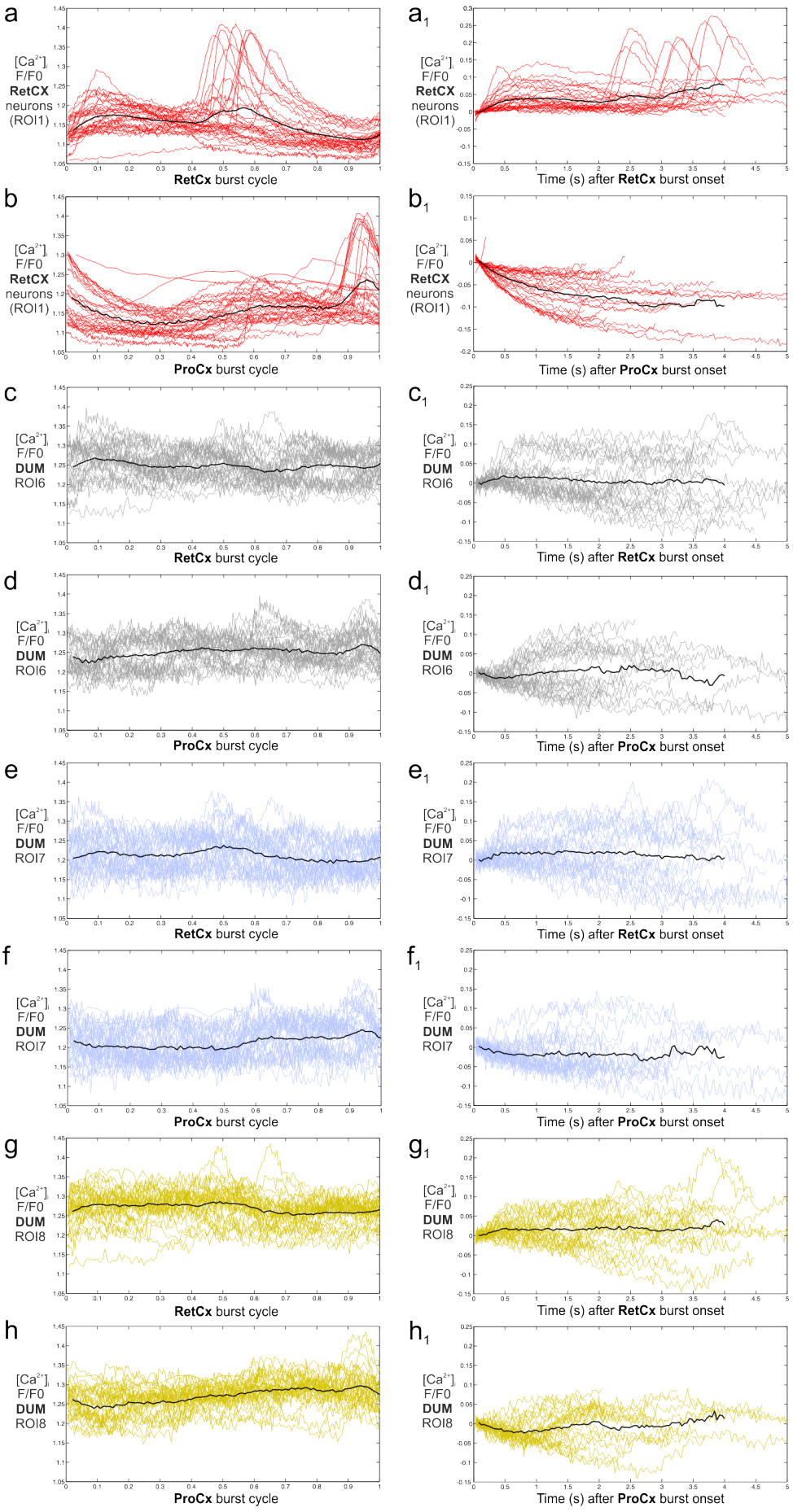

Figure 3.39. – **a-h: $[Ca^{2+}]_i$ transients of RetCx MNs and lateral DUM neurites overlaid against RetCx and ProCx burst cycle (defined from burst onset to the next). a_1-h_1: $[Ca^{2+}]_i$ transients of RetCx MNs and lateral DUM neurites overlaid against the time of RetCx and ProCx burst onsets to the end, respectively.** $[Ca^{2+}]_i$ transients were aligned to start together at 0 (a_1-h_1). Black lines in both columns show averaged $[Ca^{2+}]_i$ transients. None of these plots show any systematic coupling of DUM neurite $[Ca^{2+}]_i$ oscillations to ProCx or RetCx motor activity.

3.3.4. Ca^{2+} transients in RetCx neurons elicited by tactile stimulation

The methodological approach presented here allows not only to measure $[Ca^{2+}]_i$ transients induced by pilocarpine, in addition, it also permits to examine $[Ca^{2+}]_i$ transients in mesothoracic RetCx neurites elicited by tactile stimulation of the animal's abdomen. During the stimulations, the intact left front leg (ipsilateral to the backfilled nerve) performed frequently stepping sequences.
Tactile stimulations applied to the antennae or the animal's abdomen can elicit bouts of bursts of alternating motor activity in the extensor and flexor tibiae MNs, or elicit a co-activation of antagonistic MN pools (Bässler and Wegner, 1983).
In the following two examples of experiments of tactile evoked $[Ca^{2+}]_i$ transients are shown. In the first example, bouts of RetCx burst were observed similar as the motor activity in walking animals (Fig. 3.40). $[Ca^{2+}]_i$ transients increase in-phase during these bursts (e.g., Fig. 3.40c-d). The intracellular Ca^{2+} level remained elevated during bursts in close succession, due to the longer decay time to return to baseline level. Analysis of $[Ca^{2+}]_i$ elevations and burst activities revealed a linear correlation (Fig. 3.40d) as shown above for pilocarpine experiments.

In the second example, $[Ca^{2+}]_i$ transients are shown in comparison to extracellular recorded spike activity of RetCx and ProCx MNs (Fig. 3.41). The overview of the experiment shows frequently co-activation of smaller Pro- and RetCx MN units during the tactile stimulation (Fig. 3.41a). These co-activated MN units can also be observed in the magnified traces (asterisks; Fig. 3.41c-d). Moreover, the magnified traces show alternating sequences of bursts of Pro- and RetCx MNs similar to walking animals. $[Ca^{2+}]_i$ transients increased during the RetCx bursts and the large RetCx bursts occur in-phase to the smallest MN unit apparent in the ProCx nerve recording (Fig. 3.41c-d). Due to the smallest spike in the ProCx recording, the unit is assumed to be the common inhibitory neuron 1 (CI1; Bässler and Storrer, 1980; Graham and Wendler, 1981). The amplitudes of the $[Ca^{2+}]_i$ transients of the six defined ROIs were very similar, whereas ROI3 (cyan) along anterior and secondary neurites revealed frequently larger amplitudes (Fig. 3.42c and d). The integral analysis of large RetCx bursts and $[Ca^{2+}]_i$ transients revealed again a linear correlation (Fig. 3.42). Rise and decay time constants were only calculated for three $[Ca^{2+}]_i$ elevations of ROI1 (Fig. 3.42). The rise times were calculated as 0.3 s $\pm$ 0.156 s and decay times were calculated as 1.333 s $\pm$ 0.305 s.

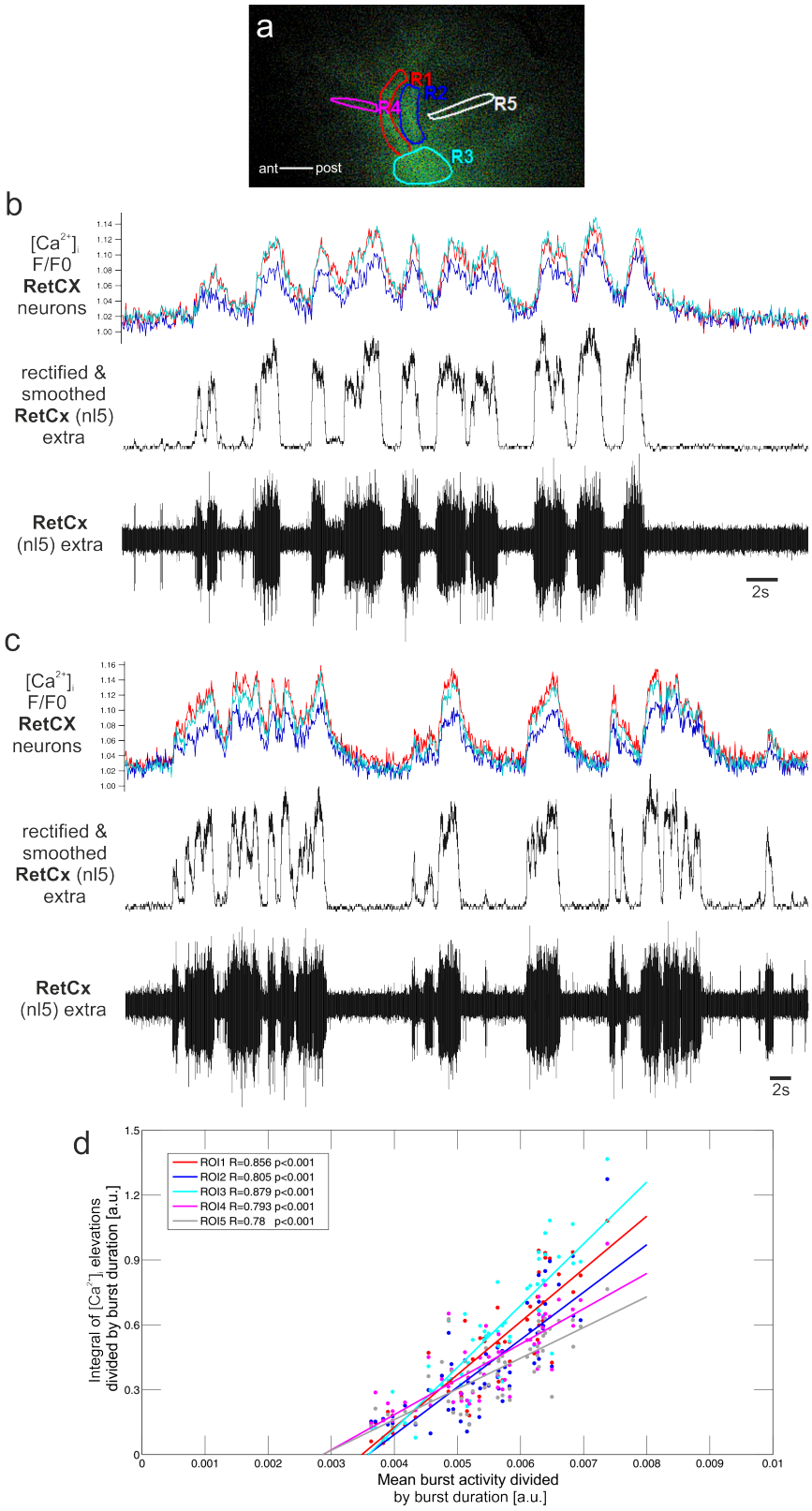

Figure 3.40. – **Spike activity and $[Ca^{2+}]_i$ transients in RetCx neurons elicited by tactile stimulation of the animal's abdomen.** **a:** Image with defined ROIs on the primary neurites (ROI4 and 5 were omitted due to better clarity). **b:** Episode of several RetCx bursts and $[Ca^{2+}]_i$ elevations of up to 14%. **c:** Episodic RetCx bursts and clear $[Ca^{2+}]_i$ elevations of up to 14%. **d:** $[Ca^{2+}]_i$ integrals and mean RetCx burst activities for five ROIs of the entire experiment show a linear correlation of recorded burst activities and measured $[Ca^{2+}]_i$ transients.

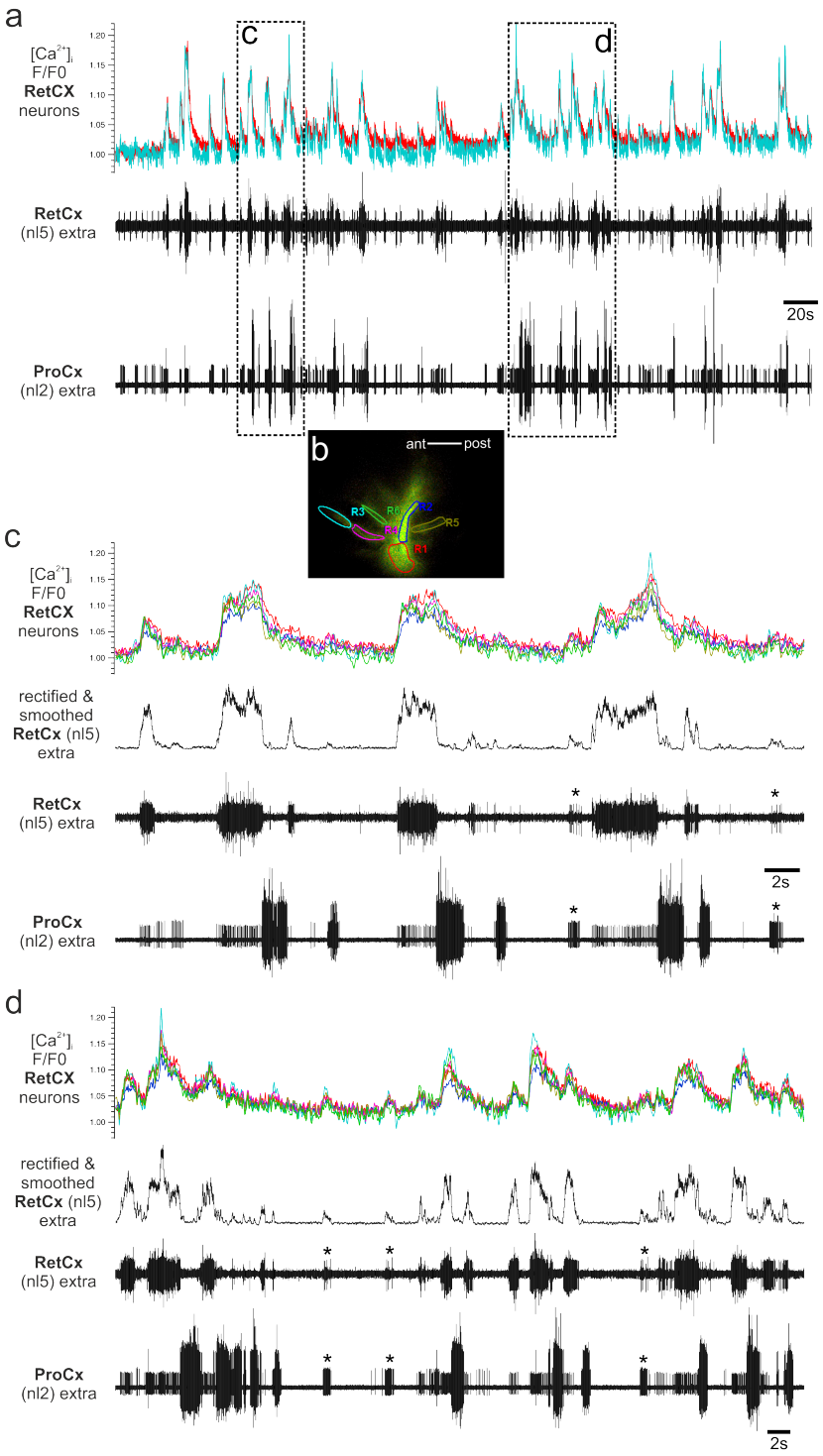

Figure 3.41. – Intracellular Ca^{2+}transients in RetCx neurons, and spike activity in RetCx and ProCx MNs elicited by tactile stimulation. a: Time-course of continuous tactile stimulation of the animal's abdomen elicited $[Ca^{2+}]_i$ transients in RetCx neurons in-phase to bouts of bursts. Apparent are also co-activated MN units in both recordings (note asterisks in c-d). Displayed are only $[Ca^{2+}]_i$ elevations of ROI1 (red) and ROI4 (cyan). **b:** Image with defined ROIs on the primary neurites **c:** Magnification of boxed traces in (a) shows an episode of several RetCx bursts and $[Ca^{2+}]_i$ elevations with amplitudes of up to 14%. Asterisks mark co-activated small MN units in both recordings. **d:** Magnification of boxed area in (a) shows episodic RetCx bursts and clear $[Ca^{2+}]_i$ elevations of up to 14%. Asterisks mark co-activated small MN units apparent in both recordings.

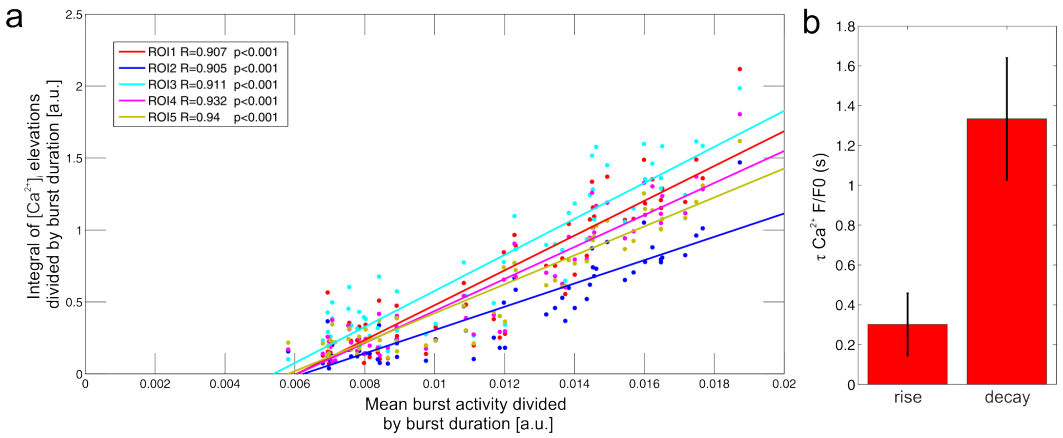

Figure 3.42. – **$[Ca^{2+}]_i$ integrals and mean RetCx burst activities, and time constants for Ca^{2+}transients of Fig. 3.42. a:** Ca^{2+} integrals and mean RetCx burst activities for five ROIs of the entire experiment show a linear relationship of recorded burst activities and measured $[Ca^{2+}]_i$ elevations. **b:** Calculated mean rise and decay time times for three $[Ca^{2+}]_i$ elevations of ROI1. Rise times are faster than decay times. Mean rise times: 0.3 s ± 0.156 s (mean ± SD) and average decay times: 1.333 s ± 0.305 s. Black error bars denote standard deviation.

3.3.5. Summary

Backfilling the high-affinity Ca^{2+}sensor OGB-1 dextran into cut ends of the RetCx nerve nl5 allows stable optical measurements of free intracellular Ca^{2+} in stick insect RetCx MN neurites *in situ*. $[Ca^{2+}]_i$ transients were induced either by the application of the ACh agonist pilocarpine into the thoracic cavity or by tactile stimulation of the animal's abdomen. The measured intracellular Ca^{2+} dynamics are very similar and temporarily uniform across primary and secodary neurites. $[Ca^{2+}]_i$ elevations have a sharp rise and a longer decay time after burst termination. The integrals of measured $[Ca^{2+}]_i$ transients and integrals of RetCx bursts revealed a linear correlation. This suggest that MN action potentials are the determinant of the observed $[Ca^{2+}]_i$ transients by activating voltage-gated Ca^{2+} channels. Frequently, very large $[Ca^{2+}]_i$ transients were observed. Their origin is unclear, but spontaneous, recurrent patterns of activity (SRP; Büschges et al., 1995) could be their origin (see discussion). Moreover, $[Ca^{2+}]_i$ transients of lateral DUM neurites can simultaneously be investigated with $[Ca^{2+}]_i$ elevations in RetCx MN neurites. For that, it is necessary that neurites of DUM neurons and neurites of MNs are found in the same focal plane of the ganglion. A first analysis of the lateral DUM neurite $[Ca^{2+}]_i$ dynamics, induced by pilocarpine, revealed regular and in-phase $[Ca^{2+}]_i$ oscillations of the three measured ROIs. These DUM neurite $[Ca^{2+}]_i$ oscillations did not show a fixed phase relation to either the ProCx nor RetCx spike activity.

4. Discussion

This thesis consists of three different chapters. In the first chapter the morphology of antennal afferents, MNs, and DINs in stick insect brains and suboesophageal ganglia (SOG) have been investigated. The second chapter deals with neuronal tracing of stick insect mesothoracic MNs, DUM neurons, and sensory neurons with a central cell body. In the third chapter, Ca^{2+} transients of retrogradely labeled mesothoracic retractor coxae neurons have been optophysiologically investigated, under pharmacological influence and by tactile stimulation of the animal. The results for each chapter will be discussed independently in detailed, separate sections.

4.1. Morphology of antennal afferents and descending interneurons in stick insect brain and suboesophageal ganglion

After antennal contact blindfolded stick insects approaching a vertical rod showed re-targeting of the front leg (when the leg was in swing phase) or aimed reaching movements of the front leg (when the leg was in stance phase) (Schütz and Dürr, 2011). In order to fulfill such aimed leg movements, it is necessary that the antennal contact site is measured by antennal sense organs. Furthermore, sensory information about antennal posture is needed to generate an aimed leg movement via fast connections to the motor centers in thoracic ganglia. Sensory organs for measuring the antennal posture are scapal and pedicellar HFs located at the base of the segments. Ablation experiments of the HF sensilla led to drastic changes in the antennal working range, indicating their function as important antennal joint angle sensors (Krause et al., 2013). Antennal HFs are therefore necessary for the antennal movement pattern and also for the spatial coordination of the front leg movement. To understand the neuronal mechanism underlying the antennal movement patterns, information about neuropil regions for processing of

mechanosensory signals is required. For insects it was shown that the deutocerebrum (DC) of the brain is an important integration center for signals of antennal sense organs (e.g., Rospars, 1988; Homberg et al., 1989), but neuroanatomical data about the stick insect DC is not present. This is why I addressed the question in chapter 3.1 of how the antennal sensorimotor system of the stick insect is centrally organized and how many descending interneurons (DINs) are involved in transmitting signals from the brain and SOG to thoracic motor centers. The stainings provided here are first insights into the neuroanatomical organization of the DC in the stick insect and are compared to findings in other insect species.

4.1.1. Antennal HFs and deutocerebral neuropils for processing of antennal mechanosensory signals

In chapter 3.1.1, the central projection patterns of all seven antennal HFs of the stick insect were described. They all send fibers into the dorsal lobe (DL) also known as the 'antennal mechanosensory and motor center' (AMMC; Rospars, 1988; Homberg et al., 1989) and in tract 6I (T6I). Moreover, the HF afferents travel posteriorly through T6II to descend to the SOG, where they terminate in ipsilateral and intermediate neuropil regions (Fig. 3.1). According to these results, the first integration center for antennal HF signals is the DL and a second center is located in the SOG. At least two different pathways for the processing of antennal HF signals are possible.

Identified tracts of sensory afferents in the DC of stick insects are in general very similar to tracts in crickets and honeybees (reviewed in Staudacher et al., 2005). For the honeybee was shown that antennal mechanosensory fibers enter the DL through tracts T5 and T6, whereas afferents in T6 travel further from the DL to divide into tracts T6I, T6II, and T6III (Suzuki, 1975; Mobbs, 1982; Maronde, 1991). The afferents in T6I and T6III terminate near the posterior protocerebral lobe (PPL) and their origin are neurons from the Johnston's organ (Ai et al., 2007). Antennal afferents in tract T6II terminate in the SOG (also T6IV afferents; Maronde, 1991). In the stick insect, it was frequently observed that afferents from the scape and pedicel travel upon entry into the DC in different tracts, presumably T5 and/or T6. Moreover, T6I correspond to the tract where the anteromedially traveling HF collaterals terminate and T6II is assumed to be the tract where the afferent fibers travel posteriorly in the direction of the ipsilateral connective. For the stick insect pedicellar HP dorsomedial (pHPdm) it was observed that the anteromedial collaterals in T6I performed sometimes a slight lateral turn to terminate shortly after (Fig. A.2 in the appendix). Stainings of the antennal nerve close to the brain revealed also a similar turn (Fig. 3.8c), and it is possible that the turn

of T6I afferents represents T6III described for bees. In contrast, afferents in T6IV projecting into the SOG as described by Maronde (1991) for the bee were not found. Furthermore, a seventh tract (T7) was reported for flagellar afferents in crickets (Staudacher and Schildberger, 1999).
The observed central projection pattern of stick insect HFs is comparable to stained sensilla of the dorsal scapal HP of the locust (Bräunig et al., 1983). Antennal HF afferents of honeybees and ants project also to the DL and send neurites into the SOG (bee: Maronde, 1991; Kloppenburg, 1995; Ai et al., 2007; Brockmann and Robinson, 2007; ant: Ehmer and Gronenberg, 1997). Interestingly, the anteromedially traveling HF collaterals in T6I described for the stick insect are lacking in central projections of honeybee HFs completely.
Stainings in the stick insect revealed variability in the central projection patterns of the same HF in different animals. Differences appeared in the length of the anteromedial terminals in T6I, but this observation was inconsistent in different animals. The noticed discrepancy in the staining pattern is probably due to variability in the number of sensilla per HF between different animals. For example Krause et al. (2013) list the range of the dorsal scapal HP (sHPd) sensilla as eleven to 22. Besides, it is possible that not all neurons of ablated sensilla have been labeled with fluorescent dye, adding a methodological cause for variability.

For the processing of sensory signals, an arrangement of sensory terminals in a somatotopic manner might be important. Preserving the position of the receptor in the periphery may aid spatial discrimination of sensory stimuli. Somatotopic maps in insects have been described, for example, for mechanosensory leg hairs (Mücke and Lakes-Harlan, 1995; Newland et al., 2000), chordotonal organ afferents (Nishino, 2000), antennal Johnston's organ afferents (Ignell et al., 2005; Kamikouchi et al., 2006; Ai et al., 2007), antennal afferents of bimodal flagellar bristles (Nishino et al., 2005), photoreceptors (Strausfeld, 2012), or auditory afferents (Römer et al., 1988; Imaizumi and Pollack, 2005). For stick insect HF afferents, I expected that the central projections differ according to the segments where the HFs are located and also differ according their direction specificity. Nishino et al. (2005) reported that mechanosensory afferents of bimodal bristles on the same longitudinal row of the cockroach antenna are arranged on the medioventral axis in the brain and SOG according their proximodistal somata position. Here, the double-stained specimens of scapal and pedicellar HF sensilla revealed so far no obvious shifts in their staining pattern, neither in the horizontal plane nor in depth within in the DL or SOG. The exception are spatially segregated boutons in the brain and SOG, with only a slight overlap of different HF varicosities. A similar co-occurrence of terminal synaptic varicosities was found for auditory afferents of a medial terminating (MT) receptor type and an ultrasound receptor in the same

depth of the prothoracic neuropil of the field cricket, which is tonotopically organized (Imaizumi and Pollack, 2005). Reconstructions of central projections of three subgroups of Johnston's organ afferents in the honeybee, revealed a somatotopic organization only for the terminal region in T6I (Ai et al., 2007). No separation in T6II, T6III, and the DL was found for the three Johnston's organ subgroups. Instead, their terminal arborizations were intermingled (Ai et al., 2007), similar to stick insect HF afferents described above.

The physiology of scapal antennal HF sensilla in cockroaches was investigated by Okada and Toh (2001). They showed that scapal HF neurons have a phasic on-transient and a sustained tonic response characteristic, dependent on the amplitude of the hair deflection. The HFs in the stick insect have specific locations along the scape and the pedicel, and during antennal movement different sensilla are deflected by different angles of the antennal segments. The signals of afferents belonging to the same HF are needed to be integrated centrally in order to represent the orientation of the antennal segments in space. Staudacher et al. (2005) assume that for the discrimination of self-motion-induced or external stimulations of antennal sense organs a somatotopic arrangement is not sufficient. They suggest that additional central modifications or gating of the sensory input are necessary, like the 're-afference principle' (von Holst and Mittelstaedt, 1950). Furthermore, to understand the processing of HF signals and the functionality of the observed differences in bouton formation of different HFs, it is necessary to have information about the physiology and morphology of DL interneurons. In the honeybee, about 200 interneurons with cell bodies in the brain and SOG were found to innervate the DL, but only two of them have been physiologically and morphologically characterized (Ai et al., 2009). Both of these interneurons are vibration-sensitive and related to the processing of Johnston's organ signals. The DL interneuron 1 (DL-Int-1) has dense arborizations in the DL, the dorsal SOG, and the posterior protocerebral lobe, whereas DL interneuron 2 (DL-Int-2) has neurites within the DL, the SOG, and in the lateral and posterior protocerebral lobe (Ai et al., 2009). The stick insect HF stainings provide no obvious neuroanatomical evidence for a somatotopic organization. The functionality of the different antennal HFs might be established by their specific non-overlapping bouton formations, but that is speculative. Future studies should therefore examine the connectivity of HF afferents with DL interneurons related to the processing of HFs signals.

Antennal HFs and MNs

In section 3.1.3, it was shown that scapal HF afferents overlap spatially with antennal MN neurites in the DL. The observed numbers of MNs backfilled through N2/N3 and N4 are generally in agreement with the results by Dürr et al. (2001).

Descending axons of DUM neurons located in the SOG as reported for locusts and crickets (Bräunig et al., 1990; Allgäuer and Honegger, 1993) were not found in the stick insect.
Overlapping fields of HF afferents and antennal MN neurites were observed in the DL of honeybees (Kloppenburg, 1995) and recently in the Oleander hawk moth (Krishnan et al., 2012). The vicinity of dendritic fields of HF afferents and antennal MNs suggests that direct monosynaptic contacts are possible which could improve the coordination of the antennal segments. The stainings showed, for example, overlapping fields of afferents from sHPv sensilla with neurites of levator (Lv) MNs and also depressor (Dp) MNs. This may imply a feedback mechanism, where Dp MN firing is inhibited due to the deflection of sHPv sensilla and Lv MNs are excited to change the movement direction and to lift the scape. In contrast, the sHPv afferents have also overlapping dendritic fields with Dp MNs. This may suggest a feedback loop, where the Dp MN firing is reinforced during deflection of sHPv sensilla to support the movement into the direction.

In the Oleander hawk moth, stimulation of HF sensilla while recording electromyographic (EMG) antennal muscles, showed short latency muscle activation after the stimulus (Krishnan et al., 2012). Krishnan et al. (2012) hypothesize that the antennal positioning behavior in flying moths underlies a monosynaptic negative feedback loop, in which the antennal movement from a set point position stimulates sensory HF sensilla that activates monosynaptically antennal MNs and their innervating muscles to cause the antenna to return to the set point. This ensures that the antennal position is maintained during flight of the moth. In cockroaches and stick insects ablation of HFs results in changes in the antennal working range (Okada et al., 2002; Krause et al., 2013). For example, ablation of stick insect antennal sHPd sensilla caused a dorsal shift of the upper boundary of the HS joint working range (Krause et al., 2013). Okada et al. (2002) and Krause et al. (2013) suggest also an involvement of a possible negative feedback loop, in which the HF afferents could deliver a stop signal to the MNs that drive movement into the direction that caused the afferents to fire.
Similarly, an involvement of coxal HPs in a negative feedback loop for posture control in stick insects was proposed by Wendler (1964). Bässler (1977b) removed HRs and stimulated continuously HPs of the stick insect thoraco-coxal joint and he showed that during walking the leg was moved far backwards, which results in an unnatural leg movement. In the cockroach, ablation of metathoracic trochanteral HPs (deflected during femur flexion) leads also to an overstepping of the leg by an exaggerated flexion movement (Wong and Pearson, 1976). Furthermore, Pearson et al. (1976) stimulated electrically trochanteral HP afferents during intracellular recordings of MNs and they revealed short-latency excitatory post synaptic po-

tentials (EPSP) in extensor MNs and longer latencies for inhibitory post synaptic potentials (IPSP) in flexor MNs. This suggest that the IPSPs are not monosynaptically elicited and presumably involves a non-spiking interneuron (Pearson et al., 1976). However, direct connections of sensory neurons onto MNs were also shown, for example, for the locust (e.g., Burrows, 1975; Laurent and Hustert, 1988; Kuenzi and Burrows, 1995), the larval tobacco hornworm (Weeks and Jacobs, 1987), or for the blowfly (Fayyazuddin and Dickinson, 1996). However, to prove the existence of monosynaptic contacts of antennal HF afferents onto MNs, intracellular MN recordings during stimulation of HF sensilla are needed.

Two antennal neuropils in the deutocerebrum for sensory afferents

Section 3.1.4 revealed that antennal HF afferents and sensory afferents of the flagellum project into two different neuropils situated in the DC: (i) the dorsal lobe (DL) and (ii) the ventral area of flagellar afferents (VFA; Staudacher and Schildberger, 1999).

The present finding of two non-olfactory sensory brain neuropils for processing of antennal signals in the stick insect is in agreement to crickets and for the Madagascar hissing cockroach *Gromphadorhina portentosa* (Staudacher and Schildberger, 1999; Staudacher et al., 2005). For the cockroach *Periplaneta americana* was reported that scapal and pedicellar mechanosensory afferents of unknown origin and flagellar tactile afferents of bimodal bristles project into the DL, whereas contact-chemosensory afferents of bimodal bristles project into a region medioventrally to the DL (Nishino et al., 2005). In contrast to *P. americana* no flagellar afferents were found in the DL of stick insects (Fig. 3.8). The terminal neuropil regions described by Nishino et al. (2005) seem similar to stick insect HF afferents terminating in the DL and flagellar afferents terminating in the VFA, but these neuropils were not distinguished in *P. americana.* However, it is possible that antennal gustatory/contact-chemosensory afferents of stick insects project into the VFA, too. Nevertheless, the second antennal neuropil, the VFA, is possibly a special feature for primarily nocturnal insects with a long filiform antenna, which use mainly the tactile sense to explore their near-field environment. Honeybees rely on vision for orientation. In contrast to crickets and stick insects they possess only the DL and the antennal lobe (AL) (Suzuki, 1975; Mobbs, 1982; Maronde, 1991), whereas the VFA is lacking.

Staudacher and Schildberger (1999) described a striped appearance of the VFA in crickets, with an orderly structured projection pattern of flagellar fibers that might indicate a somatotopic arrangement. In the stick insect, the VFA seems to be highly organized too, with a dense core neuropil and a diffuse looking neuropil region on top of the core (Fig. 3.9). A striped appearance, as in crickets,

was not found. Moreover, Nishino et al. (2005) assume a somatotopic organization for flagellar bimodal bristle afferents (tactile and contact-chemosensory). As mentioned earlier, tactile afferents of cockroaches with somata located more distally on similar longitudinal antennal rows project to more medioventral regions of the DL, whereas the overall branching patterns remain unchanged (Nishino et al., 2005). Future studies should therefore perform selective antennal nerve or sensilla stainings in different flagellum regions, to study if flagellar afferents follow a somatotopic organization in the DC of stick insects as reported by Nishino et al. (2005).

Section 3.1.4 showed furthermore that the term used for the ventral area of flagellar afferents (VFA) is only partially appropriate, because stainings of solitary presumed mechanosensory hairs located dorsally on the pedicel (not arranged in HFs) project also into the VFA. The VFA is therefore a neuropil in which all exteroceptive sensory sensilla situated on the pedicel and the flagellum, and most likely from the scape as well, converge. This assumption is supported by the finding that flagellar and pedicellar fibers of sensilla project into the same region within the SOG (Fig. 3.7; Fig. 3.8). This neuropil is separated from the terminal area of HF afferents that project and terminate slightly more laterally than flagellar fibers. However, few flagellar afferents were found that terminate in the same region like HFs afferents. It might be that these projections result from campaniform sensilla (CS) situated on the flagellum. Bräunig et al. (1983) showed that the CS located at the distal pedicel of locusts have a similar projection pattern as HF afferents in the brain and SOG. In the stick insect, projections into the DL were not found in the antennal nerve stainings of the flagellum. It would be interesting to know if CS from the flagellum and the pedicel have different projection patterns in the DC or if the observed pattern results from a different sensory structure located on the flagellum. Interestingly, it was observed that afferents from the flagellum descend to the prothoracic ganglion (not shown). It seems therefore possible that antennal touch information is transmitted to thoracic ganglia without intercalated interneurons.

Anti-synapsin immunohistochemistry stainings revealed that the stick insect possesses an antennal lobe (AL), but stainings of the antennal nerve resulted only in a diffuse staining of glomeruli within the AL (Fig. 3.9). For the study here, it was of no importance to stain olfactory sensilla because the mechanosensory system of the stick insect antenna was investigated. Nevertheless, the method using dextran fluorescent dyes failed to stain olfactory sensilla within the AL. For stainings of the antennal nerve in ants (Nakanishi et al., 2010) and cockroaches (Watanabe et al., 2010), a combination of biotin with dextran dyes, so-called Microruby or

Microemerald (both Invitrogen) was used successfully. It was possible to visualize olfactory afferents and glomeruli in the AL. To receive more insights of the organization of the AL in stick insect, future studies should try these dyes for antennal nerve stainings.

Central projections of other antennal sensory structures

In section 3.1.5, central projections of other sense organs were described in the brain that differ from stainings of antennal HF afferents.
At the protocerebral bridge, one cell body per hemisphere was stained that probably innervates a connective tissue strand in the head of the stick insect. Bräunig (1985) described four to five neurons in a similar location for the locust and these neurons innervate a connective tissue strand that spans between the scape to the head (tentorium). Electrophysiological recordings revealed during elongation of the strand an increased afferent activity, whereas shortening decreased the activity (Bräunig, 1985). Four neurons on a similar location were also found in crickets (Staudacher and Schildberger, 1999). The arborization pattern was described by Bräunig (1985) and these neurons send collaterals into a region homolog to the DL, with additional collaterals in the anterior DC and medial protocerebrum. In the stick insect, the arborization pattern of the strand receptor neuron was masked by antennal MN neurites within the DL, but its primary neurite could be traced from the cell body to at least a region close the DL. The discrepancy in number of strand receptor cell bodies between the stick insect and to the cricket or locust cannot be explained. Either the stick insects possesses only one strand receptor neuron per hemisphere, or the number is the same as in locusts and crickets, but only one could be stained with the method used here.
Stainings of the antennal nerve N1 close to the brain revealed sensory structures that differ in their projection patterns from those of antennal HFs. For honeybee Johnston's organ afferents was shown that collaterals terminate, among others, in the medial and central posterior protocerebral lobe (PPL; Ai et al. 2007). The observed afferents in the stick insect terminate, similarly to honeybees, in the medial posterior protocerebrum (Fig. 3.10c). Thus, it seems that the described pattern results from Johnston's organ afferent fibers. Nevertheless, it cannot be excluded that the projections shown in Fig. 3.10d have their origin in HF sensilla, but afferents of HFs tend to terminate earlier. To unravel the entire projection pattern of stick insect Johnston's organ afferents, selective stainings are needed.
Stainings of campaniform sensilla (CS) in the locust showed a similar projection pattern to those of HF sensilla, but their terminal projection pattern appeared dense and plexus-like (Bräunig et al., 1983). A plexus-like appearance in T6I was also observed here in the stick insect (Fig. 3.10c). Whether the observed pattern

results from CS or from HFs is unknown. This too, requires additional investigations.

Furthermore, stainings of the antennal nerve N1 showed a sensory afferent that leaves the AL to travel anteromedially to the β-lobe where it terminates in a protocerebral brain region (Fig. A.5 in the appendix). The appearance is similar to afferents in the cockroach, were it is assumed that they belong to hygro-, thermo- or olfactory neurons (Watanabe et al., 2010). Recent stainings in the locust show similar projection patterns and electrophysiological investigations indicate that these sensory neurons are cold-receptive (P. Bräunig, personal communication). The stick insect *C. morosus* possesses at the 12th antennal segment a 'mound-shaped' sensillum with sensory neurons responding to downward temperature steps (Tichy and Loftus, 1987). It is possible that the observed pattern here results from these receptors.

Table 4.1. – Summary of tracts and terminal neuropil regions of stick insect antennal afferents in brain and SOG. AL=antennal lobe; DL=dorsal lobe; DC=deutocerebrum; PC=protocerebrum; T=tract; VFA=ventral area of flagellar afferents; ?=hypothesized.

Segment	Types of antennal afferents	Tracts and terminal neuropil regions of afferents	
		Brain	SOG
Head-scape	presumed strand receptor	T5/T6: DL?	unknown
Scape	hair fields	T5/T6: DL; T6I and T6II: anterior DC	medial, slightly lateral, and intermediate neuropil regions
Pedicel	hair fields	T5/T6: DL; T6I, T6II (and T6III?): anterior DC	medial, slightly lateral, and intermediate neuropil regions
	presumed Johnston's organ	T5/T6: DL?; T6I, T6II and T6III: posterior PC?	unknown
	presumed campaniform sensilla	T5/T6: DL?; T6I: anterior DC?	unknown
	presumed mechanosensory afferents on dorsal pedicel	T7: VFA	medial and intermediate regions
Flagellum	mechanosensory and presumed gustatory	T7: VFA	majority medial and intermediate regions; few similar to HFs; minor descending to prothoracic ganglion
	olfactory	AL	unknown
	presumed cold-receptive	PC	unknown

4.1.2. Descending interneurons (DINs) in stick insect brain and SOG

DINs transmit signals from the brain and SOG to thoracic motor centers. The experiments of backfilling axons of cervical (neck) connectives and connectives between the pro- and mesothoracic ganglia showed up to 410 neurons in the brain and SOG (brain DINs: 205, SOG DINs: 205) which have axons to the prothoracic ganglion, whereas up to 173 neurons (brain DINs: 83, SOG DINs: 90) project to the mesothoracic ganglion. These findings are in agreement for brain DINs backfilled through cervical connectives in the cricket, with at least 181 pairs of neurons (Staudacher, 1998), and to the cockroach with at least 235 pairs (Okada et al., 2003). In contrast, only 106 DINs in the brain and 88 DINs in the SOG were stained through cervical connectives of cockroaches by Gal and Libersat (2006). The numbers of counted SOG DINs stained through cervical connectives or pro- and mesothoracic connectives, exceeded or fall below to the reported 153 SOG DINs in the locust (Kien et al., 1990). Kien et al. (1990) stained either cervical connectives or connectives between pro- and mesothoracic ganglia and therefore it is unclear if the numbers of SOG DINs counted here are higher or lower. Numbers of DINs projecting to the mesothoracic ganglia were not found in the literature. For the cockroach, Burdohan and Comer (1996) stained approximately 50 brain DINs and around 35 SOG DINs projecting at least to the metathoracic ganglia.
Almost all studies about DINs reported variability in the number of counted cell bodies in different specimens. Here, variability was also observed in stainings here between different animals and it is most likely that the actual number of DINs is higher than counted. Okada et al. (2003), for instance, estimated 284 brain DINs by counting the maximum numbers of cell bodies of different clusters, whereas the numbers in different specimens revealed 160 to 212 neurons. Reasons for the variability are the long dye traveling distance, failure to fill all axons with dye, and errors in counting dense clusters of cell bodies.

Soma clusters of DINs in the brain

Stick insect DINs were assigned to 19 soma clusters in the brain. The locations of these clusters correspond to the 17 described for the cricket: i1-i5, i5n, i6, i7a, i7b, i8, pi, and c1-c6 (Staudacher, 1998). In contrast to the cricket, additional cell bodies were found in clusters i9 and c7. It is possible that neurons from cluster i9 in the stick insect resemble solitary neurons at a similar location described for the cricket (Staudacher, 1998). Compared to DINs of the cockroach, 14 clusters (out of 22; Okada et al. 2003) have matching locations in stick insect. These clusters are i1-i5, i5n, i7a, i7b, pi, and c1-c4. Okada et al. (2003) adjusted the

nomenclature of Staudacher (1998) for the cockroach. Therefore, renamed clusters in the cockroach appear to be homologs to the stick insect. These cockroach clusters are i9 (i9, stick insect), c7 (c5, stick insect), c8 (c7, stick insect), and c9 (c6, stick insect). Additionally, Okada et al. (2003) described two clusters (i6a and c6) near the β-lobes of the mushroom bodies. Somata at a similar location to this, were also found in stick insects, but only very rarely (Fig.3.11-3.12, question mark and unnamed soma clusters). Taken together, the clustering of DINs in the brain of crickets, cockroaches, and stick insects appears to be very similar. However, the locations of neurons of specific soma clusters are variable. For instance, cluster i1 is located laterally and more posteriorly in the PC of the stick insect than those of cockroaches and crickets, where it can be found near the ipsilateral calyx.

Distribution of dendrites in the brain

Stainings of connectives revealed distinct areas in the brain of the stick insect with extensive dendritic arborizations. Whether these arborizations belong to ascending interneurons (AIN) or descending interneurons (DIN) is not discernible. Nevertheless, dendritic arborizations were observed in the ipsilateral posterior protocerebrum (PC) throughout ventral, intermediate, and dorsal parts. Dendritic branches occur in the ipsilateral lateral accessory lobe (LAL), in the ipsilateral and contralateral medial PC, and in the VFA and DL neuropils on both brain hemispheres (see below). The lateral and medial protocerebra receive signals from mushroom body (MB) output neurons (Li and Strausfeld, 1999). Similar to the stick insect, Okada et al. (2003) observed numerous dendritic branches in the protocerebrum of the cockroach and they suggest that at least some mushroom body output neurons have direct connections to DINs. In the protocerebrum seems to be a considerable overlap of AINs with DINs neurites (e.g., Fig. 3.12). Okada et al. (2003) suggest that this overlap may indicate a rapid feedback transmission from AINs to DINs which could be important to form descending signals for motor control. The LAL seems to play a role in visual integration and it appears to be a neuropil which connects ascending and descending pathways with the central complex, the anterior optic tubercles, and posterior parts of the protocerebrum (Homberg, 1994). This is supported by lesioning experiments of the LAL in cockroaches, which results in striking abnormalities in obstacle negotiation (Harley and Ritzmann, 2010). In the stick insect, no dendritic arborizations were observed in the AL, the central complex, and the mushroom bodies. This is in agreement with studies by Staudacher (1998) and Okada et al. (2003).

The stainings of whole connectives here in the stick insect provides only first insights into the distribution of DIN neurites. For a detailed analysis only parts of

connectives should be stained. Therefore, I want to recommend to the interested reader the study by Staudacher (1998), who described the branching of various single cell DINs in the cricket brain, and to the study by Okada et al. (2003), who analyzed the distribution of AINs and DINs dendrites in the cockroach brain.

Neurites of DINs appear in vicinity to HF afferents

The present findings of brain DIN neurites and antennal HF afferents in close vicinity could indicate a direct pathway that transmits antennal mechanosensory signals to thoracic ganglia. As yet, neuroanatomical observations alone are not sufficient to prove the existence of direct functional synaptic contacts. Therefore, the observations here are needed to be considered critically due to the limitations in confocal microscopy (Pawley, 2006). Further investigations with electrophysiological methods, volume electron microscopy (Briggman and Denk, 2006), or 'stimulation emission depletion microscopy' (STED; Hell and Wichmann, 1994) are needed.

However, few brain DINs have been identified in different insect species that receive mechanosensory signals from the antenna. In the cricket and cockroach, the descending brain neurons with a contralateral descending axon and branches in the DC respond to antennal touch with short latencies (cricket: DBNc1-2 and DBNc2-2, Schöneich et al., 2011; cockroach: DMIa-1, Burdohan and Comer, 1990, 1996). Morphologically similar neurons were found in cluster c1 and c3 in the stick insect brain (Fig.3.11a and 3.13a). The cricket ipsilateral descending neurons (DBNi1-2 and DBNi2-1) also respond to deflection of the pedicel or the flagellum (Gebhardt and Honegger, 2001; Schöneich et al., 2011). These neurons can possibly be found in clusters c1 and c2 in the stick insect (Fig. 3.11a and Fig. 3.13a). The DMIs in the cockroach are assumed to be involved in the tactually elicited escape turns (Burdohan and Comer, 1996; Comer and Baba, 2011). Schöneich et al. (2011) also suggest that the DBNs in crickets evoke fast turning responses towards or away from obstacles, predators, or conspecifics. Indeed, intracellular recordings of DBNi2-1 revealed recently that the spike frequency was correlated with walking velocity and steering towards the contralateral side (Zorović and Hedwig, 2013). In the stick insect, intracellular recordings of DINs during ramp-and-hold staircase stimulations applied to the SP joint were performed by Ache and Dürr (2013). They revealed DINs sensitive to movement direction, velocity, and antennal joint angle. Moreover, Ache and Dürr (2013) were able to categorize five groups of simple position-sensitive, dynamic position-sensitive, unspecific movement-sensitive, and On- and Off-type DINs. Some of the movement-sensitive DINs convey spikes to the thorax within 11 ms (Ache and Dürr, 2013).

It is interesting to note the branching pattern of descending neurons in the DC of crickets. The cricket DBNs have fan-shaped branches mostly in the ventral posterior DC region, where the VFA is located (Staudacher and Schildberger, 1999; Schöneich et al. 2011). The exception is the ipsilaterally descending neuron DBNi2-1 that has branches in the DC more dorsally than the other DBNs (Staudacher and Schildberger, 1999; Schöneich et al. 2011). Staudacher and Schildberger (1999) reported additionally that branches of the DBNi2-1 were found in the DL and overlap with antennal afferents that project into this neuropil region. This finding is similar to the situation found in the stick insect, where an overlap of a DIN branch and HF afferents was found ipsilaterally to the stained connective (Fig. 3.15a-a_3). In contrast to the contralateral descending neurons in crickets, DIN branches in stick insects were observed not only in the VFA but also near or within the DL and in T6I and T6II, where an overlap was found with antennal HF afferents (Fig. 3.14 and Fig. 3.15b). The extensive branching of DIN neurites in the stick insect DL and VFA neuropils could indicate that these neurons receive several signals from a variety of different mechanoreceptors distributed along all antennal segments.
Furthermore, SOG DINs were identified that transmit antennal-tactile signals to thoracic ganglia. Two neurons in the cricket (SOG-dc1 and SOG-dc2) were found by Schöneich et al. (2011), whereas one SOG DIN (DMIb-1) was described by Burdohan and Comer (1996) in the cockroach. All SOG DINs transmit antennal signals with fast conduction velocities. Unfortunately, for the stick insect it is not known where the DINs investigated by Ache and Dürr (2013) have their origin. Nevertheless, the finding of stained stick insect HF afferents in the SOG could indicate that direct functional contacts onto SOG DINs are established within neuropils located there (Fig. A.7 in the appendix).
The fast re-targeting of stick insect front legs after antennal contact (Schütz and Dürr, 2011), the electrophysiological investigation of DINs by Ache and Dürr (2013), and the neuroanatomical data presented here, indicate that a pathway for proprioceptive and tactile information to thoracic motor networks exists.

Functional aspects of DINs

External stimulations are often used to elicit walking in the stick insect. This can be achieved by optomotor stimulations of moving stripes in the visual field of the stick insect to induce straight or curve walking (Jander and Volk-Heinrichs, 1970; Dürr and Ebeling, 2005; Gruhn et al., 2009). Backward walking is induced by tactile stimulations of the head or by pulling the antenna (Graham, 1985; Hellekes, 2012; Rosenbaum, 2013). The applied stimuli need to be transmitted to thoracic ganglia in order to elicit or to tune the motor activity. This is accomplished by DINs responding fast and directly to the stimulus (Ache and Dürr, 2013), or

through secondary pathways involving the central complex (Ritzmann et al., 2008). For the cricket, a descending neuron was reported that respond to moving gratings in the visual field, whereas the neuronal activity of another descending neuron was correlated with the translational velocity of the walk of the animal (Böhm and Schildberger, 1992). DINs with a similar morphology can presumably found in the pi cell cluster or in soma clusters i1 or i2 of the stick insect brain. A recently discovered DIN in *Drosophila* triggers after activation the initiation of backward directed walking (MwDN1; Bidaye, 2012), according to its soma position the neuron can possibly be found in the pi cluster of stick insects. The neuroanatomy of DINs presented here are, therefore, targets for future physiological experiments to understand the descending control of motor behavior.

4.2. Mesothoracic MNs, DUM cells, and sensory neurons with a central cell body[1]

Backfills of lateral nerves of insect thoracic ganglia stain excitatory and inhibitory motoneurons (MN), dorsal unpaired median neurons (DUM), and sensory neurons. The majority of insect sensory cells have cell bodies in the periphery (Burrows, 1996). The only exception known are strand receptor neurons that have cell bodies in the respective segmental ganglion (Bräunig and Hustert, 1980; Bräunig, 1982a, 1982b). These cell bodies cluster in a typical position and their primary neurites and branches take a typical course (Bräunig, 1982a, 1982b). These features and considerable smaller cell bodies allow to discriminate sensory neurons from MNs. Therefore, I will refer to cells that do not meet the above characteristics and that have a single axon as MNs. This practice, of course, bears a small risk of a wrong classification. Cases of doubt, however, will be discussed.
The tracing studies here revealed MN numbers that considerably differ from previous data (see Tab. 3.3). The MN cell body positions and clusters are shown, which were resolved by depth color-coding and transverse ganglia sections, and pathways of primary neurites and finer arborizations within the neuropil. The number of labeled cell bodies, their positions, and cell body diameters is well in the range of orthopteran MNs (e.g., Wilson, 1979; Phillips, 1981; Siegler and Pousman, 1990a). In contrast to Storrer et al. (1986), I was able to backfill DUM cells and determine their number and type. I also looked at the structure and terminal regions of sensory afferents as, for example, hair plates that have axons in the examined nerves.

4.2.1. Comparison with previous tracing studies in stick insects and other orthopteran insects

Tab. 4.2, Tab. 4.3 and Tab. 4.4, at the end of the chapter, allow a comparison of stick insect data from the backfill study here with data from locusts and cockroaches. I list the destination of homolog nerves (homology based on Bullock and Horridge, 1965) and the number and location of neurons that have axons in these nerves. In the following all backfilled nerves will be discussed in detail. A shortened version of the discussion can be found in Goldammer et al. (2012).

[1]Parts of the discussion in this section are already published: Goldammer J, Büschges A and Schmidt J. *Motoneurons, DUM Cells, and Sensory Neurons in an Insect Thoracic Ganglion: A Tracing Study in the Stick Insect Carausius morosus.* Journal of Comparative Neurology, 520(2), 230-257, 2012. The author contributions are as followed: JG, AB and JS designed research. JG performed experiments, analyzed data, prepared figures, tables and drafted the manuscript. JS edited the manuscript.

Nervus anterior (na)

Backfills of nervus anterior labeled up to nine MN cell bodies including a previously undescribed small cell body contralaterally in the anterolateral group and a dorsal cell body at the ganglion midline. The dorsal position of the cell body and the bifurcating lateral neurites identify this neuron as a DUM cell. This DUM cell was previously described by Mentel et al. (2008) and termed DUMna nl2 because of its branches in both nerves. Interestingly, DUM neurites were observed in a simultaneous staining of nl5 branches A and B (Fig. B.2 in the appendix), that project in the direction of the na nerve root. Therefore, it is possible that a DUMna nl2,5 type exists (see below) that did not show up in nl2 backfills. Backfills of na made by Storrer et al. (1986) in the stick insect *C. morosus* labeled seven MNs contralaterally to the side of dye application. A DUM cell is lacking in their stainings.

Backfills of specific nerves in different insect species revealed similar staining patterns as described for nerve na in stick insects. The similarity may indicate homologies of nerves and their innervated muscles in different insect species. For example, Breidbach and Kutsch (1990) stained the nerve innervating mesothoracic dorsal longitudinal flight muscles (dlm) in larval and adult locusts species (Nerve N1; *Schistocerca gregaria* and *Locusta migratoria*) and in the American beetle *Zophobas morio*. They showed in their studies two MNs with contralateral soma position (termed dlm 1 and 2) in the metathoracic ganglion of both species but one cell body (dlm 1) appeared more dorsally with a larger diameter than the other neuron. Besides these neurons they revealed also a single DUM neuron (probably DUMDL, dorsal unpaired median cell of the dorsal longitudinal muscle; Hoyle, 1978) and a cell body more ventrally located than the DUM, which they termed 'central cell'. Comparable are stainings of the homolog nerve 2 (B+C) of the prothoracic ganglion of *Periplaneta americana* (for homologies see Bullock and Horridge, 1965) performed by Iles (1976). Iles (1976) labeled also two contralateral cell bodies, one neuron in a dorsomedian position and another neuron located posterodorsomedian. Because of its cell body position and the course of its primary neurite it is possible that the latter neuron is a homolog of the 'central cell' and of the medioventrally labeled neuron in stick insects. I am not sure which cell bodies in stick insects are homologs of the dlm 1 and 2 MNs because in the stick insect two larger cell bodies in the anterodorsal cluster were found with similar cell body diameters and two neurons slightly more medial with equal diameters. Therefore, a differentiation of MNs by size as reported for the locust Breidbach and Kutsch (1990) is not possible. However, the neurons with the slightly more medially positioned cell bodies are likely to be the homologs with dlm 1 and dlm

2 because their primary neurites follow a similar curved pathway.
Another tracing study was performed by Siegler and Pousman (1990a) in the metathoracic ganglion of the desert locust *S. gregaria*. They stained through nerve 1 (N1) five small cell bodies and a large MN on the contralateral ganglion region supplying the dorsal longitudinal (M112) muscle. A second DUM neuron as shown for the mesothoracic ganglion in locusts (DUM1b; Bräunig et al., 1994; Duch et al., 1999) was not found in stick insects.
Furthermore, sensory afferents were stained that descend through the ipsilateral connective to the metathoracic ganglion. From locusts is known that mesothoracic N1 carries afferents of forewing stretch receptors and of forewing tegulae. Stainings of these sense organs showed afferents descending to the metathoracic ganglion (Burrows, 1975; Büschges et al., 1992) but tegula central projections showed more similarities with labeled stick insect afferents.

Nervus lateralis (nl2)

The backfills of nerve nl2 revealed up to 17 anterolaterally stained MN cell bodies, the CI1 neuron, and at least four DUM cells. Previous tracing studies of nl2 in stick insects by Storrer et al. (1986) labeled eight cell bodies in the anterolateral ganglion region and the ventrally situated CI1 neuron at the midline (for identification of CI1 in stick insects: Bässler and Storrer, 1980; Graham and Wendler, 1981; locust: Burrows, 1973). In contrast to Storrer et al. (1986) nine additional neurons were found in the anterolateral region and at least four DUM cells with clearly visible lateral neurites projecting in the direction of nerve roots na, nl2-4, and ncr. In one preparation a fifth cell body in a dorsomedial position was stained. It is possible that the cell body is a DUM cell but lateral neurites typical for DUM neurons were not identified, which is why I parenthesized the neuron in Tab. 3.3 and Tab. 4.2.
According to Mentel et al. (2008), in stick insects, three different DUM neurons have axons in nl2 and other side nerves: DUMncr nl2,4,5; DUMnl5 nl2; and DUMna nl2 (possibly DUMna nl2,5; see above). Because four DUM neurons were stained it is possible that one type exists in two copies within the mesothoracic ganglion or an undescribed neuron was labeled. Backfills of branch C of nl2, that innervates the protractor coxae muscle, showed six to nine MN cell bodies anterolaterally, the CI1 neuron, and up to four DUM cells. Stainings by Graham and Wendler (1981) of nerve nl2C showed only five to eight cell bodies anterolaterally. The prothoracic nerve 3A in *P. americana* is assumed to be homolog to nl2 (Bullock and Horridge, 1965). Backfills of nerve 3A by Iles (1976) revealed 15 neurons anteroventrally and a single posteroventromedian cell body, the common inhibitory

neuron D3 (Pearson and Iles, 1971). A similar cell body number was labeled in *S. gregaria* by Siegler and Pousman (1990a) through backfills of the metahoracic nerve 3A that is assumed to be homolog to nl2 (Bullock and Horridge, 1965). They stained 14 MNs anterolaterally, eight of which innervate elevators (M113, M118) and depressors (M127, M128) of the hindwing and the remaining six neurons innervate the abductors of the coxa (M125, 126). Compared to stainings of nerve nl2C it is conspicuous that the stick insect protractor muscle appears to possess a more complex innervation than the abductor muscles in locusts. Additionally, Siegler and Pousman (1990a) identified the CI1 neuron and a 'lateral cell' on the contralateral ganglion region. The latter neuron was never observed in any of the nl2 backfills. When considering the identity of neurons in the anterolateral region it is interesting, that Siegler and Pousman (1990a) not only stained 14 cell bodies in the anterolateral region but also a variable number of smaller cell bodies (dia. ~15 µm). They speculate that these cell bodies either belong to larval MNs (Pflüger et al., 1986) or to strand receptors, similar to those stained through nerve 3B in locusts (Bräunig and Hustert, 1980; Bräunig, 1982b). The nl2 stainings showed small cell bodies as well. However, neither do I think that the small cell bodies in the backfills belong to larval MNs nor that strand receptors were filled. Selected were only fully matured stick insect imagos at least one week after the adult molt to avoid the occurrence of larval MNs in whole-mounts as reported for locusts (Pflüger et al., 1986). Furthermore, the primary neurite pathway of the small cell bodies differs from the pathways of primary neurites of strand receptors of nerve nl3 in stick insects (Fig. 3.18a, dashed yellow line). But still, whether the small cell bodies belong to functional adult MNs or sensory cells remains to be clarified.

Nervus lateralis 3 (nl3) and femoral branch 2 (F2) of nervus cruris (ncr)

In backfills of nerve nl3 the FETi MN and up to 23 small cell bodies were labeled in the anterolateral ganglion region. A maximum of seven MNs, including SETi were stained laterally, and one DUM cell at the ganglion midline. Backfills of the same nerve by Storrer et al. (1986) revealed approximately 20 neurons in the anterolateral region (including the FETi cell body), five to eight neurons laterally and anterior of the origin of nl3 (including the SETi cell body), and the CI1 cell body at the ganglion midline.

Sensory afferents where barely included into the drawings of Storrer et al. (1986). In contrast, numerous afferent fibers were stained. The location of which is the one of the dorsal and ventral coxal hairplates (HP) projections (cxHPd, cxHPv;

Schmitz et al., 1991). Other sensory fibers that run ventrally through the ganglion to terminate in the ventral association center (VAC) have similar central projections as single coxal hairs of locusts, cricket, and cockroaches (Bräunig, 1982b). Furthermore, a so far undescribed sensory afferent was stained that bifurcates and descends through the ipsilateral and contralateral connective to the metathoracic ganglion.

According to Mentel et al. (2008) two types of DUM cells with axons through the nl3 are present in the mesothoracic ganglion of stick insects: DUMncr nl3 and DUMncr nl3,4,5. In the preparations I never stained more than one DUM neuron which I was not able to assign to either type.

The small cell bodies distributed around the FETi MNs most likely belong to sensory neurons because their position matches the position of strand receptor cell bodies in other orthopteran insects (Bräunig, 1982a). In the locust strand receptors innervate a small connective tissue strand in the thoraco-coxal joint of the hind leg (Bräunig and Hustert, 1980). In a comparative anatomical study, Bräunig (1982a) found in metathoracic ganglia of orthopteran insects 17 strand receptors cells in *L. migratoria*, 15 in *Acheta domesticus* (Grillidae), 23 in *Extatosoma tiaratum* (Phasmidae), and 21 in *P. americana* (Blattidae). The results with up to 23 strand receptors matches exactly the number obtained by Bräunig (1982a) in the phasmid species *E. tiaratum*. In general, the arrangement and number of sensory neurons and MNs and projections of sensory afferents that were labeled in nl3 stainings are very similar to backfills of metathoracic nerve 3B in other orthopteran insects (Bräunig, 1982b), except for a larger number of neurons in the lateral group in cockroaches and crickets (10-13 cell bodies in *P. americana* and eight for *A. domesticus* instead of seven neurons in *C. morosus*). Backfills of the locust pro- and mesothoracic nerve 3B by Bräunig (1982a) showed three neurons in the lateral cell group.

Stainings of nerve F2 allows more insights into the dendritic branching of FETi and SETi neurites compared to backfills of nerve nl3 where primary neurites are masked extensively by sensory afferents of coxal HPs. The gross morphology of FETi's branching pattern in stick insects is very similar to the branching pattern of FETi in pro- and mesothoracic ganglia of locusts (Wilson, 1979). The main differences in stick insects are three large dendritic branches that arise shortly after the primary neurite leaves the FETi cell body to run in posterolateral direction to terminate close to SETi's cell body. Such dendritic branches are not present in pro- and mesothoracic FETis in the desert locust *S. gregaria* (Wilson and Hoyle, 1978; Wilson, 1979). The stick insect and locust (Wilson, 1979) primary neurite pathway of SETi and its dendritic branching pattern are almost identical, including the prominent primary neurite loop. Beside FETi, SETi and CI1, three DUM

cells were stained in backfills of nerve F2. Neurites of these cells enter nerve ncr but no projections into other lateral nerves were found. Therefore, these neurons appear to belong to the DUMncr type (Mentel et al., 2008). Nerve F2 is also a mixed nerve that houses axons of tactile hairs on the femur, the RDPL (Récepteur dorso-postéro-latérale), RVPL (Récepteur ventro-postéro-latérale; both receptors described for the locust by Coillot and Boistel, 1968) and the apodeme-receptor (Bässler, 1977a). It is most likely that the sensory afferents terminating in the VAC belong to tactile hairs on the femur because stick insect trochanteral hair afferents terminate in the VAC (Schmitz et al., 1991) as do afferents from locust tactile hairs located ventroposterior on the coxa (Pflüger et al., 1981). The origins of the remaining sensory structures stained through nerve F2 cannot be related to any of the sense organs known to have axons in the nerve. Besides, comparable central projections patterns of femoral sensory structures were not found in the literature for other insect species.

Nervus lateralis 4 (nl4)

In the experiments nine MN cell bodies were labeled anterolaterally, which is close to 10 cell bodies labeled by Storrer et al. (1986). In addition, CI1 and three DUM cells were stained at the ganglion midline. The number of DUM neurons corresponds to the three DUM neuron types (DUMncr nl2,4,5; DUMncr nl3,4,5; and DUMnl5 nl4) that were identified by Mentel et al. (2008) using dye filled microelectrodes. Nerve 3C of locust thoracic ganglia is assumed to be homologous to nl4 (Bullock and Horridge, 1965). This nerve innervates the anterior rotator and adductor of the coxa and depressors of the trochanter. Stainings of locust metathoracic nerve 3C showed also nine cell bodies in the anterolateral region and the CI1 soma at the ganglion midline (Siegler and Pousman, 1990a). While the number of anterior cell bodies is identical in stick insects and locusts it is unclear if in locusts two of these neurons are situated dorsally as in stick insects.
In the stick insect few sensory afferents were stained that terminate in the VAC similar to tactile hair afferents in locusts (Pflüger et al., 1981). A sensory neurite through the ipsilateral anterior connective as described by Storrer et al. (1986) was never observed in any of the preparations.

Nervus lateralis 5 (nl5)

The stainings revealed up to 18 MNs in the posterolateral (PL) cell cluster, seven cell bodies in the posteroventromedial (PVM group), the CI1, six DUM cells, and

one to two anterolateral MN cell bodies. The anterolateral neurons appeared in stainings of all nl5 branches together and in a specimen where only the p branch was stained. Marquardt (1940) reported a fusion of nerve branch nl4C with nerve nl5. Therefore, it is possible that a nerve anastomosis was contaminated with fluorescent dye because labeled nl4 cell bodies are located in the same ganglion region as the backfilled anterolateral nl5 cell bodies. The maximum number of cell bodies counted in a preparation was up to 31 neurons but if the highest number of cell bodies labeled in the different clusters of different specimens is summed-up, it is possible that a total of 34 neurons (including the anterolateral cell bodies and six DUM cells) can be stained via all side branches of nerve nl5. In great contrast, backfills of nerve nl5 (assumed branches A and B) by Graham and Wendler (1981) showed eight MNs. Some more neurons were stained by Storrer et al. (1986), eleven cell bodies in the PL cell group, six neurons in the PVM and the CI1 at the ganglion midline. The reason for such a great difference in cell body number is unclear but the cell bodies cover each other and it might be that confocal laser scanning microscopy is much better to disintegrate such a cell body conglomeration.

Mentel et al. (2008) identified four different types of DUM neurons with axons through nerve nl5: DUMncr nl2,4,5; DUMncr nl3,4,5; DUMnl5 nl2; and DUMnl5 nl4. It is possible that a fifth DUM neuron type exists that project into na, nl2 and nl5. In one of the nl5 backfills branches of a DUM neuron enter nl2 and sent a neurite in the direction of na (the stains fades; Fig. B.2 in the appendix). A similar observation was published by Mentel et al. (2008). Therefore, because only five types of DUM cells with axons in nl5 appear to exist one of these types comes possibly in a copy of two cells.

In the locust nerves 4C and 4D are assumed to be homologs to nl5 in stick insects (Bullock and Horridge, 1965). Backfills of nerve 4C by Siegler and Pousman (1990a) showed two cell bodies in the PL cluster, six neurons in the PVM cell group and the CI1 as found for nerve nl5p in the stick insect. Stainings of nerve 4D revealed eleven neurons but mainly located in the PL cluster with a MN and the CI1 at the midline (Siegler and Pousman, 1990a). This situation is comparable to neurons labeled through branches A and B of nerve nl5 in stick insects. Nerve 4D in locusts innervates bifunctional muscles that are involved in flight and in walking (Ramirez and Pearson, 1988), whereas in stick insects these MN innervate unifunctional retractor coxae muscles only. In prothoracic ganglia of cockroaches Iles (1976) stained nerves that are assumed to be homologs to nl5 in stick insect (Bullock and Horridge, 1965). Through nerve 6A which innervates the tergal remoter coxae he stained fourteen cell bodies in the PL cluster, one neuron in the PVM group and the D3 inhibitory neuron at the midline. Backfills of nerve 6Br

(1+2) in the cockroach labeled seven neurons more medial, which is comparable to the nl5p neurons in the stick insect PVM cluster, and two neurons (including the D3) at the midline.

Coxa branch 1 (C1) of nervus cruris (ncr)

Backfills of C1 revealed eight MN cell bodies anterolaterally and three cell bodies in the posterolateral cell cluster and up to three DUM neurons. Storrer et al. (1986) stained through backfilling C1 only seven neurons anterolaterally and two cell bodies in the posterolateral ganglion region, whereas Hess and Büschges (1997) labeled in addition the CI1 neuron posterior at the ganglion midline. In the posterolateral cell cluster a small cell body was labeled (Fig. 3.21a and c) that might belong to a neuron innervating the levator stretch receptor organ (LvSR; Schmitz and Schöwerling, 1992). Because its location is similar to a neuron that innervates the receptor muscle of the coxo-trochanteral muscle receptor organ (cxtrMRO) in locusts through nerve 4A (Bräunig, 1982b) which is homolog to nerve C1 in stick insects (Bullock and Horridge, 1965). The number of cell bodies stained by backfilling nerve C1 is very similar to the number of neurons labeled through the homolog nerves 4A and B of locusts (Bullock and Horridge, 1965). Bräunig (1982b) backfilled mesothoracic nerve 4A and labeled eight neurons anterolaterally and three neurons posterolaterally, including the cxtrMRO MN. In metathoracic ganglia of locust Siegler and Pousman (1990a) labeled through nerve 4A and B together only seven cell bodies anterolaterally, three neurons posterolaterally and the CI1 neuron, whereas the most anterior cell body labeled in mesothoracic ganglia of locusts and stick insect is lacking. In the prothoracic ganglion of *P. americana* stainings of nerve 6Br4 (homolog to C1; Bullock and Horridge, 1965) showed seven neurons in the anterior cell cluster, two neurons posterolaterally, the inhibitory D3 cell body and a cell body in the posterodorsomedian ganglion region (Iles, 1976). Overall, backfills of C1 homologs in orthopteran insects reveal a comparable number of neurons.

Coxa branch 2 (C2) of nervus cruris (ncr)

Backfills of C2 revealed the fast depressor trochanteris (FDTr), the slow depressor trochanteris (SDTr), and the CI1 neuron. Three cell bodies at the dorsal midline were labeled but only two of these could be clearly identified as DUM neurons by their typical neurite branching pattern. Unexpectedly, two neurons with large cell bodies posteroventromedially were stained in the locations of common inhibitory neurons 2 and 3 (CI2 and 3; Storrer et al., 1986). Previous C2 stainings only

showed the FDTr, the SDTr, and the CI1 (Storrer et al., 1986; Hess and Büschges, 1997). The finding is unexpected but not completely surprising because the innervations pattern of the intrinsic depressor in crickets and the coxal depressor in cockroaches show a similar inhibitory innervation pattern of three MNs (Laurent and Richard, 1986; Pearson and Iles, 1971; Iles, 1976). In contrast, the depressor trochanteris of locusts is innervated by CI1 only (Hale and Burrows, 1985; Siegler and Pousman, 1990a). The excitatory innervation of the depressor muscles appears to be similar in all three insect species (Laurent and Richard, 1986; Pearson and Iles, 1971; Siegler and Pousman, 1990a).

Flexor tibiae branches of nervus cruris (ncr)

Simultaneous backfills of flexor tibiae branches of ncr revealed a variable number of neurons usually showed 19 to 29 cell bodies. These include 17 to 25 anterolateral positioned MN cell bodies, the CI2 and CI3 neurons posteriorly, and one to three DUM cells. In contrast previous stainings of flexor tibiae branches of ncr in stick insects showed twelve to 18 cell bodies, including eight to 14 MN cell bodies anterolaterally and two dorsomedially cell bodies (Storrer et al., 1986). The dorsomedially neurons are probably CI2 and CI3 but it remains unclear why Storrer et al. (1986) notice a dorsal position whereas their drawings indicate a ventral position as in the stainings here. Electrophysiological measurements by Debrodt and Bässler (1989) revealed that the flexor tibiae muscle in *C. morosus* has at least thirteen and *E. tiaratum* (Phasmidae) at least 14 or 15 excitatory flexor MNs and they propose that *C. morosus* possesses probably more than 13 excitatory flexor MNs.

Backfilling flexor branches of ncr showed a great variability in number of stained cell bodies. This results from the fact that the flexor branches are very small and distributed along the entire femoral part of nerve ncr. It is difficult to dissect all of the flexor branches without crushing axons and to fill all neurons because of the long dye traveling distance. Furthermore, the dissection needs to be performed very careful to avoid dye contamination of nerve F4 and F5 of nerve ncr. How many MNs are actually innervating the stick insect flexor tibiae muscle cannot be definitely answered. It is possible that about six more flexor MN are present than previously revealed by Debrodt and Bässler (1989) and Storrer et al. (1986). Probably, neurons take up fluorescent dyes more easily than cobalt ions. This, in combination with confocal microscopy uncovers a more complete innervations pattern than previous studies.

The flexor tibiae muscle in middle legs of the desert locust *S. gregaria* is innervated by twelve excitatory, two inhibitory and two DUM neurons (Theophilidis

and Burns, 1983). In locusts the specialized hind leg flexor tibiae muscles are less complex innervated as the mesothoracic flexor muscle but nevertheless by at least nine excitatory (Phillips, 1981) and two inhibitory MNs (Hale and Burrows, 1985). Interestingly, cobalt backfillings of nerve 5B2 in locusts where it supplies all the anterior bundles of the hind leg flexor tibiae revealed between eleven and 15 cell bodies (Sasaki and Burrows, 1998), indicating that the hind leg flexor is possibly innervated by more than nine excitatory neurons. The authors, however, suggest that cobalt chloride may have leaked into other axons. In middle legs of cockroaches eight flexor MNs were found (Dresden and Nijenhuis, 1958). In contrast to locusts and cockroaches, the flexor muscle of crickets seems to be as complex innervated as in stick insects. Nishino (2003) estimated that the cricket hind leg flexor muscle is innervated by 19 to 21 neurons.

The questions arises why the flexor tibiae muscles in orthopteran insects possesses such a complex innervation or why its antagonist the extensor tibiae is innervated only by two excitatory neurons? Ball and Goodman (1985a, 1985b) studied the development of the extensor and flexor tibiae muscles in locust embryos. They showed that the extensor muscle develops from a single pioneer cell, whereas the flexor muscle develops, in contrast, from three pioneers. This observation indicates that the flexor muscle might originate from a fusion of three muscles. In support of this view, Theophilidis and Burns (1983) suggested that the flexor tibiae does not function as a single muscle and that some muscle parts are used to achieve rapid movements and other parts to produce fine controlled tensions for posture. Other authors propose that specific slow MNs may be used to control limb muscles for reflex responses while others are used for generating locomotory movements (Zill and Moran, 1982). Duch and Pflüger (1995) revealed through electromyographic recordings that flexor MNs with large spikes are active during horizontal walking, occasionally during vertical climbing and never during upside-down walking. In the stick insect middle leg the flexor muscle is a stance phase muscle (Rosenbaum et al., 2010) and slow and fast MNs are recruited sequentially during stance phase (Gabriel et al., 2003). Perhaps the multitude of MNs allows a fine tuning of force during stance phase that is not necessary for the stereotypical swing movement to which extensor MNs contribute.

Femoral branches 4 and 5 (F4/5) of nervus cruris (ncr)

Combined backfills of nerves F4 and F5 showed up to six MN cell bodies, at least three, in the anterolateral ganglion region. Common inhibitory neurons CI2 and CI3 were labeled in six preparations and up to two DUM cells in three preparations. The number of up to ten neurons that were labeled by far exceeds the

number of three cell bodies in the anterolateral cluster that were stained by Storrer et al. (1986). However, the data here approximately match anatomical data by Walther (1980). Transverse sections of the distal nerve (F5) revealed three large diameter profiles and up to ten smaller ones. Therefore, I assume that in Storrer et al. (1986) and in experiments in which only three cell bodies were labeled, dye reached the ganglion via large diameter axons only. Walther (1980) examined also the innervation of the femoral RU muscle in two locust species (*S. gregaria* and *L. migratoria*) and revealed that the femoral RU muscle in *L. migratoria* is innervated by two fast and two slow excitatory, two inhibitory neurons and a neurosecretory neuron, whereas the femoral RU in *S. gregaria* is supplied by two excitatory, two inhibitory and a neurosecretory neuron as well. Therefore, the data of Walther (1980) and the stainings of nerve F4/5 here demonstrate that the femoral RU muscle in stick insect possesses a more complex innervation than its homolog in locusts.

Nervus unparis (nup)

Backfills of nup labeled 14 to 15 MNs, four to five of which midline in the posterior ventral cortex and the laterally located stained cell body clusters at the dorsal side. Previous nup stainings by Storrer et al. (1986) showed a different picture: 14 cell bodies in the posterior ventral location and four neurons that are situated dorsally at the midline. Comparable stainings of retrogradely labeled median nerves of insects were not found in the literature, but Burrows (1982) examined intracellulary MNs with axons within the median nerve of thoracic ganglia of locusts. He revealed two MNs that innervate the mesothoracic spiracular closer muscles. These cell bodies are located ventrally in a median region similar to those of the nup neurons. Interestingly, the mesothoracic spiracles of locusts lack opener muscles, whereas metathoracic spiracles possess these muscles and as a consequence four neurons are arranged in pairs as found frequently in stick insects except for one preparation that showed also a fifth neuron. However, in stick insects these MNs supply common intersegmental lateral muscles and not regular spiracle muscles as in abdominal ganglia (Marquardt, 1940).

Nervus posterior (np)

The number of MN cell bodies labeled in backfills of nerve np exactly match data by Storrer et al. (1986) who found also 18 cell bodies in mesothoracic ganglia of stick insects. In contrast, an undescribed large cell body was found situated dorsally at the ganglion center and an anterolaterally cell body on the contralateral

side that were not detected by Storrer et al. (1986). Similar numbers were found in other insect species. In prothoracic ganglia of cockroaches Iles (1976) injected cobalt iontophoretically into nerve 2Ar2 (assumed to be homolog to np; Bullock and Horridge, 1965) and labeled 15 cell bodies in posterior and ventral ganglion regions. Breidbach and Kutsch (1990) examined the dorsal longitudinal muscles in larval and adult locust species (*S. gregaria* and *L. migratoria*) and of the American beetle *Z. morio*. In locusts these flight muscles are innervated via a nerve that is a merger of nerve 1 in the muscle containing segment and nerve 6 (recurrent nerve, RNa) from the preceding ganglion (Neville, 1963). Their stainings showed in prothoracic ganglia a cell body cluster with four large and three smaller ipsilateral cell bodies and occasionally a ventral midline cell (missing in *Z. morio*), whereas Kutsch and Heckmann (1995) stained in addition three neurons more (including an contralateral neuron, see below). Furthermore, Siegler and Pousman (1990a) performed backfills of nerve N1 in locusts distal to the juncture with nerve branch RNa (mesothoracic N6) to show four cell bodies ipsilateral in the mesothoracic ganglion, whereas stainings of branch RNa alone displayed four neurons arranged in two pairs in posterior regions of the mesothoracic ganglion and an anterolateral cell body contralaterally to the filled nerve. Such an anterolateral neuron on the contralateral side was also found in stick insects but in locusts, interestingly, the neuron possesses axons in nerves N1, N3, and N6 (Siegler and Pousman, 1990a; Kutsch and Heckmann, 1995). Multiple axons of this neuron in stick insects were never observed.

DUM cell population in the mesothoracic ganglion

When the tracing study of mesothoracic nerves was started it was still unclear how many DUM neurons exists in the mesothoracic ganglion of stick insects. Mentel et al. (2008) assume that a minimum of nine DUM neurons should be located in the mesothoracic ganglion. The data here confirm this assumption because up to nine DUM cells were stained. By intracellular staining Mentel et al. (2008) discriminated eight different DUM cell types. According to lateral neurite projections through peripheral nerves or through connectives the cell types were named DUMncr; DUMncr nl3; DUMncr nl2,4,5; DUMncr nl3,4,5; DUMnl5 nl2; DUMnl5 nl4; DUMna nl2; and DUM H-cell. The H-cell possesses only projections through the anterior and posterior connectives. I suggest that the DUMna nl2 type possesses axons also in nerve nl5 because I observed in a single nl5 backfill neurites of a DUM cell entering nl2 and sent a neurite in the direction of na. I could not clearly observe DUM cell neurite projections contralateral to the dyed nerves because of a fading label.

The posterior DUM cell clustering in stick insects is comparable to the situation in locusts, crickets, and cockroaches. In the locust 20 to 21 DUM neurons were found by octopamine immunohistochemistry (Stevenson and Spörhase-Eichmann, 1995), 19 cells are efferent (Duch et al., 1999). In crickets ten DUM cells and in cockroaches eight octopaminergic DUM neurons were labeled dorsally in mesothoracic ganglia (Stevenson and Spörhase-Eichmann, 1995). The tracing study here revealed nine efferent DUM neurons. Together with the DUM H-cell the total number is the same as in crickets.

4.2.2. Concluding remarks

The backfill technique of axons is a convenient method for labeling afferent and efferent neurons. Disadvantages of this method are its preference for large diameter axons and problems that come with handling very small side nerves, e.g., crushing or misplacing nerve branches. As shown here, the first problem can be reduced by using dextran-coupled fluorescent dyes instead of cobalt chloride (compare the data here and data by Storrer et al., 1986 in Tab. 3.3). Problems with handling are probably the main reason for the variability of neuron numbers between experiments. These problems also impede the comparison of published data. However, the total number of excitatory MNs that innervate leg muscles in different insect species appear to vary considerably. In the cockroach prothoracic ganglion 122 different paired MNs were stained by Iles (1976). A majority of these neurons are leg MNs because the respective segment lacks wing muscles (Carbonell, 1947). In the stick insect middle leg up to 106 MNs were stained (without unpaired nerves), a number that is comparable. Locust hind leg muscles are served by 70 MNs (Burrows, 1996) and prothoracic *Drosophila* leg muscles are driven by 48 to 56 MNs (Brierley et al., 2012; Baek and Mann, 2009). Small differences in numbers may be due to comparing MNs from different legs. For example, Theophilidis and Burns (1983) report 12 and Sasaki and Burrows (1998) nine excitatory MNs that innervate the locust middle and hind leg flexor muscle respectively. While differences in numbers are interesting and ask for an explanation one has to have in mind that differences might at least partly be due to different staining techniques and improvements in microscopy techniques.

Table 4.2. – Assumed homolog nerve roots and efferent neurons in thoracic ganglia of stick insect, locust, and cockroach.

Stick insect	Locust	Cockroach
Nervus anterior (na) Target muscles and specific features: meso.: dorsal longitudinal, intersegmental, muscles of the heart; joins prothoracic nerve np and nerve nup [1,2] Neurons meso. g.: (MNs) 7–9; (DUM) 1; locations: (ALC) 7–8; (M) 2 (central cell and DUM cell) DUM cell type meso.g.: DUMna nl2,5 [5, present study]	**Nerve 1** Target muscles and specific features: meta.: dorsal longitudinal (dlm), fifth ventral longitudinal, lateral oblique intersegmental; joins mesothoracic recurrent nerve and mesothoracic tergal and spiracular nerve [7,8,9] Neurons meta. g.: (MNs) 3; (DUM) 1; locations: (ALC) dlm1 and dlm2; (M) central cell and DUM cell [10] meta. g.: (MNs) 6; locations: (ALC) 6 (probably include larval MNs) [11] DUM cell types DUMDL; DUM1b [25,26]	**Nerve 2 (B+C)** Target muscles and specific features: pro.: first and second protergal, second cervical muscle of head, foregut suspensor, dorsal longitudinal, oblique dorsal, transverse dorsal; branch of nerve 2B joins intergang. connective [29] Neurons pro. g.: (MNs) 3; (DUM) 1?; locations: (ALC) 2; (M) 2 [30] DUM cell types[3]
Nervus lateralis 2 (nl2) Target muscles: meso.: pleuro-sternal, tergo-pleural ventilatory, protractor coxae, tergo-trochatinal [1,2] Neurons meso. g.: (MNs) 13–18; (DUM) 4 (5?); locations: (AL) 12–17; (PM) CI1 and 4 (5?) DUM cells DUM cell types meso. g.: DUM na nl2,5; DUMncr nl2,4,5; DUMnl5 nl2 [5]	**Nerve 3A** Target muscles: meta.: 1st tergosternal, anterior tergocoxal (promotor), 1st pleurocoxal/abductor, 3rd pleurocoxal/abductor, 1st basalar, 2nd basalar [8,11] Neurons meta. g.: (MNs) 16[1]; locations: (AL) 14; (PM) CI1; (C) 1 [11] DUM cell types[2] meso. g.: 5 DUM3(A); 3 DUM3(A),4; 3 DUM3 (A,C),4; 4 DUM3,4,5 [27]	**Nerve 3A** Target muscles: pro.: cephalic, protergal muscle of the neck, 2nd, 3rd and 4th tergal, tergal promotor, 1st, 2nd 3rd and 4th tergopleural, sternopleural promotor [29] Neurons pro. g.: 5 (stained through nerve branch 3Apr1); locations: (AV) 4; (PM) D3 [30] pro. g.: 16 (stained through nerve branch 3Ar2); locations: (AV) 15; (PM) D3 [30] pro. g.: 8 (stained through nerve branch 3Ar3); locations: (AV) 7; (PM) D3 [30] DUM cell types[3]
Nervus lateralis 3 (nl3) Target muscles and specific features: meso.: accessory depressor and accessory levator trochanteris, extensor tibiae; joins nerve F2 [3,4] Neurons meso. g.: (MNs) 9; (SR) 9–23; (DUM) 1; locations: (AL) FETi and 23 SR; (L) SETi and 6 cell bodies; (PM) CI1 and one DUM cell DUM cell types meso. g.: DUMncr nl3 or DUMncr nl3,4,5 [5]	**Nerve 3B** Target muscles: meta.: anterior levator of trochanter, extensor tibiae [13,15] Neurons meso. g.: (MNs) 5; (SR) 20; locations: (AL) FETi and 20 SR; (L) 3; (PM) CI1 [13] meta. g.: (MNs) 9; (SR) 15–20; locations: (AL) SETi and 15–20 SR; (L) 7; (PM) CI1 [11] DUM cell types[2] meso. g: 4 DUM3,4,5 [27]	**Nerve 3B** Target muscles: meta.: anterior coxal levator (not classified in the prothorax) [29] Neurons pro. g.: (MNs) 10; locations: (AV) 9; (PVM) D3 [30] meta. g.: (MNs) 12–15; (SR) 21; locations: (AL) 1 cell body and 21 SR; (L) 10–13; (PM) D3 [31] DUM cell types[3]
Nervus lateralis 4 (nl4) Target muscles: meso.: pleural, tergal and sternal depressors of trochanter, pleural remotor coxae [2] Neurons meso. g.: (MNs) 9–10; (DUM) 3; locations: (AL) 9, (PM) CI1 and 3 DUM cells DUM cell types meso. g.: DUMncr nl2,4,5; DUMncr nl3,4,5; DUMnl5 nl4 [5]	**Nerve 3C** Target muscles: meta.: anterior rotator of coxa, adductor of coxa, depressors of trochanter [13,15] Neurons meta. g.: (MNs) 10; locations: (AL) 9; (PM) CI1 [11] DUM cell types[2] meso. g.: 3 DUM3(A,C),4; 4 DUM3,4,5 [27]	**Nerve 4** Target muscles: pro.: sterno-coxal, pleural and tergal depressors [29] Neurons pro. g.: (MNs) 8 (stained trough nerve branch 4r2); locations: (AL) 5; (PM) D1–3 [30] pro. g.: (MNs) 7 (stained through nerve branch 4r3); locations: (AL) 6; (PM) D3 [30] DUM cell types[3]

Refer to Tab. 4.4 for footnotes.

Table 4.3. – (continued)

Stick insect	Locust	Cockroach
Nervus unparis (nup) Target muscles and specific features: meso.: intersegmental lateral; joins mesothoracic np and metathoracic na [1] Neurons meso. g: (MNs) 9–14 (15?); locations: (PVM) 4 (5?); (PL) 10 (5 in each lateral cell body cluster on the left and right hemiganglion) DUM cells not observed	**Median nerve** Target muscles meso.: spiracular; joins nerve 1 of metathoracic ganglion [9] Neurons meso. g: 9 (backfilled through one side branch) [19]; (MNs) at least 2; locations: (PVM) 2 spiracle closer MNs [20]; (PL) 7 (up to 5 in each lateral cell body cluster on both sides of ganglion), 8–10 cell bodies in each lateral cluster showed bovine pancreatic polypeptide-like and myomodulin-like immunoreactivity [19,21] DUM cells not available [27]	**Nerve 8** Target muscles: pro.: closing muscle of first spiracle; joins nerve 2 of mesothoracic ganglion [29] Neurons pro. g.: (MNs) 4; locations: (PVM) 4 [30] DUM cells unknown
Nervus posterior (np) Target muscles and specific features: meso.: ventral longitudinal; joins mesothoracic nerve nup and metathoracic nerve na [1] Neurons meso. g: (MNs) 11–18; locations: (PM) 11–18 DUM cells not observed	**Nerve 6 (RNa)** Target muscles and specific features: meso.: third and fourth ventral longitudinal; joins nerve 1 of metathoracic ganglion [9] Neurons pro. g.: (MNs) 7–8; locations: (PM) 7–8 [10] pro. g. and meso. g.: (MNs) 11; locations: (ALC) 1; (PM) 10 [16] meso. g.: (MNs) 4 (stained through metathoraic N1 distal to juncture with RNa); locations: (PM) 4 [11] meso. g.: (MNs) 5 (stained through branch RNa); locations: (ALC) 1; (PM) 4 [11] DUM cells: no DUM cells [27]	**Nerve 2A** Target muscles and specific features: meso.: ventral oblique, sterno-spinal, ventral longitudinal, sternal-spinal intersegmental; branch 2Ar2 anteriorly joins intergang. connective [30] Neurons pro. g.: (MNs) 15 (stained through mesothoracic nerve branch 2Ar2); locations: (PM) 15 [30] DUM cells unknown
Nervus lateralis 5 (nl5) Target muscles: meso.: tergal retractor coxae, sternal remotor, sternal adductor [1,2] Neurons meso. g.: (MNs) 23–26 (without 1-2 AL neurons); (DUM) 5–6; locations: (AL) 1–2; (PL) 18; (PVM) 7; (PM) CI1 and 5–6 DUM cells DUM cell types meso. g.: DUMncr nl2,4,5; DUMncr nl3,4,5; DUMnl5 nl2; DUMnl5 nl4; DUM na nl2,5 [5]	**Nerves 4C&D** Target muscles: first, second and third posterior rotator of coxa,pleuroalar, first and second posterior tergocoxal, subalar [8,11,17,18] Neurons meta. g.: (MNs) 8 (stained through nerve branch 4C); locations: (PL) 2; (PVM) 5 and CI1 [11] meta. g.: (MNs) 13 (stained through nerve branch 4D); locations: (PL) 11; (PM) 1 and CI1 [11] DUM cell types[2] meso. g.: 3 DUM3(A),4; 3 DUM3(A,C),4; 4 DUM 3,4,5 [27]	**Nerves 6A&Br(1+2)** Target muscles: pro.: tergal remotor coxae, first, second, third and fourth tergomeral, spinal muscle of coxa, episternal muscle of coxa, sternal adductor of coxa [29] Neurons pro. g.: (MNs) 16 (stained through nerve branch 6A); locations: (PL) 14; (PM) 1 cell body and D3 [30] pro. g.: (MNs) 8 (stained through nerve branches 6Br(1þ2)); locations: (PL) 6; (PM) 1 cell body and D3 [30] DUM cell types[3]
Coxabranch 1 (C1) Target muscles and specific features meso.: levator trochanteris, levator stretch receptor organ (LvSR) [1,6] Neurons meso. g.: (MN) 10–12, (DUM) 3; locations: (AL) 8; (PL) 3; (PM) CI1 and 3 DUM cells DUM cell types unknown	**Nerves 4A&B** Target muscles and specific features: posterior levator trochanteris, coxosutral, pleurosternal, coxotrochanteral muscle receptor organ (cxtrMRO) [11,13] Neurons meso. g.: (MNs) 11; locations: (AL) 8; (PL) 3 [13] meta. g.: (MNs) 11; locations: (AL) 7; (PL) 3; (PM) CI1 [11] DUM cell types[2] meso. g.: 3 DUM3(A),4; 3 DUM3(A,C),4; 4 DUM 3,4,5 [27]	**Nerve 6Br4** Exchange Destinations for target muscles: main levator, secondary levator [29] meta. g.: (MNs) 10–11; locations: (AV) 7; (PL) 2–3; (PM) D3 [32] DUM cell types[3]

Refer to Tab. 4.4 for footnotes.

Table 4.4. – (continued)

Stick insect	Locust	Cockroach
Coxabranch 2 (C2) Target muscles: meso.: depressor trochanteris [1] Neurons meso. g.: (MNs) 5, (DUM) 2–3; locations: (AL) FDTr; (PM) SDTr , CI1–3 and 2 or 3 DUM cells DUM cell types unknown	**Nerve 5A** Target muscles: depressor trochanteris [13] Neurons meta. g.: (MNs) 3; locations: (AL) FDTr; (PM) SDTr and CI1 [11] DUM cell types[2] meso. g.: 4 DUM3,4,5 [27]	**Nerve 5r1** Target muscles: pro.: main depressor, anterior and posterior depressor of the leg [29] Neurons pro. g: (MNs) 5; locations: (AV) Df; (PL) Ds; (PM) D1–3 [30] DUM cell type meta. g.: DUM5r1 [33]
Femoral branch 2 (F2) Exchange Destination for Target muscle: extensor tibiae [3] Neurons meso. g.: (MNs) 3, (DUM) 3; locations: (AL) FETi; (L) SETi; (PM) CI1 and 3 DUM cells DUM cell types unknown	**Nerve 5B1** Target muscles: extensor tibiae [15] Neurons meta. g.: (MNs) 4; locations: (AL) SETi; (L) FETi; (PM) CI1 and 1 DUM cell [12,22] DUM cells meso. g.: 1 DUM3,4,5 [28]	**Nerve 3Br11** Target muscles: extensor tibiae [34,36] Neurons meso. g./meta. g.: (MNs) FETi, SETi and common inhibitory neuron (based upon muscle recordings) [35] DUM cell types[3]
Flexorbranches of nervus cruris Target muscles: meso.: flexor tibiae [1] Neurons meso. g.: (MNs) 10–27, (DUM) 0–3; locations: (AL) 8–25; (PM) CI2, CI3 and 0–3 DUM cells DUM cell types unknown	**Nerve 5B2** Target muscles: flexor tibiae [14] Neurons meta. g.: (MNs) at least 11; locations: (AL) 9; (PM, M) CI2 and CI3 [23] DUM cell types meso. g.: 2 DUM3,4,5 [28]	**Nerve 5** Target muscles: meso.: i.a. flexor tibiae [34,36] Neurons meso. g.: (MNs) 9 (based upon nerve sections) [36] DUM cell types[3]
Femoral branch 4 and 5 (F4/5) Target muscles: meso.: retractor unguis I [3,24] Neurons meso. g.: (MNs) 3–7, (DUM) 1–2; locations: (AL) 3–6; (PM) CI2, CI3 and 1–2 DUM cells DUM cell types unknown	**Nerve 5B2** Target muscles: meta.: retractor unguis a [12,15] Neurons meta. g.: *(MNs) 6, (DUM) 1 (based upon muscle recordings and nerve sections) [24] **(MNs) 4, (DUM) 1 (based upon muscle recordings and nerve sections) [24] DUM cell types unknown	**Nerve 5** Target muscles: meta.: i.a. retractor unguis a [34,36] Neurons meta. g.: (MNs) 2 (based upon nerve sections) [36] DUM cell types[3]

**L. migratoria.* ***S. gregaria.*

[1]A variable number of unidentified small cell bodies were excluded from the account by Siegler and Pousman (1990a).

[2]Most studies do not provide information on DUM axons in higher-order roots. In the list of neurons with axons in such roots I included DUM cells with an axon in the respective primary root (e.g., DUM3,4,5 appears in the listing for nerve 3A) although I do not know whether its axon is to be found in the higher-order root. By this, I intend to indicate possible DUM innervation of the respective muscles.

[3]According to Tanaka and Washio (1988) six different types of DUM neurons are present in the metathoracic ganglion of the cockroach: **DUM2,3; DUM2,3,4; DUM3,5; DUM3,4,6; DUM3,5,6;** and **DUM5**.

AL, anterolateral; **ALC**, anterolateral and contralateral to stained nerve; **AV**, anteroventral; **C**, contralateral; **CI1–3**, common inhibitory neurons 1–3; **D1–3**, common inhibitory neurons 1-3; **Df**, fast depressor motoneuron; **DUM**, dorsal unpaired median neuron; **FDTr**, fast depressor trochanteris motoneuron; **FETi**, fast extensor tibiae motoneuron; **L**, lateral; **M**, medial; **meso. g.**, mesothoracic ganglion; **meta. g.**, metathoracic ganglion; **MN**, motoneuron; **PL**, posterolateral; **PM**, posteromedian; **PVM**, posteroventromedial; **pro. g.**, prothoracic ganglion; **RNa**, recurrent nerve branch a; **SDs**, slow depressor motoneuron; **SDTr**, slow depressor trochanteris motoneuron; **SETi**, slow extensor tibiae motoneuron; **SR**, stretch receptor cell bodies.

Stick insect: [**1**] Marquardt, 1940; [**2**] Graham, 1985; [**3**] Bässler, 1977a; [**4**] Storrer et al., 1986; [**5**] Mentel et al., 2008; [**6**] Schmitz and Schöwerling, 1992.

Locust: [**7**] Bullock and Horridge, 1965; [**8**] Burrows, 1975; [**9**] Campbell, 1961; [**10**] Breidbach and Kutsch, 1990; [**11**] Siegler and Pousman, 1990a; [**12**] Burrows, 1996; [**13**] Bräunig, 1982b; [**14**] Phillips, 1981; [**15**] Burrows and Hoyle, 1973; [**16**] Kutsch and Heckmann, 1995; [**17**] Pflüger et al., 1986; [**18**] Kutsch and Usherwood, 1970; Kutsch and Schneider, 1987; [**19**] Myers and Evans, 1985; [**20**] Burrows, 1982; [**21**] Swales and Evans, 1994; [**22**] Wilson, 1979; [**23**] Sasaki and Burrows, 1998; [**24**] Walther, 1980; [**25**] Hoyle, 1978; [**26**] Bräunig et al., 1994; [**27**] Bräunig and Pflüger, 2001; [**28**] Duch et al., 1999.

Cockroach: [**29**] Pipa and Cook, 1959; [**30**] Iles, 1976; [**31**] Bräunig, 1982a; [**32**] Pearson and Fourtner, 1973; [**33**] Elia and Gardner, 1990; [**34**] Dresden and Nijenhuis, 1953; [**35**] Atwood et al., 1969; [**36**] Dresden and Nijenhuis, 1958.

4.3. Calcium transients in retrogradely labeled mesothoracic retractor coxae neurons

Motoneurons are the primary output elements of the central nervous system (CNS). During stick insect walking, leg MNs show a rhythmic bursting pattern based on alternating phasic excitatory and inhibitory synaptic inputs, with an underlying long-lasting (tonic) background depolarization (Schmidt et al., 2001; Ludwar et al., 2005). Experiments in the stick insect showed that inhibitory synaptic inputs onto MNs derive from central pattern generators (CPG) (Büschges, 1998; Büschges et al., 2004). The tonic excitation is assumed to has its origin in descending and/or intersegmental sources (Ludwar et al., 2005; Westmark, 2007). Additionally, MNs receive rhythmic synaptic drive of sense organs associated with the legs (Akay et al., 2001).

As yet, the mechanism for the generation of the tonic depolarization and the role of Ca^{2+} in stick insect MNs is not fully understood. Westmark et al. (2009) showed that the tonic depolarization underlying flexor MNs during walking decreased after injecting the Ca^{2+} chelator BAPTA-1 intracellularly. Moreover, patch-clamp recordings of stick insect MN cell bodies in combination with Ca^{2+} imaging revealed that a fraction of actetylcholine induced currents (I_{ACh}) was carried by Ca^{2+} (~18%; Oliveira, 2010; Oliveira et al., 2010). The latter study had the disadvantage that only MN somata were investigated and not the synaptic input sites of MN dendrites located in the dorsal and lateral ganglionic neuropils as shown in sec. 3.2. Imaging of Ca^{2+} in MN neurites in combination with electrophysiological recordings could therefore be a powerful tool to gain more insights into the intrinsic properties, the integration sites of synaptic inputs, and especially the role of Ca^{2+} in stick insect MNs. Ca^{2+} imaging allows, in contrast to intracellular and patch-clamp recordings, to investigate many neurite locations simultaneously. This is why in the third part of the thesis a method was established that allows stable *in situ* optical measurements of free intracellular Ca^{2+} after retrograde labeling axons with a Ca^{2+}-sensitive fluorescent indicator.

4.3.1. Intracellular Ca^{2+} transients in MN neurites

The pharmacological and tactile stimulation experiments showed clear intracellular Ca^{2+} transients in RetCx MNs in anti-phase to extracellular spike activity of antagonistic ProCx MNs (Fig. 3.29) and in-phase to extracellular recorded spike activity of the backfilled RetCx nerve (e.g., Fig. 3.30, Fig. 3.32, Fig. 3.41). Amplitudes of $[Ca^{2+}]_i$ elevations were highest mainly on primary neurites. Along secondary neu-

rites the $[Ca^{2+}]_i$ elevations were frequently smaller, but they can reach the same or even slightly higher amplitudes as observed in primary neurites (e.g., ROI3 in Fig. 3.41). Analyzing changes in intracellular Ca^{2+} of RetCx MNs revealed temporarily uniform $[Ca^{2+}]_i$ elevations in all defined ROIs. Uniform $[Ca^{2+}]_i$ transients were reported, for instance, for cricket MN neurites (Baden and Hedwig, 2009) and for leech heart interneuron neurites (Ivanov and Calabrese, 2000).
The time course of $[Ca^{2+}]_i$ elevations revealed sharp rise time constants (mean τ rise ranging from 0.074 s to 0.3 s) with the onset of RetCx bursts and slower decay time constants (mean τ decay ranging from 0.683 s to 1.333 s) to return to baseline level. Decay time constants are presumably underestimated because bursts follow each other with short intervals and, therefore, the decaying $[Ca^{2+}]_i$ signal to baseline level was seldom completely accomplished. When a $[Ca^{2+}]_i$ transient occurs during the decay of a preceding $[Ca^{2+}]_i$ elevation then the amplitude of the $[Ca^{2+}]_i$ signal increases and shows summation. The prolonged decay times can be related to endogenous buffer capacities, the uptake into internal stores, slow extrusion mechanisms, and can depend on the distance of the Ca^{2+} influx region (Augustine and Neher, 1992; Augustine et al., 2003; Kloppenburg et al., 2000). On the other hand, the Ca^{2+} indicator acts as a buffer and can distort the magnitude and time course of the measured signal (Augustine et al., 2003; Haag and Borst, 2000).
Baden and Hedwig (2009) studied $[Ca^{2+}]_i$ transients in neurites of cricket tibial MNs (SETi, FETi and a fast flexor MN, FFTi1) with the same Ca^{2+} indicator used here. For main neurites of the three different tibial MNs they calculated slower rise times (ranging from 0.278 s to 0.301 s) and slower decay times (ranging from 1.965 s to 2.012 s) compared to intracellular Ca^{2+} transients in RetCx neurites of the stick insect. Nevertheless, the slowest mean rise time of RetCx neurites is comparable to Baden and Hedwig (2009), whereas calculated decay time with 1.6 s is close to decay values for the cricket. However, differences in the time course of rise and decay times might be due to different staining techniques. Baden and Hedwig (2009) studied $[Ca^{2+}]_i$ transients in single MNs and I measured $[Ca^{2+}]_i$ transients of several MN neurites. Varying Ca^{2+} indicator concentrations in different experiments should also be considered as reasons for variable time courses calculated here and by Baden and Hedwig (2009).

Mode of Ca^{2+} influx into MN neurites

The experiments revealed obviously that the shapes of the measured RetCx $[Ca^{2+}]_i$ elevations reflect the rectified and smoothed extracellularly recorded spike activities of RetCx MN units. The analysis of the integrals of $[Ca^{2+}]_i$ elevations and integrals of the rectified and smoothed extracellular recorded RetCx spike activity

showed a linear correlation. This suggests that the measured intracellular Ca^{2+} transients in RetCx MNs are the result of Ca^{2+} influx through voltage-gated Ca^{2+} channels (VGCC) activated by membrane depolarizations due to sodium action potentials.
The analysis revealed frequently small integral values that seem not to be linearly correlated (Fig. 3.33a and c; Fig. 3.35). Three reasons are possible for calculated mean $[Ca^{2+}]_i$ intensities that might not reflect the actual burst activities. One reasons could be the result of dye bleaching over time. This could explain the linear correlation for integral values in the first half of experiment 1 shown in Fig. 3.31b, whereas the plot for the second half of the experiment revealed small integral values that are not linearly correlated (Fig. 3.31c). Another reason could be small $[Ca^{2+}]_i$ elevations close to noise that do not reflect properly the activity of bursts of very small MN units (compare small bursts and corresponding $[Ca^{2+}]_i$ signal in Fig. 3.34). Furthermore, in experiments with irregular motor patterns it is often difficult to classify appropriate burst criteria and oftentimes bursts that follow each other in very short intervals are grouped together. Nevertheless, a linear relationship of $[Ca^{2+}]_i$ intensity and mean burst activity is apparent in the plots.

Ca^{2+} channel types

In general, the VGCCs are classified by their voltage thresholds into high-voltage-activated (HVA) and low-voltage-activated (LVA) channels. The VGCCs of mammals are multimeric and consist of five subunits (α_1, α_2, β, γ, δ), whereas the pore-forming α_1 subunit, encoded by ten genes, affects the physiological and pharmacological profiles of these channels (Dolphin, 2009). The gene family can further be divided into three subfamilies responsible for at least six different Ca^{2+} currents: (i) Ca_v1 mediates HVA L-type ('long-lasting') Ca^{2+} currents; (ii) Ca_v2 mediate HVA P/Q ('Purkinje') type, N-type ('neural') and R-type ('residual') Ca^{2+} currents and, (iii) Ca_v3 mediates LVA T-type ('transient') Ca^{2+} currents (Dolphin, 2009). The *Drosophila* genome possess three putative homolog genes to the vertebrate VGCC subfamilies, which were termed as *DmCa1D* (Ca_v1), *DmCa1A* (Ca_v2) and *DmαG* (Ca_v3) (Littleton and Ganetzky, 2000; Ryglewski et al., 2012).
For adult *Drosophila* MN5 neurons, Ryglewski et al. (2012) revealed a transient LVA current (activation between -60 mV and -70 mV) and a sustained HVA Ca^{2+} current (activation -30 mV). Interestingly, *DmCa1A* mediates all the HVA current and 60-70% of the LVA currents in somata of MN5, whereas *DmαG* provide approximately only 30% of the transient LVA Ca^{2+} current (Ryglewski et al., 2012). HVA Ca^{2+} currents in the locust were shown for isolated thoracic neurons of *S. gregaria* by Pearson et al. (1993) and *in vivo* as well as *in vitro* for non-spiking interneurons by Laurent et al. (1993). Similar findings were shown for isolated

leg MNs of *M. sexta* by Hayashi and Levine (1992), whereas isolated somata of cockroach fast depressor MNs revealed LVA and as well HVA Ca^{2+} currents (Mills and Pitman, 1997). The mentioned studies above investigated voltage-gated Ca^{2+} currents primarily of somata, but Ca^{2+} imaging experiments revealed that voltage-gated Ca^{2+} channels are also distributed on the dendritic processes of fly visual interneurons (Haag and Borst, 2000), MN5 neurons of the moth *Manduca sexta* (Duch and Levine, 2002), and tibial MNs of the cricket (Baden and Hedwig, 2009). Interestingly, antidromically elicited sodium spikes revealed Ca^{2+} elevations in the MN5 neuron of the moth, which indicates a spike driven Ca^{2+} entry mechanism (Duch and Levine, 2002). Such a mechanism was also suggested for Ca^{2+} transients in chick, rat, and mouse spinal cord MN somata evoked during antidromic stimulations or rhythmic behavior (O'Donovan et al., 1993; Lev-Tov and O'Donovan, 1995; Bonnot et al., 2002). In contrast, Baden and Hedwig (2009) injected subthreshold depolarizing currents into SETi of the cricket and revealed small Ca^{2+} transients. In addition, they injected rhythmical depolarizing currents into cricket MNs and frequently, the spike generation failed during pulses, but the intracellular Ca^{2+} level increased. Thus, Baden and Hedwig (2009) suggested the existence of a low-voltage-activated Ca^{2+} entry mechanism that could drive directly the level of free intracellular Ca^{2+} of the neuron that possibly allows furthermore the uniform $[Ca^{2+}]_i$ elevations they observed. As mentioned above, Ivanov and Calabrese (2000) reported also uniform intracellular Ca^{2+} transients in leech heart interneurons due to activation of LVA Ca^{2+} channels, which possibly drive graded synaptic transmission. They suggest further that the uniformity of the observed $[Ca^{2+}]_i$ transients results from an evenly distributed channel density across the interneuron dendrites. The striking similarities of the uniform Ca^{2+} transients measured in the stick insect compared to results by Baden and Hedwig (2009) or Ivanov and Calabrese (2000) suggest that Ca^{2+} enters RetCx MN neurites via LVA channels. However, according to Ryglewski et al. (2012) and Mills and Pitman (1997), who found LVA and HVA Ca^{2+} currents on *Drosophila* and cockroach MN somata, it seems possible that stick insect MN neurites possess both of these Ca^{2+} channels types. To test this, I suggest to backfill into cut ends of the RetCx nerve the intracellular sodium channel blocker QX-314 together with the Ca^{2+} indicator to monitor intracellular Ca^{2+} changes in the absence of HVA currents induced by sodium spikes.

Furthermore, it was shown that stick insect leg MN somata possess two types of nicotinic ACh receptors (nAChR) with differing rates in desensitization and a fraction (~18%) of the ACh induced currents are carried by Ca^{2+} ions (Oliveira, 2010; Oliveira et al., 2010). For *Drosophila* it was shown that neurites of the MN5 neuron express the Dα7 subunit of nAChRs (Fayyazuddin et al., 2006; Kuehn

and Duch, 2013). The finding of nAChRs on stick insect MN somata and also on dendritic sites of the *Drosophila* MN5 neuron might argue for the presence of nAChRs also along stick insect MN neurites. The soma of the fast depressor (Df) MN of the cockroach possesses mAChRs and 'mixed' AChRs, which are sensitive to both nicotinic and muscarinic receptor antagonists (David and Pitman, 1995, 1996). The activation of mAChRs leads to a rise in intracellular Ca^{2+} (David and Pitman, 1996). In the stick insect, no evidence for mAChRs nor 'mixed' receptors on stick insect leg MN somata were found (Oliveira et al., 2010), but it can not excluded that they are expressed on MN neurites and if so they could be activated by pilocarpine.

Furthermore, the level of intracellular Ca^{2+} could be modulated by neuroactive substances. In the spiny lobster, Kloppenburg et al. (2000) revealed that dopamine reduced voltage-gated Ca^{2+} currents in the pyloric dilator MNs. In the stick insect, Westmark et al. (2009) showed that bath application of octopamine increased, whereas the octopamine receptor antagonist mianserin decreased the tonic depolarization underlying flexor MNs. In *Drosphila*, the activation of octopamine receptors expressed in neurons of the mushroom bodies and the central complex leads to an increase in intracellular cyclic adenosinmonophosphate (cAMP) and Ca^{2+} (Han et al., 1998). Therefore, an additional increase in intracellular Ca^{2+} after activation of AChRs or octopamine receptors could possibly explain the observation that slightly larger intracellular Ca^{2+} transient amplitudes were measured along a distal region of secondary MN neurites (ROI3, Fig. 3.41) Nonetheless, the intracellular Ca^{2+} transients in RetCx neurites are so far predominantly carried by the activation VGCCs. However, the modulation of ion channels or the activation of currently unknown receptors on stick insect MN neurites and a release of Ca^{2+} from internal stores should also considered to contribute to the intracellular Ca^{2+} signals.

Role of Ca^{2+} in MNs

Ca^{2+} conductances contribute to a variety of firing and intrinsic properties of MNs. For some MNs it was shown that they generate plateau potentials. The plateau capability is essential dependent on the support of Ca^{2+} currents and is regulated by serotonin as shown for crab STG MNs and turtle spinal cord MNs (Zhang and Harris-Warrick, 1995; Hounsgaard and Kiehn, 1993). In insects, plateau potentials were reported for locust flight MNs (Ramirez and Pearson, 1991) and cockroach leg MNs (Hancox and Pitman, 1991), but not for stick insect MNs. The activation of Ca^{2+}-dependent potassium currents (K_{Ca}) are important for spike frequency adaptation (SFA) and burst termination in the lamprey locomotor network (El Manira et al., 1994). SFA was reported for stick insect coxal and tibial MNs by Schmidt

et al. (2001). Furthermore, Ca^{2+} can act as a 2nd messenger and local Ca^{2+} signaling in postsynaptic dendrites could initiate enzymes to modify synaptic strength and structure (Augustine et al., 2003).

Apart from the studies by Westmark et al. (2009) and Oliveira et al. (2010), the role of Ca^{2+} in stick insect MNs is largely unknown. For the tonic depolarization underlying flexor MNs it was hypothesized that it is a form of cellular arousal to increase the effectiveness of phasic excitation in supporting MN firing (Ludwar et al., 2005; Westmark, 2007). The observed intracellular Ca^{2+} transients in the stick insect could as well support the generation of action potentials in RetCx MNs. Interestingly, the pilocarpine experiments revealed, just after the application, an increase in intracellular free Ca^{2+} accompanied by tonic spike activity in the extracellular recordings. Subsequently, the first intracellular Ca^{2+} elevations due to bursts of RetCx MNs occur on the elevated Ca^{2+} signal due to tonic activity of small MN units. It could be that the observed increase in free intracellular Ca^{2+} in the beginning reflects a form of cellular arousal as hypothesized by Ludwar et al. (2005) and Westmark (2007). On the other hand, it was shown that the $[Ca^{2+}]_i$ dynamics of RetCx MN neurites are slow and Ca^{2+} could just be accumulated due to tonic active MN units. Similar maintained elevated $[Ca^{2+}]_i$ signals were observed during continuous electrical stimulations of cricket MNs (Baden and Hedwig, 2009), lamprey spinal MNs (Bacskai et al., 1995), and in MNs of the neonatal rat (Bonnot et al., 2002). Thus, it is most likely that the temporal accumulation of $[Ca^{2+}]_i$ appears due to tonic active small MN units. This assumption is supported by tactile evoked $[Ca^{2+}]_i$ transients, because no large initial $[Ca^{2+}]_i$ increase was observed as in the pilocarpine experiments.

Moreover, the tonic depolarization outlast stepping sequences (Ludwar et al., 2005) and repolarization time constant τ can reach up to 3.7s (Westmark, 2007). This seems similar to the slow decaying $[Ca^{2+}]_i$ signals after burst termination and intracellular Ca^{2+} could induce Ca^{2+}-dependent secondary currents for repolarization. So far, Ca^{2+}-dependent potassium (K_{Ca}) currents as reported for the lamprey locomotor network by El Manira et al. (1994) were not found in stick insects. Whether the increase in free intracellular Ca^{2+} in the beginning of the pilocarpine experiments and the slow declining $[Ca^{2+}]_i$ transients participate in supporting the tonic depolarization cannot be answered and is currently speculative. The Ca^{2+} imaging method presented here could be useful to provide more information in the future about the role of intracellular Ca^{2+} in stick insect MNs.

Occurrence of very large Ca^{2+} transients

Another interesting finding was the occurrence of very large and short $[Ca^{2+}]_i$ transients with amplitudes of up to 30% during pilocarpine-induced activity (Fig. 3.36).

These large $[Ca^{2+}]_i$ transients were observed when very large RetCx MN units were active, during two successive ProCx burst, and in-phase with large LvTr MN units. Büschges et al. (1995) investigated the motor pattern in deafferented mesothoracic ganglia induced by the application of pilocarpine. They described three different spontaneous, recurrent patterns (SRP) of MN activity which were strongly coupled between the activity of different MN pools in about 90% of their experiments. It could be that these very large Ca^{2+} transients observed here are related to such SRP patterns. The most common SRP1 is characterized by a switch from ProCx activity to RetCx during an existing depressor bursts and by an inhibition of the excitatory extensor tibiae MNs (Büschges et al., 1995). They assumed that SRP1 is the centrally generated portion of the switch from swing to stance or the switch from searching to walking. The second SRP resembled a 'reversed SRP1', with a depressor burst coincident with a RetCx burst that stopped its activity to switch to PrCx MN activity (Büschges et al., 1995). SRP2 is assumed to be a switch from swing to stance in a backward walking stick insect (Büschges et al., 1995). The third SRP was described as a switch from ProCx activity to RetCx activity during firing of both extensor tibiae MNs that resembles a transition from stance to swing in a forward walking stick insect (Büschges et al., 1995).
The situation of large Ca^{2+} transients between two successive ProCx burst (Fig. 3.36 b) is comparable to the motor pattern of SRP3. The large Ca^{2+} transients of RetCx in-phase to large LvTr MNs (Fig. 3.36c) could be a variant of SRP2 that is assumed to be a transition in a backward walking stick insect (Büschges et al., 1995). Rosenbaum et al. (2010) showed that during backward walking the LvTr and RetCx muscle activities overlap, because the RetCx muscle becomes a functional swing phase muscle. This is similar as observed here, when large LvTr MN units and a large Ca^{2+} transient in RetCx neurites occur in-phase, whereas afterwards the rhythmicity resembles a forward walking activity pattern with in-phase activity of LvTr and ProCx MN units (Fig. 3.36c). The observation of very large Ca^{2+} transients in-phase during firing of large RetCx MN (Fig. 3.36a) units could not been assigned to one of the SRP pattern. It might be possible that this pattern is an undescribed SRP. However, in the latter case, these large $[Ca^{2+}]_i$ transients occurred after the rhythmicity changed to an irregular motor pattern. It could be that the concentration of pilocarpine diminishes over time to produce such irregular motor patterns. On the other hand, when anterior and posterior connectives were not crushed properly it could be that influences of neighboring ganglia were present. Nevertheless, it seems that these large intracellular Ca^{2+} transients appear during the recruitment of very large RetCx MN units. To proof if these large $[Ca^{2+}]_i$ transients occur during 'fictive transitions' as suggested by Büschges et al. (1995) for the SRPs, requires additional experiments with extracellular recordings

of depressor and extensor nerves.

4.3.2. Intracellular Ca^{2+} transients in lateral DUM neurites

As shown in sec. 3.3.3 it was possible to measure $[Ca^{2+}]_i$ transients in RetCx MN neurites and simultaneously in lateral DUM neurites within the same focal plane of the ganglion. It is not known if the three presumed lateral neurites were from three different DUM cells or if branched neurites of the same neuron or of two DUM cells were imaged. However, the experiment revealed an increase in free intracellular Ca^{2+} in both RetCx MN and lateral DUM neurites just after the application of pilocarpine. The co-variance analysis revealed that the Ca^{2+} transients of the three defined ROIs along lateral DUM neurites oscillate regular and nearly in-phase to each other (Fig. 3.38). This present finding is in agreement with Baudoux et al. (1998) who examined the pilocarpine-induced activity pattern of locust DUM neurons intracellularly. They showed that two recorded DUM5 neurons generate bursts of spikes during the same phase of the cycle. Pilocarpine treatment in the isolated ventral nerve cord of the *M. sexta* larvae elicited synchronous rhythmical activations of efferent unpaired median (UM) neurons as well (Johnston et al., 1999). The overlays of the $[Ca^{2+}]_i$ oscillations of lateral stick insect DUM neurites against the Pro- and RetCx burst cycle, or against the Pro- and RetCx burst onsets (Fig. 3.39) revealed no fixed phase relation to either of the Pro- or RetCx nerve activity, respectively. Baudoux et al. (1998) showed that rhythmical active DUM5 and DUM3,4,5 neurons were only coupled to the levator phase of either side of the ganglion. They found no DUM neuron activity coupled to nerve activity of another MN pool. In support, Johnston et al. (1999) revealed that all segmental *M. sexta* larval UM neurons were coupled to the levator phase during fictive crawling evoked by pilocarpine. Therefore, future projects should examine whether the activity of stick insect DUM neurons are coupled to the levator phase as shown for the locust or *M. sexta*.

The question arises, how Ca^{2+} ions may enter the lateral DUM neurites or whether Ca^{2+} ions are released from internal storages? Most of the DUM Ca^{2+} currents were investigated by patch-clamp recordings of isolated DUM somata located in abdominal and the terminal abdominal ganglion (TAG) of the cockroach. These TAG DUM neurons generate spontaneous electrical activity, similar to pacemaker neurons, with a slow pre-depolarization followed by the termination of an action potential (for review: Grolleau and Lapied, 2000). Several different voltage-activated Ca^{2+} channels of DUM neurons have been classified according to their kinetics and pharmacological properties (reviewed in Wicher et al., 2001). The transient LVA Ca^{2+} channel (tLVA) is characterized by an activation threshold

of -70 mV, whereas the maintained LVA (mLVA) Ca^{2+} channel activates at -60 mV (Grolleau and Lapied, 1996). Both tLVA and mLVA are important for the pre-depolarization of the pacemaker potential (Grolleau and Lapied, 1996). A mid/low-voltage-activated Ca^{2+} channel (M-LVA; activation -50 mV) was identified by Wicher and Penzlin (1997) in the abdominal ganglion 5 (A5) of the cockroach. The last one is a HVA Ca^{2+} channel that activates more positive than -40 mV (Wicher and Penzlin, 1997). Both, the M-LVA and HVA Ca^{2+} channels are considered to control repolarization and afterhyperpolarization of the pacemaker potential via the modulation of Ca^{2+}-activated K^+ currents (Grolleau and Lapied, 2000). In contrast to the cockroach, DUM cells of locusts possess presumably no LVA channels (Heidel and Pflüger, 2006). Instead, Heidel and Pflüger (2006) revealed by patch-clamp recordings of isolated locust DUM neurons at least two different types of Ca^{2+} currents, one inactivating at low membrane potentials (-75 mV and -45 mV) and a second current that inactivates in the range between -55 mV and -20 mV.

Cockroach TAG DUM neurons express also an α-bungarotoxin-sensitive nACh receptor, two types of mAChRs, and a 'mixed' AChR (Lapied et al., 1990; Grolleau et al., 1996). Activation of the 'mixed' ACh receptor results in influx of Ca^{2+}, but so far it is not known whether the 'mixed' ACh receptor is of ionotropic or metabotropic nature. The presence of mAChRs on DUM cells is interesting because in experiments here the mACh agonist pilocarpine was used to induce MN activity and it may be possible that pilocarpine acts directly on DUM neurons. A released of Ca^{2+} by internal storages of isolated locust DUM neurons was shown by Ryglewski et al. (2007). They found a voltage sensor in the DUM cell membrane that activates a G-protein that leads via phosholipase C (PLC) and inositol 1,4,5-triphosphate receptor (IP3R) activation to a release of Ca^{2+} from the endoplasmic reticulum.

The mechanisms of how Ca^{2+} influx or release from internal stores are mediated in DUM neurons are manifold. However, the imaged ROIs defined along lateral stick insect DUM neurites are not considered to be a synaptic integration sites due to missing arborizations in the region as shown in backfills of nerve nl5 (see Fig. B.2). Heitler and Goodman (1978) showed that locust DUM neurons possess presumably four spike initiation zones. One of these zones were suggested to be located distally from the DUM neurite T-branch at the transition from the lateral neurite to the axon on each of the two originating neurites. The region studied by Heitler and Goodman (1978) seems close-by the location where stick insect DUM neurites were imaged. Thus, it could be that the measured $[Ca^{2+}]_i$ signal of lateral DUM neurites was generated by unknown voltage-gated Ca^{2+} channels. For unraveling the generation of $[Ca^{2+}]_i$ transients in lateral DUM neurites additional

experiments are required.

4.3.3. Outlook

The presented method of retrograde loading RetCx neurons with a Ca^{2+}-sensitive indicator allows stable optical measurements of free intracellular Ca^{2+}. The currently dye loading time to measure intracellular Ca^{2+} transients is about 3 hours to ensure that enough dye entered the neurites. For studying $[Ca^{2+}]_i$ transients in a restrained but walking stick insect it would be necessary to minimize the loading times, because tactile stimulation of the animals often failed to induce stepping sequences. One approach could be to inject the Ca^{2+} indicator by depolarizing current pulses into cut ends of nerves, by means of an electrode that fits the nerve to ensure no dye leakage into the thoracic cavity. Dye leakage would presumably result in a high background staining that would blur the indicator staining of neurites. In order to study $[Ca^{2+}]_i$ transients in walking animals it is further necessary to ensure a walking like posture. Therefore, I suggest to lower the microscopy stage of the imaging platform, because in the experiments here the stick insect laid flat under the imaging objective. It should also be tested if the animals are more willingly to perform stepping sequences by using optomotor stimuli (e.g., Jander and Volk-Heinrichs, 1970).
The Ca^{2+} imaging experiments raise new questions, for instance, the mode of Ca^{2+} entry into RetCx neurites. As mentioned above, the intracellular sodium channel blocker QX-314 should be backfilled with the Ca^{2+} indicator to see if the Ca^{2+} influx is driven by sodium spikes which activate high-voltage-gated Ca^{2+}channels. Another experiment would require the blocking of sodium conductances by tetrodotoxin (TTX) and subsequently the application of pilocarpine to test where MN neurites receive synaptic inputs from nonspiking interneurons (NSI). A whole set of new experiments could adress the questions where excitatory, inhibitory or modulatory synaptic input sites are located and what kind of ionotropic or metabotropic receptors are involved. This could be achieved by blocking the complete synaptic transmission of the ganglion and the focal application of, e.g., ACh, nicotine, GABA or octopamine near the sites of stained MN neurites. Furthermore, specific sense organs should be stimulated, like campaniform sensilla located on the tibia and trochanter of stick insects (Zill et al., 2012), to test their impact on a population of RetCx neurons. An open question is also the occurrence of very large $[Ca^{2+}]_i$ transients in RetCx MN neurites induced by pilocarpine. Therefore, extracellular recordings of depressor and extensor nerves are required to prove if they are the result due to spontaneous, recurrent patterns of activity (SRP; Büschges et al., 1995).

Future experiments of intracellular Ca^{2+} transients in DUM neurites require extracellular recordings of LvTr MNs to support the findings by Baudoux et al. (1998) that DUM neuron activity of locusts, elicited with pilocarpine, are only coupled to the levator phase of the motor output. The RetCx nerve carries the axons of at least six different DUM neurons. Their activity should be investigated during walking of the stick insect by imaging their cell bodies located on the dorsal surface of the ganglion.

Closing remarks

With respect to the investigations of neuronal control of walking in the stick insect, the understanding of the neuroantomical organization of the central nervous system is sparse and is lacking depth compared to other 'model systems'. The present thesis extended the current knowledge by providing novel information about the antennal mechanosensory and motor center in the deutocerebrum of the stick insect brain. Moreover, descending brain and SOG interneurons were neuroanatomical investigated. These neurons transmit signals from the brain to thoracic ganglia, where the walking pattern generators are located. The second part featured a neuronatomical atlas of the entire population of motoneurons, modulatory DUM cells, sensory neurons with central cell bodies, and afferent sensory neurons that have axons in all lateral nerves of the mesothoracic ganglion. Apart from the development of protocols for anti-β-tubulin and anti-synapsin immunohistochemistry, a method was established that allows to investigate intracellular Ca^{2+} transients in stick insect motoneuron and DUM neurites. The method could serve to understand the synaptic input sites of motoneurons and the involved transmitters and neuromodulators that shape the motor output.

Bibliography

Ache, J. M., Dürr, 2013. Encoding of near-range spatial information by descending interneurons in the stick insect antennal mechanosensory pathway. J Neurophysiol 110 (9), 2099–2112.

Ai, H., Nishino, H., Itoh, T., 2007. Topographic organization of sensory afferents of Johnston's organ in the honeybee brain. J Comp Neurol 502 (6), 1030–1046.

Ai, H., Rybak, J., Menzel, R., Itoh, T., 2009. Response characteristics of vibration-sensitive interneurons related to Johnston's organ in the honeybee, *Apis mellifera*. J Comp Neurol 515 (2), 145–160.

Akay, T., Bässler, U., Gerharz, P., Büschges, A., 2001. The role of sensory signals from the insect coxa-trochanteral joint in controlling motor activity of the femur-tibia joint. J Neurophysiol 85 (2), 594–604.

Akay, T., Haehn, S., Schmitz, J., Büschges, A., 2004. Signals from load sensors underlie interjoint coordination during stepping movements of the stick insect leg. J Neurophysiol 92 (1), 42–51.

Allgäuer, C., Honegger, H., 1993. The antennal motor system of crickets: modulation of muscle contractions by a common inhibitor, DUM neurons, and proctolin. J Comp Physiol A 173, 485–494.

Ashcroft, F. M., Stanfield, P. R., 1982. Calcium and potassium currents in muscle fibres of an insect (*Carausius morosus*). J Physiol 323, 93–115.

Atwood, H. L., Smyth, T., Johnston, H. S., 1969. Neuromuscular synapses in the cockroach extensor tibiae muscle. J Insect Physiol 15 (4), 529–535.

Augustine, G. J., Neher, E., 1992. Calcium requirements for secretion in bovine chromaffin cells. J Physiol 450, 247–271.

Augustine, G. J., Santamaria, F., Tanaka, K., 2003. Local calcium signaling in neurons. Neuron 40 (2), 331–346.

Bacskai, B. J., Wallén, P., Lev-Ram, V., Grillner, S., Tsien, R. Y., 1995. Activity-related calcium dynamics in lamprey motoneurons as revealed by video-rate confocal microscopy. Neuron 14 (1), 19–28.

Baden, T., Hedwig, B., 2009. Dynamics of free intracellular Ca^{2+} during synaptic and spike activity of cricket tibial motoneurons. Eur J Neurosci 29 (7), 1357–1368.

Baek, M., Mann, R. S., 2009. Lineage and birth date specify motor neuron targeting and dendritic architecture in adult *Drosophila*. J Neurosci 29 (21), 6904–6916.

Ball, E. E., Goodman, C. S., 1985a. Muscle development in the grasshopper embryo. II. Syncytial origin of the extensor tibiae muscle pioneers. Dev Biol 111 (2), 399–416.

Ball, E. E., Goodman, C. S., 1985b. Muscle development in the grasshopper embryo. III. Sequential origin of the flexor tibiae muscle pioneers. Dev Biol 111 (2), 417–424.

Bässler, U., 1977a. Sense organs in the femur of the stick insect and their relevance to the control of position of the femur-tibia-joint. J Comp Physiol A 121, 99–113.

Bässler, U., 1977b. Sensory control of leg movement in the stick insect *Carausius morosus*. Biol Cybern 25, 61–72.

Bässler, U., 1983. Neural Basis of Elementary Behavior in Stick Insects. Vol. 10 of Studies of Brain Function. Springer-Verlag Berlin Heidelberg New York.

Bässler, U., Büschges, A., 1998. Pattern generation for stick insect walking movements - multisensory control of a locomotor program. Brain Research 27 (1), 65–88.

Bässler, U., Storrer, J., 1980. The neural basis of the femur-tibia-control-system in the stick insect *Carausius morosus*. I. Motoneurons of the extensor tibiae muscle. Biol Cybern 38, 107–114.

Bässler, U., Wegner, U., 1983. Motor output of the denervated thoracic ventral nerve cord in the stick insect *Carausius morosus*. J Exp Biol 105, 127–145.

Baudoux, S., Duch, C., Morris, O., 1998. Coupling of efferent neuromodulatory neurons to rhythmical leg motor activity in the locust. J Neurophysiol 79 (1), 361–370.

Berridge, M. J., 1998. Neuronal calcium signaling. Neuron 21 (1), 13–26.

Berridge, M. J., Lipp, P., Bootman, M. D., 2000. The versatility and universality of calcium signalling. Nat Rev Mol Cell Biol 1 (1), 11–21.

Bidaye, S. S., 2012. Neuronal basis for directed walking in *Drosophila melanogaster*. PhD Thesis, University of Vienna.

Böhm, H., Schildberger, K., 1992. Brain neurones involved in the control of walking in the cricket *Gryllus bimaculatus*. J Exp Biol 166, 113–130.

Böhm, L., 1911. Die antennalen Sinnesorgane der Lepidopteren. Arbeiten aus dem Zoologischen Institut der Universität Wien und der Zoologischen Station in Triest 19, 219–246.

Bonnot, A., Whelan, P. J., Mentis, G. Z., O'Donovan, M. J., 2002. Spatiotemporal pattern of motoneuron activation in the rostral lumbar and the sacral segments during locomotor-like activity in the neonatal mouse spinal cord. J Neurosci 22 (3), RC203.

Bootman, M. D., Collins, T. J., Peppiatt, C. M., Prothero, L. S., MacKenzie, L., De Smet, P., Travers, M., Tovey, S. C., Seo, J. T., Berridge, M. J., Ciccolini, F., Lipp, P., 2001. Calcium signalling–an overview. Semin Cell Dev Biol 12 (1), 3–10.

Boyan, G., Williams, L., Meier, T., 1993. Organization of the commissural fibers in the adult brain of the locust. J Comp Neurol 332, 358–377.

Brandt, R., Rohlfing, T., Rybak, J., Krofczik, S., Maye, A., Westerhoff, M., Hege, H.-C., Menzel, R., 2005. Three-dimensional average-shape atlas of the honeybee brain and its applications. J Comp Neurol 492 (1), 1–19.

Bräunig, P., 1982a. Strand receptors with central cell bodies in the proximal leg joints of orthopterous insects. Cell Tissue Res 222 (3), 647–654.

Bräunig, P., 1982b. The peripheral and central nervous organization of the locust coxo-trochanteral joint. J Neurobiol 13, 413–433.

Bräunig, P., 1985. Mechanoreceptive neurons in an insect brain. J Comp Neurol 236 (2), 234–240.

Bräunig, P., Allgäuer, C., Honegger, H.-W., 1990. Suboesophageal DUM neurones are part of the antennal motor system of locusts and crickets. Experientia 46, 259–261.

Bräunig, P., Hustert, R., 1980. Proprioceptors with central cell bodies in insects. Nature 283, 768–770.

Bräunig, P., Pflüger, H.-J., Hustert, R., 1983. The specificity of central nervous projections of locust mechanoreceptors. J Comp Neurol 218, 197–207.

Bräunig, P., Pflüger, H.-J., 2001. The unpaired median neurons of insects. Adv Insect Physiol 28, 185–266.

Bräunig, P., Stevenson, P., Evans, P., 1994. A locust octopamine-immunoreactive dorsal unpaired median neuron forming terminal networks on sympathetic nerves. J Exp Biol 192, 225–238.

Breidbach, O., Kutsch, W., 1990. Structural homology of identified motoneurones in larval and adult stages of hemi- and holometabolous insects. J Comp Neurol 297 (3), 392–409.

Brierley, D. J., Rathore, K., VijayRaghavan, K., Williams, D. W., 2012. Developmental origins and architecture of *Drosophila* leg motoneurons. J Comp Neurol 520 (8), 1629–1649.

Briggman, K. L., Denk, W., 2006. Towards neural circuit reconstruction with volume electron microscopy techniques. Current Opinion Neurobiol 16, 562–570.

Brockmann, A., Robinson, G. E., 2007. Central projections of sensory systems involved in honey bee dance language communication. Brain Behav Evol 70 (2), 125–136.

Bullock, T. H., Horridge, G. A., 1965. Structure and function in the nervous system of invertebrates II. San Francisco, London: Freeman.

Burdohan, J. A., Comer, C. M., 1990. An antennal-derived mechanosensory pathway in the cockroach: descending interneurons as a substrate for evasive behavior. Brain Res 535 (2), 347–352.

Burdohan, J. A., Comer, C. M., 1996. Cellular organization of an antennal mechanosensory pathway in the cockroach, *Periplaneta americana*. J Neurosci 16 (18), 5830–5843.

Burrows, M., 1973. Physiological and morphological properties of the metathoracic common inhibitory neuron of the locust. J Comp Physiol 82, 59–78.

Burrows, M., 1975. Monosynaptic connexions between wing stretch receptors and flight motoneurones of the locust. J Exp Biol 62, 189–219.

Burrows, M., 1982. The physiology and morphology of median nerve motor neurons in the thoracic ganglia of the locust. J Exp Biol 96, 325–341.

Burrows, M., 1996. The neurobiology of an insect brain. Oxford: Oxford University Press.

Burrows, M., Hoyle, G., 1973. Neural mechanisms underlying behavior in the locust *Schistocerca gregaria*. III. Topography of limb motorneurons in the metathoracic ganglion. J Neurobiol 4, 167–186.

Burrows, M., Siegler, M., 1984. The morphological diversity and receptive fields of spiking local interneurons in the locust metathoracic ganglion. J Comp Neurol 224, 483–508.

Büschges, A., 1989. Processing of sensory input from the femoral chordotonal organ by spiking interneurons of the stick insect. J Exp Biol 144, 81–111.

Büschges, A., 1990. Nonspiking pathways in a joint-control loop of the stick insect *Carausius morosus*. J Exp Biol 151, 133–160.

Büschges, A., 1995. Role of local nonspiking interneurons in the generation of rhythmic motor activity in the stick insect. J Neurobiol 27 (4), 488–512.

Büschges, A., 1998. Inhibitory synaptic drive patterns motoneuronal activity in rhythmic preparations of isolated thoracic ganglia in the stick insect. Brain Res 783 (2), 262–271.

Büschges, A., 2005. Sensory control and organization of neural networks mediating coordination of multisegmental organs for locomotion. J Neurophysiol 93 (3), 1127–1135.

Büschges, A., Akay, T., Gabriel, J. P., Schmidt, J., 2008. Organizing network action for locomotion: insights from studying insect walking. Brain Res Rev 57 (1), 162–171.

Büschges, A., Gruhn, M., 2008. Mechanosensory feedback in walking: From joint control to locomotor patterns. Adv Insect Physiol A 34, 193–230.

Büschges, A., Ludwar, B. C., Bucher, D., Schmidt, J., DiCaprio, R. A., 2004. Synaptic drive contributing to rhythmic activation of motoneurons in the deafferented stick insect walking system. Eur J Neurosci 19 (7), 1856–1862.

Büschges, A., Ramirez, J. M., Driesang, R., Pearson, K. G., 1992. Connections of the forewing tegulae in the locust flight system and their modification following partial deafferentation. J Neurobiol 23 (1), 44–60.

Büschges, A., Schmitz, J., Bässler, U., 1995. Rhythmic patterns in the thoracic nerve cord of the stick insect induced by pilocarpine. J Exp Biol 198, 435–456.

Büschges, A., Wolf, H., 1995. Nonspiking local interneurons in insect leg motor control. I. Common layout and species-specific response properties of femur-tibia joint control pathways in stick insect and locust. J Neurophysiol 73 (5), 1843–1860.

Campbell, J., 1961. The anatomy of the nervous system of the mesothorax of *Locusta migratoria migradorioides* R. & F. Proc Zool Soc London 137, 403–432.

Carbonell, C., 1947. Thoracic muscles of the cockroach *Periplaneta americana*. Smithson Misc Coll 107, 1–23.

Carlin, K. P., Jiang, Z., Brownstone, R. M., 2000. Characterization of calcium currents in functionally mature mouse spinal motoneurons. Eur J Neurosci 12 (5), 1624–1634.

Chrachri, A., Clarac, F., 1987. Induction of rhythmic activity in motoneurons of crayfish thoracic ganglia by cholinergic agonists. Neurosci Lett 77 (1), 49–54.

Coillot, J., Boistel, J., 1968. Localisation et description de récepteurs à l'étirement au niveau de l'articulation tibio-fémorale de la patte sauteuse du criquet, *Schistocerca gregaria*. J Insect Physiol 14, 1661–1667.

Collin, S., 1985. The central morphology of mechanoreceptor afferents in the metathoracic leg of the cockroach, *Periplaneta americana* (insecta). J Neurobiol 16, 269–282.

Comer, C., Baba, Y., 2011. Active touch in orthopteroid insects: behaviours, multisensory substrates and evolution. Philos Trans R Soc Lond B Biol Sci 366 (1581), 3006–3015.

Crossman, A. R., Kerkut, G. A., Pitman, R. M., Walker, R. J., 1971. Electrically excitable nerve cell bodies in the central ganglia of two insect species *Periplaneta americana* and *Schistocerca gregaria*. Investigation of cell geometry and morphology by intracellular dye injection. Comp Biochem Physiol 40A, 579–594.

Cruse, H., 1990. What mechanisms coordinate leg movement in walking arthropods? Trends Neurosci 13 (1), 15–21.

David, J., Pitman, R., 1995. Muscarinic agonists modulate calcium-dependent outward currents in an identified insect motoneurone. Brain Res 669, 153–156.

David, J., Pitman, R., 1996. Muscarinic receptor activation modulates ligand-gated ion channels in an insect motoneuron via changes in intracellular calcium. Proc R Soc Lond B Biol Sci 263, 469–474.

Debrodt, B., Bässler, U., 1989. Motor neurones of the flexor tibiae muscle in phasmids. Zool Jb Physiol 93, 481–494.

DiCaprio, R. A., Wolf, H., Büschges, A., 2002. Activity-dependent sensitivity of proprioceptive sensory neurons in the stick insect femoral chordotonal organ. J Neurophysiol 88 (5), 2387–2398.

Dolphin, A. C., 2009. Calcium channel diversity: multiple roles of calcium channel subunits. Curr Opin Neurobiol 19 (3), 237–244.

Dorai Raj, B. S., 1964. Diversity of crab muscle fibers innervated by a single motor axon. J Cell Physiol 64, 41–53.

Dresden, D., Nijenhuis, E., 1953. On the anatomy and mechanism of motion of the mesothoracic leg of *Periplaneta americana*. Proc K Ned Akad Wet C 56, 39–47.

Dresden, D., Nijenhuis, E., 1958. Fibre analysis of the nerves of the second thoracic leg in *Periplaneta americana*. Proc K Ned Akad Wet C 61, 213–223.

Dürr, V., Ebeling, W., 2005. The behavioural transition from straight to curve walking: kinetics of leg movement parameters and the initiation of turning. J Exp Biol 208 (Pt 12), 2237–2252.

Dürr, V., König, Y., Kittmann, R., 2001. The antennal motor system of the stick insect *Carausius morosus*: anatomy and antennal movement pattern during walking. J Comp Physiol A 187 (2), 131–144.

Duch, C., Levine, R. B., 2002. Changes in calcium signaling during postembryonic dendritic growth in *Manduca sexta*. J Neurophysiol 87 (3), 1415–1425.

Duch, C., Mentel, T., Pflüger, H. J., 1999. Distribution and activation of different types of octopaminergic DUM neurons in the locust. J Comp Neurol 403 (1), 119–134.

Duch, C., Pflüger, H., 1995. Motor patterns for horizontal and upside-down walking and vertical climbing in the locust. J Exp Biol 198, 1963–1976.

Eccles, J., Sherrington, C. S., 1930. Numbers and contraction-values of individual motor-units examined in some muscles of the limb. Proc R Soc Lond B Biol Sci 745, 326–357.

Edwards, J., Reddy, G., Rani, M., 1988. Central projections of a homoeotic regenerate, antennapedia, in a stick insect, *Carausius morosus* (Phasmida). J Neurobiol 20 (3), 101–114.

Ehmer, B., Gronenberg, W., 1997. Proprioceptors and fast antennal reflexes in the ant *Odontomachus* (Formicidae, Ponerinae). Cell Tissue Res 290 (1), 153–165.

El Manira, A., Bussieres, N., 1997. Calcium channel subtypes in lamprey sensory and motor neurons. J Neurophysiol 78 (3), 1334–1340.

El Manira, A., Tegner, J., Grillner, S., 1994. Calcium-dependent potassium channels play a critical role for burst termination in the locomotor network in lamprey. J Neurophysiol 72 (4), 1852–1861.

Elia, A., Gardner, D., 1990. Some morphological and physiological characteristics of an identifiable dorsal unpaired median neurone in the metathoracic ganglion of the cockroach, *Periplaneta americana* (L.). Comp Biochem Physiol C 95, 55–62.

Fayyazuddin, A., Dickinson, M., 1996. Haltere afferents provide direct, electrotonic input to a steering motor neuron in the blowfly, *Calliphora*. J Neurosci 16 (16), 5225–5232.

Fayyazuddin, A., Zaheer, M. A., Hiesinger, P. R., Bellen, H. J., 2006. The nicotinic acetylcholine receptor dalpha7 is required for an escape behavior in *Drosophila*. PLoS Biol 4 (3), e63.

Fetcho, J. R., O'Malley, D. M., 1995. Visualization of active neural circuitry in the spinal cord of intact zebrafish. J Neurophysiol 73 (1), 399–406.

Gabriel, J., Scharstein, H., Schmidt, J., Büschges, A., 2003. Control of flexor motoneuron activity during single leg walking of the stick insect on an electronically controlled treadwheel. J Neurobiol 56 (3), 237–251.

Gal, R., Libersat, F., 2006. New vistas on the initiation and maintenance of insect motor behaviors revealed by specific lesions of the head ganglia. J Comp Physiol A Neuroethol Sens Neural Behav Physiol 192 (9), 1003–1020.

Gebhardt, M., Honegger, H., 2001. Physiological characterisation of antennal mechanosensory descending interneurons in an insect (*Gryllus bimaculatus*, *Gryllus campestris*). J Exp Biol 204, 2265–2275.

Göbel, W., Helmchen, F., 2007. In vivo calcium imaging of neural network function. Physiology (Bethesda) 22, 358–365.

Goldammer, J., Büschges, A., Schmidt, J., 2012. Motoneurons, DUM cells, and sensory neurons in an insect thoracic ganglion: A tracing study in the stick insect *Carausius morosus*. J Comp Neurol 520 (2), 230–257.

Gozes, I., Barnstable, C., 1982. Monoclonal antibodies that recognize discrete forms of tubulin. Proc Natl Acad Sci USA 79, 2579–2583.

Graham, D., 1985. Pattern and control of walking in insects. In: Advances in Insect Physiology. Vol. 18. Academic Press Inc., London, pp. 31–140.

Graham, D., Wendler, D., 1981. The reflex behaviour and innervation of the tergocoxal retractor muscles of the stick insect *Carausius morosus*. J Comp Physiol 143, 81–91.

Grillner, S., 2003. The motor infrastructure: from ion channels to neuronal networks. Nat Rev Neurosci 4 (7), 573–586.

Grolleau, F., Lapied, B., 1996. Two distinct low-voltage-activated Ca^{2+} currents contribute to the pacemaker mechanism in cockroach dorsal unpaired median neurons. J Neurophysiol 76 (2), 963–976.

Grolleau, F., Lapied, B., 2000. Dorsal unimpaired median neurones in the insect central nervous system: Towards a better understanding of the ionic mechanisms underlying spontaneous electrical activity. J Exp Biol 203, 1633–1648.

Grolleau, F., Lapied, B., Buckingham, S. D., Mason, W. T., Sattelle, D. B., 1996. Nicotine increases $[Ca^{2+}]_i$ and regulates electrical activity in insect neurosecretory cells (DUM neurons) via an acetylcholine receptor with 'mixed' nicotinic-muscarinic pharmacology. Neurosci Lett 220 (2), 142–146.

Gruhn, M., Zehl, L., Büschges, A., 2009. Straight walking and turning on a slippery surface. J Exp Biol 212 (Pt 2), 194–209.

Haag, J., Borst, A., 2000. Spatial distribution and characteristics of voltage-gated calcium signals within visual interneurons. J Neurophysiol 83 (2), 1039–1051.

Hale, J., Burrows, M., 1985. Innervation patterns of inhibitory motor neurones in the thorax of the locust. J Exp Biol 117, 401–413.

Han, K. A., Millar, N. S., Davis, R. L., 1998. A novel octopamine receptor with preferential expression in *Drosophila* mushroom bodies. J Neurosci 18 (10), 3650–3658.

Hancox, J., Pitman, R., 1991. Plateau potentials drive axonal impulse bursts in insect motoneurons. Proc R Soc Lond B 244, 33–38.

Harley, C. M., Ritzmann, R. E., 2010. Electrolytic lesions within central complex neuropils of the cockroach brain affect negotiation of barriers. J Exp Biol 213 (Pt 16), 2851–2864.

Hayashi, J., Levine, R., 1992. Calcium and potassium currents in leg motoneurons during postembryonic development in the hawkmoth *Manduca sexta*. J.Exp.Biol. 171, 15–42.

Heidel, E., Pflüger, H.-J., 2006. Ion currents and spiking properties of identified subtypes of locust octopaminergic dorsal unpaired median neurons. Eur J Neurosci 23 (5), 1189–1206.

Heitler, W. J., Goodman, C. S., 1978. Multiple sites of spike initiation in a bifurcating locust neurone. J Exp Biol 76, 63–84.

Hell, S., Wichmann, J., 1994. Breaking the diffraction resolution limit by stimulated emission: stimulated-emission-depletion fluorescence microscopy. Optics Letters 19, 780–782.

Hellekes, K., 2012. Task-specific modulation of a proprioceptive reflex in a walking insect. PhD Thesis, University of Cologne.

Hess, D., Büschges, A., 1997. Sensorimotor pathways involved in interjoint reflex action of an insect leg. J Neurobiol 33 (7), 891–913.

Hess, D., Büschges, A., 1999. Role of proprioceptive signals from an insect femur-tibia joint in patterning motoneuronal activity of an adjacent leg joint. J Neurophysiol 81 (4), 1856–1865.

Hess, M., 2008. The role of octopamine and DUM-neurons in the modulation of motor activity in the stick insect *Carausius morosus*. Bachelor thesis. University of Cologne.

Homberg, U., 1994. Flight-correlated activity changes in neurons of the lateral accessory lobes in the brain of the locust *Schistocerca gregaria*. J Comp Physiol A 175, 597–610.

Homberg, U., Christensen, T., Hildebrand, J., 1989. Structure and function of the deutocerebrum in insects. Ann Rev Entomol 34, 477–501.

Homberg, U., Montague, R. A., Hildebrand, J. G., 1988. Anatomy of antennocerebral pathways in the brain of the sphinx moth *Manduca sexta*. Cell Tissue Res 254 (2), 255–281.

Horseman, B., Gebhardt, M., Honegger, H.-W., 1997. Involvement of the suboesophageal and thoracic ganglia in the control of antennal movements in crickets. J Comp Physiol A 181, 195–204.

Hounsgaard, J., Kiehn, O., 1993. Calcium spikes and calcium plateaux evoked by differential polarization in dendrites of turtle motoneurones in vitro. J Physiol 468, 245–259.

Hoyle, G., 1978. The dorsal, unpaired, median neurons of the locust metathoracic ganglion. J Neurobiol 9, 43–57.

Hoyle, G., Dagan, D., Moberly, B., Colquhoun, W., 1974. Dorsal unpaired median insect neurons make neurosecretory endings on skeletal muscle. J Exp Zoology 187, 159–165.

Ignell, R., Dekker, T., Ghaninia, M., Hansson, B. S., 2005. Neuronal architecture of the mosquito deutocerebrum. J Comp Neurol 493 (2), 207–240.

Iles, J., 1976. Organization of motoneurons in the prothoracic ganglion of the cockroach *Periplaneta americana* (L.). Philos Trans R Soc Lond B 276, 205–219.

Imaizumi, K., Pollack, G. S., 2005. Central projections of auditory receptor neurons of crickets. J Comp Neurol 493, 439–447.

Ivanov, A. I., Calabrese, R. L., 2000. Intracellular Ca^{2+} dynamics during spontaneous and evoked activity of leech heart interneurons: low-threshold Ca currents and graded synaptic transmission. J Neurosci 20 (13), 4930–4943.

Jander, R., Volk-Heinrichs, I., 1970. Das strauch-spezifische visuelle Perceptor-System der Stabheuschrecke (*Carausius morosus*). Z. vergl. Physiologie 70, 425–447.

Johnson, S., Murphey, R., 1985. The afferent projection of mesothoracic bristle hairs in the cricket, *Acheta domesticus*. J Comp Pysiol A 156, 369–379.

Johnston, R., Consoulas, C., Pflüger, H., Levine, R., 1999. Patterned activation of unpaired median neurons during fictive crawling in *Manduca sexta* larvae. J Exp Biol 202, 103–113.

Kamikouchi, A., Shimada, T., Ito, K., 2006. Comprehensive classification of the auditory sensory projections in the brain of the fruit fly *Drosophila melanogaster*. J Comp Neurol 499 (3), 317–356.

Kien, J., Fletcher, W., Altman, J., Ramirez, J.-M., Roth, U., 1990. Organisation of intersegmental interneurons in the suboesophageal ganglion of *Schistocerca gregaria* (Forksal) and *Locusta migratoria migratorioides* (Reiche & Fairmaire) (Acrididae, Orthoptera). Int J Insect Morphol & Embryol 19, 35–60.

Kittmann, R., Dean, J., Schmitz, J., 1991. An atlas of the thoracic ganglia in the stick insect, *Carausius morosus*. Phil Trans R Soc Lond B 331, 101–121.

Klagges, B. R., Heimbeck, G., Godenschwege, T. A., Hofbauer, A., Pflugfelder, G. O., Reifegerste, R., Reisch, D., Schaupp, M., Buchner, S., Buchner, E., 1996. Invertebrate synapsins: a single gene codes for several isoforms in *Drosophila*. J Neurosci 16 (10), 3154–3165.

Kloppenburg, P., 1995. Anatomy of the antennal motoneurons in the brain of the honeybee (*Apis mellifera*). J Comp Neurol 363, 333–343.

Kloppenburg, P., Zipfel, W., Webb, W., Harris-Warrick, R., 2000. Highly localized Ca^{2+} accumulation revealed by multiphoton microscopy in an identified motoneuron and its modulation by dopamine. J Neurosci 20 (7), 2523–2533.

Kononenko, N. L., Pflüger, H.-J., 2007. Dendritic projections of different types of octopaminergic unpaired median neurons in the locust metathoracic ganglion. Cell Tissue Res 330 (1), 179–195.

Krause, A. F., Dürr, V., 2012. Active tactile sampling by an insect in a step-climbing paradigm. Front Behav Neurosci 6, 30.

Krause, A. F., Winkler, A., Dürr, V., 2013. Central drive and proprioceptive control of antennal movements in the walking stick insect. J Physiol Paris 107, 116–129.

Krishnan, A., Prabhakar, S., Sudarsan, S., Sane, S. P., 2012. The neural mechanisms of antennal positioning in flying moths. J Exp Biol 215 (Pt 17), 3096–3105.

Kuehn, C., Duch, C., 2013. Putative excitatory and putative inhibitory inputs are localised in different dendritic domains in a *Drosophila* flight motoneuron. Eur J Neurosci 37 (6), 860–875.

Kuenzi, F., Burrows, M., 1995. Central connections of sensory neurones from a hair plate proprioceptor in the thoraco-coxal joint of the locust. J Exp Biol 198, 1589–1601.

Kurylas, A. E., Rohlfing, T., Krofczik, S., Jenett, A., Homberg, U., 2008. Standardized atlas of the brain of the desert locust, *Schistocerca gregaria*. Cell Tissue Res 333 (1), 125–145.

Kutsch, W., Heckmann, R., 1995. Motor supply of the dorsal longitudinal muscles, I: homonomy and ontogeny of the motoneurones in locusts (Insecta, Caelifera). Zoomorphology 115, 179–195.

Kutsch, W., Schneider, H., 1987. Histological characterization of neurones innervating functionally different muscles of locusta. J Comp Neurol 261 (4), 515–528.

Kutsch, W., Usherwood, P., 1970. Studies of the innervations and electrical activity of flight muscles in the locust *Schistocerca gregaria*. J Exp Biol 52, 299–312.

Lapied, B., Le Corronc, H., Hue, B., 1990. Sensitive nicotinic and mixed nicotinic-muscarinic receptors in insect neurosecretory cells. Brain Res 533 (1), 132–136.

Laurent, G., 1987. The role of spiking local interneurons in shaping the receptive fields of intersegmental interneurons in the locust. J Neurosci 7, 2977–2989.

Laurent, G., Hustert, R., 1988. Motor neuronal receptive fields delimit patterns of motor activity during locomotion of the locust. J Neurosci 8, 4349–4366.

Laurent, G., Richard, D., 1986. The organization and role during locomotion of the proximal musculature of the cricket foreleg. I. Anatomy and innervations. J Exp Biol 123, 255–283.

Laurent, G., Seymour-Laurent, K., Johnson, K., 1993. Dendritic excitability and a voltage-gated calcium current in locust nonspiking local interneurons. J Neurophysiol 69 (5), 1484–1499.

Lev-Tov, A., O'Donovan, M. J., 1995. Calcium imaging of motoneuron activity in the en-bloc spinal cord preparation of the neonatal rat. J Neurophysiol 74 (3), 1324–1334.

Li, Y., Strausfeld, N. J., 1999. Multimodal efferent and recurrent neurons in the medial lobes of cockroach mushroom bodies. J Comp Neurol 409 (4), 647–663.

Littleton, J. T., Ganetzky, B., 2000. Ion channels and synaptic organization: analysis of the *Drosophila* genome. Neuron 26 (1), 35–43.

Ludwar, B., Westmark, S., Büschges, A., Schmidt, J., 2005. Modulation of membrane potential in mesothoracic moto- and interneurons during stick insect front-leg walking. J Neurophysiol 94 (4), 2772–2784.

Macleod, G. T., Suster, M. L., Charlton, M. P., Atwood, H. L., 2003. Single neuron activity in the *Drosophila larval* CNS detected with calcium indicators. J Neurosci Methods 127 (2), 167–178.

Maronde, U., 1991. Common projection areas of antennal and visual pathways in the honeybee brain, *Apis mellifera*. J Comp Neurol 309, 328–340.

Marquardt, F., 1940. Beiträge zur Anatomie der Muskulatur und der peripheren Nerven von *Carausius (Dixippus) morosus*. Zoologische Jahrbücher Abt Anat Ont Tiere 66, 63–128.

Mentel, T., Weiler, V., Büschges, A., Pflüger, H.-J., 2008. Activity of neuromodulatory neurones during stepping of a single insect leg. J Insect Physiol 54 (1), 51–61.

Mills, J. D., Pitman, R. M., 1997. Electrical properties of a cockroach motor neuron soma depend on different characteristics of individual Ca components. J Neurophysiol 78 (5), 2455–2466.

Mobbs, P. G., 1982. The brain of the honeybee *Apis mellifera*. I. The connections and spatial organization of the mushroom bodies. Phil Trans R Soc Lond B 298, 309–354.

Monteforti, G., Angeli, S., Petacchi, R., Minnocci, A., 2002. Ultrastructural characterization of antennal sensilla and immunocytochemical localization of a chemosensory protein in *Carausius morosus* Brunner (Phasmida: Phasmatidae). Arthropod Struct Dev 30 (3), 195–205.

Mücke, A., Lakes-Harlan, R., 1995. Central projections of sensory cells of the midleg of the locust, *Schistocerca gregaria*. Cell Tissue Res. 280, 391–400.

Mujagic, S., Krause, A. F., Dürr, V., 2007. Slanted joint axes of the stick insect antenna: an adaptation to tactile acuity. Naturwissenschaften 94 (4), 313–318.

Myers, C., Evans, P., 1985. The distribution of bovine pancreatic polypeptide/FMRFamide-like immunoreactivity in the ventral nervous system of the locust. J Comp Neurol 234, 1–16.

Nakanishi, A., Nishino, H., Watanabe, H., Yokohari, F., Nishikawa, M., 2010. Sex-specific antennal sensory system in the ant *Camponotus japonicus*: glomerular organizations of antennal lobes. J Comp Neurol 518 (12), 2186–2201.

Neville, A., 1963. Motor unit distribution of the dorsal longitudinal flight muscles in locusts. J Exp Biol 40, 123–136.

Newland, P. L., Rogers, S. M., Gaaboub, I., Matheson, T., 2000. Parallel somatotopic maps of gustatory and mechanosensory neurons in the central nervous system of an insect. J Comp Neurol 425 (1), 82–96.

Nishino, H., 2000. Topographic mapping of the axons of the femoral chordotonal organ neurons in the cricket *Gryllus bimaculatus*. Cell Tissue Res 299, 145–157.

Nishino, H., 2003. Local innervation patterns of the metathoracic flexor and extensor tibiae motor neurons in the cricket *Gryllus bimaculatus*. Zoolog Sci 20 (6), 697–707.

Nishino, H., Nishikawa, M., Yokohari, F., Mizunami, M., 2005. Dual, multilayered somatosensory maps formed by antennal tactile and contact chemosensory afferents in an insect brain. J Comp Neurol 493 (2), 291–308.

O'Donovan, M. J., Ho, S., Sholomenko, G., Yee, W., 1993. Real-time imaging of neurons retrogradely and anterogradely labelled with calcium-sensitive dyes. J Neurosci Methods 46 (2), 91–106.

Okada, J., Kanamaru, Y., Toh, Y., 2002. Mechanosensory control of antennal movement by the scapal hair plate in the american cockroach. Zoolog Sci 19 (11), 1201–1210.

Okada, J., Toh, Y., 2000. The role of antennal hair plates in object-guided tactile orientation of the cockroach (*Periplaneta americana*). J Comp Physiol A 186 (9), 849–857.

Okada, J., Toh, Y., 2001. Peripheral representation of antennal orientation by the scapal hair plate of the cockroach *Periplaneta americana*. J Exp Biol 204 (Pt 24), 4301–4309.

Okada, J., Toh, Y., 2004. Spatio-temporal patterns of antennal movements in the searching cockroach. J Exp Biol 207 (Pt 21), 3693–3706.

Okada, R., Sakura, M., Mizunami, M., 2003. Distribution of dendrites of descending neurons and its implications for the basic organization of the cockroach brain. J Comp Neurol 459 (3), 158–174.

Oliveira, E. E., 2010. Properties of cholinergic currents in identied leg motoneurons of the stick insect, *Carausius morosus*. PhD Thesis, University of Cologne.

Oliveira, E. E., Pippow, A., Salgado, V. L., Büschges, A., Schmidt, J., Kloppenburg, P., 2010. Cholinergic currents in leg motoneurons of *Carausius morosus*. J Neurophysiol 103 (5), 2770–2782.

Orlovsky, G., Deliagina, T., Grillner, S., 1999. Neuronal Control of Locomotion. Oxford University Press.

Pawley, J. B., 2006. Handbook of biological confocal microscopy. Springer.

Pearson, H., Lees, G., Wray, D., 1993. Calcium channel currents in neurones from locust (*Schistocerca gregaria*) thoracic ganglia. J Exp Biol 177, 201–221.

Pearson, K., 1993. Common principles of motor control in vertebrates and invertebrates. Annu Rev Neurosci 16, 265–297.

Pearson, K., Wong, R., Fourtner, C., 1976. Connexions between hair-plate afferents and motoneurones in the cockroach leg. J Exp Biol 64, 251–266.

Pearson, K. G., Fourtner, C. R., 1973. Identification of the somata of common inhibitory motoneurons in the metathoracic ganglion of the cockroach. Can J Zool 51, 859–866.

Pearson, K. G., Iles, J. F., 1971. Innervation of coxal depressor muscles in the cockroach, *Periplaneta americana*. J Exp Biol 54 (1), 215–232.

Pflüger, H. J., Bräunig, P., Hustert, R., 1981. Distribution and specific central projections of mechanoreceptors in the thorax and proximal leg joints of locusts. II. The external mechanoreceptors: hair plates and tactile hairs. Cell Tissue Res 216 (1), 79–96.

Pflüger, H.-J., Elson, E., Binkle, U., Schneider, H., 1986. The central nervous organization of the motor neurons to a steering muscle in locusts. J Exp Biol 120, 403–420.

Pflüger, H.-J., Bräunig, P., Hustert, R., 1988. The organization of mechanosensory neuropiles in locust thoracic ganglia. Phil Trans R Soc Lond B 321, 1–26.

Phillips, C., 1981. Organization of motor neurons to a multiply innervated insect muscle. J Neurobiol 12, 269–280.

Pipa, R., Cook, E., 1959. Studies on the hexapod nervous system. I. The peripheral distribution of the thoracic nerves of the adult cockroach, *Periplaneta americana*. Ann Ent Soc Am 52, 695–710.

Plotnikova, S. I., 1969. Effector neurons with several axons in the ventral nerve cord of the asian grasshopper *Locusta migratoria*. J Evol Biochem Physiol [English translation] 5, 276–277.

Radnikow, G., Bässler, U., 1991. Function of a muscle whose apodeme travels through a joint moved by other muscles: why the *retractor unguis* muscle in stick insects is tripartite and has no antagonist. J Exp Biol 157, 87–99.

Ramirez, J., Pearson, K., 1988. Generation of motor patterns for walking and flight in motoneurons supplying bifunctional muscles in the locust. J Neurobiol 19, 257–282.

Ramirez, J., Pearson, K., 1991. Octopamine induces bursting and plateau potentials in insect neurones. BrainResearch 549, 332–337.

Rein, K., Zöckler, M., Mader, M. T., Grübel, C., Heisenberg, M., 2002. The *Drosophila* standard brain. Curr Biol 12 (3), 227–231.

Ritzmann, R. E., Ridgel, A. L., Pollack, A. J., 2008. Multi-unit recording of antennal mechano-sensitive units in the central complex of the cockroach, *Blaberus discoidalis*. J Comp Physiol A 194 (4), 341–360.

Römer, H., Marquart, V., Hardt, 1988. Organization of a sensory neuropile in the auditory pathway of two groups of orthoptera. J Comp Neurol 275, 201–215.

Rosenbaum, P., 2013. Motor flexibility: neuronal control of walking direction and walking speed in an insect. PhD Thesis, University of Cologne.

Rosenbaum, P., Wosnitza, A., Büschges, A., Gruhn, M., 2010. Activity patterns and timing of muscle activity in the forward walking and backward walking stick insect *Carausius morosus*. J Neurophysiol 104 (3), 1681–1695.

Rospars, J., 1988. Structure and development of the insect antennodeutocerebral system. Int J Insect Morphol & Embryol Vol. 17. No. 3, 243–294.

Ryckebusch, S., Laurent, G., 1993. Rhythmic patterns evoked in locust leg motor neurons by the muscarinic agonist pilocarpine. J Neurophysiol 69, 1583–1595.

Ryglewski, S., Lance, K., Levine, R. B., Duch, C., 2012. Ca(v)2 channels mediate low and high voltage-activated calcium currents in *Drosophila* motoneurons. J Physiol 590 (Pt 4), 809–825.

Ryglewski, S., Pflueger, H. J., Duch, C., 2007. Expanding the neuron's calcium signaling repertoire: intracellular calcium release via voltage-induced PLC and IP3R activation. PLoS Biol 5 (4), e66.

Sachse, S., Galizia, C. G., 2002. Role of inhibition for temporal and spatial odor representation in olfactory output neurons: a calcium imaging study. J Neurophysiol 87 (2), 1106–1117.

Sasaki, K., Burrows, M., 1998. Innervation pattern of a pool of nine excitatory motor neurons in the flexor tibiae muscle of a locust hind leg. J Exp Biol 201, 1885–1893.

Schmidt, J., Fischer, H., Büschges, A., 2001. Pattern generation for walking and searching movements of a stick insect leg. II. Control of motoneuronal activity. J Neurophysiol 85, 354–361.

Schmit-Jensen, H. O., 1914. Homoeotic regeneration of the antennae in a phasmid or walking-stick. Smithson Rep 1914, 523–536.

Schmitz, J., 1986. The depressor trochanteris motoneurones and their role in the coxo-trochanteral feedback loop in the stick insect *Carausius morosus*. Biol Cybern 55, 25–34.

Schmitz, J., Dean, J., Kittmann, R., 1991. Central projections of leg sense organs in *Carausius morosus* (Insecta, Phasmida). Zoomorphology 111, 19–33.

Schmitz, J., Schöwerling, H., 1992. No effects of coxo-trochanteral proprioceptors on extensor tibiae motor neurons in posture control. Proceedings of the 20th Göttingen Neurobiology Conference 1992, 118.

Schneider, D., 1964. Insect antennae. Annu Rev Entomol 9, 103–122.

Schöneich, S., Schildberger, K., Stevenson, P. A., 2011. Neuronal organization of a fast-mediating cephalothoracic pathway for antennal-tactile information in the cricket (*Gryllus bimaculatus* DeGeer). J Comp Neurol 519 (9), 1677–1690.

Schütz, C., Dürr, V., 2011. Active tactile exploration for adaptive locomotion in the stick insect. Philos Trans R Soc Lond B Biol Sci 366 (1581), 2996–3005.

Siegler, M., Burrows, M., 1979. The morphology of local non-spiking interneurones in the metathoracic ganglion of the locust. J Comp Neurol 183, 121–148.

Siegler, M. V., Pousman, C. A., 1990a. Motor neurons of grasshopper metathoracic ganglion occur in stereotypic anatomical groups. J Comp Neurol 297 (2), 298–312.

Siegler, M. V., Pousman, C. A., 1990b. Distribution of motor neurons into anatomical groups in the grasshopper metathoracic ganglion. J Comp Neurol 297 (2), 313–327.

Slifer, E. H., 1966. Sense organs on the antennal flagellum of a walkingstick *Carausius morosus* Brunner (Phasmida). J Morphol 120 (2), 189–201.

Staudacher, E., 1998. Distribution and morphology of descending brain neurons in the cricket *Gryllus bimaculatus* de Geer. Cell Tissue Res 780, 1–16.

Staudacher, E., Gebhardt, M., Dürr, V., 2005. Antennal movements and mechanoreception: Neurobiology of active tactile sensors. Adv Insect Physiol 32, 49–205.

Staudacher, E., Schildberger, K., 1999. A newly described neuropile in the deutocerebrum of the cricket: Antennal afferents and descending interneurons. Zoology 102, 212–226.

Stevenson, P. A., Spörhase-Eichmann, U., 1995. Localization of octopaminergic neurones in insects. Comp Biochem Physiol A Physiol 110 (3), 203–215.

Storrer, J., Bässler, U., Mayer, S., 1986. Motoneurone im Meso- und Metathorakalganglion der Stabheuschrecke *Carausius morosus*. Zool Jb Physiol 90, 359–374.

Strausfeld, N. J., 2012. Arthropod brains: Evolution, functional elegance, and historical significance. The Belknap Press of Harvard University press.

Suzuki, H., 1975. Antennal movements induced by odour and central projection of the antennal neurones in the honey-bee. J Insect Physiol 21, 831–847.

Swales, L. S., Evans, P. D., 1994. Distribution of myomodulin-like immunoreactivity in the adult and developing ventral nervous system of the locust *Schistocerca gregaria*. J Comp Neurol 343 (2), 263–280.

Takahashi, A., Camacho, P., Lechleiter, J. D., Herman, B., 1999. Measurement of intracellular calcium. Physiol Rev 79 (4), 1089–1125.

Tanaka, Y., Washio, H., 1988. Morphological and physiological properties of the dorsal unpaired median neurons of the cockroach metathoracic ganglion. Comp Biochem Physiol 91A, 37–41.

Theophilidis, G., Burns, M., 1983. The innervation of the mesothoracic flexor tibiae muscle of the locust. J Exp Biol 105, 373–388.

Tichy, H., Loftus, R., 1987. Response characteristics of a cold receptor in the stick insect *Carausius morosus*. J Comp Physiol A 160, 33–42.

Tsien, R. Y., Harootunian, A. T., 1990. Practical design criteria for a dynamic ratio imaging system. Cell Calcium 11 (2-3), 93–109.

Tsien, R. Y., Rink, T. J., Poenie, M., 1985. Measurement of cytosolic free Ca^{2+} in individual small cells using fluorescence microscopy with dual excitation wavelengths. Cell Calcium 6 (1-2), 145–157.

Viana di Prisco, G., Alford, S., 2004. Quantitative investigation of calcium signals for locomotor pattern generation in the lamprey spinal cord. J Neurophysiol 92 (3), 1796–1806.

von Holst, E. V., Mittelstaedt, H., 1950. Das Reafferenzprinzip. Wechselwirkungen zwischen Zentralnervensystem und Peripherie. Naturwissenschaften 37, 464–476.

von Uckermann, G., Büschges, A., 2009. Premotor interneurons in the local control of stepping motor output for the stick insect single middle leg. J Neurophysiol 102 (3), 1956–1975.

Walther, C., 1980. Small motor axons in orthopteran insects. J Exp Biol 87, 99–119.

Watanabe, H., Nishino, H., Nishikawa, M., Mizunami, M., Yokohari, F., 2010. Complete mapping of glomeruli based on sensory nerve branching pattern in the primary olfactory center of the cockroach *Periplaneta americana*. J Comp Neurol 518 (19), 3907–3930.

Watkins, B., Burrows, M., Siegler, M., 1985. The structure of locust nonspiking interneurones in relation to the anatomy of their segmental ganglion. J Comp Neur 240, 233–255.

Watson, A. H., Burrows, M., 1982. The ultrastructure of identified locust motor neurones and their synaptic relationships. J Comp Neurol 205 (4), 383–397.

Watson, A. H. D., Burrows, M., Hale, J., 1985. The morphology and ultrastructure of common inhibitory motor neurons in the thorax of the locust. J Comp Neurol 239, 341–359.

Weeks, J. C., Jacobs, G. A., 1987. A reflex behavior mediated by monosynaptic connections between hair afferents and motoneurons in the larval tobacco hornworm, *Manduca sexta*. J Comp Physiol A 160, 315–329.

Weide, W., 1960. Einige Bemerkungen über die antennalen Sensillen sowie über das Fühlerwachstum der Stabheuschrecke *Carausius (Dixippus) morosus* br. (Insecta: Phasmida). Wiss Z Univ Halle Math-Nat IX/2, 247–250.

Weidler, D., Diecke, F., 1969. The role of cations in conduction in the central nervous system of the herbivorous insect *Carausius morosus*. Z vergl Physiol 64, 372–399.

Wendler, G., 1964. Laufen und Stehen der Stabheuschrecke *Carausius morosus*: Sinnesborstenfelder in den Beingelenken als Glieder von Regelkreisen. Z vergl Physiol 48, 198–250.

Westmark, S., 2007. State-dependent long lasting modulation of leg motoneuron membrane potential during stick insect walking. PhD Thesis, University of Cologne.

Westmark, S., Oliveira, E. E., Schmidt, J., 2009. Pharmacological analysis of tonic activity in motoneurons during stick insect walking. J Neurophysiol 102 (2), 1049–1061.

Wicher, D., Penzlin, H., 1997. Ca^{2+} currents in central insect neurons: Electrophysiological and pharmacological properties. J Neurophysiol 77, 186–199.

Wicher, D., Walther, C., Wicher, C., 2001. Non-synaptic ion channels in insects-basic properties of currents and their modulation in neurons and skeletal muscles. Progress in Neurobiology 64, 431–525.

Wilson, J., 1979. The structure and function of serially homologous leg motor neurons in the locust. I. Anatomy. J Neurobiol 10, 41–65.

Wilson, J., Hoyle, G., 1978. Serially homologous neurones as concomitants of functional specialization. Nature 274, 374–379.

Wong, R., Pearson, K., 1976. Properties of the trochanteral hair plate and its function in the control of walking in the cockroach. J Exp Biol 64, 233–249.

Young, D., 1969. Motor neurons of the mesothoracic ganglion of *Periplaneta americana*. J Insect Physiol 15, 1175–1179.

Zhang, B., Harris-Warrick, R., 1995. Calcium-dependent plateau potentials in a crab stomatogastric ganglion motor neuron. I. Calcium current and its modulation by serotonin. J Neurophysiol 74, 1929–1937.

Zill, S. N., Moran, D. T., 1982. Suppression of reflex postural tonus: a role of peripheral inhibition in insects. Science 216 (4547), 751–753.

Zill, S. N., Schmitz, J., Chaudhry, S., Büschges, A., 2012. Force encoding in stick insect legs delineates a reference frame for motor control. J Neurophysiol 108 (5), 1453–1472.

Zorović, M., Hedwig, B., 2013. Descending brain neurons in the cricket *Gryllus bimaculatus* (de Geer): auditory responses and impact on walking. J Comp Physiol A 199 (1), 25–34.

A. Supplementary figures of chapter 3.1

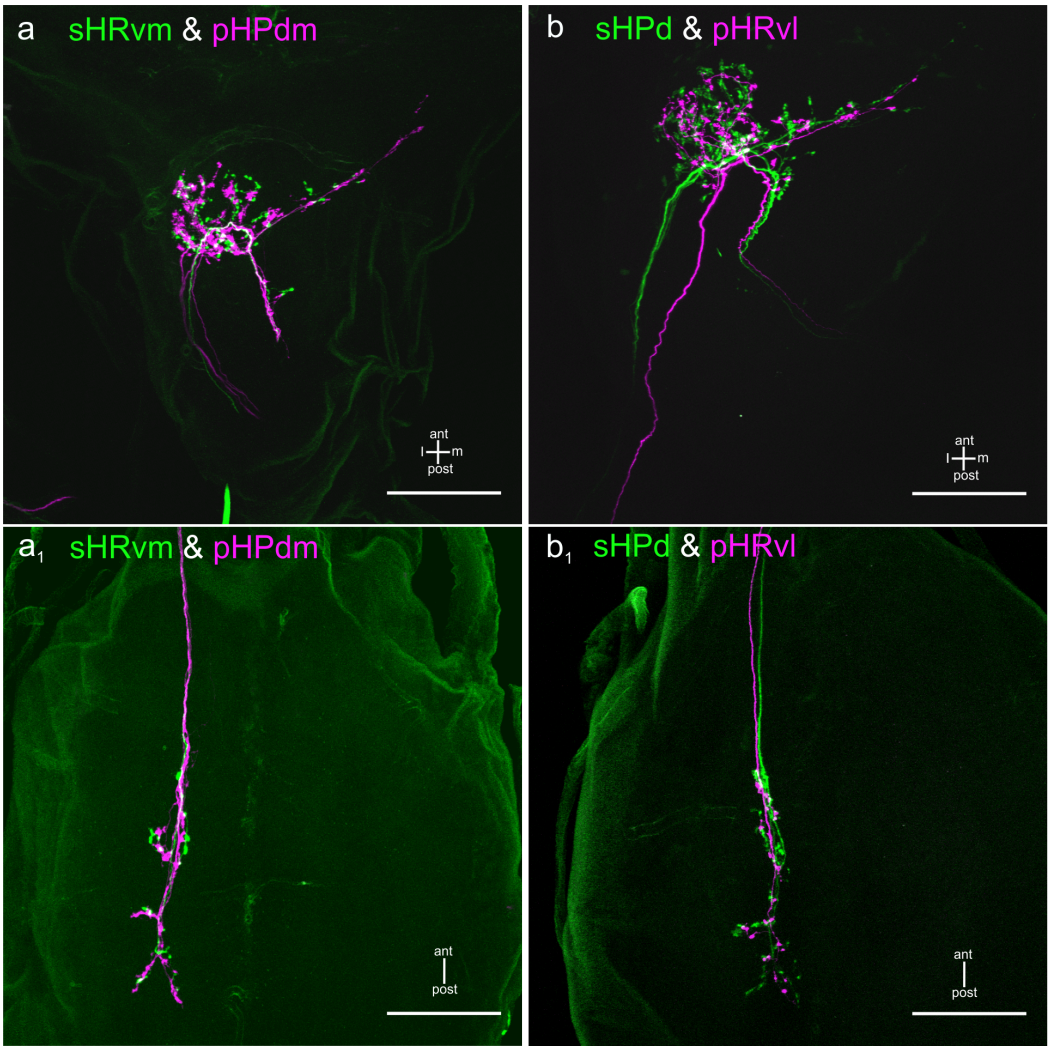

Figure A.1. – Additional stainings of dorsal and ventral HFs situated on the scape and pedicel. a and a_1: Brain and SOG whole-mounts with stained sHRvm (green) and pHPdm (magenta) sensilla. Specimens show a similar projection pattern with a different bouton formation. **b and b_1:** Brain and SOG whole-mounts with stained sHPd (green) and pHRvl (magenta) sensilla. Specimens show also a similar projection pattern with a different bouton formation. Scale bars=100 µm.

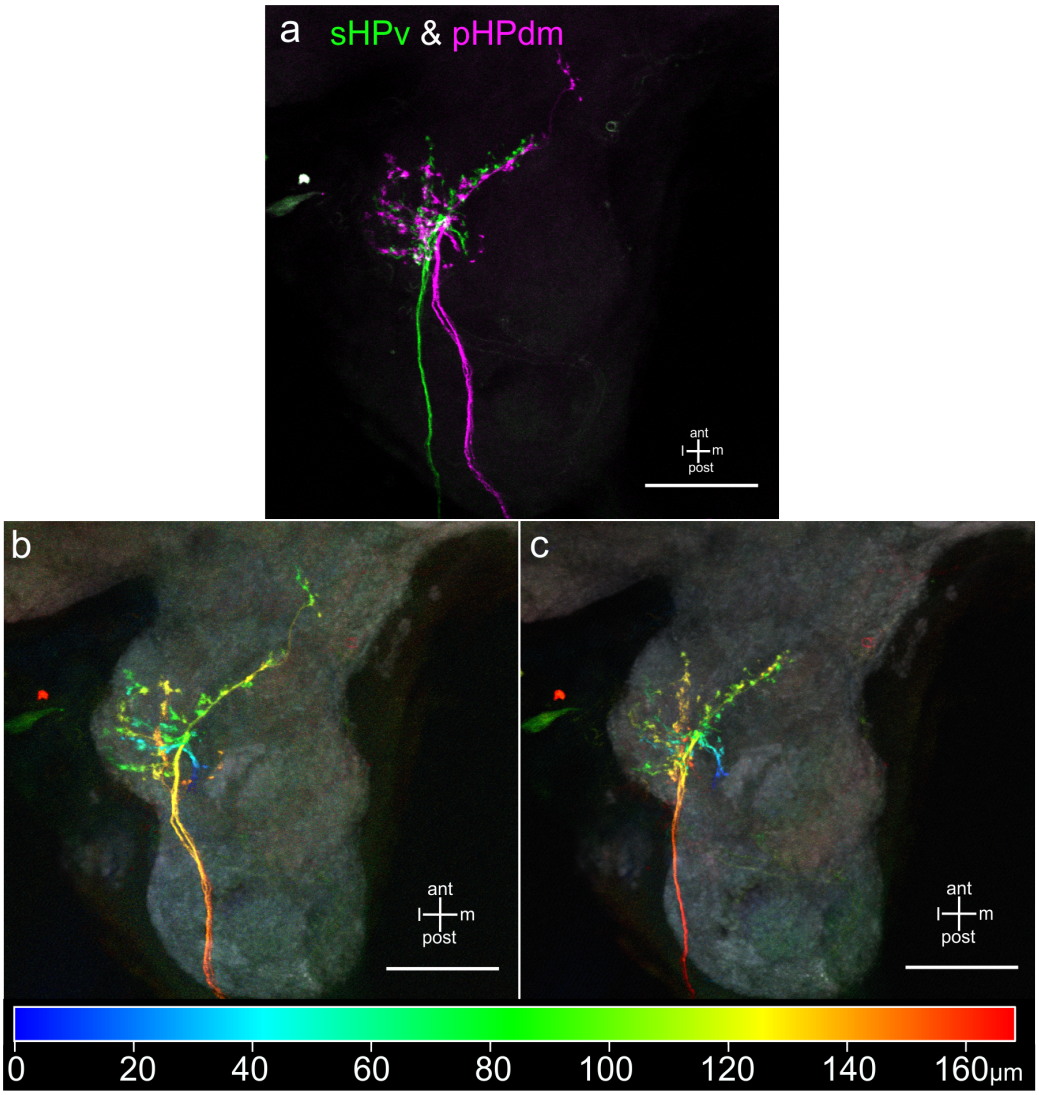

Figure A.2. – Additional brain whole-mount with stained sHPv (green) and pHPdm (magenta) sensilla combined with anti-synapsin immunostaining (gray; b-c). a: The merged image of both HF fibers shows a similar projection pattern but boutons appear on spatially different regions. Note the laterad bend of anteromedially traveling pHPdm afferents before terminating. **b:** Depth color-coded image of pHPdm afferents combined with synapsin immunostaining (gray). Depth encoded from dorsal to ventral as blue to red. **c:** Depth color-coded image of sHPv afferents combined with synapsin immunostaining (gray). Depth coding as in (b). Both images (b-c) reveal that fibers of both HF types form boutons in the entire depth of the DL on slightly different locations. Scale bars=100 µm.

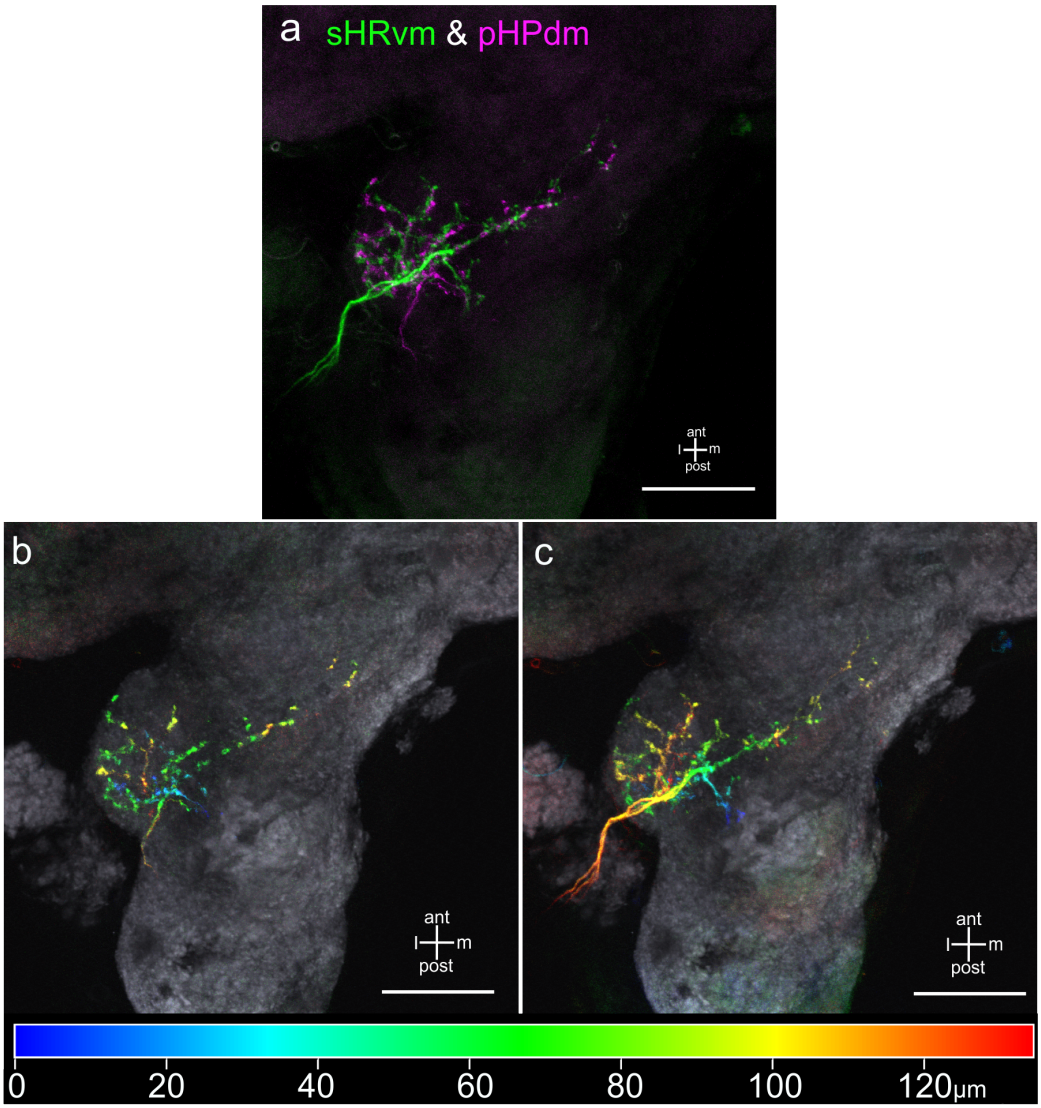

Figure A.3. – Additional brain whole-mount with stained sHRvm (green) and pHPdm (magenta) sensilla combined with anti-synapsin immunostaining (gray; b-c). a: The merged image of both HF fibers shows a similar projection pattern but boutons appear on spatially different regions. **b:** Depth color-coded image of pHPdm afferents combined with synapsin immunostaining (gray). Depth encoded from dorsal to ventral as blue to red. **c:** Depth color-coded image of sHRvm afferents combined with synapsin immunostaining (gray). Depth coding as in (b). Both images (b-c) reveal that fibers of both HF types form boutons in the entire depth of the DL on slightly different locations. Scale bars= 100 µm.

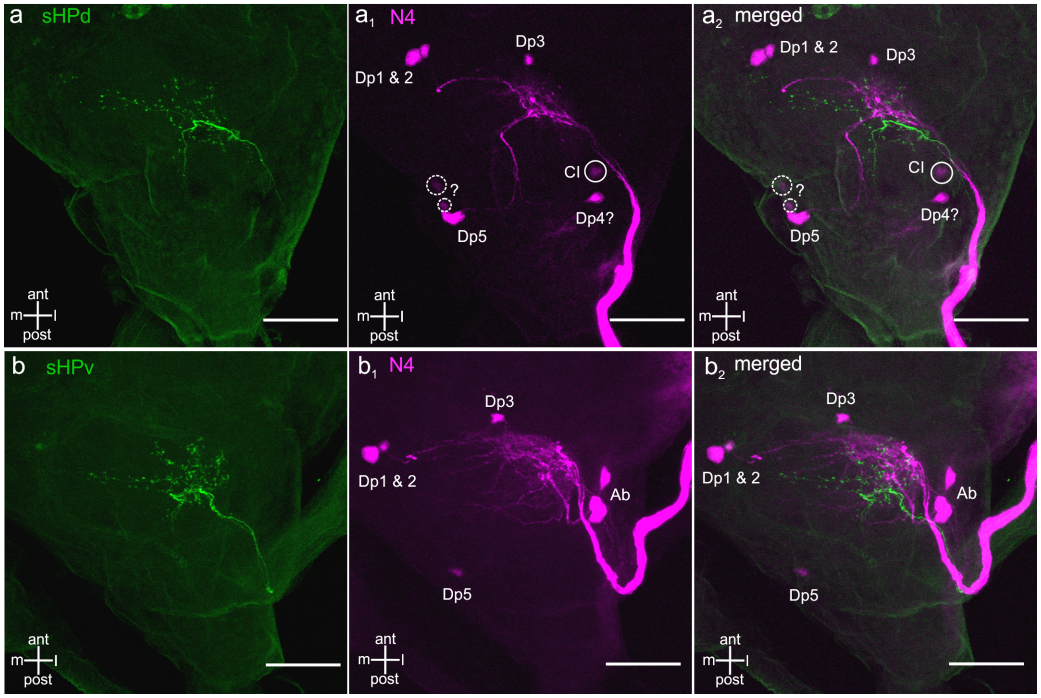

Figure A.4. – Staining of sHPd or sHPv sensilla (green) and antennal nerve N4 (magenta; innervates Dp and Ab muscles). a-a$_2$: Top views of brain whole-mount with central projections of sHPd fibers and Dp and Ab MN neurites. Boutons of sHPd can be found in vicinity to MN neurites in the DL. Circles with question mark indicate weakly stained cell bodies. **b-b$_2$:** Top views of brain whole-mount with central projections of sHPv fibers and Dp and Ab MN neurites. Boutons of sHPd can be found also in vicinity to MN neurites in the DL. Dp1-5: depressor MN cell bodies; Ab: abductor MN cell bodies and CI: common inhibitory neuron (Dürr et al., 2001). Scale bars=100 µm.

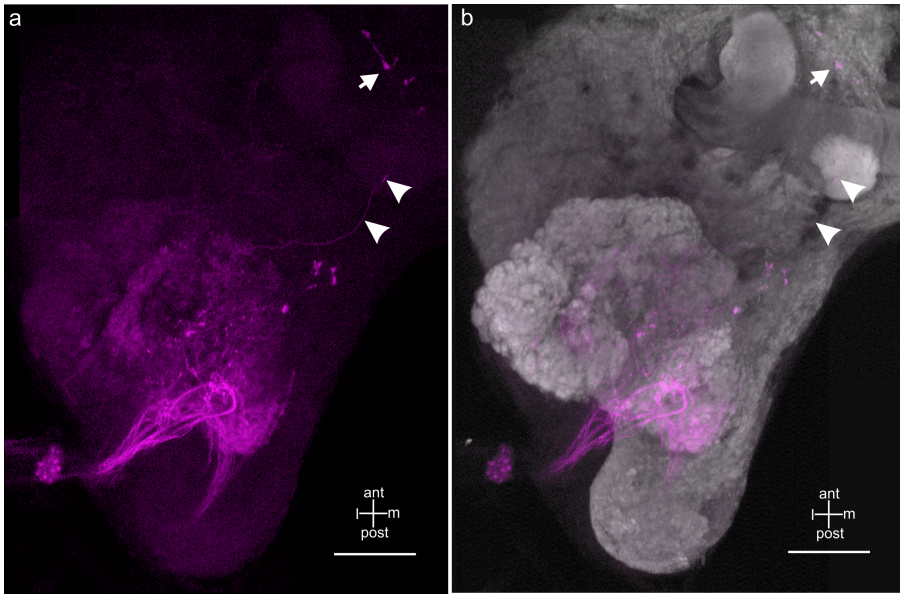

Figure A.5. – Staining of the antennal nerve N1 shows putative afferents from a cold receptor situated in the flagellum. a: Backill of nerve N1 shows a diffuse staining of afferents in the AL, DL, and VFA neuropils. Besides, an afferent from a putative cold receptor was stained that leaves the AL to terminate in an unknown neuropil region between the mushroom body and the central complex. **b:** Same specimen as in (a), combined with anti-synapsin immunostaining. Arrowheads mark primary neurite and arrow indicate afferent terminals. Scale bars=100 µm.

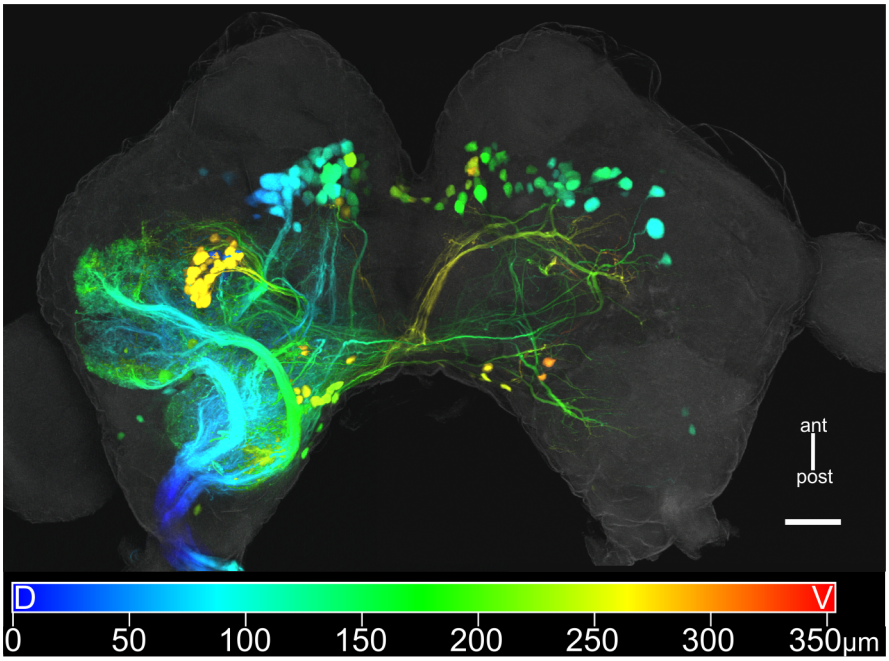

Figure A.6. – Additional depth color-coded specimen with brain DINs stained through a cervical (neck) connective. Depth encoded from dorsal to ventral as blue to red. Scale bar=100 µm.

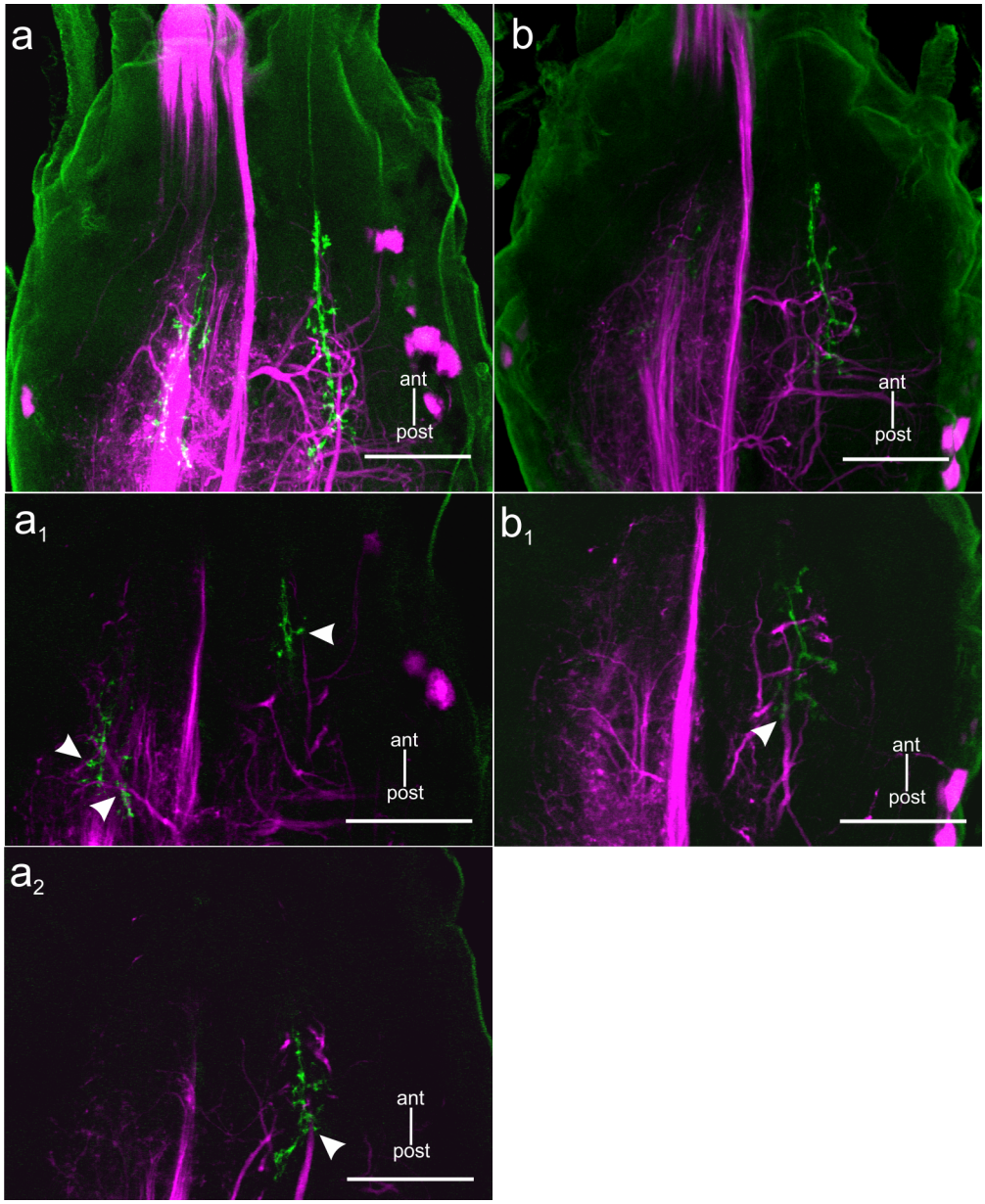

Figure A.7. – SOG with stained scapal HF afferents (green) and backfilled connectives between the pro- and mesothoracic ganglia (magenta). **a:** Overview of sHPv (green) stained on both antennae and a pro- mesothoracic connective backfill (magenta). **a_1-a_2:** Single images of (a) show possibilities of potential contacts from afferents onto DIN neurites on ipsi- and contralateral SOG parts (arrowheads). **b:** Overview of sHPd (green) stained on both antennae and pro- mesothoracic connective backfill (magenta) but only the HF afferents on the contralateral side with respect to the stained connective are visible. **b_1:** Single images of b show again possibilities of potential contacts from afferents onto a large DIN neurite along the inverted 'V'-shaped HF terminals (arrowhead). Scale bars=100 µm.

B. Supplementary figures of chapter 3.2

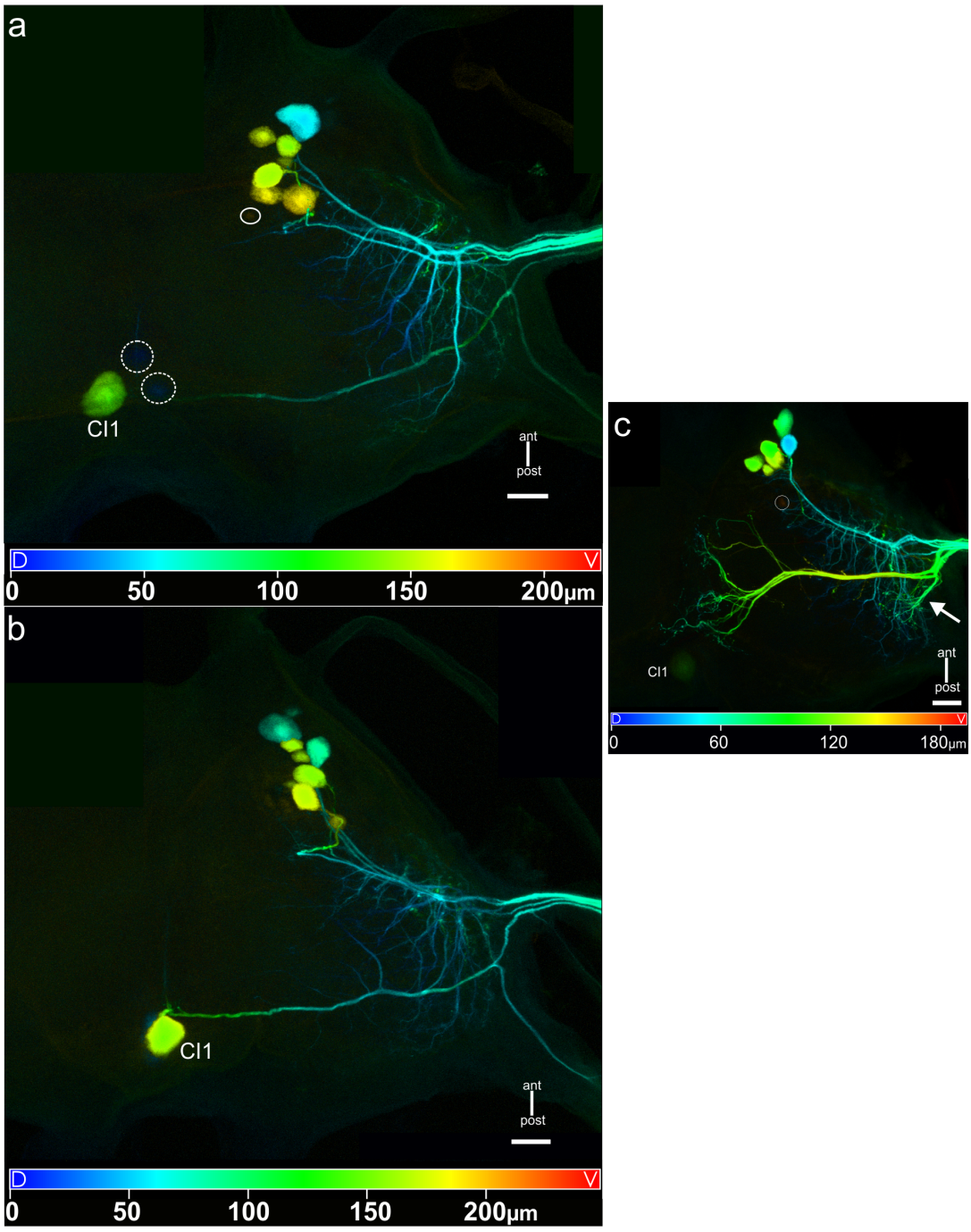

Figure B.1. – Backfill of branch C of nervus lateralis 2 (nl2C) that innervates the protractor coxae muscle. a: Depth color-coded whole-mount with an anterolateral (AL) cell cluster with eight cell bodies (one small cell body encircled) and a cluster at the ganglion midline. Midline cluster contains cell bodies of the common inhibitor 1 (CI1) cell body and at least two DUM neurons (dashed circles) Depth encoded from dorsal to ventral as blue to red. **b:** Another depth color-coded specimen. AL cell cluster contains at least nine cell bodies and at the midline the CI1 neuron is apparent. Two DUM cells are masked by the CI1 cell body. **c:** Another depth color-coded whole-mount with eight neurons (one situated more posteriorly) and the CI1 cell body at the midline. Image shows in addition sensory afferents of unknown origin terminating laterally (arrow) and near the midline. Scale bars=50 µm.

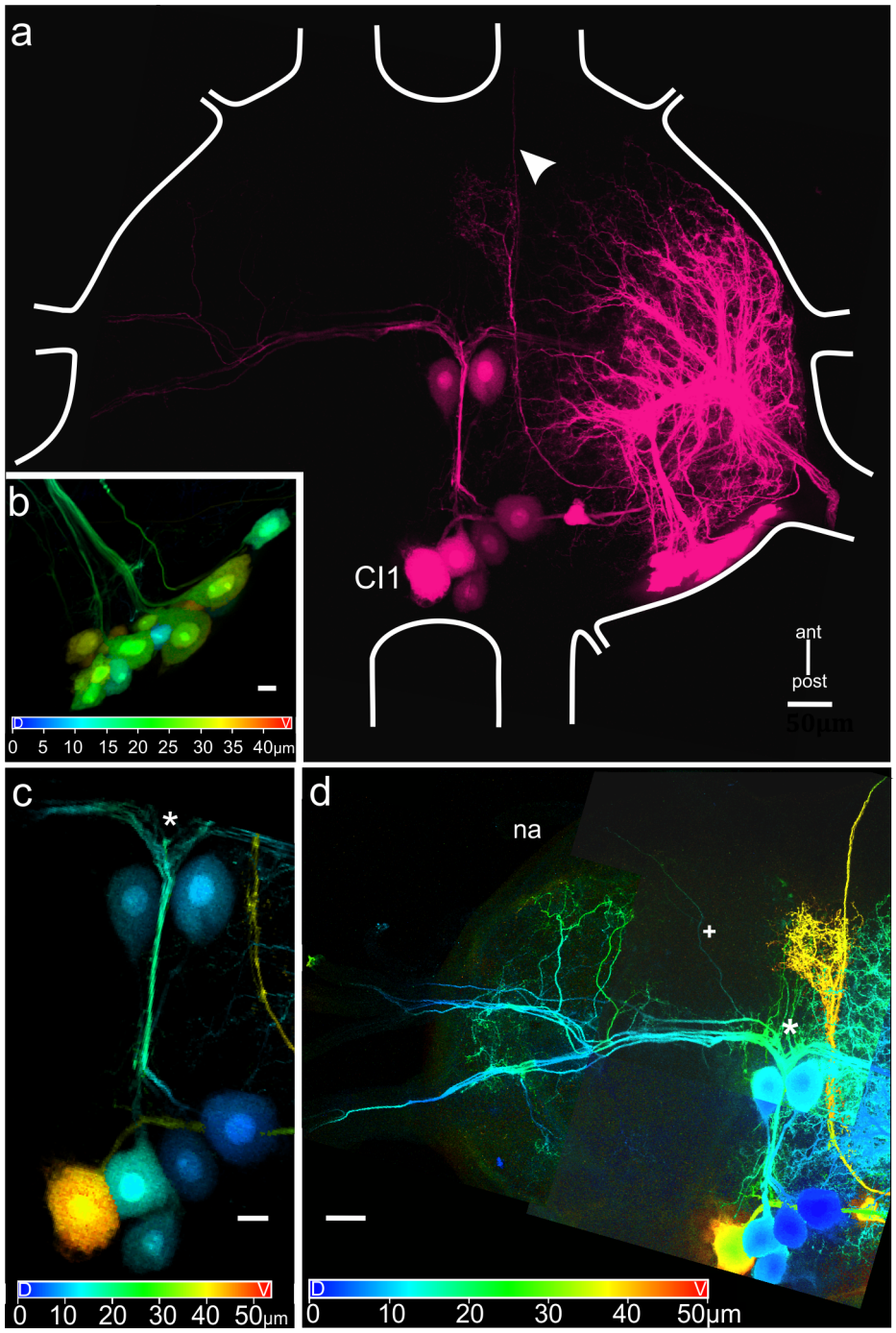

Figure B.2. – **Backfill of branches A and B of nervus lateralis 5 (nl5) that innervate the tergal retractor coxae muscles. a:** Whole-mount with stained neurons in the posterolateral (PL) cell cluster and one neuron in the posteroventromedial (PVM) cluster. At the midline six DUM neurons (note also c) and the CI1 cell body were labeled. The arrowhead indicate sensory afferents that leave the ganglion through the ipsilateral anterior connective. **b:** Depth color-coded PL neurons of a. Up to 16 cell body were stained in the cell cluster. **c:** Depth color-coded DUM cells and the CI1 at the midline. An asterisk marks the DUM neurite T-junction. **d:** Arborizations of DUM neurites on the contralateral ganglion side. Branching occurs just after the DUM neurites leave the cell bodies, at the T-junction (asterisk) and in antero- and posterolateral ganglion parts. The cross marks a neurite that travels in the direction of nerve na, possibly a neurite of a DUM na,nl2,5 neuron. Scale bars=50 µm in a and d. 20 µm in c and 10 µm in b.

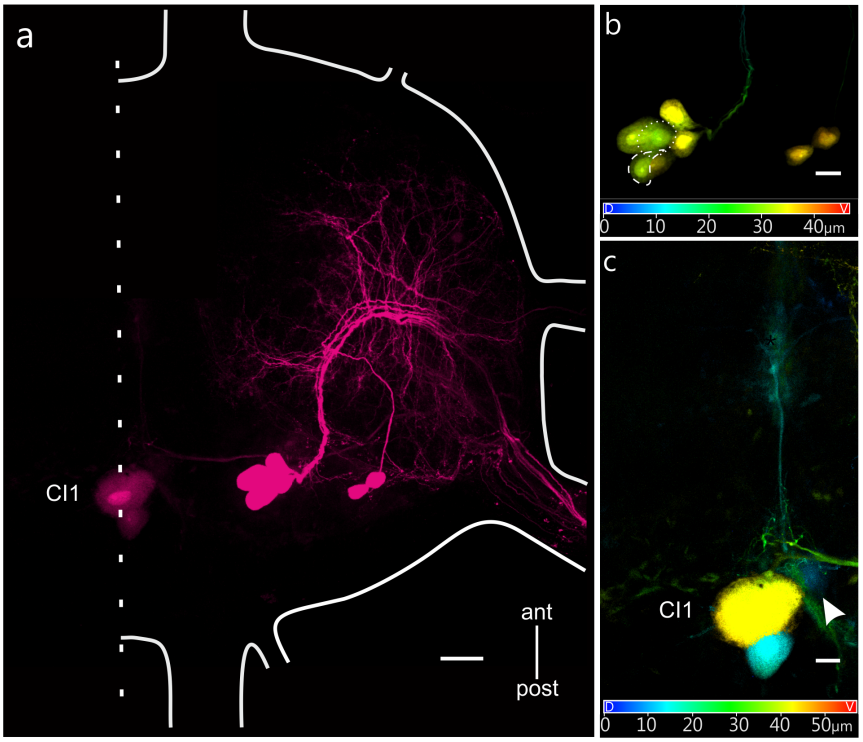

Figure B.3. – **Backfill of branch p of nervus lateralis 5 (nl5) that innervates the sternal adductor (2st-cx) and sternal remotor of coxa (3st-cx). a:** Whole-mount with two stained neurons in the posterolateral (PL) cell cluster and six neurons in the posteroventromedial (PVM) cluster. At the midline two DUM neurons (note also c) and the CI1 cell body were labeled. **b:** Depth color-coded neurons of a. Two neurons were observed in the PL cluster and up to six neurons in the PVM group. **c:** Depth color-coded DUM cells and the CI1 at the midline. An arrowhead marks a weakly stained DUM cell. Scale bars=50 µm in a and 20 µm in b and c.

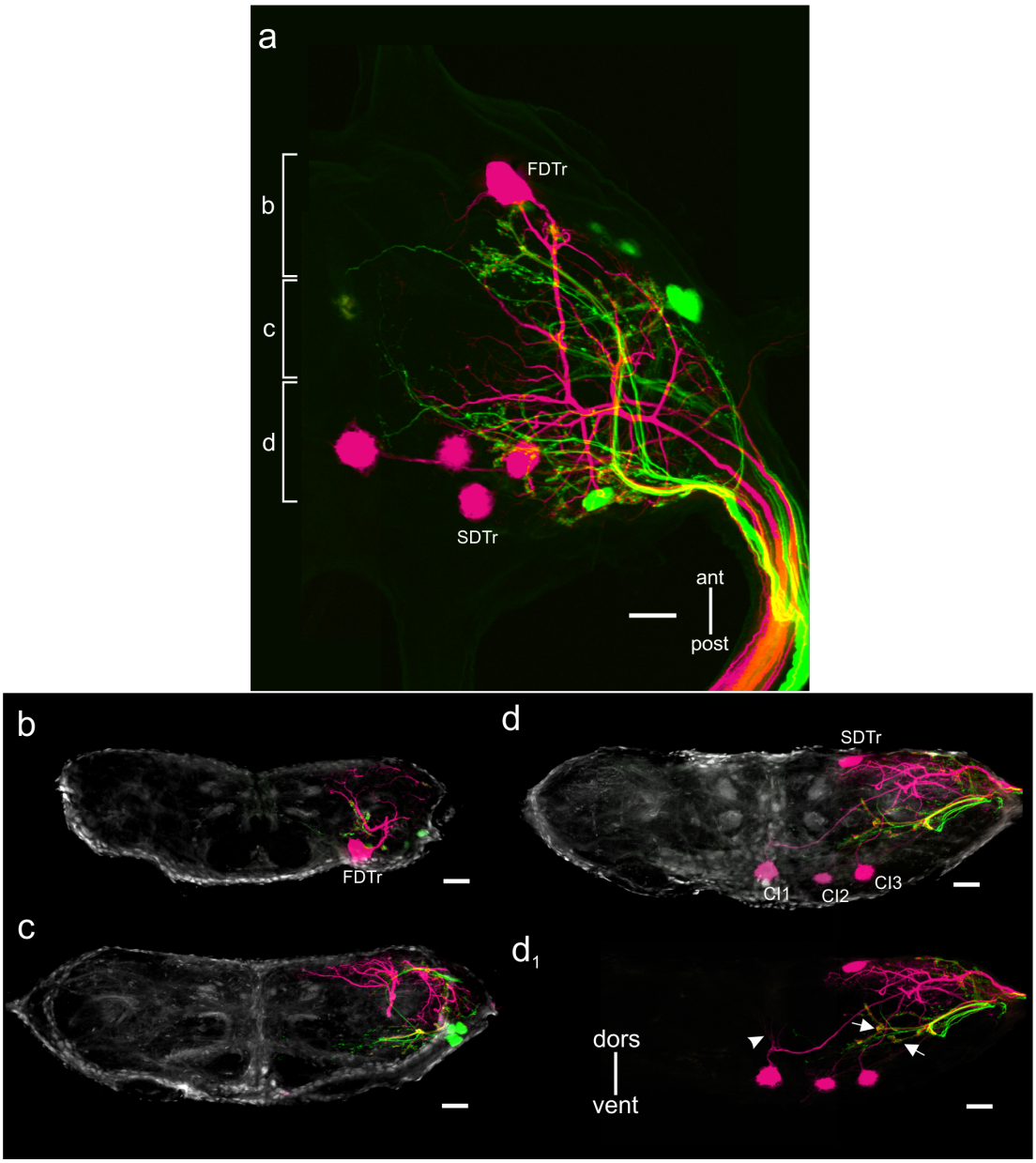

Figure B.4. – **Ipsilateral double stainings of coxa branches 1 (C1; green; innervates levator trochanteris) and 2 (C2; magenta; innervates depressor trochanteris). a:** Top view of whole-mount. Brackets indicate levels of transverse sections shown in (b–d). **b–d:** Transverse sections. Through both nerves several sensory afferents of coxal hair plates (HP) were stained that terminate in the same and mainly intermediate neuropil regions (d). The boutons at their terminal endings appear intermingled and in vicinity as shown for afferents of antennal HFs (arrows, d_1). Noticeable are also several fine branches arising just after the CI1 primary neurite leaves the cell body (d_1, arrowhead). Scale bars=50 µm.

Abbreviations

a, ant	Anterior
$a.u.$	Arbitrary units
Ab	Abductor
Ad	Adductor
AIN	Ascending interneuron
AL	Antennal lobe
$aVAC$	Anterior ventral association center
c	Contralateral
$C1-2$	Coxa branch 1 or 2 of nervus cruris
Ca^{2+}	Calcium
CB	Central body
CC	Central complex
cdl	Caudo-dorsal-lateral terminal area
$CI1-3$	Common inhibitory motoneurons 1-3
cvi	Caudo-ventro-intermediate terminal area
$d, dors$	Dorsal
DC	Deutocerebrum
DIN	Descending interneuron
DIT	Dorsal intermediate tract
DL	Dorsal lobe
Dp	Depressor
DUM	Dorsal unpaired median neuron
$F2$	Femoral branch 2 of nervus cruris
$F4/5$	Femoral branches 4 and 5 of nervus cruris
$FDTr$	Fast depressor trochanteris motoneuron
$FETi$	Fast extensor tibiae motoneuron
HF	Hair field
hN	Horseshoe neuropil

HP	Hair plate
HR	Hair row
HVA	High-voltage-activated channel
i	Ipsilateral
ilb	Intermediate longitudinal bundle
l	Lateral
LAL	Lateral accessory lobe
llb	Lateral longitudinal bundle
$Lv/LvTr$	Levator/levator trochanteris
LVA	Low-voltage-activated channel
$lVAC$	Lateral ventral association center
$LvSR$	Levator stretch receptor
m	Medial
MN	Motoneuron
na	Nervus anterior
ncr	Nervus cruris (main leg nerve)
$nl1-5$	Nervi laterali 1-5
np	Nervus posterior
nup	Nervus unparis
$OGB-1$	Oregon Green 488 BAPTA-1 dextran
$p, post$	Posterior
PB	Protocerebral bridge
PC	Protocerebrum
pi	Pars intercerebralis
PL	Posterolateral
$ProCx$	Protractor coxae
PVM	Posteroventromedial
rdl	Rostro-dorso-lateral terminal area
$RetCx$	Retractor coxae
ROI	Region of interest
RUI	Retractor unguis I muscle
rvi	Rostro-ventro-intermediate terminal area
$SDTr$	Slow depressor trochanteris motoneuron
$SETi$	Slow extensor tibiae motoneuron
SOG	Suboesophageal ganglion
SRP	Spontaneous recurrent pattern
TC	Tritocerebrum
$v, vent$	Ventral
VAC	Ventral association center
VFA	Ventral area of flagellar afferents
VIT	Ventral intermediate tract

List of Figures

List of Tables

Teilpublikationen

Article

Goldammer J, Büschges A, Schmidt J. (2012)
Motoneurons, DUM cells and sensory neurons in an insect thoracic ganglion: a tracing study in the stick insect *Carausius morosus. J Comp Neurol, 520(2):230-257*

Conference abstracts

Goldammer J, Rotte C, Schmidt J, Kloppenburg P, Büschges A. (2013)
Calcium imaging of retrogradely labeled retractor coxae neurons in the stick insect *Carausius morosus. Proc. of the 10th Meeting of the German Neuroscience Society, Göttingen. Conference Abstract T21-8A.*

Goldammer J, Rotte C, Schmidt J, Kloppenburg P, Büschges A. (2012)
Calcium imaging of retrogradely labeled retractor coxae neurons in the stick insect *Carausius morosus. 105th Annual Meeting of the Deutsche Zoologische Gesellschaft (DZG), Konstanz. Conference Abstract 147.*

Goldammer J, Rotte C, Schmidt J, Kloppenburg P, Büschges A. (2012)
Calcium imaging of retrogradely labeled retractor coxae neurons in the stick insect *Carausius morosus. 2nd Satellite Symposium of the Arthropod Neuroscience Network (ANN), Konstanz.* Best Poster Award.

Goldammer J, Dürr V. (2011)
Central projections of antennal hair fields and descending interneurons in stick insect brain and suboesophageal ganglion. *Proc. of the 9th Meeting of the German Neuroscience Society, Göttingen. Conference Abstract T20-4A.*

Goldammer J, Büschges A, Schmidt J. (2010)
Anti-β-tubulin immunohistochemistry on thick transverse ganglion sections after

retrograde labeling of mesothoracic leg nerves of the stick insect *Carausius morosus. 9th International Congress of Neuroethology, Salamanca (Spain). Conference Abstract P111.*

Goldammer J, Schmidt J. (2009)
A Tracing Study of Mesothoracic Leg Motoneurons and DUM neurons in the stick insect *Carausius morosus. Proc. of the 8th Meeting of the German Neuroscience Society, Göttingen. Conference Abstract T21-4B.*

Goldammer J, Mentel T, Büschges A. (2008)
A Tracing Study of the Leg Motoneurons in *Carausius morosus. "Load and force control in walking pattern generation of animals and robots: From sensors to local and global control function", Zoological Institute, University Cologne, Germany. February 21th-23rd.*

Goldammer J, Mentel T, Büschges A. (2007)
A Tracing Study of the Leg Motoneurons in *Carausius morosus.* 1*00th Annual Meeting of the Deutsche Zoologische Gesellschaft (DZG), Köln. Conference Abstract N3.*

Talk

"Morphology of antennal hair field projections in stick insect brain and suboesophageal ganglion" *at the Biological Cybernetics department of Prof. Dr. V. Dürr in Bielefeld (2009).*

Danksagung

An dieser Stelle bedanke ich mich ganz besonders bei:

- Prof. Dr. Ansgar Büschges für die sehr gute Betreuung, Förderung und für das Ermöglichen der neuroanatomischen Experimente dieser Arbeit.
- Prof. Dr. Peter Kloppenburg für die Übernahme des Zweitgutachtens, Ratschlägen und für die Benutzung des Calcium-Imaging Mikroskops.
- Prof. Dr. Volker Dürr für die Möglichkeit das sensomotorische System der Antenne zu untersuchen und für hilfreiche Anmerkungen für den Antennenteil dieser Arbeit.
- PD Dr. Joachim Schmidt für das Interesse an meiner Arbeit, für diverse hilfreiche Ratschläge und das Editieren des Motoneuron Papers.
- Dr. Anke Borgmann für die Hilfe bei der Matlab Auswertung, für diverse Matlab Skripte und das Korrekturlesen dieser Arbeit.
- Dr. Cathleen Rotte für die technische Beratung und Hilfestellung bei den Calcium-Imaging Experimenten.
- Eva Berg und Dr. Philipp Rosenbaum für das Korrekturlesen dieser Arbeit.
- Dipl.-Ing. Michael Dübbert, Hans-Peter Bollhagen, Jan Sydow, Sima Seyed-Nejadi, Sherylane Seeliger und Helmut Wratil für ihre zahlreichen technischen Hilfestellungen.
- Eva Berg, Dr. Katja Hellekes und Dr. Philipp Rosenbaum für zahlreiche (wissenschaftliche) Gespräche und den erheiternden Momenten in unserem gemeinsamen Büro.
- Frau Berlingen für die regelmäßigen und vorzeitigen Verlängerungen meines Stipendiums.
- den übrigen Mitgliedern der Arbeitsgruppen Büschges, Kloppenburg, Wellmann und Gruhn.
- meinen Eltern, meiner Schwester, Jörg, Emily und Jonas.

Erklärung

Ich versichere, dass ich die von mir vorgelegte Dissertation selbstständig angefertigt, die benutzten Quellen und Hilfsmittel vollständig angegeben und die Stellen der Arbeit - einschließlich Tabellen, Karten und Abbildungen -, die anderen Werken im Wortlaut oder dem Sinn nach entnommen sind, in jedem Einzelfall als Entlehnung kenntlich gemacht habe; dass diese Dissertation noch keiner anderen Fakultät oder Universität zur Prüfung vorgelegen hat; dass sie - abgesehen von oben angegebenen Teilpublikationen - noch nicht veröffentlicht worden ist sowie, dass ich eine solche Veröffentlichung vor Abschluss des Promotionsverfahrens nicht vornehmen werde. Die Bestimmungen dieser Promotionsordnung sind mir bekannt. Die von mir vorgelegte Dissertation ist von Prof. Dr. Ansgar Büschges betreut worden.

Köln, den 03.09.2013